IntechOpen

# Drilling

*Edited by Ariffin Samsuri*

# DRILLING

Edited by **Ariffin Samsuri**

**Drilling**
http://dx.doi.org/10.5772/intechopen.71179
Edited by Ariffin Samsuri

**Contributors**

Dr Sonny Irawan, Imros Kinif, Ahmed Adeniran, Omogbolahan Ahmed, Ariffin Samsuri, Paul Anthony Potter, Suzana Yusup, Yee Ho Chai, Vui Soon Chok, Junyue Tang, Shengyuan Jiang, Qiquan Quan, Jieneng Liang, Zongquan Deng, Xuyue Chen, Jin Yang, Deli Gao, Gabriel Cavalheiro, Mariana Cavalheiro, Saulo Rocha, Jun Li, Gonghui Liu, Boyun Guo, Yulong Yang



**Notice**



First published in London, United Kingdom, 2018 by IntechOpen
eBook (PDF) Published by IntechOpen, 2019
IntechOpen is the global imprint of INTECHOPEN LIMITED, registered in England and Wales, registration number: 11086078, The Shard, 25th floor, 32 London Bridge Street
London, SE19SG – United Kingdom
Printed in Croatia

British Library Cataloguing-in-Publication Data
A catalogue record for this book is available from the British Library

Additional hard and PDF copies can be obtained from orders@intechopen.com

Drilling
Edited by Ariffin Samsuri

p. cm.

Print ISBN 978-1-78984-303-3

Online ISBN 978-1-78984-304-0

eBook (PDF) ISBN 978-1-83881-531-8

# Meet the editor

Professor Dr. Ariffin Samsuri is a senior professor of Petroleum Engineering at Universiti Teknologi Malaysia with vast experience in managing R&D projects, faculties, and departments. He has more than 38 years of teaching and supervising experience in petroleum engineering, including academic program development, staffing, and faculty and facilities establishment. He has also been appointed as a visiting professor at Universiti Teknologi Petronas. He is a peer reviewer, external examiner, and has sat on expert and academic advisory panels. He has published more than 142 technical papers for conferences/seminars and journals, authored six books and three book chapters, translated four books, and edited 11 books and five research monographs. He is also involved in more than 30 research projects in drilling and production optimization, biofuel and nanotechnology application in oil and gas.

# Contents

# Preface

With regard to depleted oil and gas resources, increasing world energy demand and volatile economic and political world scenarios, oil and gas industry players are working very hard to find ways to cut exploration and production costs to sustain and progress the industry to provide the world with cheap energy without harming the environment. Therefore, this volume, which contains eight chapters, intends to provide readers with a comprehensive overview of the current state of the art in drilling, such as advanced drilling operations and techniques used by the industry, particularly in floating, underbalanced drilling, smart drilling fluid, intelligent drilling, drilling optimization, and future drilling technology and development. These eight chapters have been selected because they represent areas of drilling technology for which sufficient technical progress has been achieved with a view to technological advancement.

I have enjoyed working with the authors of this volume, who have been most diligent in preparing their chapters. Thanks for their contributions, patience, and commitment to the process. Each chapter is designed to help the reader gain an insight into the most important aspects of each topic.

On behalf of the authors, I would like to extend my heartfelt gratitude to IntechOpen and Mr. Markus Mattila, Author Service Manager, for their support, and to all the staff who have provided input, drafting, revisions, and production for this book.

It is my hope that this edition will be used as a source of knowledge and technology, and be used by all concerned for the betterment of humankind.

**Prof. Dr. Ariffin Samsuri**
Petroleum Engineering Department
Faculty of Chemical and Energy Engineering
Universiti Teknologi Malaysia
Johor Bahru, Johor, Malaysia

Chapter 1

# Proposing a Patent Information Approach for Identifying Technological Trends in the Brazilian Upstream Oil and Gas Industry

Gabriel Cavalheiro, Mariana Brandao and Saulo Rocha

Additional information is available at the end of the chapter

http://dx.doi.org/10.5772/intechopen.75377

**Abstract**

In recent years, Brazil has emerged as a leading offshore producer with extensive proven reserves yet to be explored. As a matter of fact, the discovery of huge oil deposits in the pre-salt layer of the country's Southeastern coast is motivating oil and gas exploration in great depths in Brazil, thereby also generating increasing demand for drilling capabilities. This study addresses the technological implications of this discovery by examining patent information. Here, we provide empirical evidence indicating an increased interest for patenting technologies designed to enhance not only ultra-deep drilling capabilities and build and maintain oil wells, but also technologies to increase oil production from formations.

**Keywords:** patent information, patent analytics, oil and gas, technology, drilling, technology trend

## 1. Introduction

Despite the strong increase in the use of renewable fuels and the substantial reduction in oil prices in recent years, crude oil is still considered an extremely important commodity [1, 2]. On the one hand, oil comprises the largest share in the world energy mix for several decades [3]. On the other hand, our society is heavily dependent on a well-established and complex infrastructure for exploitation and the use of oil to fulfill energy needs in industrial, commercial, and domestic scale [2].

As consequence of the central role played by oil in our society, which was consolidated primarily from the second half of the twentieth century onward, the need to identify new reserves of this non-renewable fuel in order to ensure a reliable supply of this resource became a critical necessity worldwide [4]. As such, the combination of an increasing demand for oil and the growing technical challenges associated with the remaining oil reserves found in remote locations has motivated robust technological investments by oil firms that are constantly investing huge sums to find and exploit new reserves [5].

In recent years, Brazil has emerged as a relevant offshore oil producer with extensive proven reserves yet to be explored [6]. More specifically, in 2007, the Brazilian Federal Government announced the discovery of a huge oil and natural field in the pre-salt layer of the country's Southeastern coast. This discovery was accomplished by Petroleo Brasileiro S.A. (Petrobras) and was considered to be one of the world's largest in recent years [7]. However, despite the evident economic benefits associated with this huge oil discovery, substantial resources will need to be put in place to address the operational challenges coming from the ultra-deep water environment of the largest subsea project in the world [8].

Given the promising prospects generated by the pre-salt discovery, firms operating in the oil and gas industry rapidly perceived that the operational characteristics of the pre-salt reserve would generate a huge demand for technology-intensive services and equipment. As such, as pointed out by Cavalheiro et al. [9], there was a boom in patent filings in Brazil in response to the market opportunities for new upstream technologies to enable the development of the pre-salt fields. Increasingly, market opportunities associated with technologies determine the propensity of firms to file patent applications [10]. However, despite the awareness of the increased interest of firms in protecting innovative upstream oil and gas technologies in Brazil, extant literature remains silent on the most critical technical areas protected by firms.

Consequently, this study provides a contribution for understanding the most critical technological areas associated with the pre-salt exploitation by examining patterns of patent filings in Brazil regarding upstream oil and gas technologies. As such, this paper is aimed at improving understanding of the specific technological trends regarding the exploitation of the pre-salt reserves.

This paper is structured as follows Section 2 provides a literature review on patent information and examines the context of the oil and gas industry in Brazil. Then, Section 3 describes our research method. Section 4 examines the patterns of patent applications in Brazil concerning upstream oil and gas technologies. Finally, in Section 5, our conclusions are put forward.

## 2. Literature review

### 2.1. Patent information

A firm's innovation strategy is the central to fostering innovation competence, which in turn leads to the development of new products and technologies [11]. However, innovation is characterized by a high level of uncertainty, given the difficulties in forecasting the performance

and costs of a new technology, as well as the reaction of users to it [12]. As such, the logic behind the patent system assumes that firms invest in risky R&D activities in order to generate innovative technologies or products. As a consequence of the huge investments associated with the development of new technologies or products, it is certainly fair to assume that this investment should somehow be protected [13–15]. In this way, patents can be perceived as legal instruments providing exclusive rights to enable innovative firms to prosper in a challenging, risky, and dynamic business environment [10, 16]. Hence, these firms are able to protect their investment in new technologies by filing a patent in a Patent Office [17–19].

Fundamentally, a patent can be regarded as packaged knowledge that delimits and draws boundaries around a set of technical characteristics [20, 21] and concedes an effective instrument to prevent imitation by competitors [22]. Additionally, the value of a patent is dependent upon a number of factors such as the potential for licensing to other businesses, the quality of the patent [23], the importance of the market covered by the patent [15, 24], and the effectiveness and stringency of patent enforcement [25]. Moreover, as stated by Davies [26], technologies are subject to a life cycle that suggests a decreasing rate of innovation and economic value as technologies gradually become obsolete.

As a direct consequence of the growing number of protected technologies, various authors stress that the patent system is characterized by an increasing level of complexity [23, 27, 28]. Accordingly, it is common to have single products, like smartphones and tablets, incorporating hundreds or even thousands of patents, thereby creating legal disputes involving a large set of patents, rather than just one. Hence, the costs involved in negotiating and licensing the relevant patents is continuously increasing [29].

The international patent system gained significant importance toward the end of last century. Due to many significant technological developments associated with the Second World War, a plurality of innovative technologies was developed in fields such as computer science, materials, telecommunications, biotechnology, and nuclear energy [30]. As stated by Galini [29], the large-scale adoption of these technologies has transformed society into a knowledge-based society that generates an increasing amount of inventions needing to be protected against unauthorized copy. Moreover, given the fact that innovative firms are becoming increasingly dependent on their patent portfolios to remain competitive, patent information has become an evolving and important research area.

Alongside with the rapid growth of available patent data, modern information technologies have revolutionized patent information practice in terms of both speed of access and information comprehensiveness, thereby motivating the development of sophisticated patent analysis tools. As stated by Abbas et al. [31], currently, there are several IT-based patent analytic tools capable of performing tasks such as strategic technology planning, detecting patent infringement, determining patent quality, and identifying technological hotspots. Additionally, Ernst [20] pointed out that patent information can also be used for competition monitoring, R&D portfolio management, and identification of potential sources of technological knowledge. In order to analyze patent data from dynamic, heterogeneous, and scattered information sources, researchers in this realm count with increasingly sophisticated solutions, such as patent landscape, text mining, and digital mind mapping tools to address large data volumes [32, 33].

Given the tremendous advances in patent analytic tools in recent years, patent information can be used to support a wide range of analyses in different industries. For example, Huang [34] examined the evolution of the patent portfolio of mainstream firms of the cloud computing industry. Moreover, Dubaric et al. [35] employed patent application figures as performance indicators representing evolution and level of maturity of wind power technology. Huang and Cheng [11], in turn, proposed a patenting behavior framework to identify the primary factors determining the propensity to file a patent application. Beyond examining patent applications filed by firms, there are also relevant studies addressing how universities are protecting their inventions through patents. Accordingly, Drivas et al. [16] assessed patterns associated with the licensing process of university patents, while Siegel et al. [36] developed a framework to describe the transfer of scientific knowledge from academicians to practitioners. More recently, Arunagiri and Mathew [37] demonstrated the possibility of identifying relevant business and technical patterns by assessing patent classification of implant technology patents.

As a result of improved capabilities for analyzing patent information, policy makers started to rely on the number of patent applications as a critical performance indicator for patent office attractiveness [38], global level of economic activities, and the effort level on R&D activities [18, 24]. However, Boldrin and Levine [39] stress that there is no empirical evidence indicating that patents serve to increase innovation or productivity but rather to demonstrate power in a highly competitive environment. Despite the clear benefits associated with the current international patent system, there is also criticism regarding its current configuration. Although, scientific and technical communities in different countries are currently more connected than they used to be [40], nations that lack the capacity to innovate globally tend to consider intellectual property protection as nothing more than tax.

In addition, various scholars point out structural factors hampering firms in developing countries in generating revenue from patents, which include the limited quantity and intensity of links between firms and universities [40, 41], low rate of industrial technological accumulation in industry [13], public policy makers with limited understanding of intellectual property [42], as well as a partial lack of understanding about the consequences of academic engagement for scientific and economic objectives [43].

### 2.2. Brazilian context: pre-salt discovery

Brazil has already accumulated a long experience with the discovery and production of oil. As a matter of fact, the first oil discovery in Brazil was accomplished in 1939 in the State of Bahia, while the first offshore extraction project started in 1968 [44]. However, despite the history of oil production activities in the countries, for several decades, Brazil imported large amounts of oil to complement its internal production to supply the internal demand [8]. However, in 2007, the Brazilian Federal Government announced the discovery of huge oil and natural gas resources in the pre-salt layer of the country's Southeastern coast. This discovery was accomplished by Petróleo Brasileiro S.A. (Petrobras) and created the possibility of turning the country into one of the largest oil producers in the world [7].

In order to explore this huge oil field, substantial effort will be required to develop and integrate innovative technologies to address the challenges coming from operating in the ultra-deep water environment of the largest subsea project in the world [8]. However, until the present, total oil production in Brazil has been increasing at a small pace in recent years, as illustrated in **Figure 1**.

In practice, exploring the pre-salt reservoirs is a massive technical and organizational challenge that generates significant need of investments in new technologies. The distance between the surface of the sea and the oil reservoirs under salt layer can be as much as 7000 meters [7]. Consequently, exploration and production of hydrocarbons located in ultra-deep offshore waters require a plurality of innovative technologies destined for hostile, hard-to-reach environments characterized by extremely high pressures and temperature [46].

### 2.3. Patent applications in Brazil

Prior to examining patent applications related to upstream oil and gas technologies, it is also worthwhile to assess the trend regarding patent applications regarding all fields of technologies in recent years in Brazil. In this regard, we have opted to examine the total number of Brazilian patent applications between 2001 and 2013. Clearly, **Figure 2** displays a small and continuous increase in patent applications, which started in 2004.

Although a small and continuous increase in patent applications in Brazil can be observed in recent years, this growth started prior to the pre-salt announcement. However, when it comes to upstream oil and gas technologies, Cavalheiro et al. [9] pointed out that the pre-salt announcement motivated increased interest for protecting upstream oil and gas technologies in Brazil. In this respect, the IPC subclass E21B covers a wide portion of technologies associated with upstream oil and gas exploration, such as earth or rock drilling obtaining oil, gas, water, soluble or meltable materials, or a slurry of minerals from wells. Clearly, the growth of

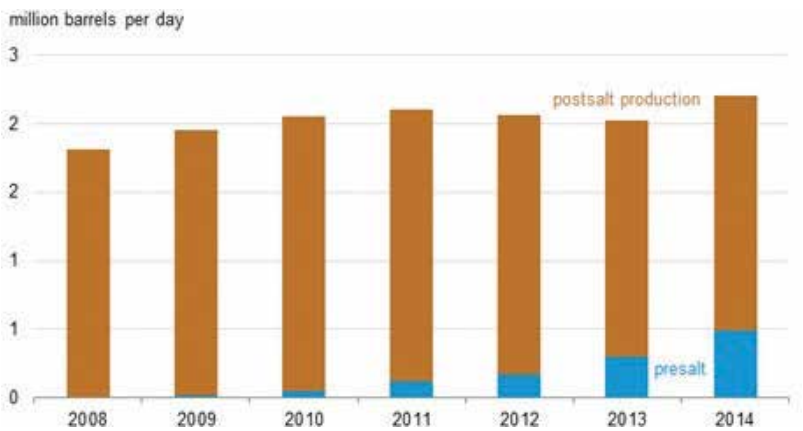


**Figure 1.** Brazil's total oil production by type: 2008–2014 (source: U.S. Energy Information Administration [45]).

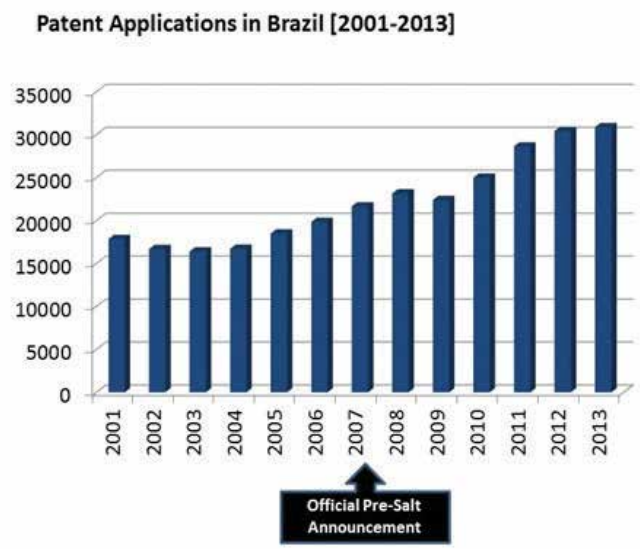


**Figure 2.** Brazil's total patent applications: 2001–2013 (source: WIPO Statistical Country Profile, Brazil, 2015).

E21B patent applications is much stronger, than the growth in both oil production and total patent applications in Brazil. Accordingly, E21B was selected for being a highly representative IPC subclass for the upstream oil and gas industry. As such, **Figure 3** displays a strong increase in patent applications in Brazil concerning the E21B.

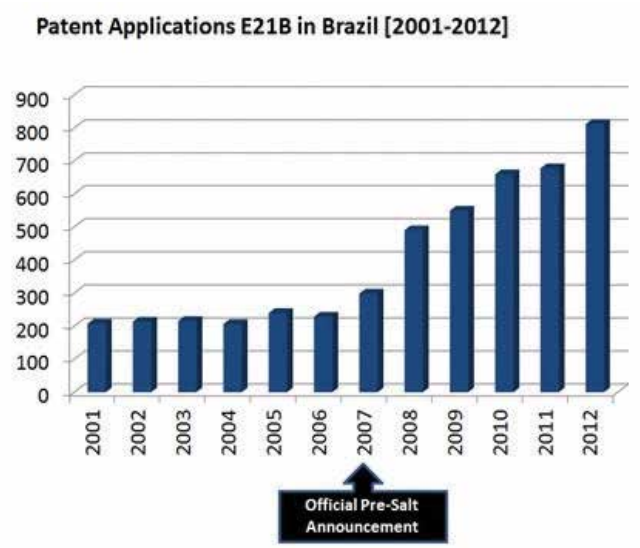


**Figure 3.** Patent applications related to upstream oil and gas technologies in Brazil: 2001–2012 (source: adapted from [9]).

## 3. Research method

Fundamentally, we adopt a qualitative and quantitative approach based on a combination of literature review and empirical analysis of patent filings. As a matter of fact, adopting a pure quantitative approach is not feasible, as the extant literature does not offer clear conventions for analyzing patent information related to upstream oil and gas technologies, such as the widely accepted and well-known rules of algebra through which the validity of mathematical deductions is known [47]. A fundamental characteristic of a qualitative approach, in turn, is that researchers may have less a priori knowledge of what the variables of interest will be and how they will be measured [48]. Accordingly, qualitative researchers are sometimes disposed toward causal determination of events but more often tend to perceive events not simply and singly caused (Stake [50]). Consequently, the combination of qualitative and quantitative approaches can be very synergistic [49].

In practice, we collected data representing the patent applications in Brazil for the period between 2001 and 2012. The choice for this period was motivated by the research objective of this study, which is aimed at improving understanding of the major technological trends associated with the upstream oil and gas industry in Brazil. Additionally, given the fact that the Brazilian patent legislation establishes that a patent application must be published 18 months after the filing date in combination with administrative delays to classify patent applications, patent data concerning the years 2013, 2014, and 2015 were not completely available during of the data collection phase of this study.

The figures regarding Brazilian patent applications were retrieved by executing queries within a system named "Sistema Integrado da Propriedade Industrial" (SINPI). SINPI regards an internal information system that processes administrative information for "Instituto Nacional da Propriedade Industrial" (INPI), which is the Brazilian national patent office. The queries concerned patent applications with filling dates between January 1, 2001, and December 31, 2012. These queries specified the patent applications classified with the International Patent Classification (IPC) scheme in the technical area of E21B, as this particular area covers a wide portion of technologies associated with upstream oil and gas exploration, such as earth or rock drilling obtaining oil, gas, water, soluble or meltable materials, or a slurry of minerals from wells.

Accordingly, E21B was selected for being a highly representative IPC subclass for the upstream oil and gas industry. The collection of patent information on patents describing technologies used in the upstream oil and industry, which are classified as E21B, was analyzed based on patent classification listed in the documents. More specifically, we have examined the total number of documents further classified in terms of the groups that belong to the E21B subclass. This decision enabled us to identify the most active technical fields within the E21B subclass.

## 4. Results

After examining the characteristics of the patent system and the context associated with the pre-salt discovery, we take up the patent applications in Brazil for the period between 2001

and 2012. As stated by Cavalheiro et al. [9], market opportunities for the oil and gas industry in Brazil associated with the pre-salt announcement motivated a substantial increase in patent filings in Brazil concerning upstream oil and gas technologies. As such, we applied the following search strings within INPI's SINPI environment to select all patent applications of interest concerning the period between 2001 and 2012—"Filing date: 01012001-31122012" and "IPC:E21B." In total, 4804 patent applications were retrieved. **Table 1** lists all groups belonging to the E21B subclass and also provides a distinction of subfields within the upstream oil and gas technologies, as proposed by WIPO's IPC diagram.

### 4.1. Most protected technologies

Beyond the six technical subareas within upstream oil and gas technologies listed in the table, it is also worthwhile to zoom in further into the IPC groups that attracted the largest number of patent applications. In order to better illustrate the dominant technical areas, we have also opted to graphically represent the most active groups. As such, **Figure 4** displays the groups that account for more than one percent of all E21B patent applications.

Since **Figure 3** indicates significant differences in terms of the number of patent application per IPC group, it is worthwhile to examine the technical characteristics of each group. As such, **Table 2** displays the total number of applications for the most active IPC groups. To this end, we selected the subgroups that received more than one percent of total E21B patent applications, which corresponds to IPC groups with more than 48 patent applications, to draw histogram.

According to Ernst [20], the information available in patent data reveals strategic decisions of firms regarding a market for a certain technologies. Accordingly, the IPC groups listed in **Table 2** can be regarded as the most strategic technologies for exploring the pre-salt reserves

| Technical subareas within upstream oil and gas technologies | IPC groups | Number of patent applications |
|---|---|---|
| Methods for drilling | E21B 1, E21B 3, E21B 4, E21B 6, E21B 7 | 268 |
| Drilling tools | E21B 10, E21B 11, E21B 12 | 198 |
| Well equipment or well maintenance | E21B 15, E21B 17, E21B 19, E21B 21, E21B 23, E21B 25, E21B 27, E21B 28, E21B 29, E21B 31, E21B 33, E21B 34, E21B 35, E21B 36, E21B 37, E21B 40, E21B 41 | 2521 |
| Obtaining fluids from wells | E21B 43 | 1080 |
| Automatic control of wells | E21B 44 | 77 |
| Surveying or testing | E21B 45, E21B 47, E21B 49 | 660 |
| Total number of E21B patent applications | | 4804 |

Source: the authors

**Table 1.** Total number of patent applications concerning upstream oil and gas technologies between 2001 and 2012 in Brazil.

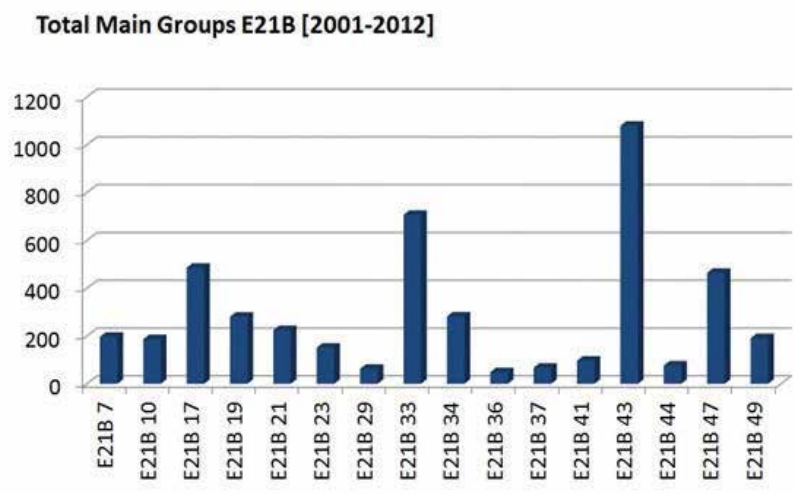


**Figure 4.** Total number of patent applications per IPC group (source: the authors).

in Brazil. Here it is worthwhile to mention that two IPC groups received special attention from firms operating in the upstream oil and gas industry. In particular, E21B 43 "Methods or apparatus for obtaining oil, gas, water, soluble or meltable materials or a slurry of minerals from wells" accounts for 1080 patent applications, representing approximately 22% of all E21B applications. Similarly, E21B 33 "Sealing or packing boreholes or wells" was responsible for 707 patent applications, or approximately 15% of all E21B applications. As such, these figures can be interpreted as an indication of the strategic importance of these technologies for exploring the offshore ultra-deep reserves of the Brazilian Pre-Salt.

Another IPC group that received substantial attention from firms regards E21B 17 "Drilling rods or pipes; Flexible drill string" and E21B 47 "Survey of boreholes or wells," as both IPC groups obtained approximately 10% of total E21B patent applications. It is possible to deduce that technologies for drilling pipes and surveying boreholes are also key areas for the companies involved in the pre-salt exploration.

### 4.2. Least protected technologies

Despite the strong increase in E21B patent applications reported by Cavalheiro et al. [9], several IPC groups belonging to E21B did not attract a large number of patent applications at all. As such, we have selected the IPC groups that received less than one percent of the total E21B applications between 2001 and 2012, which corresponds to a number of patent applications lower than 48.

As indicated in **Table 3**, several IPC groups received less than one percent of the patent applications related to upstream oil and gas technologies. Typically, these groups represent technical areas that do not attract the attention of both operating and service companies and, as a result, are not active. More specifically, a more technical interpretation of these results points out a mismatch between the requirements posed by the pre-salt reserves and the solutions

| IPC groups | Description | Number of patent applications |
|---|---|---|
| E21B 43 | Methods or apparatus for obtaining oil, gas, water, soluble or meltable materials, or a slurry of minerals from wells (applicable only to water; obtaining oil-bearing deposits or soluble or meltable materials by mining techniques; pumps) | 1080 |
| E21B 33 | Sealing or packing boreholes or wells | 707 |
| E21B 17 | Drilling rods or pipes, flexible drill strings, kellies, drill collars, sucker rods, casings, tubings | 486 |
| E21B 47 | Survey of boreholes or wells (monitoring pressure or flow of drilling fluid) | 465 |
| E21B 34 | Valve arrangements for boreholes or wells (in drilling fluid circulation systems, blowout preventers, oil flow-regulating apparatus, valves in general) | 282 |
| E21B 19 | Handling rods, casings, tubes, or the like outside the borehole, e.g., in the derrick; apparatus for feeding the rods or cables (surface drives) | 281 |
| E21B 21 | Methods or apparatus for flushing boreholes, e.g., by the use of exhaust air from motor (freeing objects stuck in boreholes by flushing, well-drilling compositions) | 225 |
| E21B 7 | Special methods or apparatus for drilling (supports for the drilling machine, e.g., derricks or masts) | 197 |
| E21B 49 | Testing the nature of borehole walls, formation testing, methods or apparatus for obtaining samples of soil or well fluids | 191 |
| E21B 10 | Drill bits (specially adapted for deflecting the direction of boring, with means for collecting substances) | 187 |
| E21B 23 | Apparatus for displacing, setting, locking, releasing, or removing tools, packers, or the like in boreholes or wells | 152 |
| E21B 41 | Equipment or details not covered by groups | 97 |
| E21B 44 | Automatic control systems specially adapted for drilling operations, i.e., self-operating systems which function to carry out or modify a drilling operation without intervention of a human operator, e.g., computer-controlled drilling systems | 77 |
| E21B 37 | Methods or apparatus for cleaning boreholes or wells | 68 |
| E21B 29 | Cutting or destroying pipes, packers, plugs, or wire lines, located in boreholes or wells, e.g., cutting of damaged pipes and of windows (perforators) | 63 |
| E21B 36 | Heating, cooling, or insulating arrangements for boreholes or wells, e.g., for use in permafrost zones (drilling by the use of heat, secondary recovery methods using heat) | 49 |

Source: the authors

**Table 2.** Most protected upstream oil and gas technologies in Brazil.

provided by the technologies belonging to the IPC groups listed in **Table 3**. As an illustration of this interpretation, Hu et al. [2] stress that the technologies belonging to E21B 1 "Percussion drilling (drives used in the borehole)" are suitable to explore onshore oil reserves with very small depths, as opposed to the offshore ultra-deep pre-salt conditions.

Consequently, given the particular conditions of the Brazilian oil reserves, only five patent applications were filed in Brazil between 2001 and 2012 related to percussion drilling. Our interpretation is that the less protected technologies within the E21B group result from the fact that these technologies are to some extent inadequate to be deployed in the Brazilian

| IPC groups | Description | Number of patent applications |
|---|---|---|
| E21B 15 | Supports for the drilling machine, e.g., derricks or masts | 37 |
| E21B 4 | Drives for drilling, used in the borehole | 33 |
| E21B 3 | Rotary drilling (drives used in the borehole, rotary drilling machines in general) | 28 |
| E21B 31 | Fishing for or freeing objects in boreholes or wells (provisions on well heads for introducing or removing objects, locating or determining the position of objects in boreholes or wells) | 27 |
| E21B 25 | Apparatus for obtaining or removing undisturbed cores, e.g., core barrels, core extractors (core bits, using explosives or projectiles in boreholes, side-wall sampling or coring) | 25 |
| E21B 27 | Containers for collecting or depositing substances in boreholes or wells, e.g., bailers for collecting mud or sand, drill bits with means for collecting substances, e.g., valve drill bits | 12 |
| E21B 28 | Vibration generating arrangements for boreholes or wells, e.g., for stimulating production (for drilling, for transmitting measuring signals, for geophysical measurements) | 8 |
| E21B 12 | Accessories for drilling tools | 7 |
| E21B 1 | Percussion drilling (drives used in the borehole) | 5 |
| E21B 6 | Drives for drilling with combined rotary and percussive action (drives used in the borehole, portable percussive machines with superimposed rotation) | 5 |
| E21B 11 | Other drilling tools | 4 |
| E21B 45 | Measuring the drilling time or rate of penetration | 4 |
| E21B 35 | Methods or apparatus for preventing or extinguishing fires (cutting or deforming pipes to control fluid flow, controlling flow of fluid to or in wells, firefighting in general) | 1 |
| E21B 40 | Tubing catchers, automatically arresting the fall of oil-well tubing | 1 |

Source: the authors

**Table 3.** Less protected upstream oil and gas technologies in Brazil.

conditions or, in some cases, may even be perceived as obsolete in the oil and gas industry, thereby not motivating firms to commit R&D resources to further develop these technologies.

## 5. Discussion

The effective management of a patent portfolio is an increasingly complex challenge in our current knowledge-based society, especially for firms with a large number of patent applications. As such, using patent information as secondary data, we have provided rich insights regarding the specific technical interest of technology-based firms operating in the Brazilian upstream oil and gas industry [20]. More specifically, we have employed patent application figures as a performance indicator representing technological hotspots [35]. To this end, we have explored a large number of patent documents by carrying out pattern analysis to identify relevant business insights (Madani and Weber [51]).

Our detailed examination of the E21B subclass has shown evidence of substantial differences in terms of the commercial potential of different types of upstream oil and gas technologies in the context of the Brazilian market. In addition, the findings on the robust growth of patent filings regarding upstream oil and gas technologies have provided evidence of a growing interest of firms operating in this particular industry in developing technical solutions to address specific operational challenges associated with the pre-salt exploration [9].

As mentioned above, it is possible to determine that within the scope of the E21B subclass, there are technologies that received greater attention from firms in the oil and gas industry, motivating more patent applications to protect inventions belonging to a small set of technical areas [39]. Clearly, we have identified a small number of highly active technical subareas that represent key technologies. However, the findings also point to several IPC classifications that comprise upstream oil and gas technologies, but did not motivate a growing number of patent applications. This was due to the existence of areas containing technologies not suitable to the Brazilian operational context of the pre-salt but also due to obsolete technologies that are not motivating patent applications anymore [26].

In practice, it was possible to identify technological hotspots within upstream oil and gas technologies [31]. Clearly, the technical subareas attracting the largest number of patent applications concern technologies designed to build and maintain wells, as well as technologies dedicated to increase productivity of existing wells. This can be seen as a strong evidence that operating companies are interested in improving technologies for building wells as maximizing production from oil formations. However, the findings also point out to that there are several technical areas attracting modest industry attention in a pre-salt context, such as percussion drilling, measuring the drilling time, preventing or extinguishing fires downhole in offshore conditions, and automatically arresting the fall of oil-well tubing.

The use of patent application figures helps us to claim that that the particular characteristics of the Brazilian pre-salt reservoirs generated specific perceptions of potential market demand for different technical areas. The concentration of patent applications in certain IPC groups, such as E21B 43 and E21B 33, highlights the value of these patents for business (Madani and Weber [51]). In fact, these patents can be perceived as instruments providing exclusive rights to commercialize critical technologies in an emerging and large-scale market. This way of perceiving decision-making regarding patenting leads us to the importance of highlighting the need to protect technologies that are perceived as strategic and generate expectations of high revenue potential in the coming years.

Thus, our research has revealed that despite the tremendous growth in patent applications concerning upstream oil and gas technologies in Brazil from 2007 onward, only a small set of very specific technical areas encompassed the wide majority of the patent applications. As such, this study contributed to the value of patent application figures as a robust performance indicator for monitoring competitive technology development efforts in the upstream oil and gas industry of a developing country.

## 6. Conclusion

This study provides further evidence of the value of exploring patent information. By exploring a sample of patent data related to upstream oil and gas technologies protected by different players in Brazil, valuable patterns were revealed. In practice, we have observed that the value of patent information goes beyond its role as a source of technical information by revealing insights of the attractiveness of certain technologies in a country. Evidence was also found that rival firms in the upstream oil and gas industry attempted to increase their competitiveness by reinforcing their patent portfolio with strategic technologies comprising high potential market value. Additionally, we believe that the paper is also valuable for readers without technical knowledge of upstream oil and gas technologies, as our study reveals patterns related to the relationship between market demand for technologies and the strategic use of patents.

## Author details

Gabriel Cavalheiro[1]*, Mariana Brandao[2] and Saulo Rocha[1]

*Address all correspondence to: gabrielmarcuzzo@id.uff.br

1 Universidade Federal Fluminense (UFF), Niterói, Brazil

2 SENAC, Rio de Janiero, Brazil

## References

[1] Coleman L. Explaining crude oil prices using fundamental measures. Energy Policy. 2012;**40**:318-324

[2] Hu W, Bao J, Hu B. Trend and progress in global oil and gas exploration. Petroleum Exploration and Development. 2013;**40**(4):439-443

[3] Brown SPA, Huntington HG. Evaluating U.S. oil security and import reliance. Energy Policy. 2015;**79**:9-22

[4] Shafiee S, Topal E. When will fossil fuel reserves be diminished? Energy Policy. 2009;**37**(1): 181-189

[5] Hayashi SHD, Ligero EL, Schiozer DJ. Risk mitigation in petroleum field development by modular implantation. Journal of Petroleum Science and Engineering. 2010;**75**(1-2): 105-113

[6] Mendes PAS, Hall J, Matos S, Silvestre B. Reforming Brazil's offshore oil and gas safety regulatory framework: Lessons from Norway, the United Kingdom and the United States. Energy Policy. 2014;**74**:443-453

[7] Haddad E, Giuberti AC. Economic impacts of pre-salt on a regional economy: the case of Espírito Santo. Brazil: Instituto de Pesquisa Economica Aplicada. Perspectivas de desenvolvimento do setor de petroleo e gas no Brasil. Comunicados do IPEA 55, (June 1). Brasília; 2010. http://agencia.ipea.gov.br/images/stories/PDFs/100601_comunicadodoipea_55.pdf [Accessed September 10, 2015]

[8] Oliveira R. Dealing with plenty: Brazil in the era of surplus oil [Master Thesis]. University of Illinois; 2011

[9] Cavalheiro GMC, Joia LA, Gonçalves AC. Strategic patenting in the upstream oil and gas industry: Assessing the impact of the pre-salt discovery on patent applications in Brazil. World Patent Information. 2014;**39**:58-68

[10] Emodi NV, Murthy GP, Emodi CC, Emodi ASA. A literature review on the factors influencing patent propensity. International Journal of Innovation and Technology Management. 2017;**14**(3):1750015

[11] Huang KF, Cheng TC. Determinant's pf firms'patenting or not patenting behaviors. Journal of Engineering Technology Management. 2015;**36**(C):52-77

[12] Pavitt K. Innovation process, in Fagerberg J, Mowery David C, Nelson, Richard R (Orgs.) The Oxford Handbook of Innovation. New York: Oxford University Press; 2005

[13] Bell M, Pavitt K. Technological accumulation and industrial growth: Contrasts between developed and developing countries. Industrial and Corporate Change. 1993;**2**(2):157-211

[14] Joia LA. Measuring intangible corporate assets: Linking business strategy with intellectual capital. Journal of Intellectual Capital. 2000;**1**(1):68-84

[15] Wang MY, Lo HC, Liao YY. Knowledge flow determinants of patent value: Evidence from Taiwan and South Korea biotechnology patents. International Journal of Innovation and Technology Management. 2015;**12**(3)

[16] Drivas K, Economidou C, Karamanis D, Zank A. Academic patents and technology transfer. Journal of Engineering and Technology Management. 2016;**40**:45-63

[17] Bessen J, Meurer MJ. What's wrong with the patent system? Fuzzy boundaries and the patent tax. First Monday. 2007;**12**(6)

[18] Godinho MM, Ferreira V. Analyzing the evidence of an IPR take-off in China and India. Research Policy. 2012;**41**:499-511

[19] Scherer FM. Nordhaus′ theory of optimal patent life: A geometric reinterpretation. American Economic Review. 1972;**62**(3):422-427

[20] Ernst H. Patent information for strategic technology management. World Patent Information. 2003;**25**:233-242

[21] Mouritsen J, Koleva G. Packing and unpacking knowledge: Patents and intellectual capital. Journal of Intellectual Capital. 2005;**6**(3):308-321

[22] Blind K, Cremers K, Mueller E. The influence of strategic patenting on companies' patent portfolios. Research Policy. 2009;**38**:428-436. http://dx.doi.org/doi:10.1016/j.respol.2008.12.003

[23] Picard PM, van Pottelsberghe B. Patent office governance and patent system quality. Center for Research in Economic Analysis, Discussion Paper 2011-06. 2011

[24] Fabry B, Ernst H, Langholz J, Koster M. Patent portfolio analysis as a useful tool for identifying R&D and business opportunities: An empirical application in the nutrition and health industry. World Patent Information. 2006;**28**:215-225

[25] Lang JC. Management of intellectual property rights: Strategic patenting. Journal of Intellectual Capital. 2001;**2**(1):8-26

[26] Davies A. The life cycle of a complex product system. International Journal of Innovation Management. 1997;**1**:1192-1216

[27] Bonino D, Ciaramella A, Corno F. Review of the state-of-the-art in patent information and forthcoming evolutions in intelligent patent informatics. World Patent Information. 2010;**32**:30-38

[28] Van Pottelsberghe B, Mejer M. The London agreement and the cost of patenting in Europe. European Journal of Law and Economics. 2010;**29**(2):211-237

[29] Galini NT. The economics of patents: Lessons from recent U.S. patent reform. Journal of Economic Perspectives. 2002;**16**(2):131-154

[30] Castells M. The Information Age: Economy, Society and Culture. Updated ed. Oxford: Blackwell; 2000

[31] Abbas A, Zhang L, Khan SU. A literature review on the state-of-the-art in patent analysis. World Patent Information. 2014;**37**:3-13

[32] Dirnberger D. The use of mindmapping software for patent search and management. World Patent Information. 2016;**47**:12-20

[33] Pargaonkar YR. Leveraging patent landscape analysis and IP competitive intelligence for competitive advantage. World Patent Information. 2016;**45**:10-20

[34] Huang JY. Patent portfolio analysis of the cloud computing industry. Journal of Engineering and Technology Management. 2016;**39**:45-64

[35] Dubaric E, Giannocaro D, Bengtsson R, Ackermann T. Patent data as indicators of wind power technology development. World Patent Information. 2011;**33**(2):144-149

[36] Siegel DS, Waldman DA, Atwater LE, Link AN. Toward a model of the effective transfer of scientific knowledge from academicians to practitioners: Qualitative evidence from the comercialization of university technologies. Journal of Engineering and Technology Management. 2004;**21**(1-2):115-142

[37] Arunagiri S, Mathew M. Exploring technology evolution using patent classification: A case of cochlear implant technology patents. International Journal of Innovation and Technology Management. 2017;**14**(1)

[38] Galini NT. Patent policy and costly imitation. RAND Journal of Economics. 1992;**23**(1): 52-63

[39] Boldrin M, Levine DK. The case against patents. Journal of Economic Perspectives. 2013;**27**(1): 3-22

[40] Nelson RR. The changing institutional requirements for technological and economic catch up. International Journal of Technological Learning, Innovation and Development. 2007;**1**(1):4-12

[41] Chiarini T, Silva ALG. Intellectual property rights and innovation system: Some lessons from Brazil. International Journal of Innovation and Learning. 2016;**20**(3):265-288

[42] Lall S. Technological capabilities and industrialization. World Development. 1992;**20**(2): 165-186

[43] Perkmann M, Tartari V, McKelvey M, Autio E, Broström A, D'Este P, Fini R, Geuna A, Grimaldi R, Hughes A, Krabel S, Kitson M, Llerena P, Lissoni F, Salter A, Sobrero M. Academic engagement and commercialisation: A review of the literature on university–industry relations. Research Policy. 2013;**42**:423-442

[44] Rodriguez MB, Suslick SB. An overview of Brazilian petroleum exploration lease auctions. Terrae. 2009;**6**(1):6-20

[45] United States Energy Information Administration. Brazil is the 8th-largest total energy consumer and 9th-largest liquid fuels producer in the world; 2015. Available from: http://www.eia.gov/beta/international/analysis_includes/countries_long/Brazil/brazil.pdf [Accessed July 26, 2016]

[46] National Petroleum Council. Oil and gas technology development. Topic Paper #26, National Petroleum Council Global Oil & Gas study. 2007. Available from: http://downloadcenter.connectlive.com/events/npc071807/pdf-downloads/Study_Topic_Papers/26-TTG-OGTechDevelopment.pdf [Accessed: February 17, 2014]

[47] Lee A. A scientific methodology for MIS case studies. MIS Quarterly. 1989;**13**(1):33-50

[48] Benbasat I, Goldstein D, Mead M. The case research strategy in studies of information systems. MIS Quarterly. 1987;**11**(3):369-386

[49] Eisenhardt KM. Building theories from case study research. Academy of Management Review. 1989;**14**(4):532-550

[50] Stake RE. Case studies. In: Denzin NK, Lincoln YS, editors. Handbook of qualitative research. Thousand Oaks, CA: Sage; 1988. pp. 236-247

[51] Madani F, Weber C. The evolution of patent mining: Applying bibliometrics analysis and keyword network analysis, World Patent Information. 2016;**46**:32-48

Chapter 2

# Intelligent Drilling and Coring Technologies for Unmanned Interplanetary Exploration

Junyue Tang, Qiquan Quan, Shengyuan Jiang,
Jieneng Liang and Zongquan Deng

Additional information is available at the end of the chapter

http://dx.doi.org/10.5772/intechopen.75712

**Abstract**

The robotic technology, especially the intelligent robotics that can autonomously conduct numerous dangerous and uncertain tasks, has been widely applied to planetary explorations. Similar to terrestrial mining, before landing on planets or building planetary constructions, a drilling and coring activity should be first conducted to investigate the in-situ geological information. Given the technical advantages of unmanned robotics, utilizing an autonomous drill tool to acquire the planetary soil sample may be the most reliable and cost-effective solution. However, due to several unique challenges existed in unmanned drilling and coring activities, such as long-distance time delay, uncertain drilling formations, limited sensor resources, etc., it is indeed necessary to conduct researches to improve system's adaptability to the complicated geological formations. Taking drill tool's power consumption and soil's coring morphology into account, this chapter proposed a drilling and coring characteristics online monitoring method to investigate suitable drilling parameters for different formations. Meanwhile, by applying pattern recognition techniques to classify different types of potential soil or rocks, a drillability classification model is built accurately to identify the current drilling formation. By combining suitable drilling parameters with the recognized drillability levels, a closed-loop drilling strategy is established finally, which can be applied to future interplanetary exploration.

**Keywords:** interplanetary exploration, drilling and coring, intelligent robotics, planetary soil simulant, closed-loop drilling strategy

## 1. Introduction

Just as some imaginative descriptions on the interplanetary traveling in scientific fictions, human beings through decades' striving have made a great step forward to that scenery. From the successful launch of Sputnik, the first man-made earth satellite in 1957 [1] to the first man-made lunar landing in 1969 to collect lunar soil samples [2] and the Rosetta Landing Project launched in 2014 on Comet 67P to collect asteroid rocks [3], mankind's extraterrestrial explorations have covered the vast majority of planets, satellites and asteroids in the solar system. However, it should be noted that although tremendous advancements are achieved in space exploration, mankind also suffered a great loss, especially when astronauts encounter emergency risks even lost their lives for various technical reasons [4, 5]. Hence, as deep space exploration having been conducted, an up-and-coming replaceable solution by employing unmanned robots has been gradually acceptable to carry out some uncertain and dangerous tasks, such as interplanetary drilling and coring activities [6–8].

For future interplanetary exploration, there is an urgent demand for a reliable method to pierce the planetary surface to a specified depth and effectively collect soil samples [9, 10]. Once the in-situ soil sample acquired, the original geological information at the sampling site can be investigated for further usage. Compared with other soil failure technological solutions, such as explosion, melting, etc., the traditional drilling and coring method by only utilizing the compound motion of rotation and penetration still has great advantages in extracting the subsurface soil sample in a relatively efficient and convenient way [11, 12]. Therefore, this method has been widely applied to previous interplanetary missions. Considering the technical advantages of unmanned robots and the unique space drilling and coring conditions, interplanetary drilling and coring compared with terrestrial drilling could be more dependent on intelligent drilling techniques.

Commonly speaking, interplanetary drilling control architecture contains remote control from Earth and autonomous drilling control on the planet [13]. Since time delay inevitably exists in the long distance remote communication, remote control mode is usually employed to deal with serious drilling faults and in the majority of the cases the sampling drill should work in an autonomous way [14, 15]. Furthermore, restricted by the delivery capacity of rocket and limited power consumption, interplanetary drilling system can hardly apply plenty of sensor resources and sufficient penetrating force to accomplish the online control. On the other hand, in most planetary drilling missions, there is not enough prior geological information in a longitudinal direction on sampling sites to guide the online drilling [16]. Given the uncertain and variable mechanical properties of drilling formations, the drill tool under above strict resources should adjust suitable drilling parameters correspondingly to overcome potential drilling faults and acquire as much as volume of the soil sample. To resolve the problems, researchers have been striving for decades to find effective solutions.

So far, the former Soviet Union's Luna series is the only unmanned detectors that successfully implemented the lunar subsurface soil's sampling and returning [17, 18]. Among them, the Luna 16 detector launched in 1970 with a stretched out arm mounted rig sampling method successfully drilled into 350 mm beneath the lunar surface, acquiring 101 g soil sample finally

[19]. The following Luna 20 detector launched in 1972 landed on a lunar plateau with a similar sampling device to the Luna16 and was forced to stop drilling at 250 mm depth due to multiple times of overheat fault, eventually sampling only 55 g lunar soil [20]. The last sampling task Luna 24 in 1976 applied a threshold-based approach to autonomously control the drill tool. When the detected penetrating force exceeds a preset threshold, the impact motor will be activated in time to overcome the drilling resistance. Based on this drilling strategy, the received remote data revealed that in the Luna 24 detector's drilling process the impact motor was frequently switched on and finally the sampler reached to a depth about 2250 mm, returning about 171 g lunar soil sample [21]. Although the applied threshold-checking strategy indeed improved the automation level of the unmanned drill tool, it should point out that there exists a high probability of tripping and need a long time to wait (often hours to days) for human troubleshooting from afar [22]. Hence, this simple limit-checking strategy may be more suitable for shallow drilling missions like Mars Science Laboratory drill (50 mm depth).

After laboratory tests aboard NASA's Phoenix Mars Lander identified water in a soil sample at Green Valley, Mars (Arctic pole) in 2008 [23], NASA has been preparing for an another Mars exploration mission to search for biomolecular evidence for life around 2018. The proposed "Icebreaker" mission would use an automated rotary-percussive drill to reach and retrieve samples from up to 1.2 m deep in the ground ice at Mars Arctic pole [24]. To support for this drilling mission, NASA Ames, together with Honeybee Robotics Ltd., and Georgia Tech., proposed a novel drilling faults diagnosis control method by acquiring the vibration signals from external laser doppler vibrometers (LDVs) to identify drilling faults [25, 26]. Based on two diagnostic methods of rules and model prediction, the "Icebreaker" drill can recognize six types of drilling faults (e.g. auger chocking, hard material, etc.) and switch to the preset recovery parameters. Test results from the recent Arctic and Antarctic field campaigns demonstrated this drill has been already capable of a hands-off ability [27].

The above drilling strategy relatively improved the automation level of the system, however, besides drilling loads or power consumption, soil's coring morphology should also be considered in designing its control method. As the primary goal of interplanetary exploration is to exam the evidence of lie by scamping the subsurface soils, it is extremely important to acquire as much soil core as possible under acceptable drilling loads. Furthermore, as the stratification information of planetary samples reflects the evolutionary history of early stars [28], it is necessary to preserve its stratification during the coring process for further analysis. Therefore, the authors proposed a novel flexible tube coring method to preserve the stratification of soil sample [29]. In order to comprehend the core flowing characteristics and optimize the final coring results, a non-contact type measurement based on ultrasonic wave reflection mechanism and vision techniques is applied to online monitor the coring and removal characteristics [30]. Once the drill-soil interaction mechanism comprehended, suitable drilling parameters for different types of drilling formations considering both power consumption and coring morphology can be optimized then.

Apart from suitable drilling parameters, to identify what kind of formation the drill bit is currently drilling is another key point to the unmanned drill tool. Only if these two key parameters matched correspondingly, the unmanned drill tool may be smoothly penetrated into the

uncertain formations and finally retrieve valuable core samples. Since planetary regolith has a considerable number of geological and mechanical properties, it is rather difficult to identify all the parameters individually online. Hence, the authors proposed a control strategy based on planetary regolith drillability (PRD) recognition [31]. Herein, the drillability of formation is a consolidated index to stand for drilling difficulty. A recognition model based on support vector machine (SVM) has been established to evaluate the drillability of current formation and subsequently control the algorithms that can tune drilling parameters to adapt to the current drilling conditions.

The remainder of this paper is organized as follows. The unique challenges in interplanetary drilling and coring are discussed first. Next, the specific drilling and coring characteristics containing the drilling loads characteristics and soil flowing characteristics are elaborated. A drillability recognition method is proposed based on monitoring the signals then. Finally, an intelligent real-time drilling strategy is achieved based on drillability recognition and drilling experiments in multi-layered drilling formations indicated that this unmanned control method could effectively reduce the drilling loads and keep a relatively complete stratification.

## 2. Challenges in interplanetary drilling

In general, if neglecting the economic factors, terrestrial drilling can be conducted with advanced auxiliary facilities to investigate the in-situ drilling formations and can automatically apply liquid lubricant to improve the drilling conditions [32, 33]. Compared with terrestrial drilling, interplanetary drilling and coring restricted by the extreme environmental conditions on the planet will have to solve several unique challenges. To assure the operability of the required drill tool and its control strategy, it is thoroughly necessary to comprehend the in-situ environment conditions and existing applicable resources. The following drilling and coring characteristics investigation and recognition based drilling strategy will be both based on these understandings. The following subsections will discuss four main challenges in interplanetary drilling.

### 2.1. Long-distance between planet and Earth

At present, wireless teleoperation is widely used in the monitoring and control of spacecraft operation status. For example, in the second phase of China lunar exploration, based on acquired visual images the lunar rover completed the entire inspection survey mission by means of ground teleoperation [34]. However, different from rover's navigation control, the buried drilling and coring activity is a quite dynamic and rapid process and any signal delay caused by long-distance teleoperation may directly result in a serious drilling fault. Once the drilling faults happened, specialists from Earth also need a long time to diagnose and recovery, making the drilling and coring process last for hours or days. Even though the drilling faults can be handled successfully, the final coring quality and core's stratification could be destroyed during this long time recovery process. Considering for future deeper

space explorations, for example, the round-trip delay between Mars and Earth will be as long as 40 min, this long time delay by teleoperation will definitely not acceptable for interplanetary drilling and coring operations [35]. Hence, in general only when a serious abnormality occurs in the sampling process, the sampling device could be automatically forced to stop drilling and wait for the ground specialists to make a fault judgment and determine the corresponding treatment plan. Otherwise, the sampling device should work in a thoroughly autonomous condition.

### 2.2. Complicated and uncertain drilling formations

Given the short execution time of Mars and asteroid exploration compared with the lunar exploration, the data of soils on Mars and asteroids are rarely found yet. Herein, this chapter mainly focuses on the physical properties of lunar soil. According to previous investigations on the material returned from the moon, the terrestrial term "regolith" is also used for the interplanetary exploration [36]. Regolith has been defined as a general term for the layer or mantle of fragmental and unconsolidated rock material. According to the published literature, lunar regolith ranges from granular soil to hard rocks [37, 38], and it mainly consists of five types of material: rock detritus, mineral dust, breccia, agglutinate and impacting molten glass. The physical characteristics of above lunar soil components are quite different and the distribution of different components of lunar soil in the depth direction at the sampling site is also uncertain. During future planetary drilling processes, either soil or rock will be randomly encountered, resulting in that the final coring quality and drilling loads may both be influenced by unpredictable properties. There are numerous parameters, including cohesion, friction angle, relative density, compression ratio, particle size distribution, etc., to describe the physical properties of lunar soil [39], further increasing the difficulty to identify the physical parameters of lunar soil at different depths one by one. Therefore, it is necessary to simplify the mechanical parameter identification of lunar soil.

### 2.3. Lacking of prior investigation on sampling site

Similar to terrestrial mining, prior investigation on the sample site will extraordinarily guide the following drilling and coring activities. In the second phase of China lunar exploration, a novel lunar penetrating radar (LPR) has already been applied to detect the morphology of the lunar surface and stratification information of subsurface lunar regolith for supporting further detector's landing site's selecting, however, it should be noted that until now due to the mass and power constraints its detection accuracy can only reach to about 30 cm [40]. Considering that any unclear detected drilling formation may bring out a serious drilling fault once inappropriate drilling parameters are operated. Therefore, it is still difficult to apply the LPR's detecting geological layering information to guide the sampling drill before drilling begins. It indicates that the drill tool should better work in a passive adaptive control mode, in which the drill tool during the whole drilling and coring process should online switch suitable drilling parameters according to the recognized current drilling formation on the drill bit, nor in the active control mode.

### 2.4. Limited on-orbit sensor resources

According to the discussion in above subsection, the control architecture of unmanned interplanetary drill should better work in a passive adaptive control, in which the drill tool will totally rely on the feedback data by sensors. However, compared with the planetary rover's surface navigation control, the planetary unmanned drilling has a more limited sensing resources. In addition to the constraints of quality, power consumption and high and low temperature vacuum environment, the sensors used for drilling condition's monitoring also need to overcome the restrictions like small installation space of drilling tools and the prevention of sample contamination as well as the high frequency vibration caused by the impact of drilling tools, etc. Combing above tough working conditions together, perhaps only traditional load cells and displacement transducers can be applied to the interplanetary drilling. Hence, to realize the intelligent drilling control the sample drill need to fully integrate the existed sensors' information, which should all be imported to the controller to decide its online strategy.

Besides above challenges, there also exists some negative factors affecting the interplanetary drilling. For example, the non-water environment on the planet surface that will cause the drill tool will work in a dry condition without any liquid lubricant to improve the drilling conditions. The only effective removing cutting chips solution is the spiral auger flute. Due to the fact that drilling loads or power consumptions are highly dependent on the removal condition [41], during this dry drilling process drilling loads will be more sensitive to the drilling parameters. Overall, these harsh working conditions will definitely aggravate the risk of the interplanetary drill, which all require a more robust and reliable control strategy.

## 3. Drilling and coring characteristics

The ultimate goal of interplanetary sampling exploration is to acquire as much as possible planetary regolith for further scientific analysis. Apart from the volume of planetary regolith, the stratification of the sample should also be seriously considered in the drilling process. If the geological information of soil sample was not be preserved completely, its geological value would be significantly reduced. In China Chang'e drilling and coring mission, a novel flexible tube coring (FTC) method referred from Luna 24 mission is being adopted to solve the above problem [42]. As shown in **Figure 1**, its drilling and coring process is illustrated.

In the FTC penetrating process (rotary speed $n$ and penetrating velocity $v_p$), the in-situ subsurface regolith destroyed by the cutting edge of drill tool can be divided into two parts: the wrapped sample into the flexible tube and the cutting chips conveyed along the spiral flute. Since the wrapped core soil is adjacent to the cutting soil through the holes at the bottom, it may result in a sudden collapse of the inner surface of the flexible tube when cutting chips are removed, resulting in a decline in the height of core. However, considering that there is no relative locomotion between the sample and the flexible tube in stable conditions, the sample can be continuous along the depth direction. Although the adopted FTC method has a great advantage in maintaining the core stratification, there still exists a considerable possibility that a very small amount of core soils are finally acquired in drilling process. Therefore, to

http://dx.doi.org/10.5772/intechopen.75712

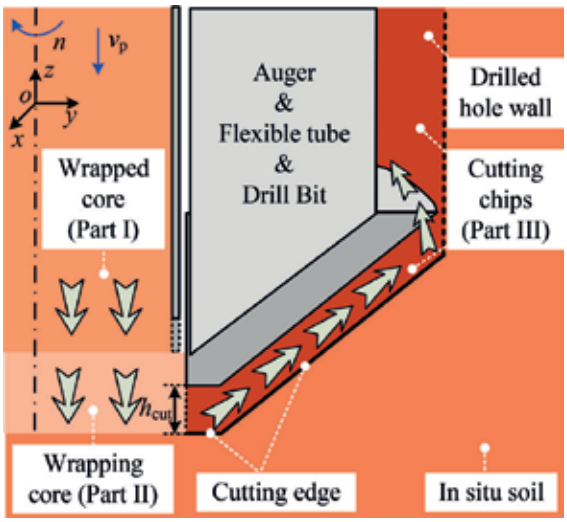


**Figure 1.** Illustration of drilling and coring process in flexible tube coring.

a certain degree, the height of core index $H_s$ or the coring ratio $K_c$ index (the ratio of coring height $H_s$ to drilling depth $H_d$) can represent the core flowing characteristics and should be monitored in real-time.

It can be also found that there inevitably exists a vertical distance between the bottom of the flexible tube and the bottom of the drill bit, connecting the internal core to the external cutting chips, as shown in **Figure 1**. Due to the fact that the external cutting chips' removal flowing characteristics is heavily determined by the operated drilling parameters [43, 44], the removed cutting chips may have a negative influence on the inner coring soil and make the coring results drop correspondingly. Therefore, besides monitoring the coring characteristics, the soil removal characteristics should also be online detected. As shown in **Figure 2**, in order to comprehend the drilling and coring characteristics, a noncontact soil flowing characteristics monitoring method has been proposed for experimental verification.

Since the cored soil is wrapped into the closed space, it's fairly difficult to measure the cored soil without affecting soil's original states. To solve this problem, an ultrasonic displacement sensor is deployed into the hollow flexible tube, as shown in **Figure 2(a)**. To assist measurement, a protective hollow tube is installed at the front of the sensor, allowing the sonic wave to pass through it without disturbance. Besides that, avoiding unnecessary disturbing reflection from the uneven upper surface, one Teflon made reflect board with a small mass (4 g) is elaborately designed to put on the in situ soil. As a result, the online coring ratio $K_c$ can be indirectly calculated by acquiring the ultrasonic sensor's online value $H_u$, its initial value $H_{uo}$, and the online drilling depth $H_d$. Apart from the coring states, soil removal characteristics are acquired by measuring the accumulation morphology on a PE plastic wrap by an external camera, as shown in **Figure 2(b)**. By converting the colorful images into binary images, the outline of accumulation soil can be obtained thereby. Meanwhile, by searching the right, left, and upward points of current outline and summing up each accumulation volume, the total

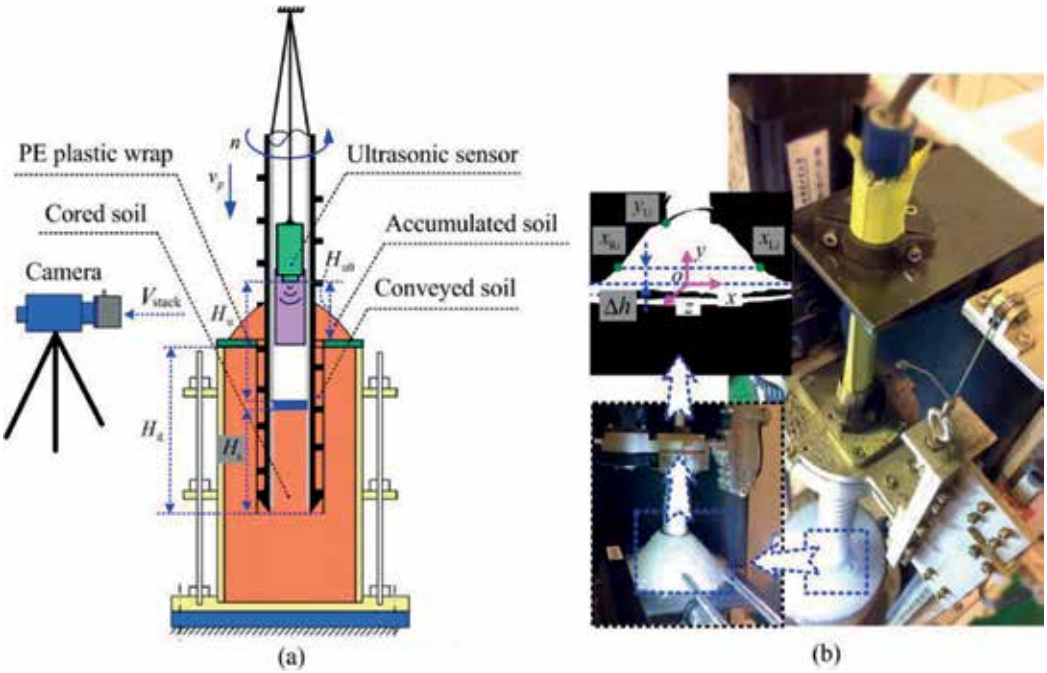


**Figure 2.** Scheme of the noncontact soil flowing characteristics monitoring method. (a) Scheme of monitoring method; (b) Acquired images in monitoring process.

volume of accumulated soil $V_{acc}$ can be finally online acquired. Hence, based on above non-contact measurement the soil flowing characteristics during the drilling and coring process can be accurately monitored without any damage.

To verify the proposed measurement, drilling experiments under the condition of $n = 400$ rev/min, $v_p = 150$ mm/min are conducted. The online coring results containing the ultrasonic sensor's value, the coring height, and the coring ratio are illustrated respectively in **Figure 3**. It can be seen that during the first 105 mm drilling depth, the ultrasonic sensor's value keeps stable, meaning that the coring soil stays at the original position making the coring height climb stably to the 105 mm and coring ratio keeps around the 100%. After then, the monitored sensor's value reveals that it has a sudden increase, resulting in a turning point at the 105 mm drilling depth. According to the definition, the corresponding coring height and coring ratio both has a sharp decline. Finally, during the 200 mm depth, the coring height slips to approximately 70 mm and the coring ratio reaches to less than 40%.

Based on above founding, it can be inferred that there exists a sudden collapse of the cored soil in the flexible tube. Actually, this interesting phenomenon can be explained by the state of the cored soil. As shown in **Figure 1**, the cored soil and the conveyed soil are inevitability connected at the bottom of the drill bit. Under proper drilling parameters or penetration per revolutions ($PPR = v_p/n$, mm/rev), once the drill bit drills into the regolith the cutting chips will be conveyed from the bottom by auger's spiral locomotion, which may make the cored soil stays in a positive stress, and vice versa. Since there exists a small side failure zone at

http://dx.doi.org/10.5772/intechopen.75712

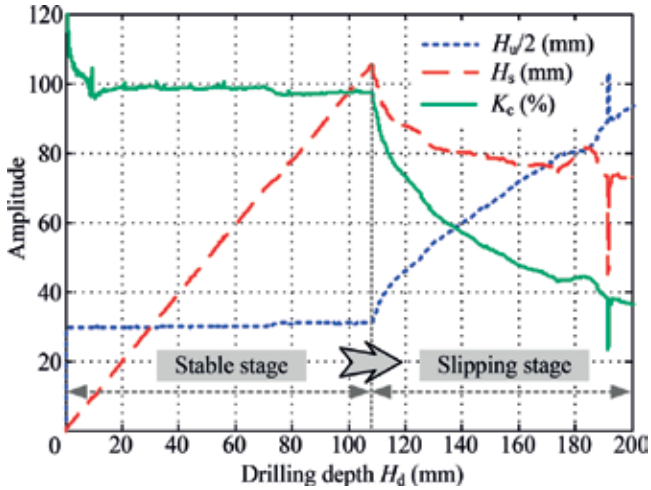


**Figure 3.** Monitored height of core and coring ratio in experiments.

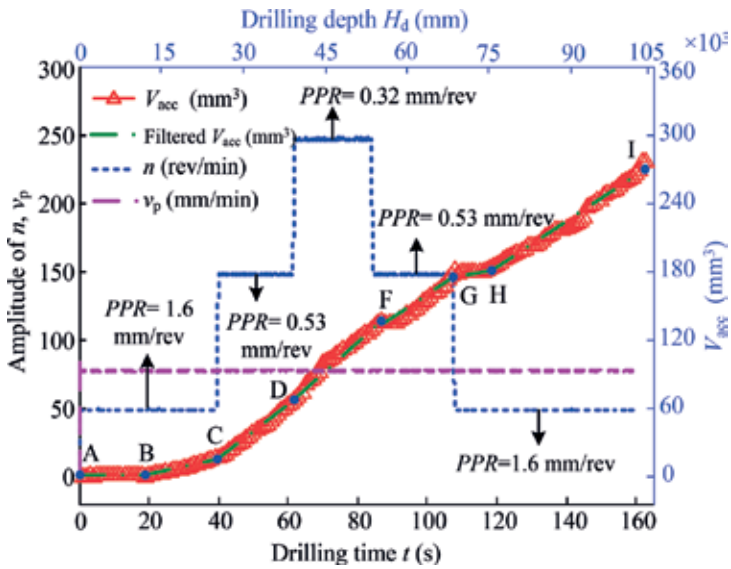


**Figure 4.** Monitored volume of accumulated soil $V_{acc}$ under different *PPR*s.

the outer annular space of cored soil by the inner edges of cuter [45], once the bottom of soil become totally granular at a certain depth, cannot be able to sustain the upward positive stress, it will result in a sudden broken or collapse along the longitudinal direction.

Apart from the core flowing characteristics, cutting chips' removal flowing characteristics is also investigated. By identifying the outline image of the wedge-shaped of the removed soil outside the surface and calculating its 3D volume per second, the online volume of removed soil $V_{acc}$ under three different *PPR*s (1.6, 0.53, and 0.32 mm/rev) is shown in **Figure 4**. It can be

seen that during above drilling and coring process, the penetrating velocity is kept constant (80 mm/min), while the rotary speed will be adjusted (50 rev/min → 150 rev/min → 250 rev/min → 150 rev/min → 50 rev/min). Meanwhile, the monitored volume $V_{acc}$ can be divided into seven stages (AB → BC → CD → DF → FG → GH → HI).

During the AB stage of the first 20 s, since drill bit constantly cuts the in situ soil simulant without spiral auger's participant, there is almost no soil accumulated upon the surface. After then, the drill bit is buried in the soil, the auger starts to remove soil from the borehole bottom with a low removal speed during the BC stage. At the 40 s moment (C point), the rotary speed is suddenly switched to 150 rev/min with the result of the sudden increase of $V_{acc}$. It can obviously be seen that the removal speed during CD stage is higher than that during BC stage. Above phenomenon is almost same with that in conditions between DF stage and CD stage. At the 85 s moment (F point), the corresponding PPR is regulated back to 0.53 mm/rev, which results in a slow increase trend of the $V_{acc}$. After about 5 s, the removal speed becomes normal. This slow increase trend of the $V_{acc}$ also exists in the sudden change on G point. Based on above experimental results, it can be concluded that the monitored volume of accumulated soil can reflect the online removal states well and the PPR index has a great effect on the removal states and should be optimized further.

According to preliminary experiments, the proposed non-contact drilling and coring characteristics monitoring method has been validated well. Next, to provide suitable drilling parameters database for the following intelligent drilling strategy, more drilling and coring experiments taken the drilling loads and core's quality into account will be conducted in several different drilling formations, such as limestone, sandstone, compacted soil, etc.

## 4. Recognition based drilling strategy

Intelligent drilling control algorithm needs to be able to effectively identify the drilling formation, and timely adjust appropriate drilling parameters according to the recognition result. As an effective pattern recognition method, support vector machine (SVM) has been widely applied for several linear and nonlinear separable problems because of its high generalization ability [46, 47]. In previous works, a drillability classification covering from granular soil to hard rocks has been established based on the mechanical penetrating tests [48]. Herein, both rotary torque and penetrating force are selected as the drilling states monitoring signals $x$ to imported into the proposed support vector machine recognition model to predict the corresponding drillability level $y$, as shown in **Figure 5**. Once the current formation's drillability level recognized, control algorithm will switch the optimized drilling parameters to drive the rotary motor and penetrate motor.

Actually, traditional SVM algorithm is based on the two classification mode, which is not suitable for multiple patterns of drillability classification. Compared with other classification methods, the decision directed acyclic graph (DDAG) based on the decision tree has a better training speed and a higher classification accuracy on the normal scale separation problems [49]. Considering that for covering potential drilling formations on the planets there are

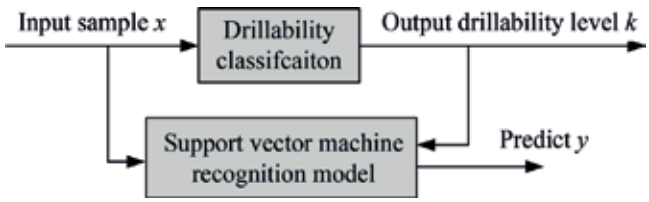


**Figure 5.** Scheme of drillability recognition based on SVM.

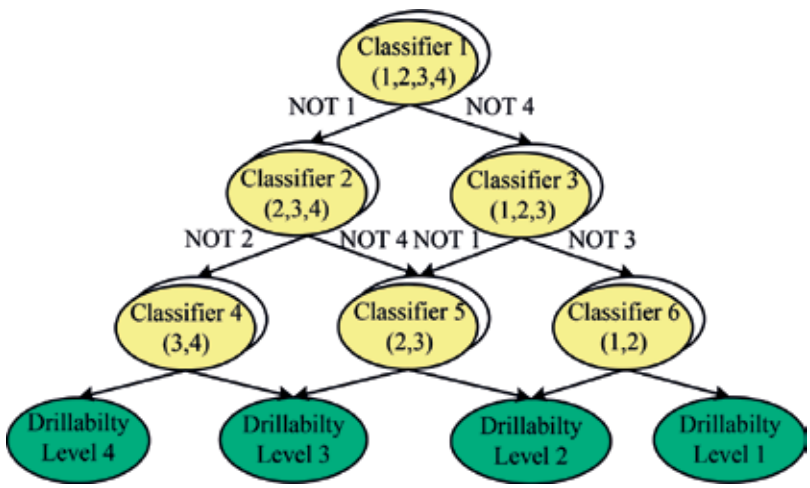


**Figure 6.** Drillability recognition algorithm based on DDAG.

at least three different formations for validation. Herein, DDAG is adopted to conduct the drillability recognition. The classification's structure diagram for four levels of lunar regolith simulants' drillability is shown in **Figure 6**.

As can be seen from the above algorithm structure, this method constructs a classifier with a two-way directed acyclic graph. Among them, the classifier 1 is located at the top of the root node to complete the first and second levels of drillability level 1–4 drillability comparison. By comparing the drillability level of 1 and drillability level of 4, the most samples may not belong to drillability level 1 (drillability level 4) can be excluded. After 3 times of excluding, the remaining category will be the drillability 1. Experiments indicated that by successive comparison this classification algorithm can guarantee a higher recognition accuracy.

In fact, model parameters in SVM play an important role in affecting recognition's accuracy. In the kernel function of SVM, scale parameter $g$ and penalty coefficient $C$ have the most significant effect on recognition's accuracy. When the two parameters do not match well, SVM will be overtraining or overfitting, which is an unstable situation in recognition. Herein, based on a grid search method, these two SVM model are optimized. To verify the optimized SVM model's generalization ability, drilling characteristics of different drillability samples under constant drilling parameters should be imported to conduct recognition training. Herein, a combination

of rotary speed $n$ = 100 rev/min and penetrating velocity $v_p$ = 10 mm/min is used as recognized drilling parameters. Typical simulants of drillability level 1, 3, 5 and 6 are selected as drilling media. Recognition results of un-optimized and optimized are shown in **Figure 7**. It can be found that the recognition accuracy of optimized SVM model is about 94.37%, which is obviously higher than the 78.15% of un-optimized model. When recognizing the closed drillability level 5 and level 6, the un-optimization model identifies 109 samples in 160 test samples and the recognition accuracy is just 68.13% in total. However, under the same conditions, the optimized model identifies 150 samples and the accuracy reaches roughly 93.75% in total. Therefore, it indicated that the optimized SVM recognition model indeed improves its recognition accuracy and becomes more practical in recognizing multilayered drilling media's drillability.

Once the optimized drillability SVM recognition model has been acquired, a multi-layered simulant mixed with granular soil and rocks has been constructed for conducting closed-loop validation experiments. There are five layers of three different compositions including granular soil (level 1), limestone (level 5) and marble (level 6) along the depth. As shown in **Figure 8**, signals acquired in the closed-loop drillability real-time recognition experiment are the drilling

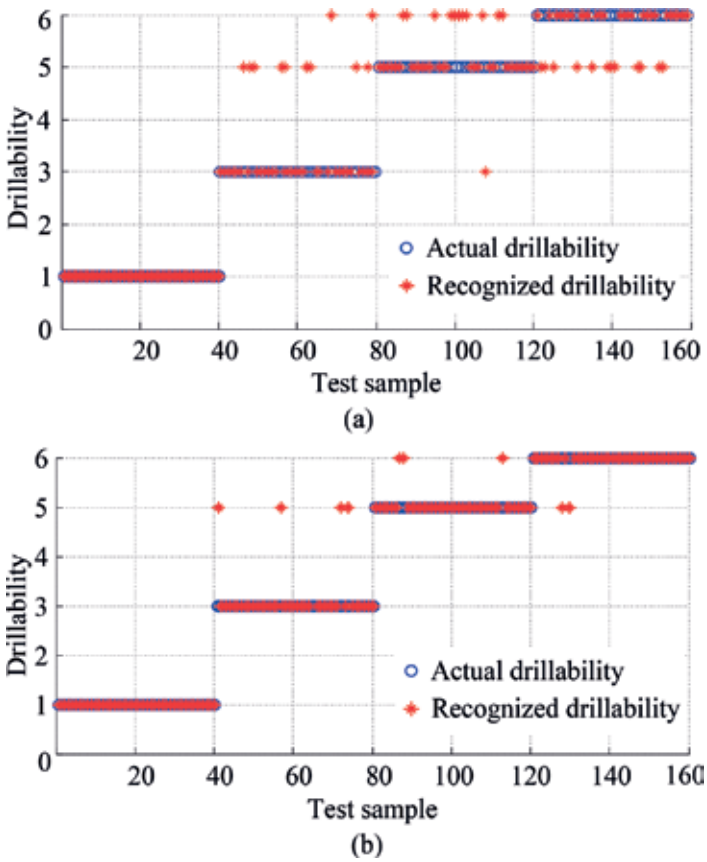


**Figure 7.** Comparison of drillability recognition before and after optimization.

http://dx.doi.org/10.5772/intechopen.75712

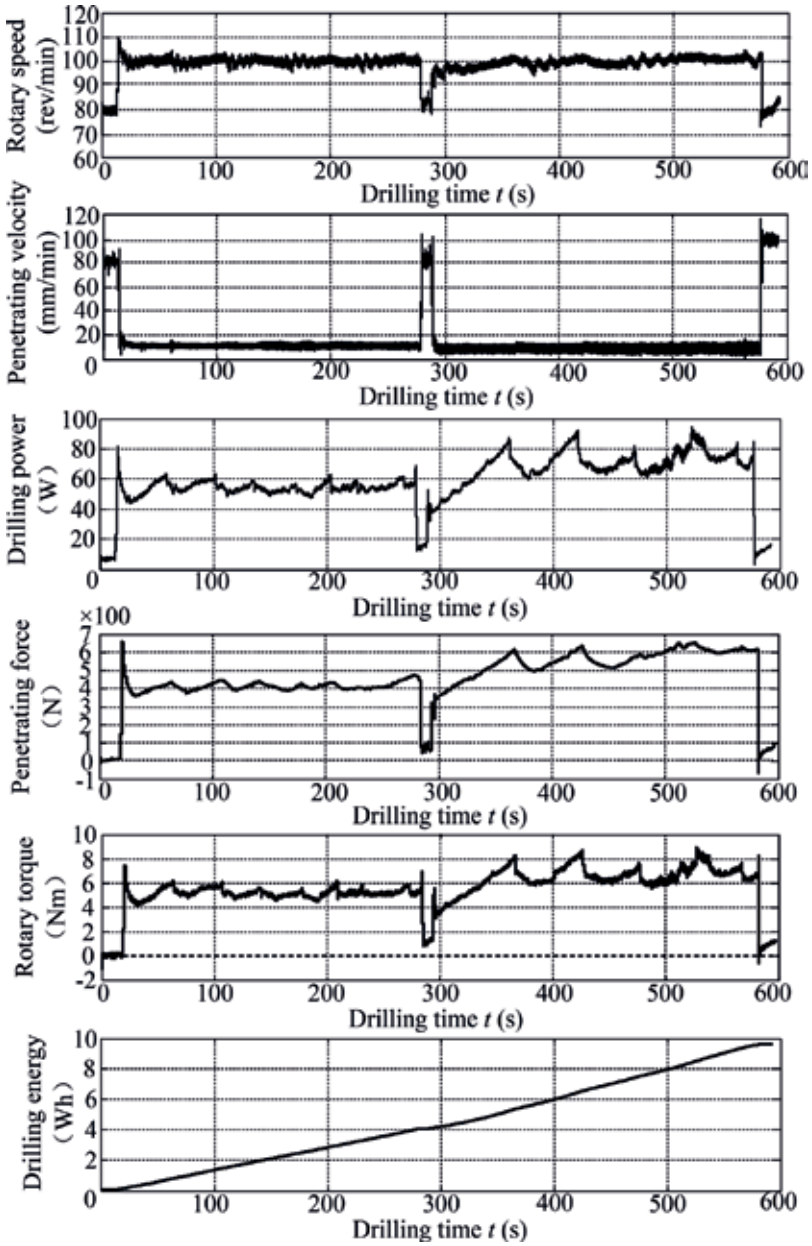


**Figure 8.** Drilling states during the multi-layered simulant drilling process.

state signals such as rotary torque, penetrating force, rotary speed, penetrating velocity, drilling power, and drilling energy. Among these signals, rotary torque and penetrating force were chosen as the recognition signals to identify drillability, and rotary speed and penetrating velocity are the corresponding drilling parameters adjusted to adapt to different drilling formations. For granular soil, rotary and penetrating control mode is adopted while rotary

and percussive control mode are employed for rocks. When penetrating the granular soil from 0 to 22 s, the rotary motor keeps a constant rotary speed 80 r/min and penetrating motor exerts a constant velocity 80 mm/min. In this period, penetrating force is less than 50 N, rotary torque is no more than 0.6 Nm and drilling power is less than 10 W. When penetrating to the formation of limestone, penetrating force booms up meanwhile recognition drilling parameters are adopted to start real-time recognition. When recognizing limestone's drillability level, rotary motor switches rotary speed to 100 r/min and penetrating velocity is maintained a constant value 10 mm/min. In this period, penetrating force maintains a low level of less than 650 N, rotary torque is also no more than 10 Nm and drilling power is controlled no more than 90 W.

According to the monitored drilling states, by matching the appropriate drilling parameters with corresponding drillability level, the drilling loads in penetrating five formations keep relatively stable and do not surpass drill tool's load limits. As a result, it takes only 600 s and 10 Wh drilling energy in the 0.5 m drilling process. Overall, this drillability real-time recognition drilling strategy has been verified by this multi-layered drilling experiments.

## 5. Prospect for future application

Although the proposed non-contact drilling and coring characteristics monitoring method, SVM pattern recognition method, and drillability recognition based drilling strategy in this chapter are more specific to the interplanetary drilling actives, it should point out that these technologies may also be applied to terrestrial oil and gas well drilling operations. Specially speaking, even although by detecting devices applied into terrestrial oil and gas well drilling operations, the in-situ geological information can be acquired before, due to the unpredicted and variable online drilling conditions, there still exists great challenges in drill bits' selection, fluid system monitoring and parameters' optimization, adjustment of drilling parameters, well drilling faults' diagnosis, etc., [50, 51].

To solve the above problems, intelligent drilling technologies have been gradually widely employed in oil and gas well drilling activities. However, so far more attention was paid into the drill bit's wearing recognition, drilling faults' identification, formations' lithology evolution, etc. [52–54], few works were conducted to focus on the coring characteristics monitoring and adjustment. Since the ultimate goal of commercial drilling is to extract oil as much as possible, it perhaps is better to apply some facilities to monitor the online coring results into the inner tube. Herein, the proposed non-contact drilling and coring characteristics monitoring method is developed to conduct experimental validations, but once its specific structure parameters and installation conditions can be optimized further it may be employed into practice to enhance the online coring monitoring performance.

Given suitable drilling parameters in oil and gas well drilling are more dependent on the empirical formula concluded by experts [55], it is also urgently necessary and important to conduct rigorously theoretical calculation and experimental validation works on the soil-machine interaction, wherein the soil or rock's flow monograph can be comprehended more basically and the minimum power of the actuator under specific formation could then be referenced for future

application. Therefore, the proposed drilling and coring characteristics monitoring method may be applied to further experiments. Moreover, considering the increasing costs of human resources in the future, the unmanned oil and gas drilling is being more popular than before. The proposed drillability recognition based online drilling strategy is exactly developed for this issue. By only required some basic force sensor resources, it can be simply applied to recognize different drillability levels of uncertain drilling formations in practice. However, it should be noted that for future application, more considerations should be taken into optimizing the fluid system's disturbance on the recognition and the longer depth's coupling influence on the mechanical system.

## 6. Conclusions

This chapter elaborates the unique challenges in interplanetary drilling and coring mission. To comprehend the specific drilling and coring characteristics, a non-contact drilling and coring characteristics monitoring method has been proposed and verified. By establishing a drillability classification model, different types of drilling formations are evaluated by a combined index. Based on the SVM pattern recognition method, a drillability recognition model has been built up that can accurately identify four different drillability levels after optimization. Experiments under a multi-layered drilling simulant revealed that this intelligent drilling strategy can effectively reduce the drilling loads and can be applied to future interplanetary unmanned drilling and coring exploration.

## Acknowledgements

The authors greatly thank to the financial support by the fundamental research fund from the National Natural Science Foundation (Nos. 61403106, 51575122) and the Program of China Scholarship Council (No. 201706120153).

## Author details

Junyue Tang, Qiquan Quan, Shengyuan Jiang*, Jieneng Liang and Zongquan Deng

*Address all correspondence to: jiangshy@hit.edu.cn

State Key Laboratory of Robotics and System, Harbin Institute of Technology, Harbin, PR China

## References

[1] Harvey B. Soviet and Russian Lunar Exploration. Chichester: Praxis; 2007. DOI: 10.1007/978-0-387-73976-2

[2] Bar-Cohen Y, Zacny K. Drilling in Extreme Environments: Penetration and Sampling on Earth and Other Planets. Weinheim: Wiley-VCH; 2009. pp. 347-541. DOI: 10.1002/9783527626625

[3] Finzi A, Zazzera F, Dainese C, et al. SD2-how to sample a comet. Space Science Reviews. 2007;**128**(1):281-299. DOI: 10.1007/s11214-006-9134-6

[4] Elizabeth, H. Columbia Disaster: What Happened, What NASA Learned [Internet]. 2017. Available from: https://www.space.com/19436-columbia-disaster.html [Accessed: 2017-11-14]

[5] Elizabeth, H. Apollo 13: Facts about NASA's near-Disaster [Internet]. 2017. Available from: https://www.space.com/17250-apollo-13-facts.html [Accessed: 2017-10-9]

[6] Parnell J, Cullen D, Sims MR, et al. Searching for life on mars: Selection of molecular targets for ESA's aurora ExoMars mission. Astrobiology. 2007;**7**(4):578-604. DOI: 10.1089/ast.2006.0110

[7] Quan Q, Tang J, Jiang S, et al. Control system for a drilling & coring device in lunar exploration. In: Proceedings of the IEEE International Conference on Information and Automation (ICIA '13); 26-28 August 2013; Yinchuan. New York: IEEE; 2013. pp. 579-584

[8] Zacny K, Bar-Cohen Y, Brennan M, et al. Drilling systems for extraterrestrial subsurface exploration. Astrobiology. 2008;**8**(3):665-706. DOI: 10.1089/ast.2007.0179

[9] Gao Y, Thomas E, Pitcher C. Piercing the extraterrestrial surface: Integrated robotic drill for planetary exploration. IEEE Robotics & Automation Magazine. 2015;**22**(1):45-53. DOI: 10.1109/MRA.2014.2369293

[10] Tang J, Deng Z, Chen C, et al. Review of planetary drilling & coring technologies oriented towards deep space exploration. Journal of Astronautics. 2017;**38**(6):555-565. DOI: 10.3873/j.issn.1000-1328.2017.06.001

[11] Anttila M. Concept evaluation of mars drilling and sampling instrument [thesis]. Helsinki University of Technology: Helsinki; 2004

[12] Ran H, Zhang J, Xie W, et al. Applications study of geo drilling technology. Acta Geologica Sinica. 2011;**85**(11):1806-1822. DOI: 11-1951/P.20111025.0834.007

[13] Tang J, Deng Z, Quan Q, et al. Real-time drilling strategy for planetary sampling: Method and validation. Journal of Aerospace Engineering. 2016;**29**(5):04016033. DOI: 10.1061/(ASCE)AS.1943-5525.0000619

[14] Tang J, Quan Q, Jiang S, et al. Investigating the soil removal characteristics of flexible tube coring method for lunar exploration. Advances in Space Research. **61**(3):799-810. DOI: 10.1016/j.asr.2017.10.043

[15] Lian Y, Chen S, Meng Z, et al. Geological analysis of lunar middle and low latitude brightness temperature anomaly area based on chang'e-2 mrm data. Acta Geoscientica Sinica. 2014;**35**(5):643-647. DOI: 10.3975/cagsh.2014.05.15

[16] Huntress W, Moroz V, Shevalev I. Lunar and planetary robotic exploration missions in the 20th century. Space Science Reviews. 2003;**107**(3):541-649. DOI: 10.1023/A:1026172301375

[17] Zacny K, Paulsen G, Szczesiak M, et al. Lunarvader: Development and testing of lunar drill in vacuum chamber and in lunar analog site of Antarctica. Journal of Aerospace Engineering. 2013;**26**(1):74-86. DOI: 10.1061/(ASCE)AS.1943-5525.0000212

[18] Harvey B, Zakutnyaya O. Russian Space Probes: Scientific Discoveries and Future Missions. Chichester: Praxis; 2011. DOI: 10.1007/978-1-4419-8150-9

[19] Dave A, Thompson S, McKay C, et al. The sampling handling system for the mars ice-breaker life mission: From dirt to data. Astrobiology. 2013;**13**(4):354-369. DOI: 10.1089/ast.2012.0911

[20] Glass B, Cannon H, Branson M, et al. Dame: Planetary-prototype drilling automation. Astrobiology. 2008;**8**(3):653-664. DOI: 10.1089/ast.2007.0148

[21] Glass B, Thompson S, Paulsen G. Robotic planetary drill tests. In: Proceedings of the International Symposium on Artificial Intelligence, Robotics and Automation in Space (I-SAIRAS '10), August 29 to September 1 2010. Sapporo, Japan, Tokyo: JAXA; 2010. pp. 464-470

[22] Moskowitz C. NASA Makes Shaved Ice on Mars [Internet]. 2008. Available from: https://www.space.com/5632-nasa-shaved-ice-mars.html [Accessed: 2008-7-16]

[23] McKay C, Stoker C, Glass B, et al. The icebreaker life mission to mars: A search for biomolecular evidence for life. Astrobiology. 2013;**13**(4):334-353. DOI: 10.1089/ast.2012.0878

[24] Statham S. Autonomous structural health monitoring technique for interplanetary drilling applications using laser doppler velocimeters [thesis]. Georgia Institute of Technology: Atlanta; 2011

[25] Zacny K, Bar-Cohen Y. Drilling and excavation for construction and in-situ resource utilization. In: Badescu V, editor. Mars Prospect Energy and Material Resources. Berlin: Springer-Verlag; 2009. pp. 431-459. DOI: 10.1007/978-3-642-03629-3

[26] Glass B, Dave A, McKay C, et al. Robotics and automation for "icebreaker". Journal of Field Robotics. 2014;**31**(1):192-205. DOI: 10.1002/rob.21487

[27] Heiken G, Vaniman D, French B. Lunar Sourcebook: A user's Guide to the Moon. Cambridge: Cambridge University Press; 1991. pp. 475-567

[28] Quan Q, Chen C, Deng Z, et al. Recovery rate prediction in lunar regolith simulant drilling. Acta Astronautica. 2017;**133**:121-127. DOI: 10.1016/j.actaastro.2017.01.002

[29] Tang J, Quan Q, Jiang S, et al. Experimental investigation on flowing characteristics of flexible tube coring in lunar missions. Powder Technology. 2018;**326**:16-24. DOI: 10.1016/j.powtec.2017.12.013

[30] Tang J, Quan Q, Jiang S, et al. A soil flowing characteristics monitoring method in planetary drilling and coring verification experiments. Advances in Space Research. 2017;**59**(5):1341-1352. DOI: 10.1016/j.asr.2016.12.009

[31] Quan Q, Tang J, Jiang S, et al. A real-time recognition based drilling strategy for lunar exploration. In: Proceedings of the IEEE International Conference on Intelligent

Robots and Systems (IROS '14); 14-18 September 2014; Chicago. New York: IEEE; 2014. pp. 2375-2380

[32] Kozan E, Liu Q. A new open-pit multi-stage mine production timetabling model for drilling, blasting and excavating operations. Mining Technology. 2016;**125**(1):47-53. DOI: 10.1179/1743286315Y.0000000031

[33] Ersoy A. Automatic drilling control based on minimum drilling specific energy using PDC and WC bits. Mining Technology. 2013;**112**(2):86-96. DOI: 10.1179/037178403225001629

[34] Dai S, Jia Y, Zhang B, et al. Chang'e-3 scientific payloads and its checkout results. Sci. Sin. Tech. 2014;**44**(4):361-368. DOI: 10.1360/092014-42

[35] Zacny K, Cooper G. Considerations, constraints and strategies for drilling on mars. Planetary and Space Science. 2006;**54**(4):345-356. DOI: 10.1016/j.pss.2005.12.003

[36] Mitchell J, Bromwell L, Carrier WD III, et al. Soil mechanical properties at the apollo 14 site. Journal of Geophysical Research Atmospheres. 1972;**77**(29):5641-5664. DOI: 10.1029/JB077i029p05641

[37] Anand M, Crawford I, Balat-Pichelin M, et al. A brief review of chemical and mineralogical resources on the moon and likely initial in situ resource utilization (ISRU) applications. Planetary and Space Science. 2012;**74**(1):42-48. DOI: 10.1016/j.pss.2012.08.012

[38] Cherkasov I, Mikheev V, Smorodinov M, et al. 20 years of soviet investigation of lunar soils. Soil Mechanics & Foundation Engineering. 1986;**23**(6):241-244. DOI: 10.1007/BF01716690

[39] Rickman D, Edmunson J, McLemore C. Functional Comparison of Lunar Regoliths and Their Simulants. Journal of Aerospace Engineering. 2013;**26**(1):176-182. DOI: 10.1061/(ASCE)AS.1943-5525.0000223

[40] Lian Y. Inversion of composition and analysis of structure in the lunar subsurface from chang'e microwave data [thesis]. Changchun: Jilin University; 2014

[41] Quan Q, Tang J, Yuan F, et al. Drilling load modeling and validation based on filling rate of auger flute in planetary sampling. Chinese Journal of Aeronautics. 2017;**30**(1):434-446. DOI: 10.1016/j.cja.2016.05.003

[42] Shi X, Jie D, Quan Q, et al. Experimental research on lunar soil simulant drilling load analysis. Journal of Astronautics. 2015;**35**(6):648-656. DOI: 10.3873/j.issn.1000-1328.2014.06.005

[43] Yu Y, Arnold P. Theoretical modelling of torque requirements for single screw feeders. Powder Technology. 1997;**93**(2):151-162. DOI: 10.1016/S0032-5910(97)03265-8

[44] Roberts A. The influence of granular vortex motion on the volumetric performance of enclosed screw conveyors. Powder Technology. 1999;**104**(1):56-67. DOI: 10.1016/S0032-5910(99)00039-X

[45] Zhao D, Tang D, Hou X, et al. Soil chip convey of lunar subsurface auger drill. Advances in Space Research. 2016;**57**(10):2196-2203. DOI: 10.1016/j.asr.2016.02.027

[46] Vapnik V, Levin E, Cun Y. Measuring the vc-dimension of learning machine. Neural Computation. 1994;**6**(5):851-876. DOI: 10.1162/neco.1994.6.5.851

[47] Ling Y, Lu W, Song A, et al. In situ regolith bulk density measurement for a coiling-type sampler. Journal of Aerospace Engineering. 2014;**27**(2):359-368. DOI: 10.1061/(ASCE) AS.1943-5525.0000271

[48] Tang J, Quan Q, Jiang S, et al. Control method of lunar drilling based on online identification of drilling ability. Journal of Deep Space Exploration. 2015;**2**(4):325-332. DOI: 10.15982/j.issn.2095-7777.2015.04.005

[49] Cristianimi N, Shawe-Taylor J. An Introduction to Support Vector Machines and other Kernel-based Learning Methods. Paris: Cambridge University Press; 2000. ISBN-13: 978-052178019

[50] Bello O, Holzmann J, Yaqoob T, et al. Application of artificial intelligence methods in drilling system design and operations: A review of the state of the art. Journal of Artificial Intelligence and Soft Computing Research. 2015;**5**(2):121-139. DOI: 10.1515/jaiscr-2015-0024

[51] Eski I. Vibration analysis of drilling machine using proposed artificial neural network predictors. Journal of Mechanical Science and Technology. 2012;**26**(10):3037-3046. DOI: 10.1007/s12206-012-0813-9

[52] Guilherme I, Marana A. Papa J, et al, Petroleum well drilling monitoring through cutting image analysis and artificial intelligence techniques. Engineering Applications of Artificial Intelligence. 2011;**24**(1):201-207. DOI: 10.1016/j.engappai.2010.04.002

[53] Yu J. Online tool wear prediction in drilling operations using selective artificial neural network ensemble model. Neural Computing & Application. 2011;**20**(4):473-485. DOI: 10.1007/s00521-011-0539-0

[54] Brezak D, Starvoski T, Stiperski I, et al. Artificial neural network model for tool condition monitoring in stone. Applied Mechanics and Materials. 2015;**772**:268-273. DOI: 10.4028/www.scientific.net/AMM.772.268

[55] Liu H, Ma L, Huang Z. Integrated Artificial Intelligence Technology and its Application in Petroleum Engineering. Beijing: Petroleum Industrial Press; 2008. ISBN: 9787502165970

Chapter 3

# Making the Connection for Well Control on Floaters: Evolving Design Rationales for BOP Control Systems

Paul A. Potter

Additional information is available at the end of the chapter

http://dx.doi.org/10.5772/intechopen.77998

**Abstract**

In this chapter, a broad technical overview is offered to illustrate the technological advancements that have made the original direct hydraulic system reach those system design features that are shown in figure overleaf, which is a modern general arrangement of the "multiplexing" type of the BOP control system. Behind each discrete advancement, it goes without saying, there was a lot of design work, influenced by the radically different conditions in the subsea marine environment than those that we experience on land. Each step of this enabling technology is reviewed with in-depth reasoning explaining the "whys" and "wherefores" of each particular development. Let us start, as the drilling industry did for the development of BOP designs, at the beginning of the industry's step offshore around 60 years ago. Not least, it should be emphasized that the ways in which the systems' architecture has evolved have, in large part, been "driven" by the statutes laid out by the American Petroleum Institute (API) and later by other class societies that govern design compliance within the industry. The learning objectives of this chapter are to provide factual insights into evolving BOP control system designs as the industry moved from onshore to offshore and subsequently from bottom-supported drilling installations to floating drilling installations. This technology also forms the basis of the underpinning principles of hydraulic/electro and multiplexing subsea control systems that are currently used in the control of all kinds of production trees, subsea production centers, subsea distribution, and pipe line end manifolds (PLEMs). This chapter can be considered as a foundation and introductory overview for the development of control systems used in the subsea environment and those engineering challenges and obstacles that have been successfully surmounted, resulting in the technology basis in use today in the manufacture of subsea control systems.

**Keywords:** multiplexing, direct hydraulic, volumetric expansion characteristic (VEC) , signal time, sonic speed, closure time limits

## 1. Introduction

The challenge! How do you make this system?

It can be seen from **Figures 1** and **2** that there are a number of significant differences. Perhaps, the most noticeable difference is that the multiplexing BOP control system depicted, in the previous figure, features dual redundancy hydraulic supplies and command paths (blue/yellow BOP control pods). These are not evident in the direct hydraulic BOP control system shown in **Figure 1** [1–3].

Both command and hydraulic pathways are extended very considerably in the subsea multiplexing version over the direct hydraulic surface BOP control system. Whether it has been considered by the reader at the point of reading the introduction, another very major and significant system design characteristic that is evident is the Class Society rules governing maximum closing times for BOP wellbore functions that represent the underlying design rationale in the development of the control system suited for the use in deep and ultra-deep water locations.

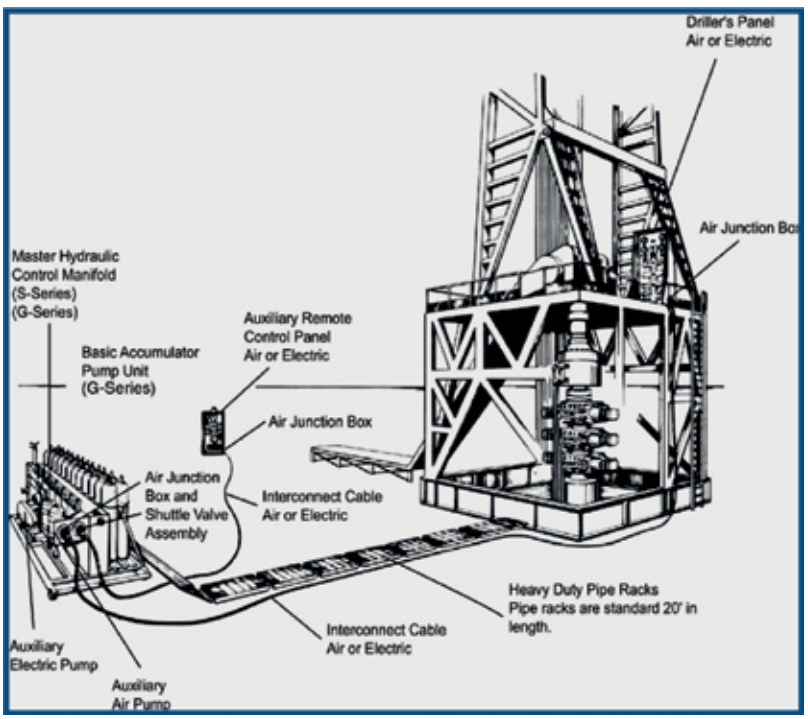


**Figure 1.** The fundamental BOP control system for a surface BOP stack.

http://dx.doi.org/10.5772/intechopen.77998

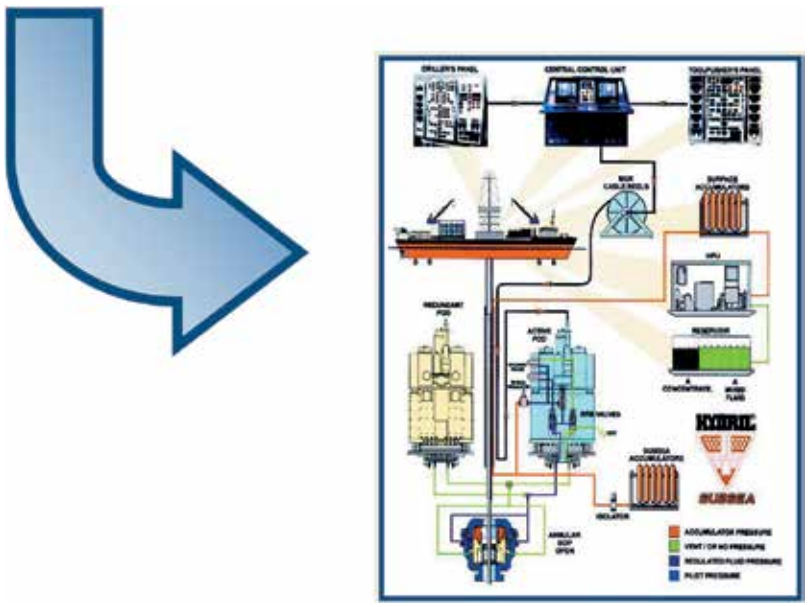

**Figure 2.** BOP multiplexing control system.

## 2. Conceptualizing the initial problems

### 2.1. Introduction

So, the starting baseline design is a system that is illustrated in **Figure 1**.

Essentially, this system is still in use today on land rigs, jack-ups, and tenders. Certainly, there are a number of design refinements on the basic system but the functionality and practical operability remain.

At this point, it should also be made clear that the core system requirements for the first land-based control systems and those encountered on sixth-/seventh-/eighth-generation ultra-deep water rigs are identical.

The BOP control system's main purpose is:

To exercise efficient and reliable control over the blowout preventer stack in the event of a well influx when the primary well control barrier of the hydrostatic column of drilling fluids in the well has not contained the well influx in the hole. Hence, we can say here that primary well control has been lost.

Put another way, we can state that the blowout preventer is the very last mechanical barrier between the well and us and is known as "secondary well control." All exploratory, appraisal, and development well barriers contain a secondary well control boundary.

### 2.2. Adaptation of land-based BOP control system for subsea service

In the most simplistic approach, we can now look at the immediate identified obstacles that reared up when the designers were contemplating the reality of making the current land-based system work subsea.

Let's refer once again to **Figure 1** in greater detail.

The normal hydraulic medium used in this closed system is 10 W (10 weight—density reference) mineral-based oil, and there are no environmental "leak" concerns because the system is shore-based or in the case of a bottom-supported drilling installation offshore (jack-up) surface application.

The following two figures further highlight the material requirements in a closed hydraulic control system where each end-user function (blowout preventer and valve hydraulic actuator) requires both a hydraulic supply and return line; this is in contrast to a subsea control system, which is an open hydraulic system (**Figure 2**).

The open hydraulic system, by definition, is one in which the displaced hydraulic fluid from the return/exhaust side of a hydraulic function is not routed via a dedicated return line back the accumulator unit reservoir but allowed to exhaust locally to the environment. In considering the application of BOP control subsea and in the marine environment, an open system must, essentially, employ a hydraulic medium which does not pollute or contaminate the environment in which displaced hydraulic fluid is being released into. Hence, a water-based hydraulic medium is utilized in all subsea BOP control systems (**Figures 3** and **4**).

The fifth figure in this chapter (**Figure 5**) is a simple block diagram of the most simple of a subsea control system maintaining closed hydraulic flow paths, while **Figure 6** shows the hydraulic flow path for one single BOP function, in this instance, a pair of ram type preventers. It should be appreciated that the single function hydraulic flow path depicted in **Figure 6** must be repeated to provide control over all BOP functions. This multiplicity of hydraulic flexible hoses is the basis of the perceived problem.

Let us imagine that we are in the design team that were tasked back in the early 1950s to get this control system working subsea.

Armed with the system architecture described briefly in the previous three pages, a simple approach may have been along these lines.

1. Provide a frame for the surface stack[1].
2. Install the hydraulic power unit on the rig topsides and run rigid pipe for the hydraulic supply and return lines to the moon pool area.
3. Install a hose reel to accommodate a hose bundle.

[1]In this chapter, we are not considering the choke and kill lines. This becomes an integral topic in the marine drilling riser topics in the appropriate chapter

http://dx.doi.org/10.5772/intechopen.77998

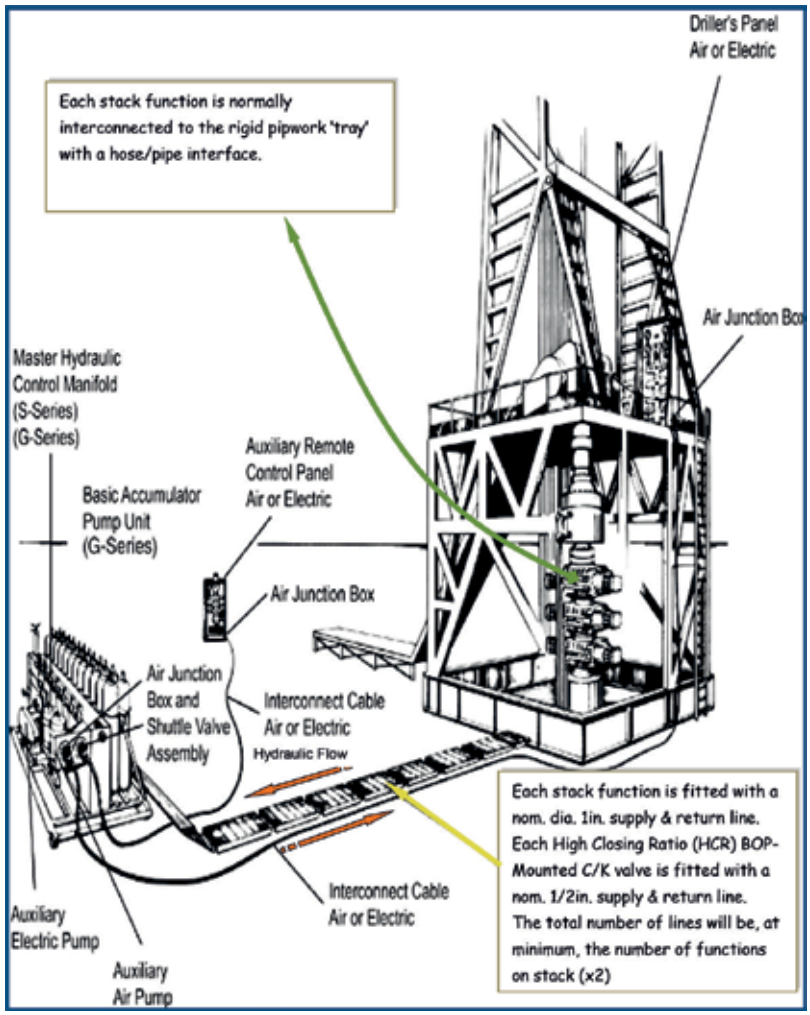


**Figure 3.** Dimensional details for the land-based BOP control system.

4. Interface the rigid pipework and arrange the hydraulic supply and return lines with flexible hoses to a removable hose stab plate to the hose reel end plate.

5. Spool sufficient hose bundle, containing the required number of supply and return hydraulic hoses, for the maximum operational water depth of the rig (let us say 750 feet).

6. On the BOP stack, connect the appropriately assigned hose (supply and return to each function) to that function.

**Figure 7** here inserted as an A3 fold-out schematic is a labeled depiction of a typical surface stack hydraulic power unit (HPU) and its hydraulic manifold. This is for reference in the forthcoming explanations.

**Figure 4.** Typical surface BOP stack, connected to BOP control system and hydraulic power unit via flexible hoses.

So, assuming that we have suitably stabilized and secured the hose bundle through the water column, is this going to work [3]?

No, of course not! The reasons why not are many and varied and the following list attempts to capture all the impossible shortfalls. These are not listed in the order of importance and relevance necessarily that were facing the first design team as they struggled with all the obvious obstacles.

http://dx.doi.org/10.5772/intechopen.77998

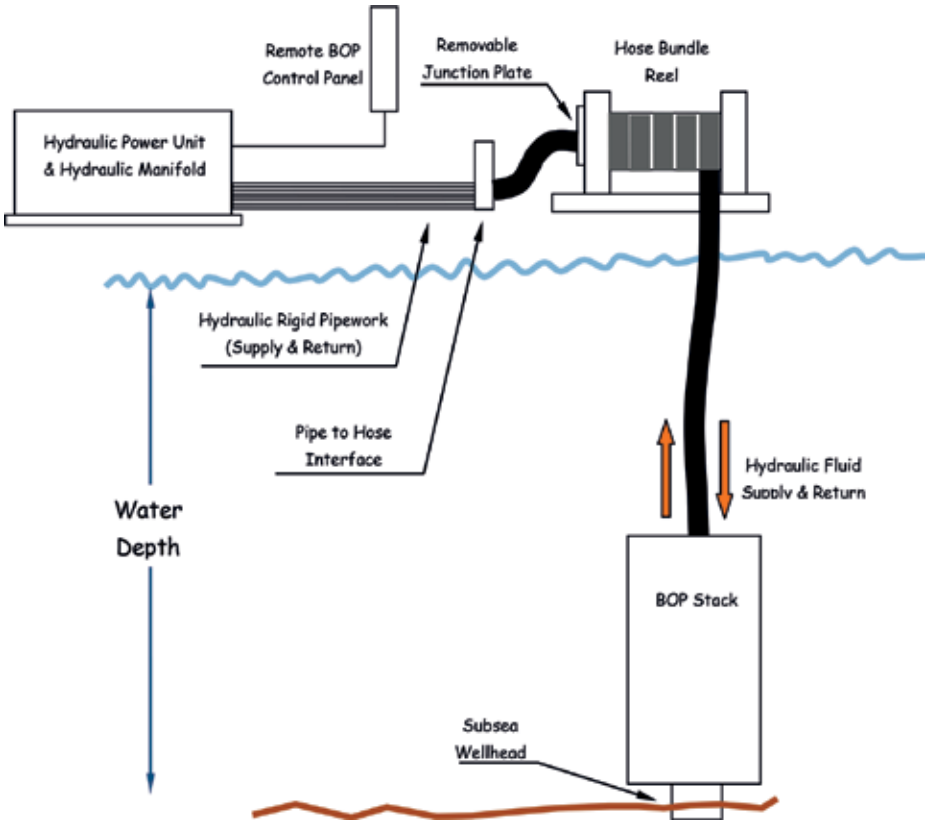


**Figure 5.** Fundamental but not practical proposed subsea adaptation of the former surface BOP control system.

*2.2.1. Hydraulic communication, "surface—subsea" issues*

Let us assume that the surface BOP stack has now been submerged for service subsea. Let us use the stack shown in **Figure 4** on page 77. This basic stack shown, using today's nomenclature (API Standard 53) [4] is a Class 4 A1-R3, interpreted this means a total of four preventers, one of which is an annular and the remainder are ram type preventers. The hardware at the base of the stack is a NT2 adapter which nipples up to the riser down on a jack-up. The NT2 adapter is not a hydraulic function on a surface BOP stack and is manually operated by a circular array of mechanical locking dogs [5].

And let us add that the stack has two hydraulically actuated BOP mounted valves (one on the choke line and the other on the kill line) [6, 7].

Therefore to now sum the quantity of supply and return hydraulic hoses required to control the functions of this stack if it were underwater would be:

| | |
|---|---|
| Annular preventer | 2 each 1 in. nominal diameter |
| Upper pipe rams | 2 each 1 in. nominal diameter |
| Shear blind rams | 2 each 1 in. nominal diameter |

| | |
|---|---|
| Lower pipe rams | 2 each 1 in. nominal diameter |
| Choke high closing ratio valve (HCR) | 2 each ½ in. nominal diameter |
| Kill HCR | 2 each ½ in. nominal diameter |

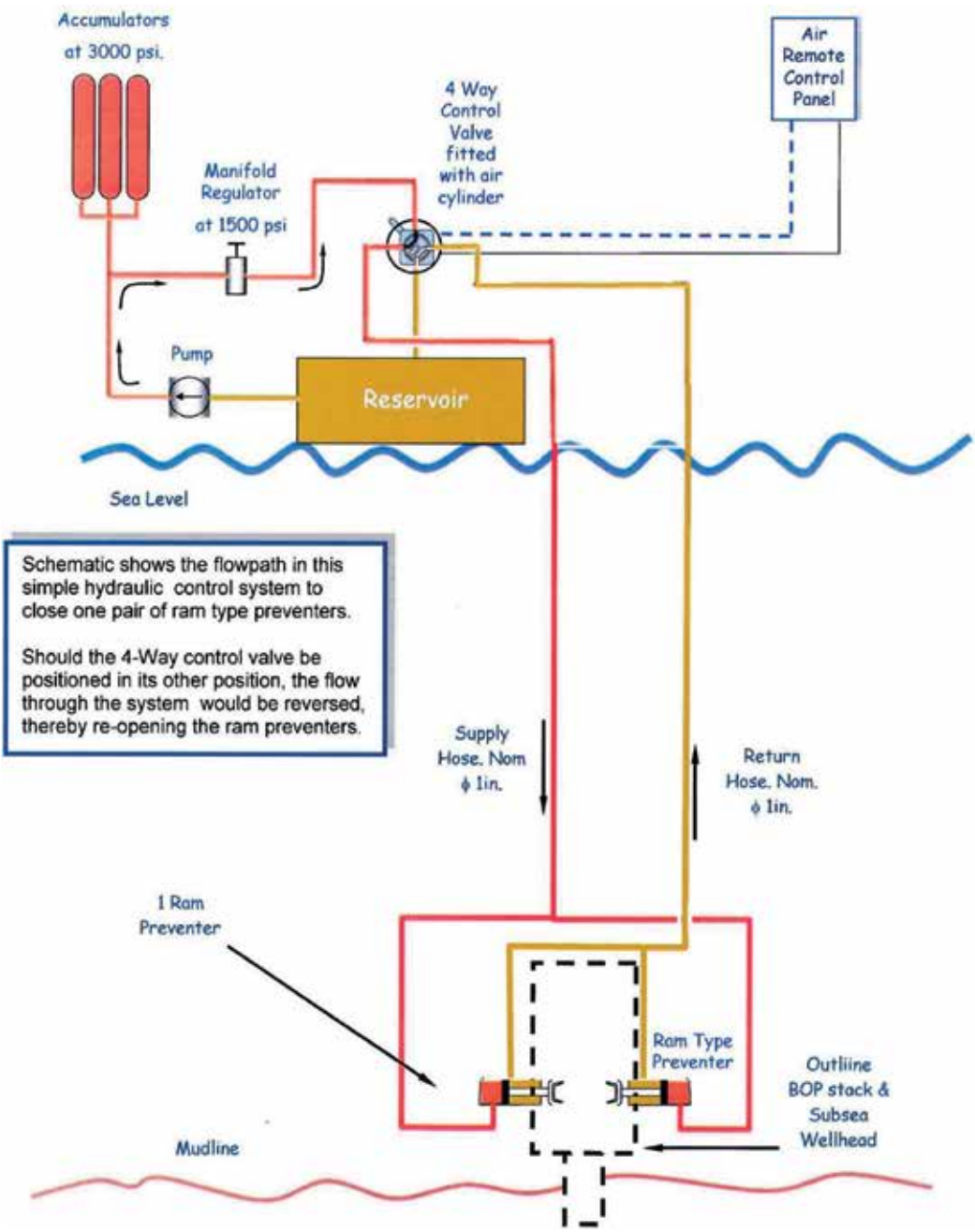


**Figure 6.** Direct hydraulic system with pneumatic control, one function.

http://dx.doi.org/10.5772/intechopen.77998

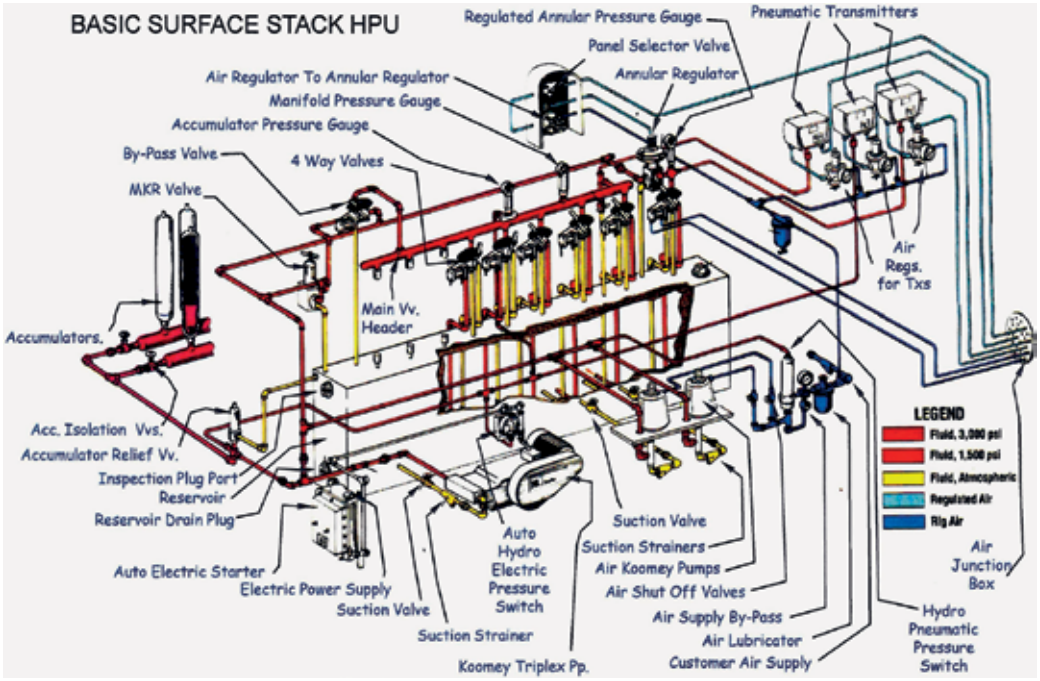


**Figure 7.** Skid Mounted Surface BOP Control HPU and Control Manifold.

**Figure 8** overleaf shows a scaled cross section of a hose bundle that satisfies the requirements to provide the above functions with hydraulic power. We can see, with some spare hoses surplus to requirements, the OD of the entire bundle is only ~6 in.

However, if we consider a BOP stack designed and built for subsea service (not a surface stack submerged!), the story is very different (**Figure 8**).

The subsea blowout preventer stack shown overleaf is an 18¾ in. nominal wellbore diameter, rated at 15000 psi maximum working pressure. This is denoted as "18¾—15 M."

This particular blowout preventer stack is somewhat dated; "third generation" puts its age genre at around 15–20 years (**Figure 9**).

Given that the minimum outside diameter (OD) for the hose bundle is going to be around 7½ in. (with no spare lines in the bundled matrix) and the minimum critical bend radius (MBR) for this bundle, let us give the reel some arbitrary dimensions, as indicated in **Figure 11**.

With these dimensions, the first wrap on this drum would store around 365 feet. Two wraps then would cover the water depth requirement of 750 feet. However, for the "storm loop" hose allowance in the moon pool to accommodate rig heave, another 250 feet would be required. This necessitates three wraps on this reel assembly.

The end plates' diameter would be in the order of 22 feet diameter. The reel assembly, its prime mover, and brake assembly are large scale!

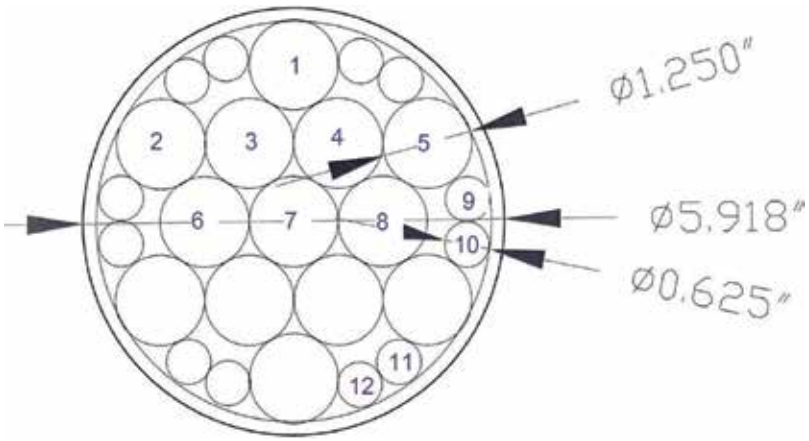


**Figure 8.** Cross section, hose bundle for minimum outfitted. BOP stack. Hose # 1: annular preventer close; Hose # 2: annular preventer open; Hose # 3: upper pipe ram close; Hose # 4: upper pipe ram open; Hose # 5: shear/blind ram close; Hose # 6: shear/blind ram open; Hose # 7: lower pipe ram close; Hose # 8: lower pipe ram open; Hose # 9: choke HCR close; Hose # 10: choke HCR open; Hose # 11: kill HCR close; Hose # 12: kill HCR open.

Typically, hose reel assemblies are installed at an intermediate elevation above the moon pool weather deck elevation on a mezzanine deck. Two such typical arrangements are shown in **Figures 12** and **13**.

*2.2.1.1. Summarizing the impracticalities and identifying the system requirements*

It has been shown that using bundled hoses of the required dimensions for the appropriate volumes demanded by the various BOP stack functions is impractical in terms of the physical challenges to build and install such hose reel topsides on a floating drilling installation. However, there are other issues with this concept, which can be summarized in the following list:

- The hydraulic system is closed and therefore the friction losses encountered in the return hoses will effectively slow down the response times, which are clearly detailed and stated in the current specification of API 16D, Edition 4, 2004 [7].
- The system offers zero redundancy and this is considered unacceptable for such a critical control system which must operate reliably and remotely in the "not-unlikely" event that the last mechanical barrier must be put in place immediately (shutting in the well). The prospect of building and installing an identical arrangement to the one illustrated is not in any way a practical solution whatsoever.
- The hydraulic medium is environmentally unfriendly and illegal. The hydraulic medium used in surface BOP stack control systems cannot be used in subsea versions of the system (water-based, as described on page 75).
- The system concept, as shown on previous pages, offers no hydraulic usable volume in storage on the subsea BOP stack, hence the drawdown effect on this system would be formidable and further exacerbate the response time issue for pipe and annular type preventers. Volumetric storage of hydraulic fluid subsea will be discussed in later sections.

http://dx.doi.org/10.5772/intechopen.77998

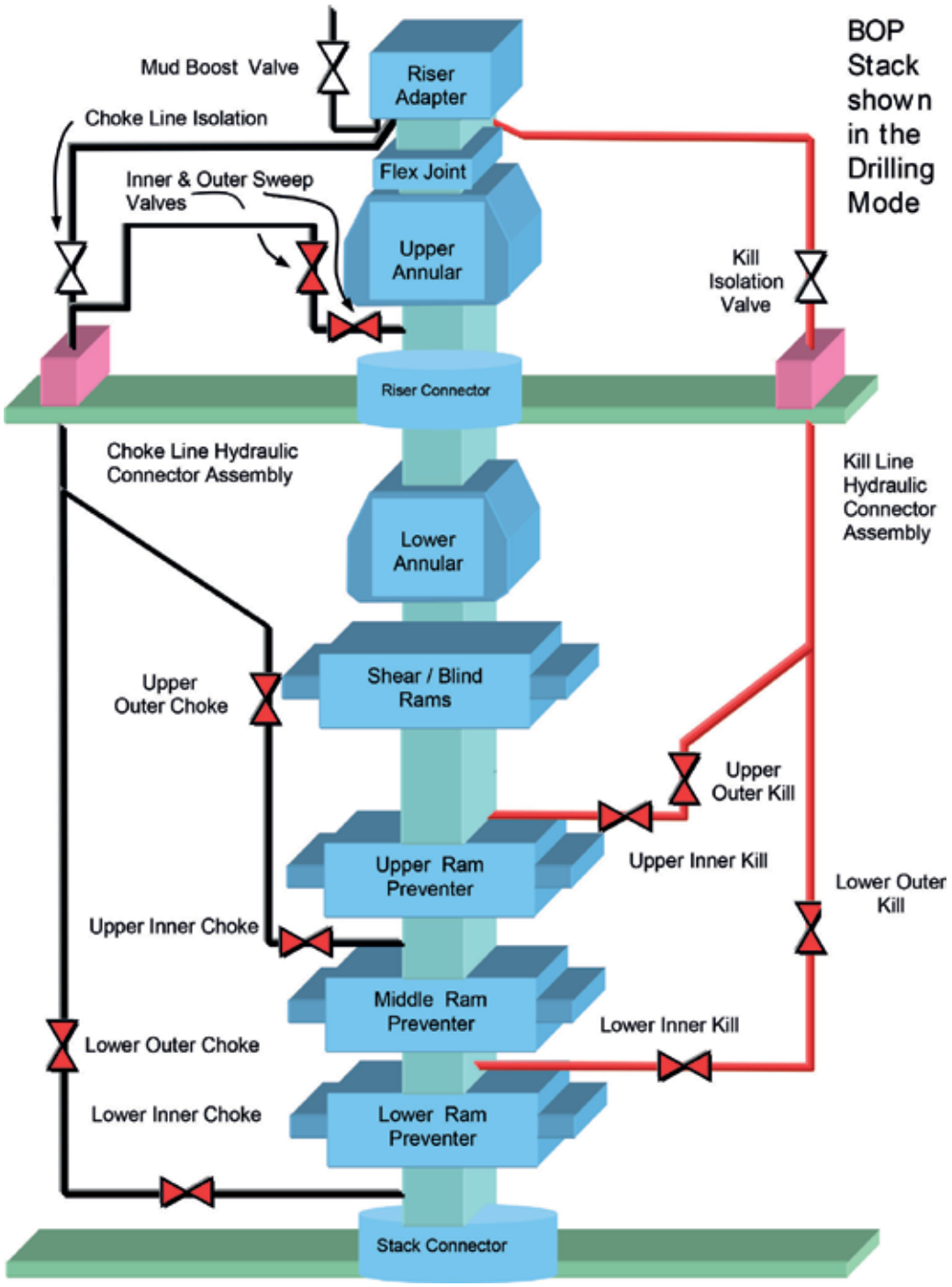


**Figure 9.** Third-generation BOP stack. Glomar Celtic Sea (**Figure 10**). 18¾ in.—15 M. Hose requirement—Mud boost valve: 2 × ½ in.; upper annular: 2 × 1½ in.; kill isolation valve: 2 × ½ in.; kill line connector: 2 × ½ in.; choke isolation valve: 2/½ in.; riser connector sec. unlock 1 × ½ in.; lower annular: 2 × 1½ in.; S/B rams: 2 × 1 in.; upper pipe rams: 2 × 1 in.; middle pipe rams: 2 × 1 in.; lower pipe rams: 2 × 1 in.; wellhead connector: 2 × ½ in.

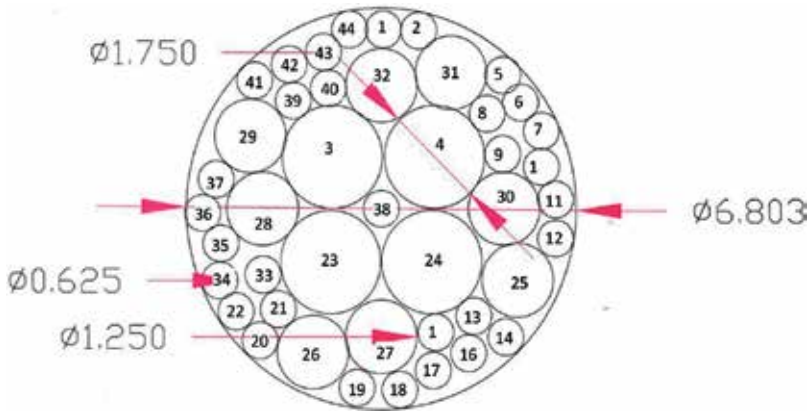


**Figure 10.** Cross section, hose bundle for third-gen. BOP stack (scaled). Hose # 1: mud boost valve close; Hose # 2: mud boost valve open; Hose # 3: upper annular close; Hose # 4: upper annular open; Hose # 5: kill isolation valve close; Hose # 6: kill isolation valve open; Hose # 7: kill line connector extend; Hose # 8: kill line connector retract; Hose # 9: choke isolation valve: Close; Hose # 10: choke isolation valve open; Hose # 11: choke line connector extend; Hose # 12: choke line connector retract; Hose # 13: inner sweep valve close; Hose # 14: inner sweep valve open; Hose # 15: outer sweep valve close; Hose # 16: outer sweep valve open; Hose # 17: riser connector lock; Hose # 18: riser connector unlock; Hose # 19: riser connector sec. unlock; Hose # 20: upper outer choke close; Hose # 21: upper outer choke open; Hose # 44: lower outer kill close; Hose # 23: lower annular close, Hose # 24: lower annular open; Hose # 25: shear blind rams close; Hose # 26: shear blind rams open; Hose # 27: middle pipe rams close; Hose # 28: middle pipe rams open; Hose # 29: lower pipe rams close; Hose # 30: lower pipe rams open. Estimating size of hose reel required, rig operational water depth: 750 feet.

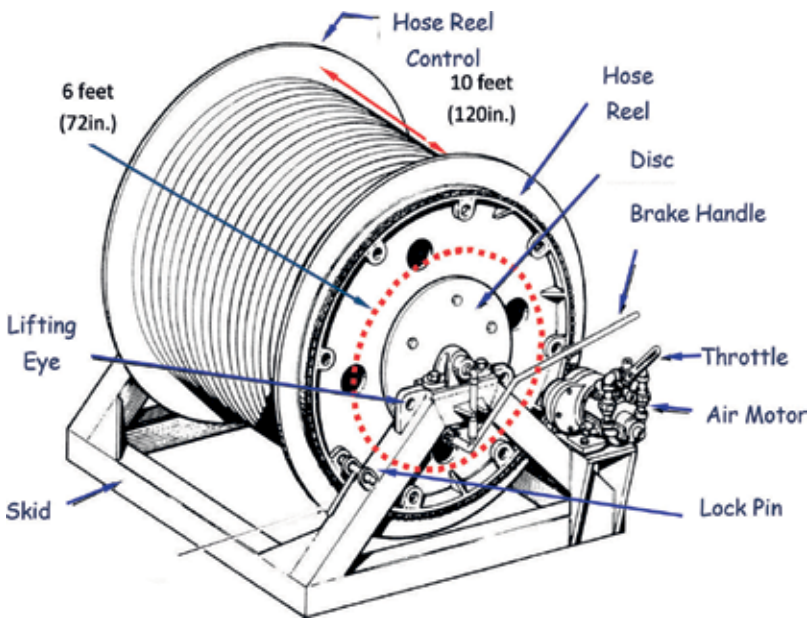


**Figure 11.** Typical hose reel.

- What has not been discussed are the issues surrounding the realities of topsides and subsea terminations for hydraulic hoses, the minimum multiplicity exampled here is by no means the total number of stack functions now supplied to modern deep and

http://dx.doi.org/10.5772/intechopen.77998

**Figure 12.** Typical BOP hose reel: mezzanine-deck mounted.


**Figure 13.** Cameron hose reel installed on the Iran Alborz GVA 6000 semi-submersible drilling installation.

ultra-deep water BOP stacks. The number of functions presented here for this illustrative exercise is 44, and to put that into today's context, modern stacks boast in excess of 110 functions!

- To this point in our design rational discussion on evolving control systems, the requirement for a BOP stack split disconnection has not been introduced. There is a myriad of situations in subsea drilling operations when we need to achieve a disconnection whereby the lower BOP is left latched on the subsea wellhead and the lower marine riser package is retrieved, either to surface or "positioned" in a stand-by location in the water column. The design architecture surrounding this design feature will be discussed in due course.
- In light of the above, we can list the design features that are required for a reliable and fit-for-purpose subsea BOP control system [7]:
    - Provide redundancy
    - Comply with legislation
    - Practical installation
    - Install stored hydraulic fluid
    - Compliance: anti-pollution laws
    - Enhance functional multiplicity
    - Design allowance: disconnect

## 2.3. Design features, first subsea BOP control system

### *2.3.1. Introduction*

The ingenious design of the first BOP control system, which is now presented as an overview, was developed in the first half of the 1950s when the maximum rated water depth for drilling offshore off floaters was still under 1000 feet (305 m) [8].

The reasons for the water depth limitation are varied and not directly attributed to the restraints of the BOP control system. Some of these were marine, drilling plant topsides' limitations and to a lesser extent, and capabilities of marine drilling riser (the mechanical connection between the subsea BOP stack and the drilling installation).

### *2.3.2. Concept of the hydraulic pilot-operated control system*

The immediate problems facing the pioneering design group:

How do we overcome the excessive dimensions of a simple closed hydraulic system deployed subsea?

How do we diminish the friction losses in the closed hydraulic system where the displaced fluid from the "other" side of the function slows the overall response times of the ram type and annular type preventers?

How do we build in redundancy to a point where the critical control system can satisfy the most stringent of regulators for reliability?

http://dx.doi.org/10.5772/intechopen.77998

What can be done to minimize the risks of pollution to the marine environment?

Is there some way in which the volume/pressure drawdown effect can be reduced in the direct closed hydraulic system?

How should the topside equipment be arranged for optimum operation and account for rig motions?

What is required to configure the BOP stack to enable a disconnect while leaving the well secured in the coincidental event of a well influx?

Pictorially shown here are the basic principles that were proposed (**Figure 14**).

Pivotal to the success of the prototype design was the use of hydraulic relay valves which are installed in the newly conceived control pod(s) which are activated by a hydraulic pilot signal commanded from the surface. By the use of hydraulic relay valves and agreement that the displaced fluid volume from the "other" side of the function should exhaust directly through the "other side of the function" relay valve directly to the marine environment, it was immediately understood that the prior formidable size of the hose bundles could be greatly reduced, not least caused by using 3/16 in. pilot hoses in the bundle. The main hydraulic supply consequently consisted of one only nominal 1 in. diameter core hose within the bundle (see top right of the previous figure for details).

In order to have an open hydraulic system that exhausted hydraulic fluid directly to the marine environment, the hydraulic medium was changed from lightweight mineral oil to potable water dosed with additives in small percentages of dilution. This new hydraulic medium necessarily influenced careful material selection of both metal and rubber sealing components of the hydraulic valves, regulators, and other subsea control system components. Not only was the marine environment a factor in dispelling the consideration of the use of an oil-based hydraulic medium, but also differential pressure experienced across the thermoplastic wall of flexible hose at increasing hydrostatic pressure from the water column depth. This is discussed in the next sub-section.

100% redundancy was provided by furnishing two identical systems which became color-coded blue and yellow. The system is arranged whereby one to the two identical sides of the system may be used at any given moment but never both. The redundancy satisfied both operators, oil companies, and more importantly, class societies and legislative bodies. Since the early systems, levels of redundancy have been revised, and standard operating procedures adopted formerly have been revised reflecting greater caution and conservatism. This will be discussed in due course.

By the introduction of gas pre-charged hydraulic accumulators, nominally 11 US gallons capacity each, the early problems of system drawdown effects were satisfactorily banished as the 1 in. hydraulic supply in either hose bundle maintained full system working pressure in the stack-mounted accumulator bottles.

This system quickly became field proven and a number of proprietary vendors produced their own systems, however it has to be said that all were based on the principles put forward originally by Paul Koomey and his design team.

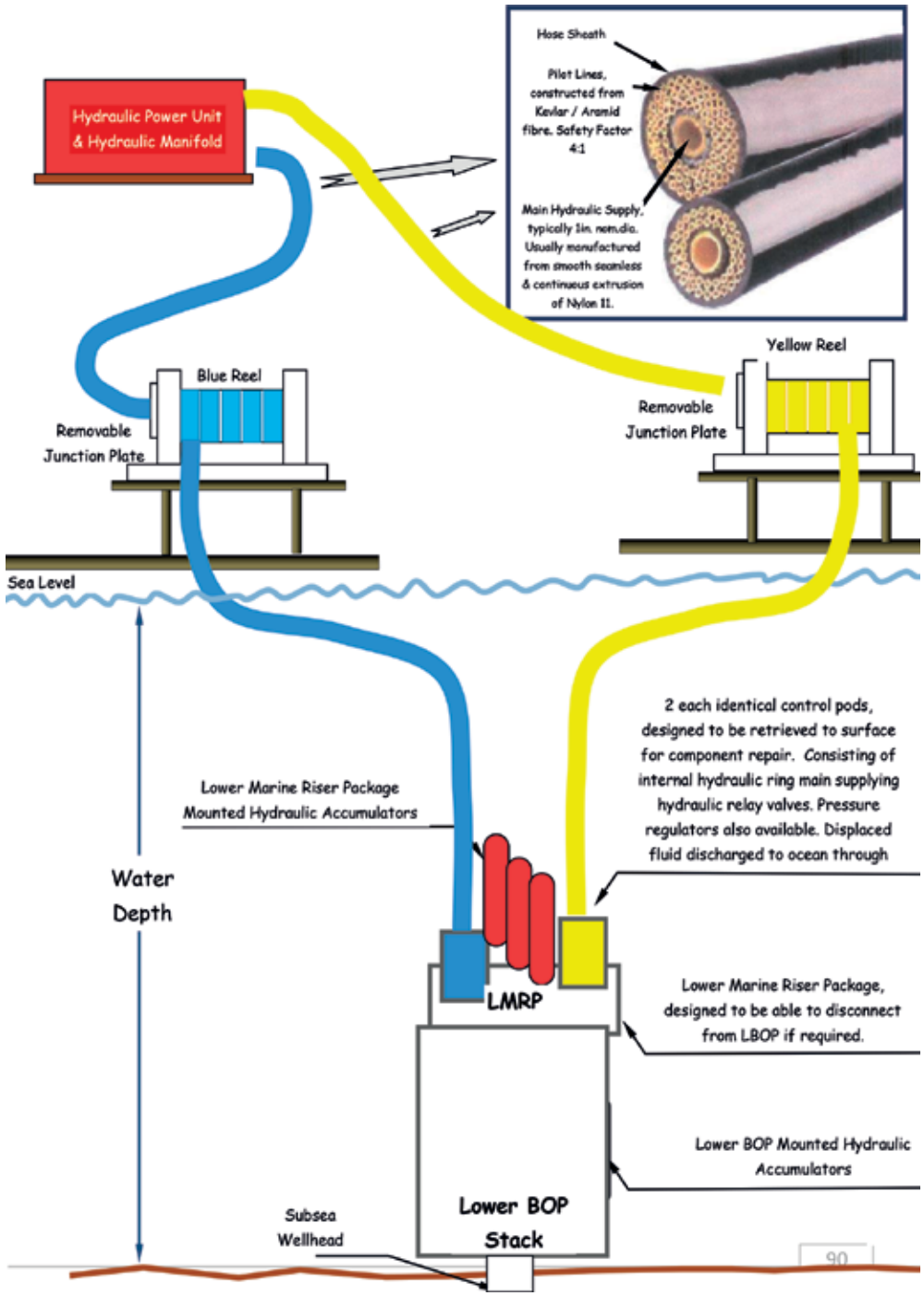


**Figure 14.** Concept and principles of the open BOP control system.

The remainder of this sub-section concentrates on the general arrangement detail of the system and its operational characteristics and finally limitations identified for this system.

*2.3.3. The basic control pod*

The hydraulic control system is always equipped with two control pods, designated as the blue or yellow pod. To maintain a fully redundant control system, both pods must be operational at all times.

Formerly, if a control pod becomes inoperable, drilling operations would be normally suspended and the BOP stack controlled with the working pod until repairs are completed and tested. This involved the retrieval to the surface of the defective pod, repair and test on surface before re-deploying subsea to latch back into its dedicated receptacle on the LMRP.

More recently with the advent of deep water drilling, the majority of oil companies will not allow continued drilling operations for the retrieval of one pod to surface for repair. If repairs are to be performed in the midst of a drilling program, drilling operations are suspended, and the well made safe and the entire LMRP retrieved to surface to repair the faulty control pod.

The active and selected control pod is normally alternated between the pods weekly or after a BOP stack test.

Koomey Shaffer introduced a 42 line retrievable pod which featured a double female receptacle design. The separate receptacles enable both the pod to be retrieved or else the entire LMRP (**Figure 15**).

Later, as the drilling contractors began to use BOP stacks with greater number of functions, Shaffer and others introduced a 64 line control pod, which, while featuring a different geometry (cubical rather than cylindrical) operated in the same manner and was intended for retrieval during drilling operations (**Figure 16**).

*2.3.4. Control system hoses*

*2.3.4.1. Introduction*

Proprietary manufacturers of subsea hose bundle strive to provide a product which has a low volumetric expansion characteristic (VEC). This ensures that API closing times are not exceeded for ram type and annular type preventers. In the electro-hydraulic control system, the single greatest contributor to lengthening response times is the hydraulic pilot pressure build time and transport time.

*2.3.4.2. Pressure characteristics of the control fluid*

The fluid parameters that govern the transmission time of a hydraulic signal through a thermoplastic tube are:

- The density of the fluid
- The viscosity of the fluid
- The un-dissolved gas in the fluid
- The bulk modulus of the fluid

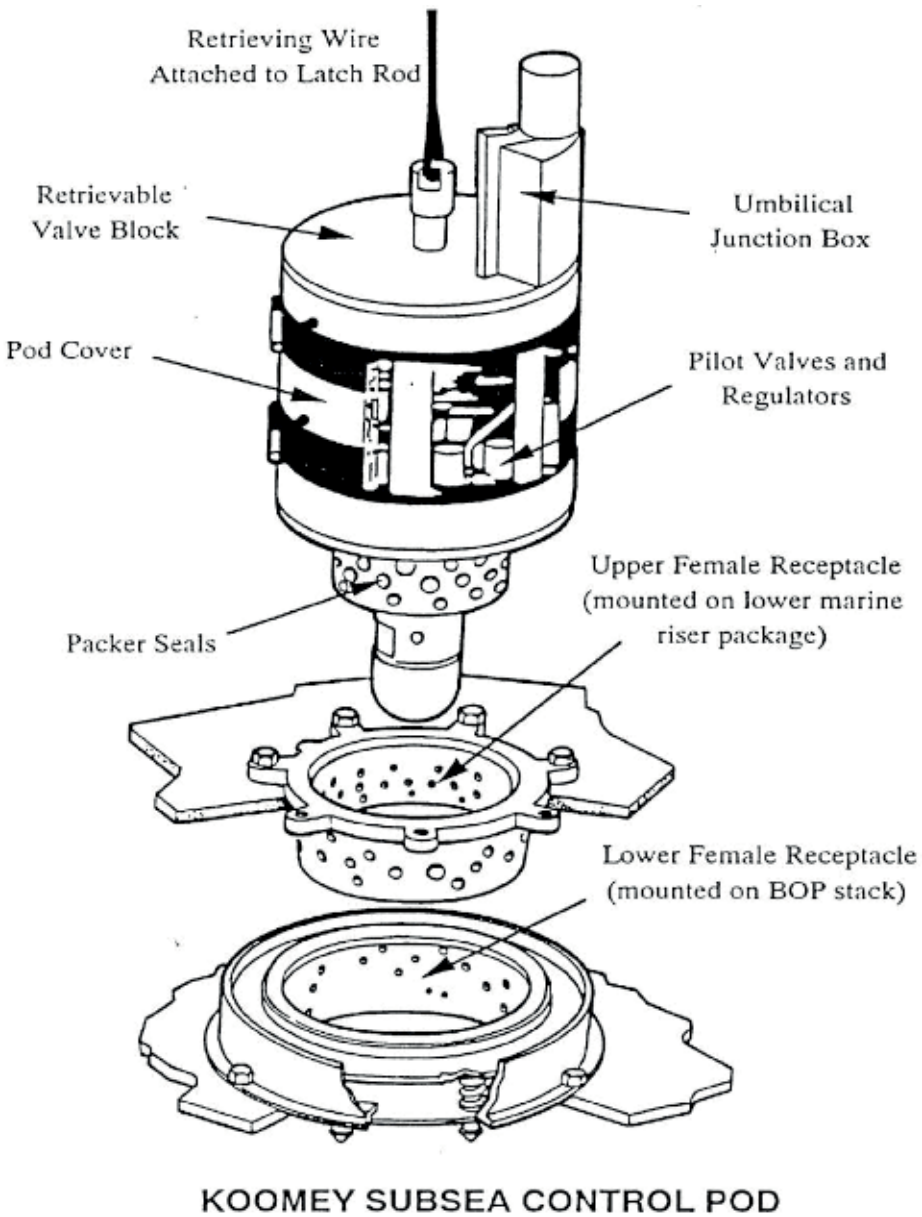


**Figure 15.** The 42 line Koomey control pod.

http://dx.doi.org/10.5772/intechopen.77998

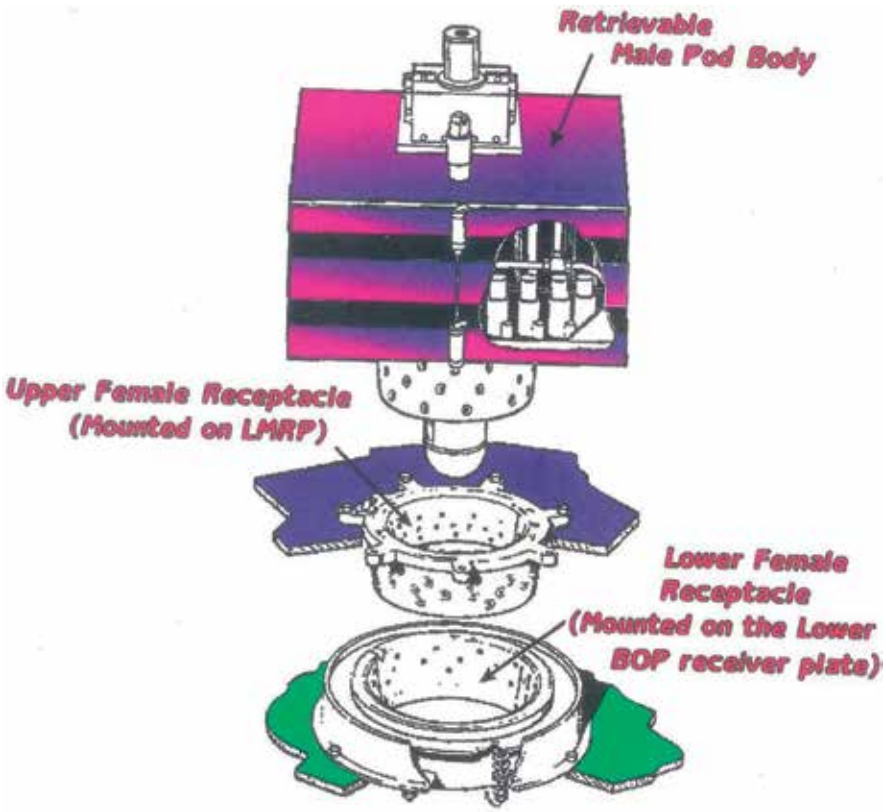


**Figure 16.** The Koomey Shaffer 64 line retrievable control pod.

The values may change, but this is usually associated with significant changes in the ambient operating temperatures. An extreme example is the difference in control fluid parameters in tropical climates. As opposed to climates in far northerly and southerly latitudes, there will be no monoethyleneglycol (MEG) added to the control fluid medium since the seawater temperature at the mudline is significantly above freezing point. (This is applicable for the relatively shallow water depths in which this type of BOP control system is used, and the previous statement is not true for ultra-deep water: >6000 feet.)

We can say that the density and viscosity of the fluid will remain close at their optimum values in this operational water depth.

*2.3.4.3. Factors influencing time response*

One of the basic concerns in regard to using thermoplastic hose to transport hydraulic fluids to great depths is differential pressure across the tube wall. At great depths, the external pressure may be sufficient to collapse the hose. The pressure at which collapse takes place is dependent upon the hose construction and the nominal diameter of the hose [4, 7].

The dominant property of differential pressure in this application arises from the differences between seawater and control fluid densities. Wherever in this type of system, there exists a degree of density difference across the hose tube wall, a chance of invoking hose collapse is possible. For instance, at a depth of 5000 feet, a thermoplastic hose containing a typical mineral oil as the hydraulic medium found in surface stack control systems will experience an overburden of around 220 psi, which is quite sufficient to collapse a hose. Pressures as little 30 psi can cause collapse of hoses with nominal diameters in the range of 3/8–½ in.

*API specification 17E: specification for subsea production control umbilicals, states for collapse pressure* [9]:

*"The minimum value of external collapse pressure shall be 150% of the difference in the static head due to hydrostatic pressure at the maximum design depth less the static head at that depth due to the service fluid (hydraulic medium)."*

Further unwanted differential pressure will be generated if the hydraulic lines are not 100% fluid filled. If any entrapped air is present in the tube length, the hydrostatic pressure will dominate and tube collapse will occur. This is easily eradicated by thorough purging and venting of all lines in the subsea umbilical hose bundle. The presence of air, however small, also dramatically increases response times due to the compressibility of gases [3].

The differential problem is overcome by choosing a hydraulic medium which has a specific gravity that is close to seawater.

Seawater has a gravity of ~1.03 and water is 1.00. Providing that the hydraulic medium is water-based with additives that only change the specific gravity to a new value remains close to that of the specific gravity of seawater then the possibility of hose collapse is virtually obviated.

*2.3.4.3.1. Viscoelasticity*

Hoses, being composites with polymeric constituents are found to behave in a time dependent viscoelastic manner when applied load is a hydraulic charge as found within a pilot line hose.

The result of the viscoelasticity manifests itself in a pressure decay after initial pressurization. This is not detrimental for the pilot signals in this application since the hydraulic pilot-operated relay valves subsea "fire" and "vent" at pressures well below the nominal pilot pressure of 3000 psi. **Figure 17** shows the pressure decay versus time. The typical time constraints are well beyond time of the hydraulic relay valves "firing" in this control system.

*2.3.4.3.2. Hose geometry changes during pressurization*

Extensive laboratory testing has been performed to assess the changes in hose geometry subjected to a step positive change in internal pressure. The changes in geometry were measured using strain gauges, both axially and circumferentially affixed to the outer surface length of the hose under test.

http://dx.doi.org/10.5772/intechopen.77998

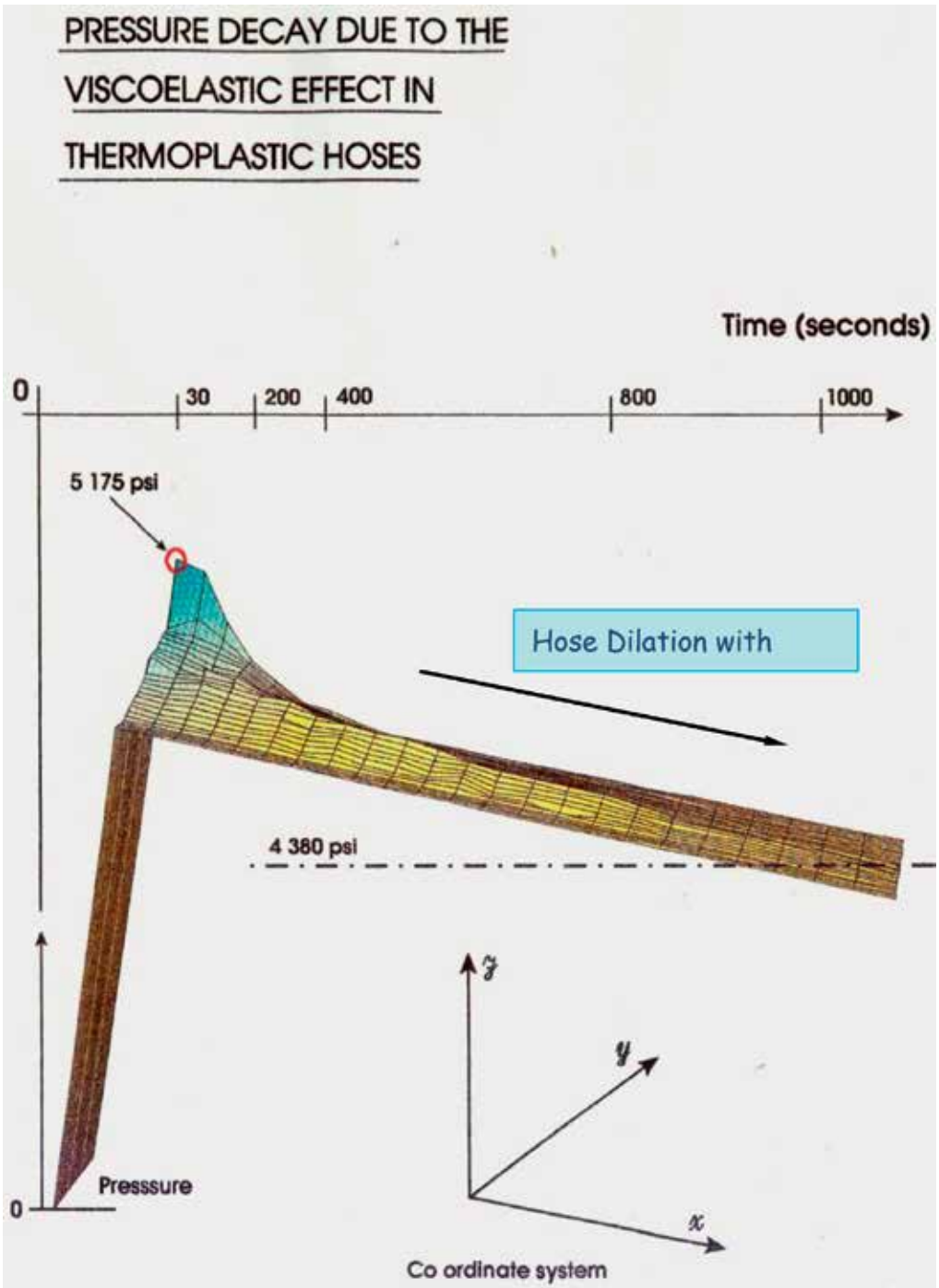


**Figure 17.** Pressure decay in thermoplastic hoses due to viscoelasticity.

The axial gauges measured any bending strains incurred and the circumferential gauges monitored hoop stresses. It was found that the hose length shortened with pressurization and this is explained by the layers of hose braiding attempting to establish a neutral lay angle during the buildup of pressure. The effect is almost instantaneous and remains constant, and hence the axial strain is not responsible for the viscoelastic effect.

Measured hoop strains correlate to observed pressure responses and shown typical viscoelastic behavior. In tandem with strain measurements, volume measurements have been recorded to estimate the variation in wall thickness. Such measurements have been quantified using two equations which account for the bulk modulus and pressure decay following initial viscoelastic expansion of the hose under test.

Results from these tests showed that both the internal and external diameters of the hose increased with pressurization although the OD significantly less than the ID of the hose.

Overall, this indicates that all hydraulic pilot hoses will "accept" more fluid when a pressure signal is initiated from the source and will duly expand in direct correlation with the VEC of the hose: dependent upon construction and materials. At pressure equilibrium (e.g., 3000 psi), the hydraulic pressure peak will transit the length of the hose at approximately the speed of sound.

*2.3.4.3.3. Behavioral phenomena of thermoplastic hose*

All hoses that are constructed of material that use a composition of polymers and fibers may be classed as thermoplastic hoses. When subjected to pressure changes internally and externally, they exhibit a viscoelastic time-related response. After an initial pressurization, the pressure decays over a period of time as the hose dilates (see the previous figure) [3].

The extent of the dilation is dependent upon a number of factors such as hose material, construction, age, environment, and so on. A similar effect occurs when the hose is depressurized, this being a time-related contraction effect.

Against logical intuition, hoses bundled together exhibit greater volumetric expansion (VE) than identical hoses pressurized in isolation. There is a mathematical proof for these phenomena but suffice it to say that the reason is simply because there are effects from adjacent bundled hoses which remain pressurized against those vented to zero gauge.

It is known that aging in hoses reduces VE which acts in our favor (in drilling BOP controls) but is considered detrimental in production control systems.

Minimizing the effects of VE promotes faster response times in hydraulically piloted BOP control systems since the pod-mounted relay valves will not "fire" until they have sufficient pressure in the hydraulic pilot signal: normally around 500–700 psi.

The following figures illustrate some of the effects of the volumetric expansion characteristic in thermoplastic hoses (**Figures 18–20**).

http://dx.doi.org/10.5772/intechopen.77998

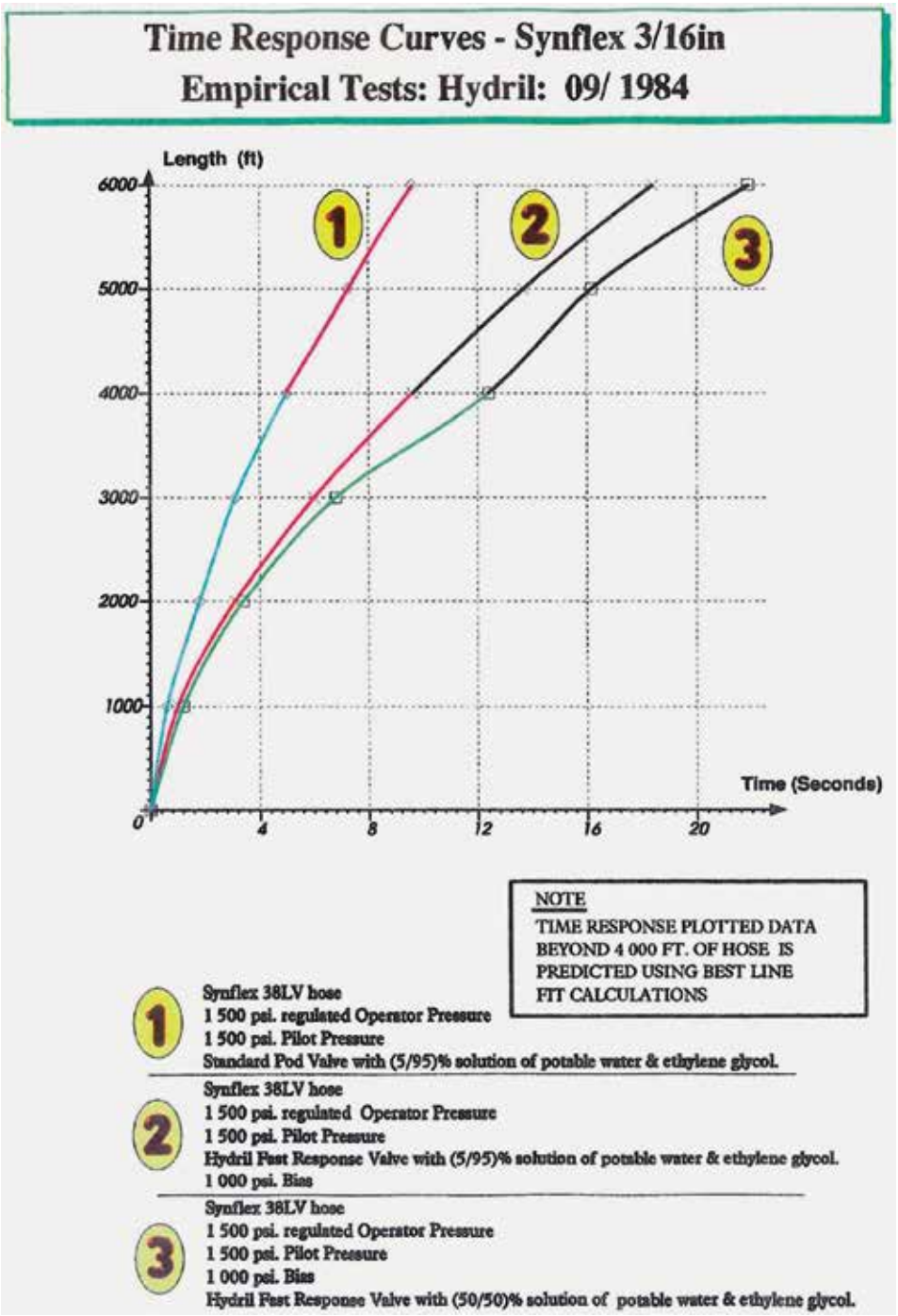


**Figure 18.** Time response curves from Hydril® empirical testing.

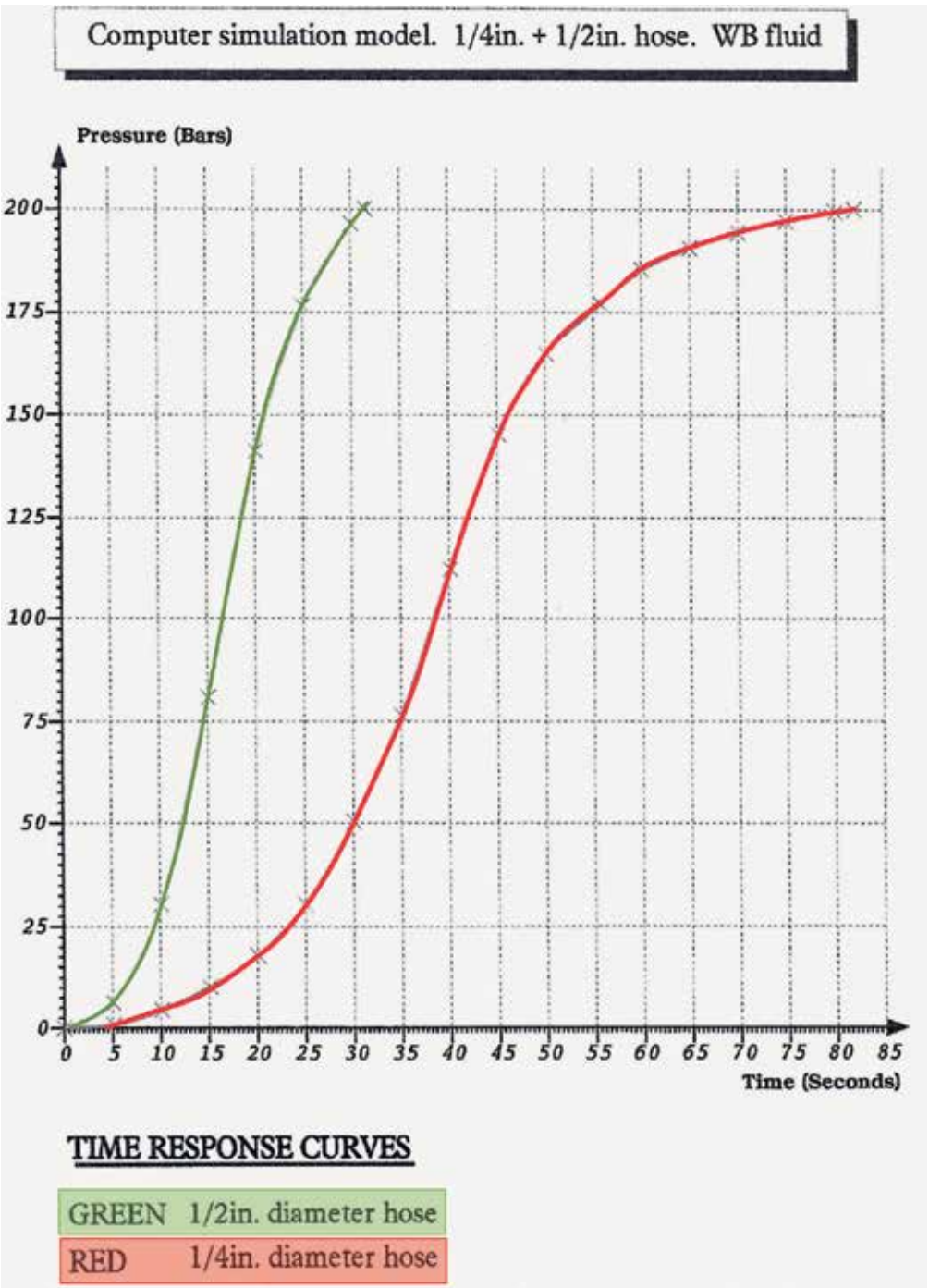


**Figure 19.** Typical response times for 1/4 in. and 1/2 in. Diameter thermoplastic hose.

http://dx.doi.org/10.5772/intechopen.77998

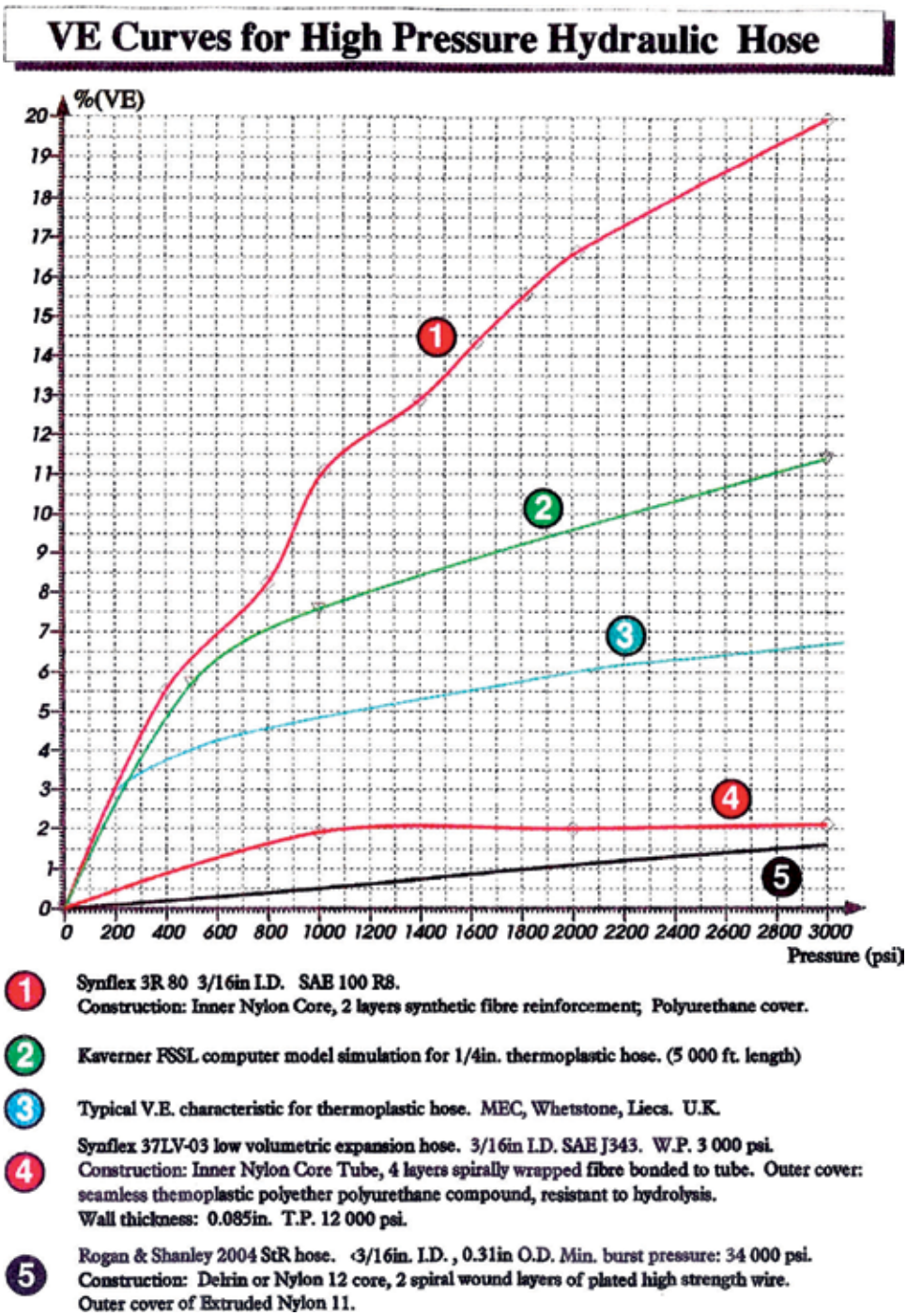


**Figure 20.** VE curves for high pressure thermoplastic hose.

## 3. Summary

In this chapter, we have explored the evolving design technology that enabled a surface land-based BOP control system to be used reliably in the subsea marine environment. Further, design teams have provided the following system features to the subsea BOP control system:

- 100% inbuilt design redundancy: based on the high level of safety criticality of the subsea BOP control system (the last barrier). Given fundamental design principles of the subsea hydraulic control pod.
- The use of hydraulic devices (such as relay valves and regulators) to satisfy legislative close times on BOP preventers and BOP-mounted valves (Choke and Kill).
- An insight into the development of flexible hydraulic hose to maximize short response times by the limitation of the design VEC of elastomeric hose materials.
- The principles employed to overcome hydraulic drawdown through extended lengths of hydraulic line/hose (accumulator introduction).

## Author details

Paul A. Potter

Address all correspondence to: paul@Subceng.com

SUBC Engineering Ltd, Unit 2, Springfield Centre, Aberdeen, United Kingdom

## References

[1] Quilici M, Roche T, Fougere P, Juda D. Risk assessment of a BOP and control system for 10000 ft water depth. Journal of Petroleum Technology. 1998;**50**(8):42-44

[2] Vigeant SP. Deep water driven advancements in well control equipment and systems. In: IADC/SPE Asia Pacific Drilling Technology Conference, APDT; 1998. pp. 65-75. Paper No. 39298

[3] Potter PA. Subsea blowout preventer control systems in deep water [MSc thesis]. UK: Cranfield University; 1998

[4] API Standard 53 'Blowout Prevention Equipment Systems for Drilling Wells'. 4th ed; 2012

[5] API Specification 16A "Specification for Drill Through Equipment"; 1997

[6] API Specification 16C "Specification for Choke and Kill Systems"

[7] API Specification 16D "Specification for Control Systems for Drilling Well Control Equipment". 1st ed; 1993

[8] Bradley HB. Petroleum Engineering Handbook. Richardson, Texas, USA: Society of Petroleum Engineers; 1987

[9] API Specification 17E: 'Specification for Subsea Production Control Umbilicals, Appendix G, Test Method for Determining the Collapse Pressure of a Hose when Subject to External Hydrostatic Pressure

Chapter 4

# Bio-Based Oil Drilling Fluid Improvements through Carbon-Based Nanoparticle Additives

Yee Ho Chai, Suzana Yusup, Vui Soon Chok and Sonny Irawan

Additional information is available at the end of the chapter

http://dx.doi.org/10.5772/intechopen.74674

**Abstract**

Performance issues of vegetable oil or bio-based oil drilling fluids are generally inferior as compared to synthetic based drilling fluids. This chapter focuses largely on thermal conductivity and rheological properties of bio-based oil drilling fluid as its core issues. Unstable drilling fluids do not only incur in downtime for maintenance, but it indirectly affects production capacity as well. To overcome these issues, nanoparticles acts as additives to improve the thermo-physical traits of bio-based oil drilling fluid. The scope of this chapter focuses on dispersion of graphene oxide at very low concentration, namely 25, 50 and 100 ppm, to improve the thermal conductivity and rheological properties of bio-based oil drilling fluid. The data obtained from thermal conductivity and rheological experimental works were validated with various thermal conductivity and rheological models.

**Keywords:** bio-based oil drilling fluid, nanoparticles, thermal conductivity, rheology, graphene oxide

## 1. Introduction

Statistics have shown world energy consumption continues to experience growth rate sine year 1990 with oil, natural gas and coal remaining as the major energy consumer [1]. Market report [2] has outlined increment in drilling activities and exploration as well as development of unconventional gas reserves will meet product's demands. The report also reported key players in the oil and gas industry to shift their focus in developing nanotechnology-based

solutions to overcome technological and environmental challenges. Asia Pacific was evaluated to have the highest market growth by 5.8% from 2016 to 2024 period [2].

Drilling fluids are highly regarded as one of the most important component in any drilling operations as it acts as a heat and solid circulating system, and a lubricant. It is reported that more than half of present global oil reserves stands at 4200 m below sea level at extreme temperature and pressure conditions [3]. However, extreme temperature and pressure conditions will cause drilling fluids to deteriorate. Deterioration in drilling fluids incurs downtime for maintenance and affects production capacity indirectly. Additives such as barite and bentonite are used to maintain density, rheology, temperature stability and fluid loss control properties of drilling fluids. However, this imposes several limitations including costly treatment cost and its inability to perform under HTHP conditions. For example, oil based muds have good lubricity properties, low torque and drag resistance [4] but performs poorly in terms of fluid loss circulation and elastomer compatibility [5], expensive and proved to be costly in terms of treatments and disposal of its cuttings. In addition, contaminated oil-based muds are often disposed to the surroundings, prompting environmental pollution to the surrounding seabed life and killing off coral reefs [6, 7]. Therefore, emphasis on drilling fluid containing biodegradable and environmental-friendly properties is inexorable for the preservation of marine environment.

The need to develop an environmental friendly drilling fluid system containing desirable attributes such as low toxicity, biodegradable and environmental friendly properties are highly demanded [8]. Some of the vegetable oils considered to be prospective base fluids are rapeseed oil, sunflower oil, palm oil and groundnut oil [5]. The ester composition within vegetable oils has intrinsic ability to biodegrade at the presence of "built-in" oxygen in esters [9]. However, esters contain high viscosity properties due to the presence hydrogen bonding of –OH groups in unsaturated fatty acids [5]. However, hydrogenation process is able to convert double bonds of unsaturated fats into saturated fats, thus altering the viscosity properties of vegetable oils to be less viscous. Vegetable oils such as Jatropha oil have higher flash point, better thermal stability and lower toxic compositions are advantageous over to diesel based muds [10]. Agwu et al. [11] had proven diesel oil to be chemically unstable in pour point and fire point analysis at extreme temperatures as compared to soybean oil. While chemical modifications such as hydrogenation process converts vegetable oils into less viscous states, it cannot be denied that oil-based fluids still possess low thermal conductance. To resolve such challenges faced by ester-based drilling fluids, incorporation and assimilation of nanotechnology into bio-based drilling fluids, such as nanoparticle additives, to be able to perform equally or better than the current conventional drilling fluids.

Nanofluids are binary systems [12] consisting of a base liquid suspended with metallic or non-metallic nanoparticles that acts as a colloidal suspension within the fluid with nanoparticles at average sizes of 100 nm or less [13]. Although nanofluids are often focused towards heat transfer applications, Choi [14] had proposed an important role for nanofluids for cooling and lubrication of drilling bits in future drilling operations. Nanoparticles are known to improve the rheological, mechanical and thermal properties of a given base fluid as they have higher specific surface areas, mechanical strengths and lower melting points [15]. Comparing

http://dx.doi.org/10.5772/intechopen.74674

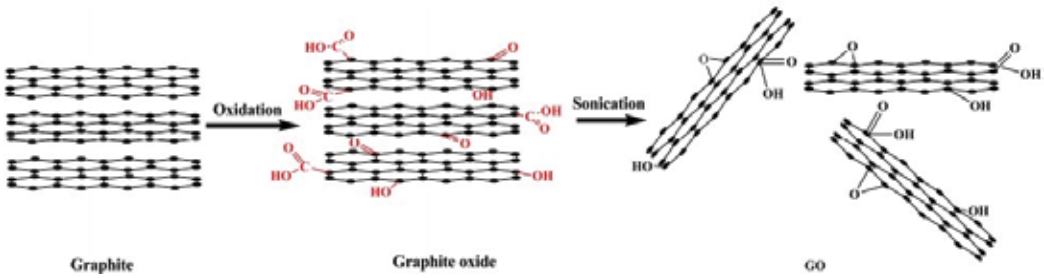


**Figure 1.** Schematic model of a graphene oxide sheet [18].

to micrometre and millimetre sized additives, nanomaterials also possess better dispersion stability, reduced pumping power [16] and clogging issues [17] In general, oil-based drilling fluids are known to possess low thermal conductance, thus requiring nanoparticle additive to achieve better conductivity properties.

Graphene oxides are heterogeneous compounds which contain oxygen groups bonded to graphene sheets via oxidation process. Oxidized from graphite, graphite oxides readily exfoliate when undergoing ultrasonic process [18] as shown in **Figure 1**. Carbonyl and carboxyl groups are attached to the basal plane of graphene oxide [19]. Interestingly, graphene oxide possesses both soluble and non-soluble behaviours, which makes it versatile for production of nanofluids with a wide range of compatibility.

Presence of oxygen atoms can lead to alteration in vibrational characteristics of scattered phonons and subsequently reduce the free mean path [20]. The reduction of mean free path of phonons can lead to reduction in thermal conductivity properties. However, Mahanta and Abramson [21] suggested oxygen atoms paved interlayer interactions that induces higher phonon frequency and contributes to thermal conductivity increment. Functionalization of oxygen-groups on graphene sheets were used to enhance stability of nanoparticle suspensions in fluids through electrostatic stabilization from the media polarity [22].

## 2. Thermal conductivity and rheological properties

Thermal conductivity enhancement is influenced by several factors, such as Brownian motion of nanoparticles, nanolayer, nanoparticle clustering and other external parameters such as volume fraction, nanoparticle size and temperature [23]. Jang and Choi [24] discovered the random motion of Brownian motion contributed to 6% of total thermal conductivity enhancement. Nanolayers shown in **Figure 2** act as a barrier for thermal conductance which lowers the overall thermal conductivity of nanofluid. There are instances where clustering of nanoparticles by Van der Waals forces induces local percolation structure that can enhance thermal conductance of nanofluids [23].

However, a fractal model developed [25] showed no changes in thermal conductivity properties of nanofluid from clustering effects as the enhancement effects are counterbalanced from

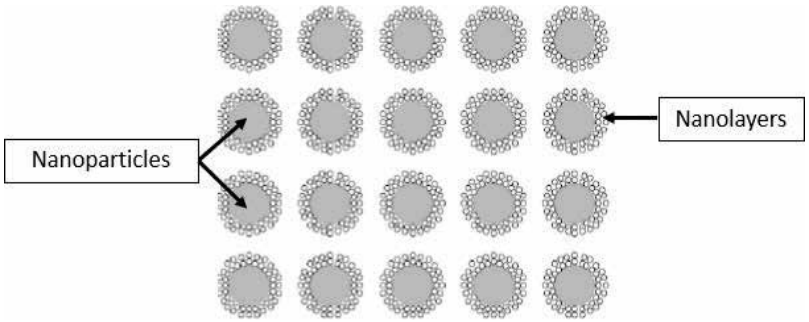


**Figure 2.** Schematic cross diagram of nanolayers at solid/liquid interface of nanoparticles and liquid [38].

reduced convection of particles. This claim was in good agreement that clustering effect performs poorly on stability and thermal conductivity of nanofluid [26].

Hadadian et al. [22] prepared different masses of graphene oxide in 50 mL of distilled water and ethylene glycol and were subjected to 15 min of ultrasonication to produce a homogenous suspension. They yielded a maximum 30% thermal conductivity enhancement with 0.07 mass fraction graphene oxide, owing to the excellent geometry of graphene oxide such as high interfacial area and comprised of sheet-like arrangements favourable for formation of a percolation structure. Ijam et al. [27] added graphene oxide nanosheets ranging from 0.01 to 0.10 wt% into deionized water to be sonicated for 10 min before further diluted with ethylene glycol to obtain deionized water/ethylene glycol mixing ratio of 60:40. Their findings showed maximum thermal conductivity enhancement of 10.47% was obtained from maximum graphene oxide loading at 45°C in which they have highlighted the effects of sheet sizes to form a percolation pathway according to the percolation theory.

It is important to know the rheological behaviour of various types of fluids. The addition of nanoparticles into base fluids can alter the liquid's thermo-physical properties. Such enhancements are useful in heat transfer applications because of the high transfer enhancement in nanofluids. Therefore, the viscosity of fluid is greatly increased even at very low nanoparticle loadings [28]. Nevertheless, high viscosity properties enable solids such as drill cuttings to be suspended at stagnant conditions and prevents sagging process [29]. The trade-off for having high fluid viscosity incurs higher pumping costs of the fluid. Vajjha and Das [30] had proven nanoparticle concentrations greater than 3 vol% increases cost of pumping. Therefore, consideration for suitable nanoparticle selection should be taken into account for certain applications such as drilling purposes. Ijam et al. [27] compared shear stress and viscosity of graphene oxide-water nanofluids and concluded viscosity to function with respect to temperature. The increase in temperature weakens the intermolecular forces between particles to lower viscosity of nanofluids. Under high shear rate, viscosity of graphene oxide-water decreases exponentially until it reaches a point where it is independent of shear rate.

However, the rheological properties of nanofluids are still widely debatable among researchers. Fluctuating results were reported by various researchers stating addition of nanoparticles gives an increment or decrement of viscosity properties of nanofluids [31]. For example,

Wang et al. [32] dispersed graphene nanoparticles at low loadings into ionanofluid and was found to possess slightly lower viscosity at higher temperatures as compared to its counterpart base fluids due to the self-lubrication of graphene nanoparticles. Lu et al. [33] concluded rheological properties to be highly dependent on nanoparticle concentrations. At very low loadings, nanofluids with Newtonian behaviours can produce shear-thinning non-Newtonian behaviour when subjected to high nanoparticle concentrations due to strong particle-particle interactions interrupted by shear rates exceeding a specific critical value.

## 3. Thermal conductivity and rheological models

### 3.1. Thermal conductivity models

Conventional thermal conductivity models are used for the prediction of thermal conductivity of nanofluids based on several main key parameters such as nanoparticle volume fraction ($\phi$), thermal conductivity of nanoparticle ($k_p$), thermal conductivity of base fluid ($k_{bf}$) and shape factor ($n$) for nanoparticle types. Effective medium theory (EMT) models, such as, Maxwell model [34], Hamilton-Crosser model [35] and Bruggeman model [36], are static models that predict based on the assumptions that particles are motionless and heat transfer between both continuous and dispersed phases are diffusive [37].

#### *3.1.1. Maxwell model*

Maxwell had developed the first EMT model to predict suspensions containing diluted particles (< 1 vol% concentration) [34]. The assumption basis of this model is that the particles are non-interacting with each other and is spherical in shape. Maxwell model is expressed as:

$$k_{nf} = \left[\frac{k_p + 2k_{bf} + 2(k_p - k_{bf}\varphi)}{k_p + 2k_{bf} - 2(k_p - k_{bf}\varphi)}\right] k_{bf} \tag{1}$$

where $k_{nf}$ is thermal conductivity of nanofluid, $k_p$ is thermal conductivity of nanoparticle, $k_{bf}$ is thermal conductivity of base fluid and $\phi$ is the volume fraction of nanoparticle. The Maxwell model was reported to predict well for relatively large particle size at micro- and millimetre scales.

#### *3.1.2. Hamilton-Crosser model*

The Hamilton-Crosser (HC) model is expressed when the thermal conductivity of particle is greater than the thermal conductivity of liquid by 100 times ($k_p/k_{bf} > 100$). The HC model is an extension of Maxwell's model which takes shape factor, $n$, of particles into account in calculation. The shape factor is defined as the ratio of surface area of the sphere with constant volume as particle to the surface area of the particle.

$$k_{nf} = k_{bf}\left[1 + \frac{k_p + (n-1)k_{bf} + (n-1)(k_p - k_{bf})\varphi}{k_p + (n-1)k_{bf} - (k_p - k_{bf})\varphi}\right] \tag{2}$$

where $n$ can be represented with $n = 3/\psi$, $\psi$ is the sphericity of the particle. Generally, n = 3 is taken for spherical particles while n = 6 is considered for cylindrical shape particles.

*3.1.3. Bruggeman model*

Unlike Maxwell model, Bruggeman model is applicable for two binary mixtures with no particle concentration limitations. However, Bruggeman model tends to deviate from Maxwell model at higher concentrations. The Bruggeman model is similar to that of Maxwell model as both models use the same assumption basis that the shape of particles are spherical. The Bruggeman model is written as follows:

$$\varphi\left(\frac{k_p - k_{eff}}{k_p + 2k_{eff}}\right) + (1-\varphi)\left(\frac{k_p - k_{eff}}{k_p + 2k_{eff}}\right) = 0 \tag{3}$$

where $\phi$ is the volume fraction of nanoparticles dispersed, $k_{bf}$ is the thermal conductivity of base fluid, $k_p$ as the thermal conductivity of nanoparticles and $k_{eff}$ as the effective thermal conductivity of nanofluid.

**3.2. Rheological models**

Rheological models are used to determine the relationships between shear stress and shear rate as different applications possess different characteristics. Non-Newtonian models such as Bingham Plastic model [39] and Power Law model [40] are commonly used to predict rheological behaviours and are considered in this study.

*3.2.1. Bingham Plastic model*

Bingham Plastic fluids are unique as it has "infinite" viscosity until adequate stress is applied to initiate flow process. The Bingham Plastic model is as follows:

$$\sigma = \sigma_0 + \mu\gamma \tag{4}$$

where $\sigma$ is the shear stress, $\sigma_o$ is the limiting shear stress, $\mu$ is the viscosity and $\gamma$ is the shear rate. The limiting shear stress is often referred to as Bingham Yield Stress of the material. This model is suitable for concentrated mixtures and colloidal systems possessing Bingham behaviours.

*3.2.2. Power Law model*

Generally known as Ostwald model, non-Newtonian materials behave with respect to shear rate to produce two effects, namely shear thinning and shear thickening. Shear thinning yield lower viscosity when subjected to higher shear rate while shear thickening contradicts. The thickening is normally associated with the increase in sample volume and is known as dilatancy. The Power Law model is as follows:

http://dx.doi.org/10.5772/intechopen.74674

$$\sigma = \mu.\gamma^n \tag{5}$$

where μ is the fluid viscosity, σ is the shear stress, γ is the shear rate and n is the power law index of the material. Shear thinning behaviour exhibits itself at n < 1 while n > 1 converts the material into a shear thickening fluid. This model is only limited to a small shear rate range as predictions from the model will deviate at a higher shear rate range.

## 4. Experimental study

### 4.1. Homogenization process

In this study, hydrogenated base oil (HBO) as base fluid and graphene oxide paste are supplied by a local company supplier. HBO is derived from vegetable oil through catalytic hydrotreating process and contains alkane chain branch between C15-C18. For the characterization of nanoparticles, graphene oxide paste was subjected to FTIR (Perkin Elmer) with wavenumber ranging from 500 to 4000 $cm^{-1}$ and TEM (Zeiss Libra 200FE) analysis at magnification range at 20,000x to 800,000x values. The HBO and graphene oxide paste were homogenized through a hydrodynamic cavitation unit at a constant flow rate of 1.5 L/min for 3 hours duration with an average of 10 bars pressure. The orifice diameter and length are 1 mm and 30 mm respectively. The schematic diagram is as shown in **Figure 3**. The hydrogenated oil-based nanofluids were transferred to an ultrasonic bath (Bath Ultrasonic Branson 8510E – DTH) for further homogenization.

### 4.2. Thermal conductivity properties analysis

Thermal conductivity analysis of hydrogenated oil-based nanofluids are carried out with KD2 Pro Thermal Properties Analyser equipped with KS-1 sensor with dimension

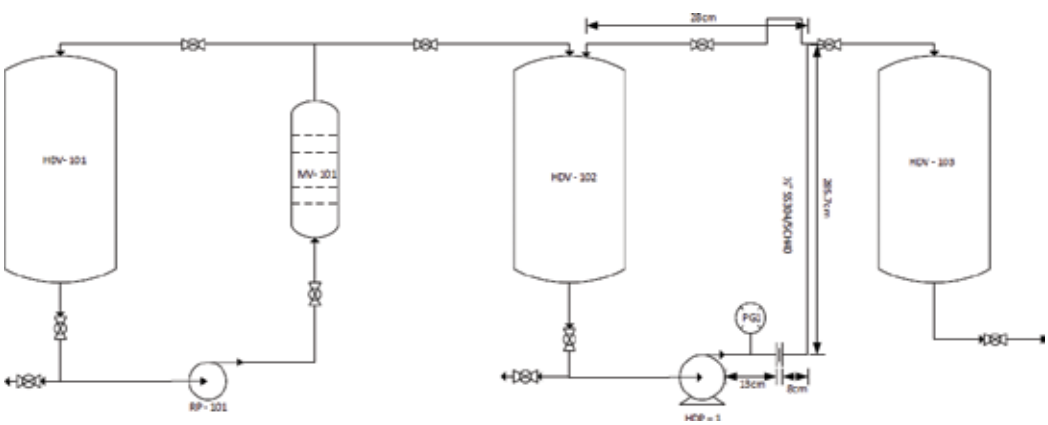


**Figure 3.** Schematic diagram of hydrodynamic cavitation unit (HDV: hydrodynamic vessel, MV: mixer vessel, PG: pressure gauge, RP: rotary pump, HDP: hydrodynamic pump).

1.3 mm diameter × 60 mm length) which complies with ASTM D5334-14 standards. The parametric studies in thermal conductivity analysis are divided into three categories, mainly the effect of temperature, the effect of nanoparticle concentrations and the effect of nanoparticle types. The temperature parameter in this study is set within the ranges of 30–50°C with a 5°C increase at each interval step. The presence of nanoparticles suspended within each sample move freely under elevated temperature, prompting fluctuations in thermal conductivity results. Therefore, each sample was repeated three times to ensure mean thermal conductivity is obtained. Further detailed explanation on the method can be found in our earlier work [48].

### 4.3. Rheological properties analysis

The parametric studies considered for the rheological properties analysis are viscosity values and shear stress values of hydrogenated base oil nanofluid with respect to shear rate and temperature. Rheological properties were measured using Malvern Bohlin Gemini II Rheometer following the method discussed in our earlier work [56].

## 5. Results and discussions

### 5.1. Characterization of graphene oxide

**Tables 1** and **2** show the product specification of graphene oxide paste and vegetable oil by the local supplier respectively.

| | |
|---|---|
| Carbon content (%) | >99.8 |
| Oxygen content (%) | <0.05 |
| Thermal conductance (W/m K) | 2800 |
| X-Y dimensions (μm) | 0.06–1 |
| Z dimensions (μm) | 0.002–0.005 |

**Table 1.** Product specification of graphene oxide paste.

| **Parameters** | **Specifications** |
|---|---|
| Density (kg/m$^3$) | 780 (at 15°C) |
| Initial boiling point (°C) | <300 |
| Final boiling point (°C) | <330 |
| Flash point (°C) | 90 |
| Kinematic viscosity (mm$^2$/s) | 2–2.6 (at 40°C) |

**Table 2.** Product specification of hydrogenated oil-based fluid.

http://dx.doi.org/10.5772/intechopen.74674

Two characterizations were used to characterize graphene oxide paste, namely FTIR analysis and TEM analysis. **Figures 4** and **5** show FTIR spectra analysis and TEM imaging of graphene oxide paste respectively.

At 3500 $cm^{-1}$ range, O-H group is present in graphene oxide as shown in **Figure 4** and is further supported by the findings of Farbod et al. [17]. Absorption peak between 1630 and

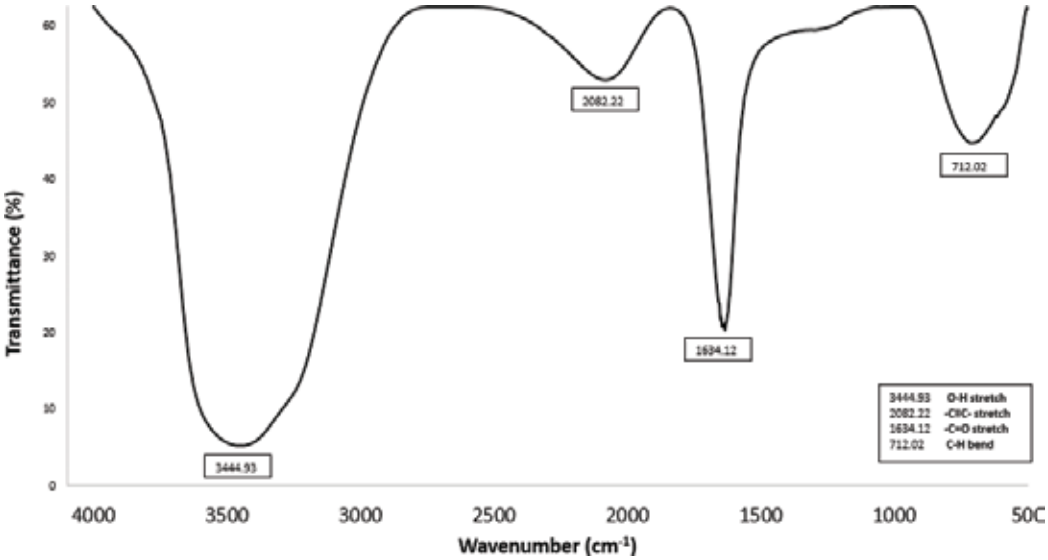


**Figure 4.** FTIR spectra analysis of graphene oxide.

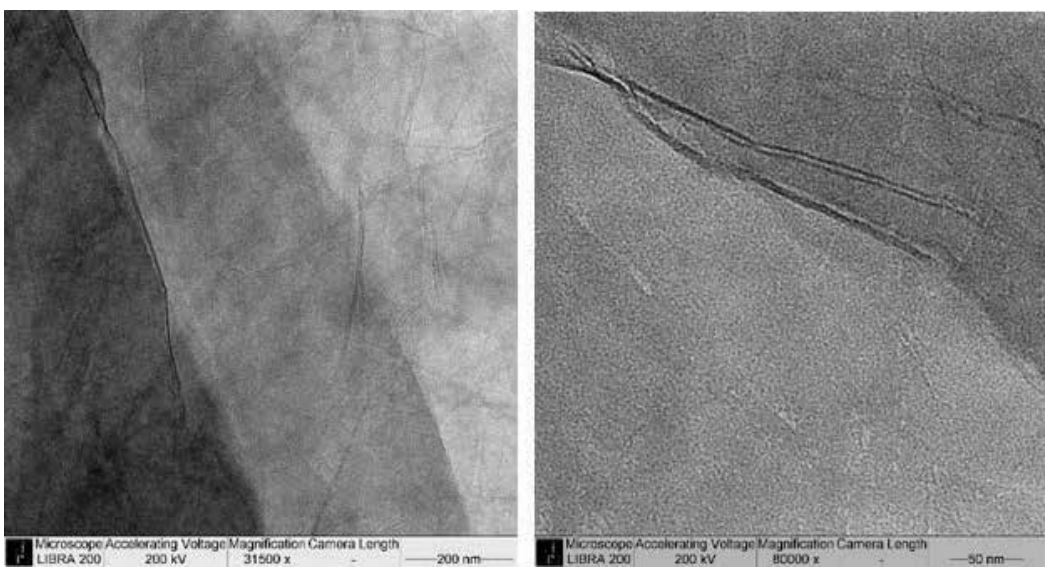


**Figure 5.** TEM image of graphene oxide at 31,500× (left) and 80,000× (right) magnifications.

1730 $cm^{-1}$ is assigned to C=O stretching of carboxylic and specific carbonyl functional groups [41]. The remaining peaks confirms the presence of carbon–carbon bonds which constitutes primarily from graphene sheets.

Stacking of graphene oxide sheets were outlined at 31,500× magnification in **Figure 5** that shows folds and bends existing on the surface of graphene oxides. Schniepp et al. [42] explained that functionalized graphene sheets are distinctively different from graphene with the attachments of epoxy, hydroxyl and carboxyl groups on graphene sheets. The attachments of these groups posed lattice defects during thermal reduction process leading to the formation of defects on the surface of graphene oxides [42].

### 5.2. Thermal conductivity analysis

The effects of temperature and nanoparticle concentrations on thermal conductivity analysis was investigated. The analysis for graphene oxides dispersed in hydrogenated oil-based fluids were carried out at temperature of 30°C, 40°C and 50°C nanoparticle concentrations at 25 ppm, 50 ppm and 100 ppm.

Thermal conductivity of hydrogenated oil-based nanofluids as shown in **Figure 6** and **Table 3** increases linearly with temperature similar to the conclusions of other researchers [21, 43]. The increased in thermal conductivity values were regarded to the effects Brownian motion and micro-convection of nanoparticles induced by at higher temperature [19]. The influences of phonons, molecular diffusion and collision, and free electrons plays a vital role in this scenario [43]. Higher temperature provides better transfer of heat with regards to high phonon vibrations while intense molecular collisions enable better thermal conductivity between nanoparticles suspended.

Furthermore, **Figure 6** highlighted the dependency of thermal conductivity with respect to nanoparticle loadings. This trend is more apparent as high particle concentration contributes to higher collision between nanoparticles which prompted better diffusion and conductance of heat [43]. The same trend can be observed from the findings of other researchers [44]. Although thermal conductivity increment rate is apparent, it does not increase anomalously. The slight fluctuations in were attributed to the clustering of nanoparticles which prompted instability of the nanofluid suspensions. The choice of base fluid with low thermal conductance influences the suspension of nanoparticles into aggregates due to the immense intermolecular attraction force at a nanoscale at increasing concentration [45]. In **Figure 6**, 100 ppm showed lower thermal conductivity as compared to 25 ppm and 50 ppm concentration at 35°C onwards. This phenomenon is regarded to clustering of nanoparticles formed from high volume concentrations resulting in nanoparticle instability in the nanofluid. Agglomerations can provide local heat percolations that improves thermal conductivity [23] at sufficient higher energy input as shown at 50°C, however, the tendency of nanoparticles clustering that leads to settling of aggregates due to lower energy input into the system will result in reduced overall thermal conductivity enhancement. Furthermore, aggregations formed leads to larger variation in particle distribution and poses stability problems at higher temperature [45]. Hence, this could also be the contributing factor to the decrease in thermal conductivity

http://dx.doi.org/10.5772/intechopen.74674

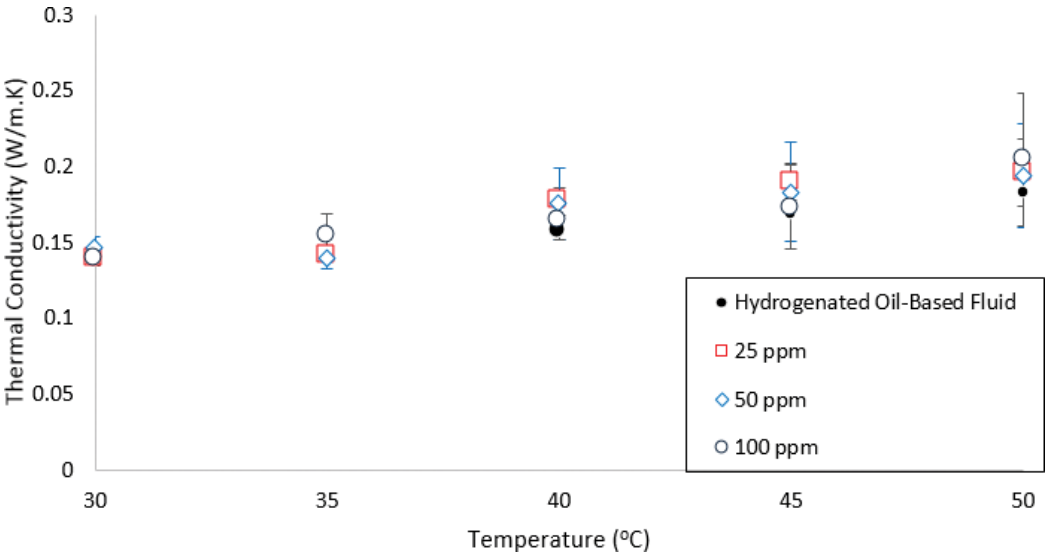


**Figure 6.** Thermal conductivity comparison of graphene oxide-hydrogenated oil nanofluid at 25 ppm, 50 ppm and 100 ppm.

| Nanofluid type | Concentration (ppm) | Temperature (°C) | Mean thermal conductivity (W/mK) | Standard deviation (W/mK) |
|---|---|---|---|---|
| Graphene oxide–hydrogenated oil | 25 | 30 | 0.1394 | 0.00518 |
| | | 35 | 0.1408 | 0.00349 |
| | | 40 | 0.1770 | 0.00914 |
| | | 45 | 0.1898 | 0.01242 |
| | | 50 | 0.1958 | 0.02191 |
| | 50 | 30 | 0.1464 | 0.00723 |
| | | 35 | 0.1396 | 0.00659 |
| | | 40 | 0.1753 | 0.02404 |
| | | 45 | 0.1830 | 0.03290 |
| | | 50 | 0.1940 | 0.03401 |
| | 100 | 30 | 0.1397 | 0.00437 |
| | | 35 | 0.1543 | 0.01409 |
| | | 40 | 0.1640 | 0.01284 |
| | | 45 | 0.1736 | 0.02755 |
| | | 50 | 0.2044 | 0.04361 |

**Table 3.** Thermal conductivity analysis of graphene oxide-hydrogenated oil based nanofluid with respect to different particle concentration and temperature.

performance at higher nanoparticle concentrations due to stability issues. Although presence of oxygen groups provides better stability and paved interlayer interactions [21] for improved thermal conductivity properties, the resulting shear pressure induced by hydrodynamic cavitation process have strained the structure of nanoparticle and in return, affects the stability of graphene oxide in this study.

The findings of this study are compared against our previous experimental work [46, 47] where graphene nanosheet and carbon nanotubes nanoparticles were selected. From **Figure 7**, graphene nanosheets have higher thermal conductivity as compared to carbon nanotube and graphene oxide by a slight margin at 50°C and 100 ppm. The high surface area to volume ratio and intrinsic thermal conductivity values of graphene nanosheets [48] contribute hugely to the increase in thermal conductivity of nanofluids at very low nanoparticle concentrations. Furthermore, larger sheet sizes attract one another and for conducting percolation pathway to conduct heat more efficiently [27], providing better thermal conductivity of graphene nanosheet and graphene oxide nanofluids as compared to carbon nanotube nanofluids.

A comparison between experimental data and the classical thermal conductivity models is shown in **Figure 8**. Similar to graphene nanosheets, graphene oxides are graphene sheets functionalized with oxide groups attached on the surface of the nanosheets. The Maxwell model is able to predict closely at 100 ppm as compared to lower particle concentrations. According to Gupta et al. [49], the contradictions between graphene nanosheets and graphene oxides is possibly influenced by different particle sizes. Gupta et al. [49] had compared the

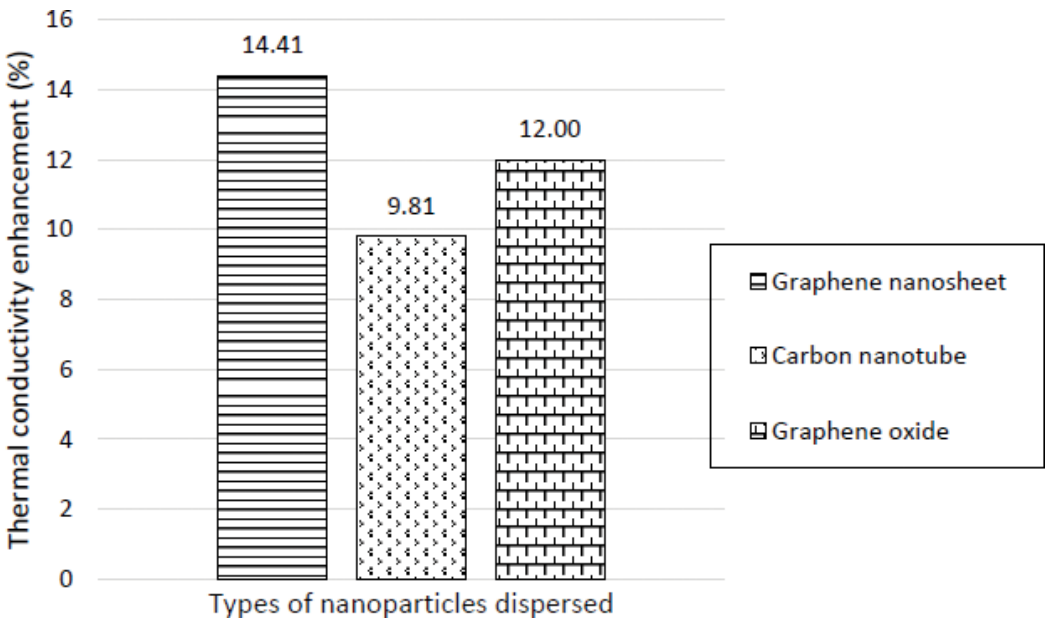


**Figure 7.** Thermal conductivity enhancement comparison between graphene nanosheets, carbon nanotubes and graphene oxide at 50°C and 100 ppm.

http://dx.doi.org/10.5772/intechopen.74674

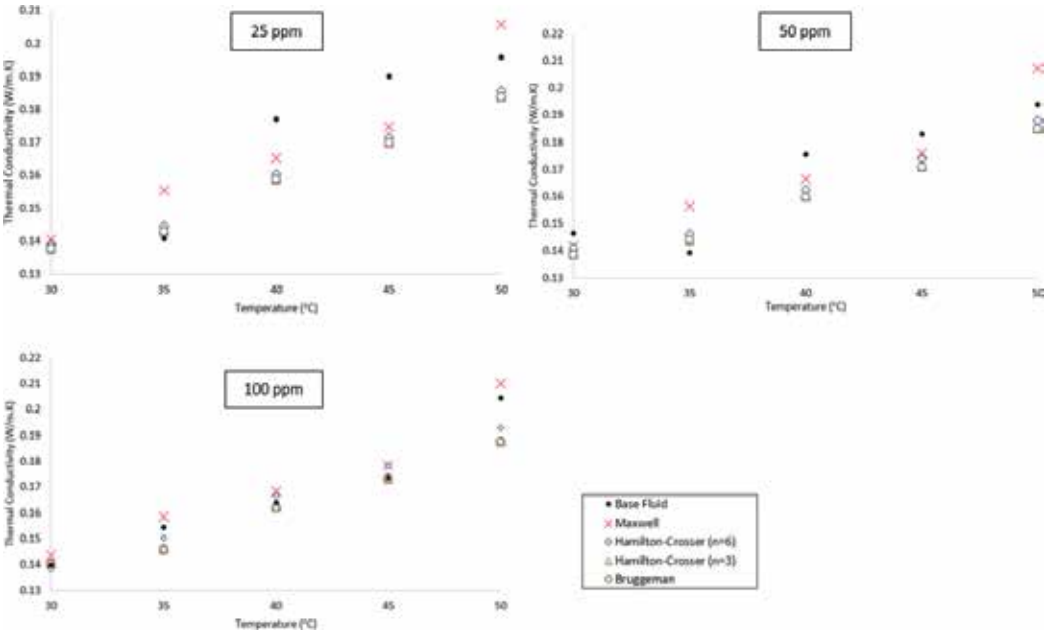


**Figure 8.** Comparison between experimental data and thermal conductivity models at 25, 50 and 100 ppm graphene oxide concentration.

sizes in their study and other researchers which lead to the conclusion of the role of particle sizes in the distribution and network formation for heat transfer. There have been various researches to improve Maxwell model with the inclusion of particle sizes [50] which can further improve the predictions of the models. In general, prediction of the models improved with respect to concentration, but consideration of higher nanoparticle concentrations should be modelled as well for a more accurate prediction by the models.

### 5.3. Rheological analysis

**Figure 9** shows the relationship of viscosity, shear rate and shear stress against the rheological behaviour of hydrogenated oil-based nanofluid. At low shear stress, Bingham fluids behave similar to a solid but flows in liquid manner when adequate stress is applied as shown in **Figure 9** (right) while Newtonian fluid will display constant viscosity regardless of the shear rate applied. From here, we can infer hydrogenated oil-based fluid to follow a non-Newtonian behaviour profile with a shear thinning behaviour.

**Figure 10** showed the comparison of viscosity profiles at 30°C, 40°C and 50°C with respect to increasing logarithmic shear rates and nanoparticle concentrations. The addition of graphene oxide does not influence the viscosity profile of pure hydrogenated oil-based fluid as shown in **Figure 9**. At higher shear rates, the viscosity of the nanofluids are closely similar at all concentrations with viscosity values overlapping each other.

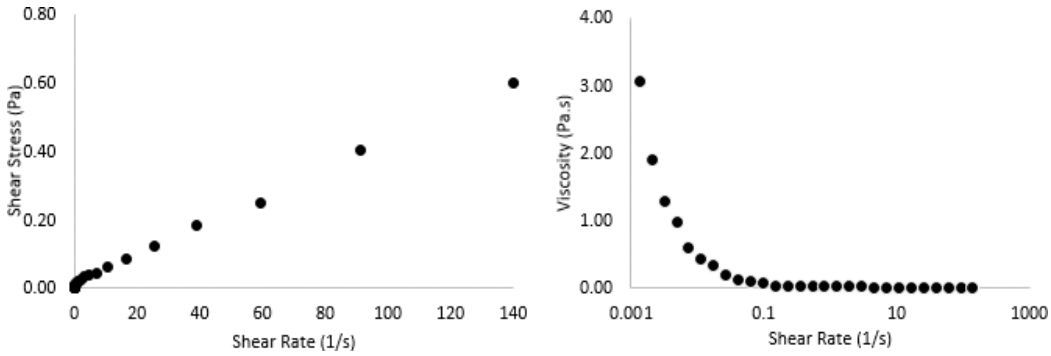


**Figure 9.** Graphical illustrations of shear stress (left) and viscosity (right) with respect to shear rate of hydrogenated oil-based fluid at 30°C.

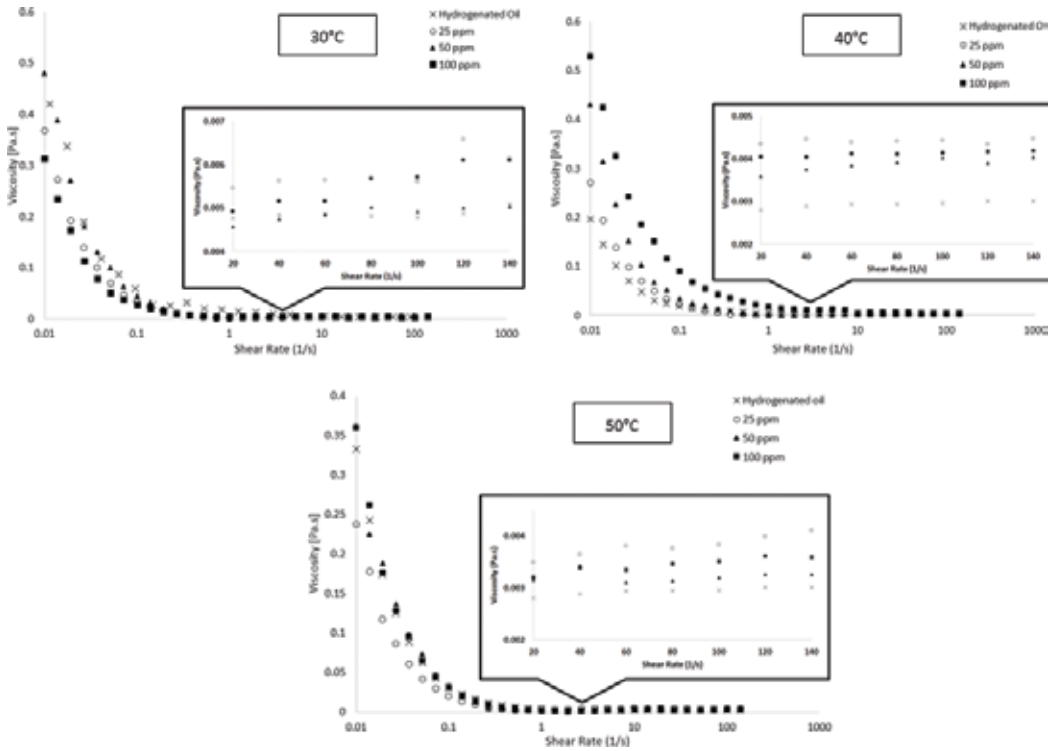


**Figure 10.** Comparison between viscosities at different concentration with respect to shear rate at 30°C, 40°C and 50°C.

At higher shear rate, the viscosity of nanofluids at various concentrations is seen decreasing exponentially towards the viscosity of the base fluid. However, upon closer inspection showed viscosity of hydrogenated oil-based nanofluids are higher compared to its base fluid counterpart. Similar to other studies carried out, the viscosity of nanofluids increases with higher concentrations but reduces when subjected to higher shear rates [51–52].

http://dx.doi.org/10.5772/intechopen.74674

Interparticle frictions increase due to higher concentrations of nanoparticle suspended, thus highlighting the fluid's resistance to flow and subsequently increased the viscosity of nanofluids [43]. Furthermore, temperature parameter plays an important role in viscosity properties. Lower viscosity values are obtained at higher temperature and vice versa for constant nanoparticle concentrations due to the influence of temperature on the intermolecular attractions between nanoparticles and base fluid's particles. Interparticle and intermolecular adhesive forces of particles decreased at higher temperature because of higher energy input into the system [53], leading to the decrease of fluid's viscosity. This phenomenon was also observed by other researchers showing the effects of temperature against viscosity of nanofluids [19].

Two different behaviours of hydrogenated oil-based nanofluids can be deduced from this study, namely shear thinning and shear thickening behaviours. The nanofluids displayed shear thinning behaviour at lower shear rate while slight shear thickening behaviour was observed at higher shear rate instead due to percolation structure effects of nanoparticles suspension in base fluid [27, 54]. At high shearing rates, the formed percolation structure is broken down to form primary particles to form higher shear stress.

The rheological behaviour of hydrogenated oil-based nanofluids over the range of 30–50°C at concentrations 25 ppm, 50 ppm and 100 ppm were compared with non-Newtonian rheological

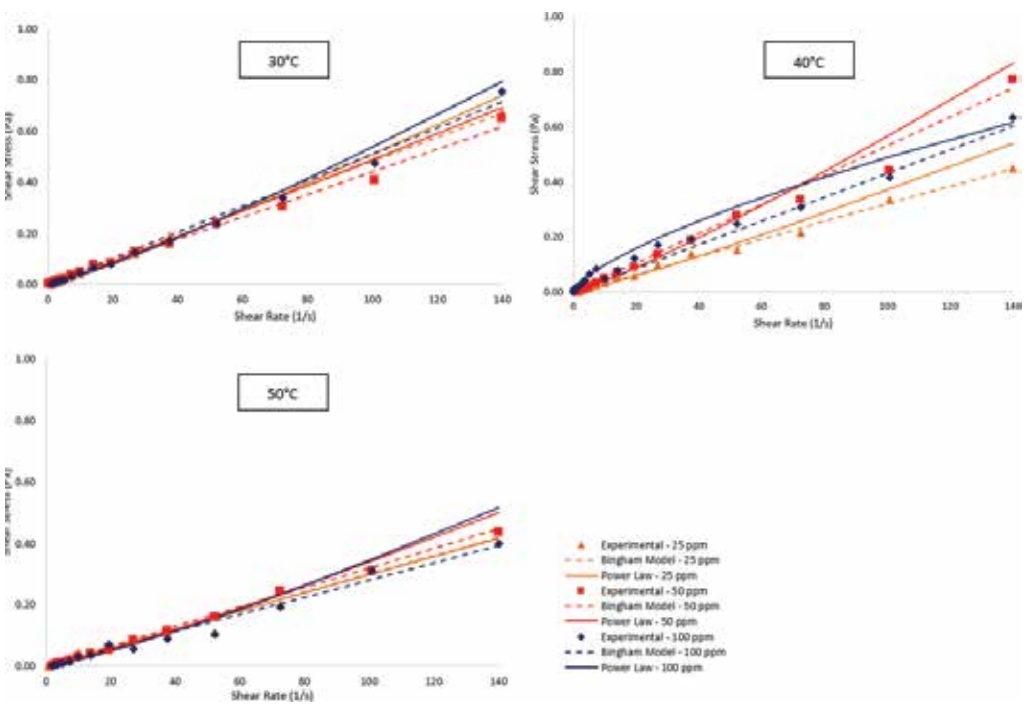


**Figure 11.** Comparison between experimental data and rheological models at different concentrations at 30°C, 40°C and 50°C.

models consisting of Bingham Plastic model and Power Law model as shown in **Figure 11** respectively. In **Figure 11**, it was observed 25 ppm concentration of graphene oxide dispersed yields the lowest shear stress while 50 ppm has the highest shear stress values at higher shear rates. A plausible explanation to this anomaly could be the increased stacking of graphene oxide sheets trapped due to the spindle's rotating movement. Comparisons have shown Bingham model gave better predictions of graphene oxide-hydrogenated oil-based nanofluids compared to Power Law model. The Power Law model over-predicted the shear stress values at higher shear rate due to the flow behaviour index at $n > 1$. Furthermore, hydrogenated oil-based nanofluid has comparatively similar yield stress values at different concentrations at higher temperatures. The rheological behaviour of hydrogenated oil-based nanofluids approaches a limit in which the shear stress values are independent to the concentration of nanoparticles at high temperature [55].

From the experimental analysis, hydrogenated oil-based fluid exhibits a non-Newtonian behaviour. Although the fluid exhibited zero shear stress at low temperature, the decreased in viscosity of hydrogenated oil-based fluid exhibited shear-thinning properties. However, the flocculation structure of nanoparticles was broken apart to form primary particle which led to slight shear thickening behaviour at higher shear rates. Similar to other findings, higher concentration of nanoparticles exhibits higher viscosity and shear stress properties but variations are insignificant upon comparison. Furthermore, the shear stress values are independent to the concentration of nanoparticles dispersed at higher temperature. The comparison between Bingham model and Power Law model showed Bingham model predicting better results data as compared to Power Law model at all concentrations, nanoparticle types and temperature.

## 6. Conclusion

In this study, graphene oxide-hydrogenated oil nanofluids were homogenized through combination of hydrodynamic cavitation and ultrasonication combination process at 25 ppm, 50 ppm and 100 ppm respectively. FTIR analysis had shown presence of large –OH groups concentration while TEM analysis shows severe defects and bends attributed to attachments of various groups on the surface. Findings have shown addition of graphene oxide into hydrogenated oil showed remarkable improvements of 12.00% in thermal conductivity enhancement at 100 ppm and 50°C. Furthermore, the rheological properties of hydrogenated oil nanofluid showed no significant changes in rheological behaviour when compared against the base fluid. Hydrogenated oil-based nanofluids have shown to possess both shear thinning and shear thickening behaviours at lower shear rates approaching higher shear rate range with increased viscosity at higher nanoparticle concentrations. Conventional thermal conductivity models were able to predict graphene oxide-based nanofluids accurately at higher particle concentration while Bingham Plastic model had shown to fit well against experimental data at all concentrations and temperature, thus proving addition of graphene oxide does not change the intrinsic behaviour of hydrogenated oil.

## Author details

Yee Ho Chai[1], Suzana Yusup[1]*, Vui Soon Chok[2] and Sonny Irawan[3]

*Address all correspondence to: drsuzana_yusuf@utp.edu.my

1 Chemical Engineering Department, Biomass Processing Laboratory, Centre for Biofuel and Biochemical Research, Institute for Sustainable Living, Universiti Teknologi PETRONAS, Perak, Malaysia

2 KL-Kepong Oleomas Sdn. Bhd, Selangor, Malaysia

3 Petroleum Engineering Department, Universiti Teknologi PETRONAS, Perak, Malaysia

## References

[1] BP Statistical Review of World Energy 2016. London, UK. 2016

[2] Grand View Research. Drilling Fluids Market Size to Reach $12.55 Billion By 2024 [Internet]. [Updated: August 2017]. Available from: http://www.grandviewresearch.com/press-release/global-drilling-fluids-market [Accessed: June 2016]

[3] Amani M, Al-Jubouri M, Shadravan A. Comparative study of using oil-based mud versus water-based mud in HPHT fields. Advances in Petroleum Exploration and Development. 2012;**4**(2). DOI: 10.3968/j.aped.1925543820120402.987

[4] Udoh FD, Itah JJ, Okon AN. Formulation of synthetic-based drilling fluid using palm oil ester derived ester. Asian Journal of Microbiology, Biotechnology and Environmental Sciences. 2012;**14**(2)

[5] Amorin R, Donsunmu A, Amankwah RK. Enhancing the stability of local vegetable oils (esters) for high geothermal drilling applications. Journal of Petroleum and Gas Engineering. 2015;**6**(8). DOI: 10.5897/JPGE2015.0215

[6] Ismail A, Kamis A. Performance of the Mineral Blended Ester Oil-Based Drilling Fluid Systems. 12-14 June; Calgary. Calgary,Alberta: Petroleum Society of Canada; 2001. p. 4. DOI: 10.2118/2001-044

[7] Al-Yasiri MS, Al-Sallami WT. How the drilling fluids can be made more efficient by using nanomaterials. American Journal of Nano Research and Applications. 2015;**3**(3):41-45. DOI: 10.11648/j.nano.20150303.12

[8] Xie S, Jiang G, Chen M, Deng H, Liu G, Xu Y, et al. An environment friendly drilling fluid system. Petroleum Exploration and Development. 2011;**38**(3). DOI: 10.1016/S1876-3804(11)60040-2

[9] Growcock FB, Patel AD. The Revolution in Non-Aqueous Drilling Fluids. April 12-14, 2011; Houston. Houston, Texas: American Association of Drilling Engineers; 2011

[10] Paswan BK, Jain R, Sharma SK, Mahto V, Sharma V. Development of Jatropha in oil-in-water emulsion drilling mud system. Journal of Petroleum Science and Engineering. 2016;**144**:10-18. DOI: 10.1016/j.petrol.2016.03.002

[11] Agwu OE, Okon AN, Udoh FD. A comparative study of diesel oil and soybean oil as oil-based drilling mud. Journal of Petroleum Engineering. 2015;**2015**:10. DOI: 10.1155/2015/828451

[12] Yu W, Xie H. A review on nanofluids: Preparation, stability mechanisms, and applications. Journal of Nanomaterials. 2012;**2012**:17 http://dx.doi.org/10.1155/2012/435873

[13] Mukherjee S, Paria S. Preparation and stability of nanofluids - A review. Journal of Mechanical and Civil Engineering. 2013;**9**(2):63-69. DOI: 10.9790/1684-0926369

[14] Choi SUS. Nanofluids: From vision to reality through research. Journal of Heat Transfer. 2015;**131**(3):9. DOI: 10.1115/1.3056479

[15] Moghaddam MB, Goshardi EK, Entezari MH, Nancarrow P. Preparation, characterization, and rheological properties of graphene-glycerol nanofluids. Chemical Engineering Journal. 2013;**231**:365-372. DOI: 10.1016/j.cej.2013.07.006

[16] Saidur R, Leong KY, Mohammad HA. A review on applications and challenges of nanofluids. Renewable and Sustainable Energy Reviews. 2016;**15**(3):1-22. DOI: 10.1016/j.rser.2010.11.035

[17] Farbod M, Ahanarpour A, Etemad SG. Stability and thermal conductivity of water-based carbon nanotube nanofluids. Particuology. 2015;**22**:59-65. DOI: 10.1016/j.partic.2014.07.005

[18] Li J, Zeng X, Ren T, Heide EVD. The preparation of grpahene oxide and its derivatives and their applications in bio-tribological systems. Lubricants. 2014;**2**(3):137-161. DOI: 10.3390/lubricants2030137

[19] Hadadian M, Goshardi EK, Youssefi A. Electrical conductivity, thermal conductivity, and rheological properties of graphene oxide-based nanofluids. Journal of Nanoparticle Research. 2014;**16**:1-17. DOI: 10.1007/s11051-014-2788-1

[20] Mu X, Wu X, Zhang T, Go DB, Luo T. Thermal transport in graphene oxide - From ballistic extreme to amorphous limit. Scientific Reports. 2014;**4**:9. DOI: 10.1038/srep03909

[21] Mahanta NK, Abramson AR. Thermal Conductivity of Graphene and Graphene Oxide Nanoplatelets. 30 May-1 June 2012; San Diego, CA, USA. IEEE; 2012. p. 6. DOI: 10.1109/ITHERM.2012.6231405

[22] Gudarzi MM. Colloidal stability of graphene oxide: Aggregation in two dimensions. Langmuir. 2016;**32**(20):5058-5068. DOI: 10.1021/acs.langmuir.6b01012

[23] Aybar HŞ, Sharifpur M, Azizian MR, Mehrabi M, Meyer JP. A review of thermal conductivity models for nanofluids. Heat Transfer Engineering. 2015;**36**(13):1085-1110. DOI: 10.1080/01457632.2015.987586

[24] Jang SP, Choi SUS. Role of Brownian motion in the enhanced thermal conductivity of nanofluids. Applied Physics Letters. 2004;**84**(21):4316-4318. DOI: 10.1063/1.1756684

[25] Wu C, Cho TJ, Xi J, Lee D, Yang B, Zachariah MR. Effect of nanoparticle clustering on the effective thermal conductive of concentrated silica colloids. Physical Review. 2010;**81**:7. DOI: 10.1103/PhysRevE.81.011406

[26] Murshed SS, de Castro C, Lourenço MJV. Effect of surfactant and nanoparticle clustering on thermal conductivity on aqueous nanofluids. Journal of Nanofluids. 2012;**1**(2):175-179. DOI: 10.1166/jon.2012.1020

[27] Ijam A, Saidur R, Ganesan P, Golsheikh AM. Stability, thermo-physical properties, and electrical conductivity of graphene-oxide/deioinized water/ethylene glycol based nanofluid. International Journal of Heat and Mass Transfer. 2015;**87**:92-103. DOI: 10.1016/j.ijheatmasstransfer.2015.02.060

[28] Mishra PC, Mukherjee S, Nayak SK, Panda A. A brief review on viscosity of nanofluids. International Nano Letters. 2014;**4**(4):109-120. DOI: 10.1007/s40089-014-0126-3

[29] Agarwal S, Phuoc TX, Soong Y, Martello D, Gupta RK. Nanoparticle-stabilised invert emulsion drilling fluids for deep-hole drilling of oil and gas. The Canadian Journal of Chemical Engineering. 2013;**91**(10):1641-1649. DOI: 10.1002/cjce.21768

[30] Vajjha RS, Das DK. A review and analysis on influence of temperature and concentration of nanofluids on thermophysical properties, heat transfer and pumping power. International Journal of Heat and Mass Transfer. 2012;**55**(15-16):4063-4078. DOI: 10.1016/j.ijheatmasstransfer.2012.03.048

[31] Ruan B, Jacobi AM. Ultrasonication effects on thermal and rheological properties of carbon nanotube suspensions. Nanoscale Research Letters. 2012;**7**(127):14. DOI: 10.1186/1556-276X-7-127

[32] Wang F, Han L, Zhang Z, Shi J, Ma W. Surfactant-free ionic liquid-based nanofluids with remarkable thermal conductivity enhancement at very low loading of graphene. Nanoscale Research Letters. 2012;**7**(314):7. DOI: 10.1186/1556-276X-7-314

[33] Lu G, Duan YY, Wang XD. Surface tension, viscosity, and rheology of water-based nanofluids: a microscopic intepretation on the molecular level. Journal of Nanoparticle Research. 2014;**16**(2564):11. DOI: 10.1007/s11051-014-2564-2

[34] Maxwell J. A Treatise on Electricity and Magnetism. 1st ed. Oxford, UK: Clarendon Press; 1873. pp. 360-366

[35] Hamilton R, Crosser O. Thermal conductivity of heteregenous two-component systems. Industrial & Engineering Chemistry Fundamentals. 1962;**7**:187-191

[36] Bruggeman D. Berechnung verschiedener physikalischer Konstanten von heterogenen Substanzen. I. Dielektrizitätskonstanten und Leitfähigkeiten der Mischkörper aus isotropen Substanzen. Annals of Physics. 1935;**416**(7):636-664

[37] Lee JH, Lee SH, Choi CJ, Jang SP, Choi SUS. A review of thermal conductivity data, mechanisms and models for nanofluids. International Journal of Micro-Nano Scale Transport. 2010;**1**(4):269-321. DOI: 10.1260/1759-3093.1.4.269

[38] Yu W, Choi SUS. The role of interfacial layers in the enhanced thermal conductivity of nanofluids: A renovated Maxwell model. Journal of Nanoparticle Research. 2003;**5**(1-2): 167-171. DOI: 10.1023/A:1024438603801

[39] Bingham E. Fluidity and Plasticity. New York: McGraw-Hill Book Co.; 1922

[40] Skelland A. Non-Newtonian Flow and Heat Transfer. New York: John Wiley and Sons; 1967

[41] Loryuenyong V, Totepvimarn K, Eimburanapravat P, Boonchompoo W, Buasri A. Preparation and characterization of reduced graphene oxide sheets via water-based exfoliation and reduction methods. Advances in Material Science and Engineering. 2013;**2013**:5. DOI: 10.1155/2013/923403

[42] Schniepp HC, Kudin KN, Li JL, Prudhomme RK, Car R, Saville DA, et al. Bending properties of single functionalized graphene sheets probed by atomic force microscopy. ACS Nano. 2008;**2**(12):2577-2584. DOI: 10.1021/nn800457s

[43] Ahammed N, Asirvathama LG, Titus J, Bose JR, Wongwises S. Measurement of thermal conductivity of graphene-water nanofluid at below and above ambient temperatures. International Communications in Heat and Mass Transfer. 2016;**70**:66-74. DOI: 10.1016/j.icheatmasstransfer.2015.11.002

[44] Keblinski P, Phillpot S, Choi SUS, Eastman J. Mechanisms of heat flow in suspensions of nano-sized particles (nanofluids). International Journal of Heat and Mass Transfer. 2002;**45**(4):855-863. DOI: 10.1016/S0017-9310(01)00175-2

[45] Li CC, Hau NY, Wang Y, Soh AK, Feng SP. Temperature-dependent effect of percolation and Brownian motion on the thermal conductivity of TiO2-ethanol nanofluids. Physical Chemistry Chemical Physics. 2016;**18**:15363-15368. DOI: 10.1039/C6CP00500D

[46] Chai YH, Yusup S, Chok VS, Arpin MT, Irawan S. Investigation of thermal conductivity of multi walled carbon nanotube dispersed in hydrogenated oil based drilling fluids. Applied Thermal Engineering. 2016;**107**:1019-1025. DOI: 10.1016/j.applthermaleng.2016.07.017

[47] Chai YH, Yusup S, Chok VS, Arpin MT, Irawan S. Thermophysical properties of grpahene nanosheets-hydrogenated oil based nanofluid for drilling fluid improvements. Applied Thermal Engineering. 2017;**122**:794-805. DOI: 10.1016/j.applthermaleng.2017.05.012

[48] Ma W, Yang F, Shi J, Wang F, Zhang Z, Wang S. Silicone based nanofluids containing functionalized graphene nanosheets. Colloids and Surfaces A: Physiochemical and Engineering Aspects. 2013;**431**:120-126. DOI: 10.1016/j.colsurfa.2013.04.031

[49] Gupta SS, Siva VM, Krishnan S, Sreeprasad T, Singh PK. Thermal conductivity enhancement of nanofluids containing graphene nanosheets. Journal of Applied Physics. 2011;**110**(8):6. DOI: 10.1063/1.3650456

[50] Li FC, Yang JC, Zhou WW, He YR, Huang YM, Jiang BC. Experimental study on the characteristics of thermal conductivity and shear viscosity of viscoelastic-fluid based nanofluids containing multiwalled carbon nanotubes. Thermochimica Acta. 2013;**556**:47-53. DOI: 10.1016/j.tca.2013.01.023

[51] Buongiomo J, Venerus DC, Prabhat N, McKrell T, Townsend J, Christianson R, et al. A benchmark study on the thermal conductivity of nanofluids. Journal of Applied Physics. 2009;**106**(9). DOI: 10.1063/1.3245330

[52] Kole M, Dey TK. Investigation of thermal conductivity, viscosity, and electrical conductivity of graphene based nanofluids. Journal of Applied Physics. 2013;**113**(8):084307-01-084307-8. DOI: 10.1063/1.4793581

[53] Thomas S, Sobhan CB. A review of experimental investigations on thermal phenomena in nanofluids. Nanoscale Research Letters. 2011;**6**(1):377. DOI: 10.1186/1556-276X-6-377

[54] Kinloch IA, Roberts SA, Windle AH. A rheological study of concentrated aqueous nanotube dispersions. Polymer. 2002;**43**(26):7483-7491. DOI: 10.1016/S0032-3861(02)00664-X

[55] Baratpour M, Karimipour A, Afrand M, Wongwises S. Effects of temperature and concentration on the viscosity of nanofluids made of single-wall carbon nanotubes in ethylene glycol. International Communications in Heat and Mass Transfer. 2016;**74**:108-113. DOI: 10.1016/j.icheatmasstransfer.2016.02.008

[56] Chai YH, Yusup S, Chok VS, Arpin MT. Rheological behaviour of graphene nano-sheets in hydrogenated oil-based drilling fluid. Procedia Engineering. 2016;**148**:49-56. DOI: 10.1016/j.proeng.2016.06.490

Chapter 5

# Solid Control System for Maximizing Drilling

Sonny Irawan and Imros B. Kinif

Additional information is available at the end of the chapter

http://dx.doi.org/10.5772/intechopen.76149

**Abstract**

This chapter focuses on the development of solid control system that is suited for drilling 12.25-inch hole. The first part discusses the performance of rate of penetration (ROP), equivalent circulating density (ECD) and drill string drag while the second part of the chapter discusses about the effect of solid control system performance to mud properties plastic viscosity (PV), yield point (YP), and low gravity solid (LGS). The input parameters were gathered from two different set up of solid control systems that were used in Well A and Well B. The result is mainly based on the performance of original solid control system new design vs. old design. Installation of distributor tank and channeling the mud to respective shale shakers significantly enhanced the system and operational performance. The ROP at 12.25-inch drilling was improved by 20%. New design, on an average, improved the ECD margin by reducing additional pressure exerted using original mud from 4.9 to 2.9%. High ECD margin is not recommended because it can break the weak formation. Mud properties while drilling the 12.25-inch hole section; PV, YP and LGS values were improved by 14, 17, and 25% respectively.

**Keywords:** solid control, 12.25-inch hole, ROP, ECD, mud rheology, LGS

## 1. Introduction

The effective performance of solid control equipment is to remove drilled solids from the drilling mud which acts as a key factor to have good mud properties [1]. Solid and particles that are not removed during the circulation will remain in the system and lead to reduction of size that may increase the difficulty on removing process using mechanical solid control equipment (SCE). Mud properties must be maintained within the acceptable specification to allow efficient cutting transport to surface [2]. Quantities of high solid content present in mud

always perceived as a vital factor affecting the operation efficiency and equipment wear issues. Ineffective solid control system and inadequate understanding of mud properties create additional risk and uncertainties to downhole condition. Drilling the 12.25 hole section using old design solid control system produced unequal distribution of the mud flow over the shakers screen. The mud flow only concentrated at middle shale shaker that connected to flow line while the others shaker received minimal flow. This situation tends to be overloaded only in the middle shale shaker unit. In rig site practice, the shakerman adjusting the baffle plate at possum belly increases the flow. However, it increased mud losses through the solid control unit and continuous plugging of the mesh in the solid control unit. Due to ineffective shale shaker and overflow of mud at possum belly, the flow was bypassed to prevent mud surface losses but it plugged the apex cones of hydrocyclone. By-passed the shale shaker unit result high drilled solids content circulated back and not remove from the system. Mud properties, such as YP, PV and LGS, were studied to investigate the significant effect of poor solid control system processing toward the performance of ROP, ECD and drag. This investigation evaluated the performance of solid control equipment before and after the introduction of mud flow distributor tank for mud return from the well while drilling the 12.25 inch hole. The methods used were gathering from various sources including case study on the rig operation, reports, personnel experience, publication and discussion for drilling the 12.25-inch hole section. The theory and literature review related to solid control system, mud properties and correlation to drilling operation also were studied to gain previous research related to the problem. Solid control system was then redesigned to investigate its affect toward mud properties and operation

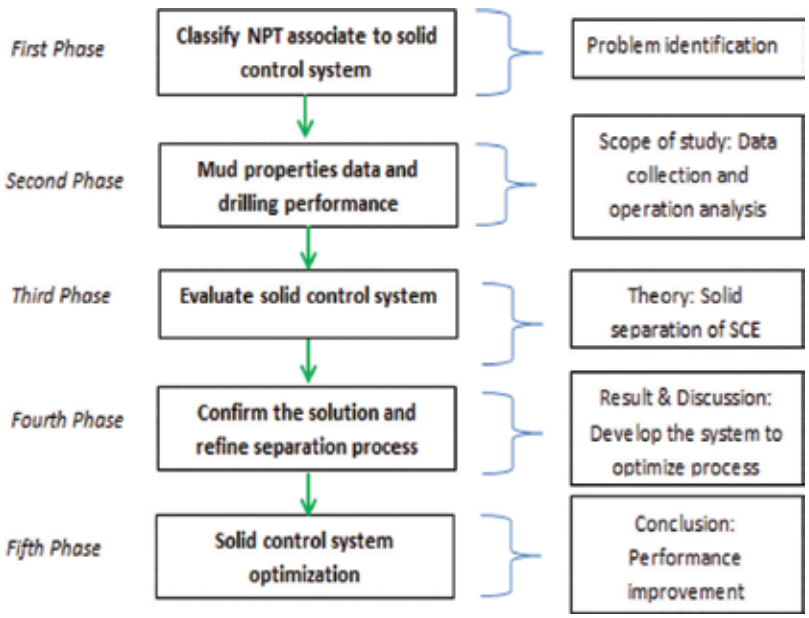


**Figure 1.** Solid control phases diagram. (Note: Personal experience).

http://dx.doi.org/10.5772/intechopen.76149

performance. Comprehensive analysis was made to discuss the relation of poor solid control system, mud properties and drilling operation (**Figure 1**).

## 2. Solid content and mechanical solid control system

The commercial solids (barite) and non-commercial solid (drilled cuttings) are two primary sources of solid particles that exist during drilling. Solid that are concentrated in the mud are classified either based on specific gravity (SG) or density and particle size. Solid SG higher than 4.2 (weight material) are categorized as high-gravity solid (HGS) while solid with SG 1.6 to 2.9 (average 2.6) is categorized as low-gravity solid (LGS) **(Figure 2).**

The solid control system sequence consists of shale shakers, hydrocyclones (desander and desilter) and centrifuge. Each mechanical equipment work independently depends on the solid particles sizes. The equipment is connected in series, and each stage of processing performance is partly dependent upon the previous equipment. By-passing the shaker screen is not recommended because failure to discard the solid particles at the shale shakers unit would overload the downstream equipment. Drilled solids that are not removed during the first circulation through the surface equipment are always subject to mechanical degradation [3]. The smaller the particle, the greater the surface area may develop, and it is causing greater effect to the mud system (**Figures 3** and **4**).

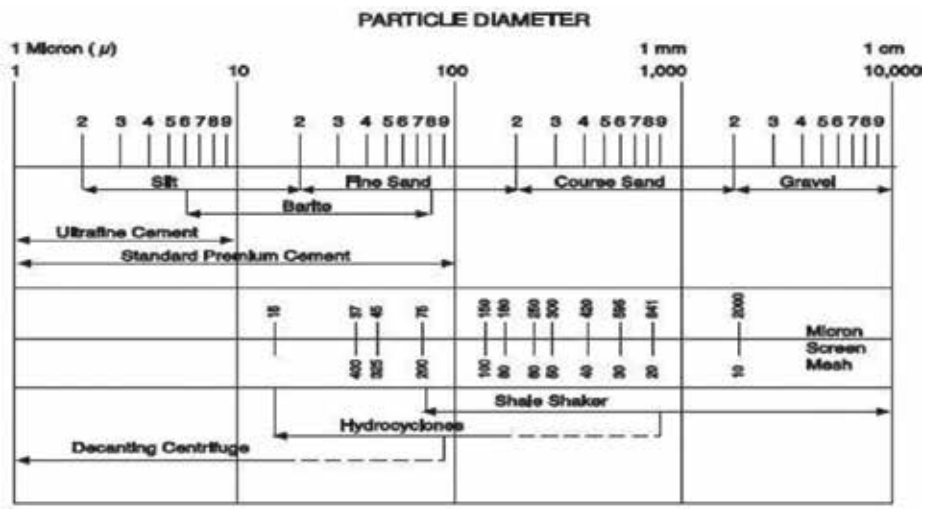


**Figure 2.** Particle diameter [7].


**Figure 3.** Old design solid control system.

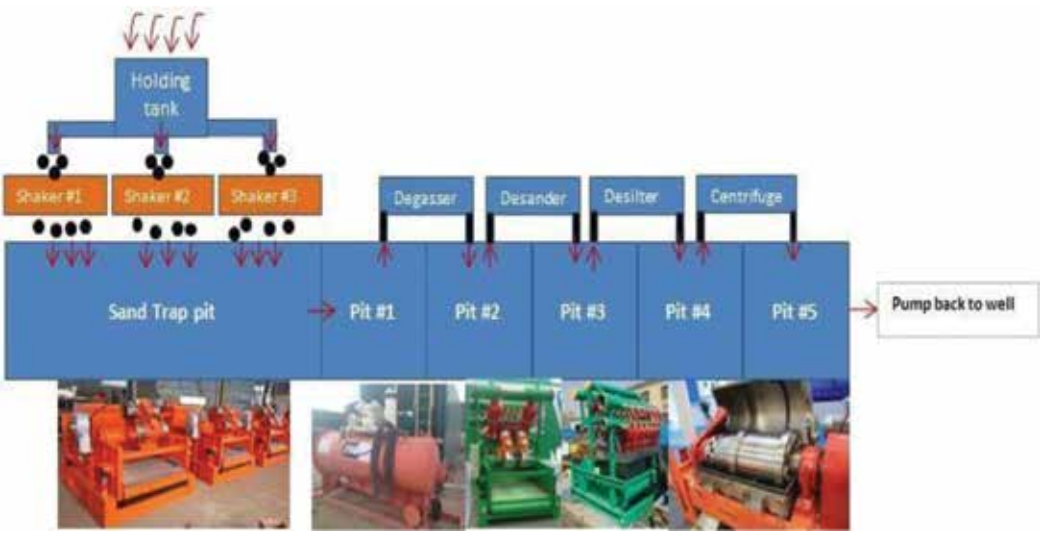


**Figure 4.** New design solid control system. (Note: **Figures 3** and **4** is based on personal experience).

## 3. Development of solid control equipment

During drilling operation, the circulated mud carries drilled cuttings to surface. These solids are then treated at mechanical solid control system by separating them from the mud according to the particles size. In this chapter, the research focuses on maximizing the efficiency of equipment performance and separation because the old design was inefficient to remove the solid from the mud. The flow line distributor was installed at the end of return line to the

shale shakers and replaced the high-pressure hose to rigid piping system for reducing pressure loss due to vibration. This system allows the solids containing drilling mud to be divided equally between the desire numbers of shale shakers. Mud circulation without any reduction in solid concentration may thicken the fluid viscosity and develops resistance to flow character of the mud. This brings to the changes in its density, rheology and other properties. The utmost advantage is to remove as much solids practically to reduce down time which contributed from plug flow lines, fluid end repair, drill string erosion and re-drilling of solids as drilling fluid recycles itself through the mud system loop [1].

### 3.1. Effect of solid particles on MW

Density or MW is measured and expressed in pounds per gallons (lb/gal), pound cubic feet ($lb/ft^3$) and grams per cubic centimeter ($g/cm^2$). It is an important property to maintain the well hydrostatic and prevent gas influx migration into the wellbore. Some of weight material such as barite and hematite are added into the mud to increase the mud weight. Mud in the wellbore column must exert a greater pressure than the fluids in porous rocks that are penetrated by the bit. The pressure exerted by the drilling mud at any depth or gradient of pressure is related to its density. Denser or viscous mud may exert excessive pressure to the wellbore and causing loss of circulation.

### 3.2. Effect of solid particles on well bottom-hole pressure

High solid content ultimately can increase the density and viscosity of the mud. Hence, it exposes the well to high BHP and mud properties contamination. Moreover, high horse power is also required to break up the gel and pump the mud for circulation. This not only triggers to hydraulic fracturing effect but also induces the tendency of mud losses into the formation. Under the primary well control requirement, the mud density must be formulated to compensate the desire BHP either meet or exceed the pore pressure of the rock formation. Failure to control the build of solid and regrinding the same drilled cutting may increase the mud surface area become very difficult to remove using mechanical solid control equipment. High solids are abrasive and can increase filter cake thickness. The higher of filter cake, the higher chances of drill string to get stuck due to differential sticking effect. Thin and impermeable filter cake is important to reduce contact area across the drill string.

### 3.3. Effect of solid particles on PV

PV is a function of solids concentration, size and shape of the solid particles and viscosity of liquid phase [4]. It is regarded as a guide to solid control for field application [5]. PV is directly proportional to the increasing of solid volume percentage, or if the volume percent remains constant, the size of the particles decreases. Decreasing particle size may increases surface area that leads to fractional drag problem. This plastic viscosity is sensitive to the concentration of solid and depends largely on the bulk volume of solids in the mud [6]. A low PV implies lower ECD exerted at bottom while high PV trigger to an increase of ECD because high pumping pressure is needed to break the gel. YP/PV ratio is a significant indicator of drilling fluid condition, low ratio indicates smaller tendency for gas cutting, swabbing pressure and greater settling velocity of cuttings whereas high ratios indicate coagulation and

flocculation [7]. Removal of drilled solids from a drilling fluid will decrease plastic viscosity, and if this solid remains in the fluids, it will grind into smaller and more numerous particles which increases plastic viscosity and decreases drilling performance [8].

### 3.4. Effect of solid particle on YP

YP is the initial resistance of the fluids to flow caused by the electrochemical forces between the particles. It is also expected to be a function of the solid concentration of the solids and those factors, such as surface charges and potential, which affect the interparticle forces [9]. YP and gel strength should be low enough to allow sand and shale cuttings to settle out and entrained gas to escape, minimize swabbing effect during pulling the string out of hole and permit the circulation to be started at low pump pressure [10]. Efficient elimination of drilled solids right after the fluid leaves the annulus was the best solution to avoid drilling fluid-cutting interaction that subsequently can increase the fluid density [11]. A change in the PV of drilling mud can cause small changes in YP. Therefore, it is always important to keep the viscosity of a mud from getting too low. The mud should have minimum viscosity properties to lift the cuttings from bottom of the hole to surface. The mud must capable to keep the weighting material and drilled cuttings in suspension while circulating or stop pumping. Normal reaction in the event of poor cutting transport is to increase the YP of the mud. However, the significant increase in YP may result poor performance of the finest mesh at shaker screen. Changing the mesh screen to a coarser screen decreases the quantity of drilled solid that can be removed [12].

### 3.5. Effect of solid particle on ROP

Rheological and filtration properties become difficult to control when the concentration of drilled solid become excessive [1]. High particulate solids in the mud reduce ROP because of increase in mud density and viscosity. The higher the mud density, the greater the differential pressure exerts. ROP decreases when differential pressure increases. Lower mud density may decrease the dynamic chip hold down and permitting faster RPM. Low viscosity mud promotes fast penetration because of good scavenging of drilled cuttings. Despite applying more WOB and RPM can comfortably achieve the desire ROP, but drilling with contaminated mud properties decreases in ROP in a long run. Darley mentioned that low concentration of noncolloidal drilled solid below 4% capable to maintain ROP at high level [3]. Mud properties such as PV and yield stress/gel strength showed that although these properties have effects on ROP, but not very significant, only annular pressure losses seemed to drastically affect the ROP which is directly related to ECD [5].

### 3.6. Effect of solid particle on drag and ECD

The fluid rheology plays an important role for solid transport and optimizes the hole cleaning [14]. The best way to pick solid is with a low viscosity fluid in turbulent flow. Hole cleaning can be optimized by the use of drilling mud with low gel strength and with low viscosity within the shear rates exposed to the annular flow [13]. In situations where ECD is not a limiting factor, high viscosity fluids with high YP/PV ratios are preferred. Under situation where ECD is a limiting factor, the use of thin fluids in turbulent flow should be considered. Driller must ensure the ECD as well as its static density is within the safe limit. ECD is the effective

density of a moving fluid and slightly more than the static density because of the friction pressure drop in the annulus. ECD depends on the pump rates and fluid viscosity. Therefore, regulation of ECD within limits means keeping viscosity low. The main cause of elevated viscosity is low gravity solid (LGS) increased. Close monitoring on solid control equipment must be performed to ensure that LGS are kept to a minimum [14].

## 4. Methodology

### 4.1. Setup of solid control system

The solids control comprises of three: shale shakers, hydrocyclones (Desander and Desilter), and centrifuge. The introduction of flow distributor tank at the end of the flowline and

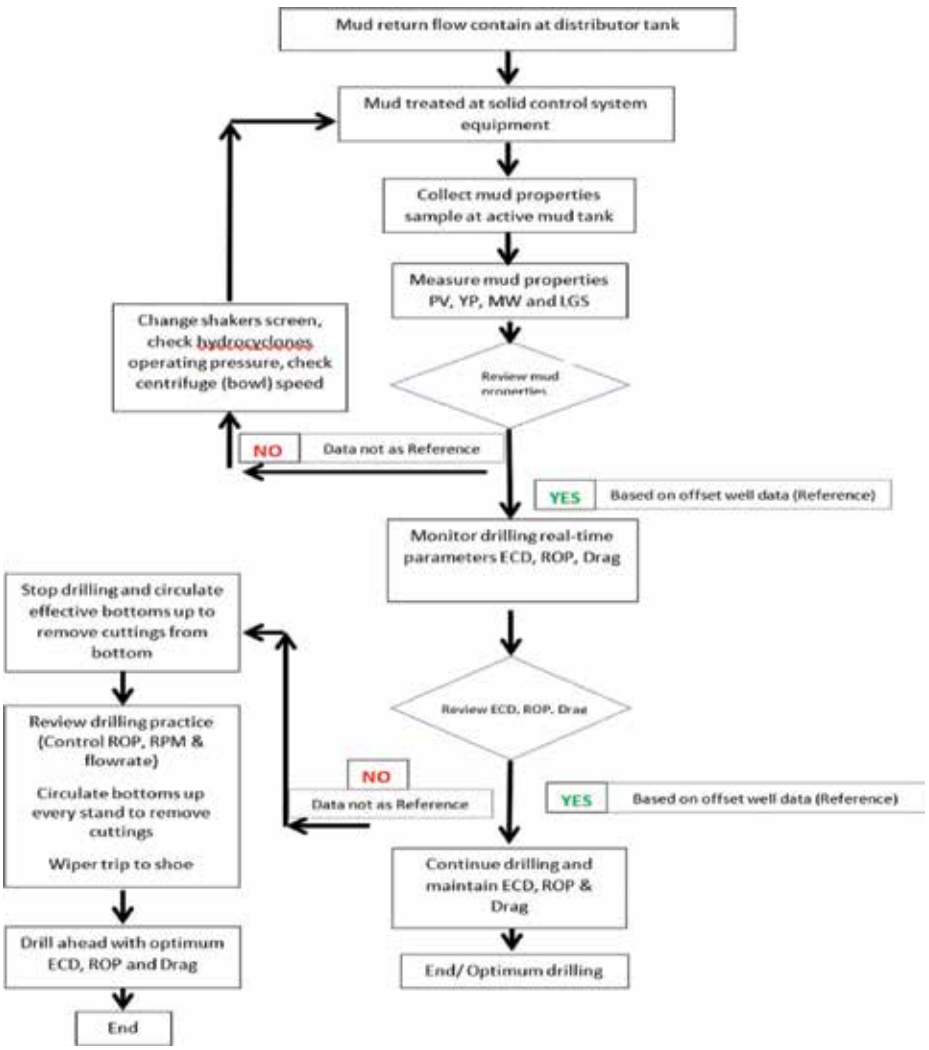


**Figure 5.** Flow diagram of the methodology. (Note: Based on personal experience).

redistribute the mud through lines to respective shale shakers is designed to optimize the mud flow performance. This improvement minimized the tendency of shale shakers overflow and reduced processing overloading (**Figure 5**).

### 4.2. Data acquisition and measurement

Data collection and evaluation of the mud properties include PV, YP and LGS. These measures are used as a tool to evaluate the efficiency of the mechanical equipment. The drilling parameters including ECD and ROP are obtained from real-time downhole acquisition tool. Drill string drag is recorded after each drill pipe connection to monitor the hole condition. Mud parameters and drilling data are correlated to oversee the drilling performance. Gradual changes in mud properties such as high ECD and poor ROP are significantly reflect to the ineffective of solid control system.

## 5. Results and discussion

Field data are obtained from onshore drilling in Borneo Block. All data are obtained from two different wells with similar lithology called Well A and Well B. The Well A was drilled using original solid control system while Well B was drilled with New developed design. The performance of both systems was compared while drilling the 12.25 inch section. A total of 40 mud samples were collected and measured to evaluate the PV, YP and LGS. These results act as a preliminary step to investigate the performance of the mud on ROP, ECD and drill string drag to justify the performance of the new design in this analysis.

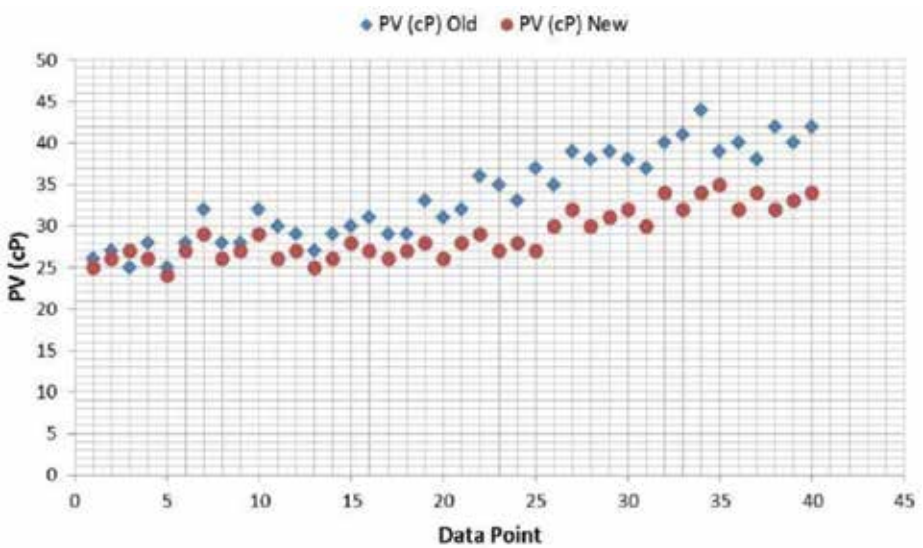


**Figure 6.** YP (lbs/100 ft²) vs. data point. (Note: Based on personal experience).

### 5.1. Performance of solid control system on plastic viscosity

**Figure 6** shows the tabulated PV of new design and old design solid control system. At the start of drilling operation, PV for both systems performed on the same trend. This reflects the solid separation and treatment was working effectively. As drilling deeper at Well A with old system and more drilled cuttings excavated, the mud viscosity was getting thicker that resulted the PV to gradually increase. Increase of PV is subjected to drilling the Well B with new system design had improved the solid removal processing by 14% as compared to old design. The performance of new system was economical and reliable as system capability justifies it to maintain the PV reading throughout the operation. The inability of the old design to eliminate rapid development of mud contamination significantly leads to overloading works at downstream equipment which increase solid contents in the drilling mud. Frequent mesh screen plugging, discharge rope from the hydrocyclone and solid recirculation contributed to poor solid removal and PV increment. Spray discharge was not achieved because the old design utilized high pressure hose as a suction line to desander and desilter. Pressure generated to feed the mud into desander and desilter through suction hose caused vibration, pressure loss and inconsistent mud flow.

### 5.2. Performance of solid control system on yield point

**Figure 7** shows the tabulated YP for old design and new design. The YP of old design gradually increased because solid in the drilling mud was not properly discarded while drilling well A. Mud overflow on the shale shakers was frequently observed, and occasionally the

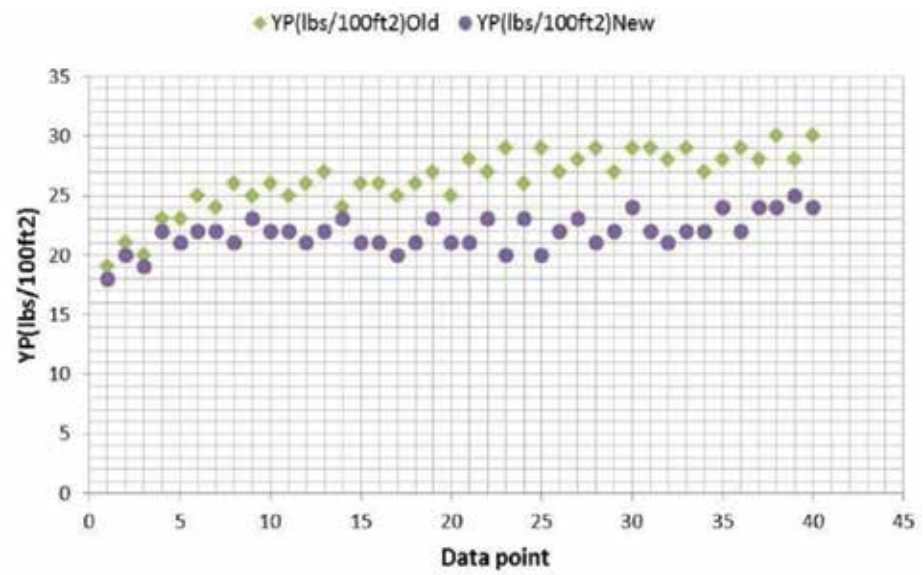


**Figure 7.** YP (lbs/100 ft$^2$) vs. data point. (Note: Based on personal experience).

unit was bypassed to minimize the surface losses. By passing the solid control unit significantly overload the downstream mechanical equipment and result the equipment incapable to remove the solid efficiently. Changes in low shear rate viscosity reflect to the mud YP. In this condition, colloidal clay platelets link together (flocculate) with consequent increase in their specific surface area. When mud is at static condition, the mud contains high solid and becomes attractive and repulsive. Stable and consistent mud flow distribution to shale shakers was helpful in controlling the YP build up. The ability of the new design to maintain the YP showed that the solids were properly separates by the system and result in low pressure loss while the drilling mud was circulated. Consistent value of YP at new design while drilling the section typically provides good cutting carrying capacity (CCC) of the drilling fluid. Good control of YP reduces the chances of pressure spike that can break the formation which may result circulation lost. Sufficient YP and gel strength were achieved at acceptable gel strength to help for cutting suspension while circulating and pump shutdown. Moreover, the mud was capable to lift the cuttings from bottom of the hole to surface.

### 5.3. Performance of solid control system on low-gravity solid

**Figure 8** shows the tabulated LGS for old design and new design. Rapid increment of LGS while drilling Well A was obvious due to inability of the old design to remove the solid efficiently from drilling mud. At the start of drilling operation, both designs removed the solid effectively from the drilling mud as the LGS was tabulated at the range of 7–8%. As drilling Well A deeper, the solid control equipment (SCE) of old design was observed getting poor in handling the mud

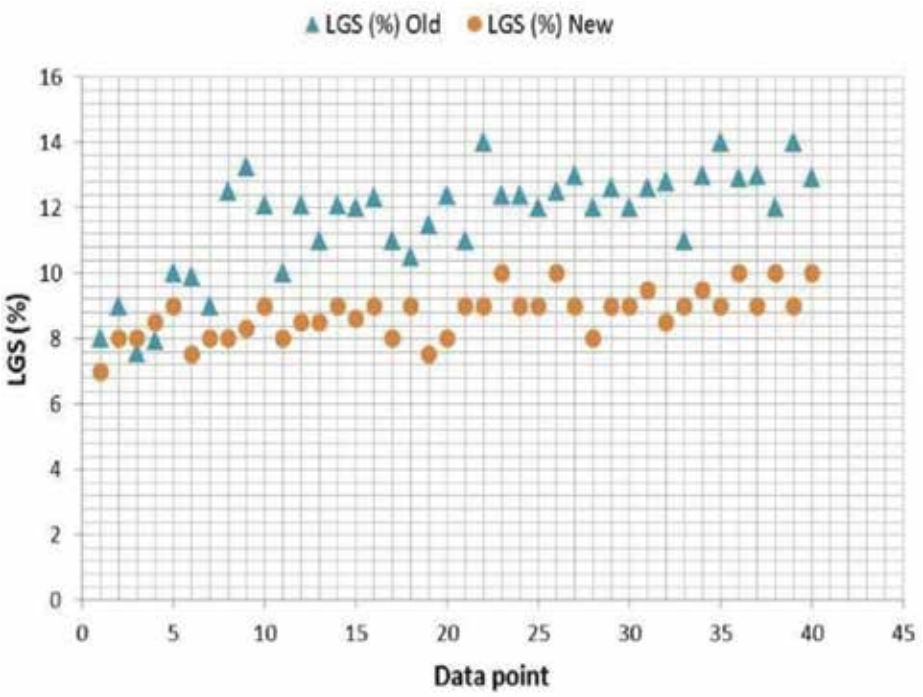


**Figure 8.** LGS (%) vs. data point. (Note: Based on personal experience).

return from the well. Frequent shale shakers overflow and bypassing the shakers in order to prevent massive surface loss of expensive fluids significantly created additional risk to the solid removal processing. The situation results of the LGS in the mud system rapidly increased to 14%. High solid content in this mud was considerably abrasive and may degrade down the drilling equipment through silt size. The smaller the particles, the more pronounced the effect on the mud properties because smaller particles are more difficult to remove or control its effect on the fluid. Recirculating of mud that contained drilled solid may gradually deteriorate mud properties. The upper limit of the solid fraction should be in the range of 6–8% by volume. The new design of solid control system as tabulated in **Figure 8** shows that the system LGS was improved with system removal by 25% when drilling Well B which showed an average reading of LGS at 8.7%.

### 5.4. Performance of solid control system on mud weight and equivalent circulating density

Well A was drilled using old design solid control system. The section was from 760 to 2163 m MDRT. MW was gradually increased from 10 to 11.6 ppg mud to maintain the hydrostatic

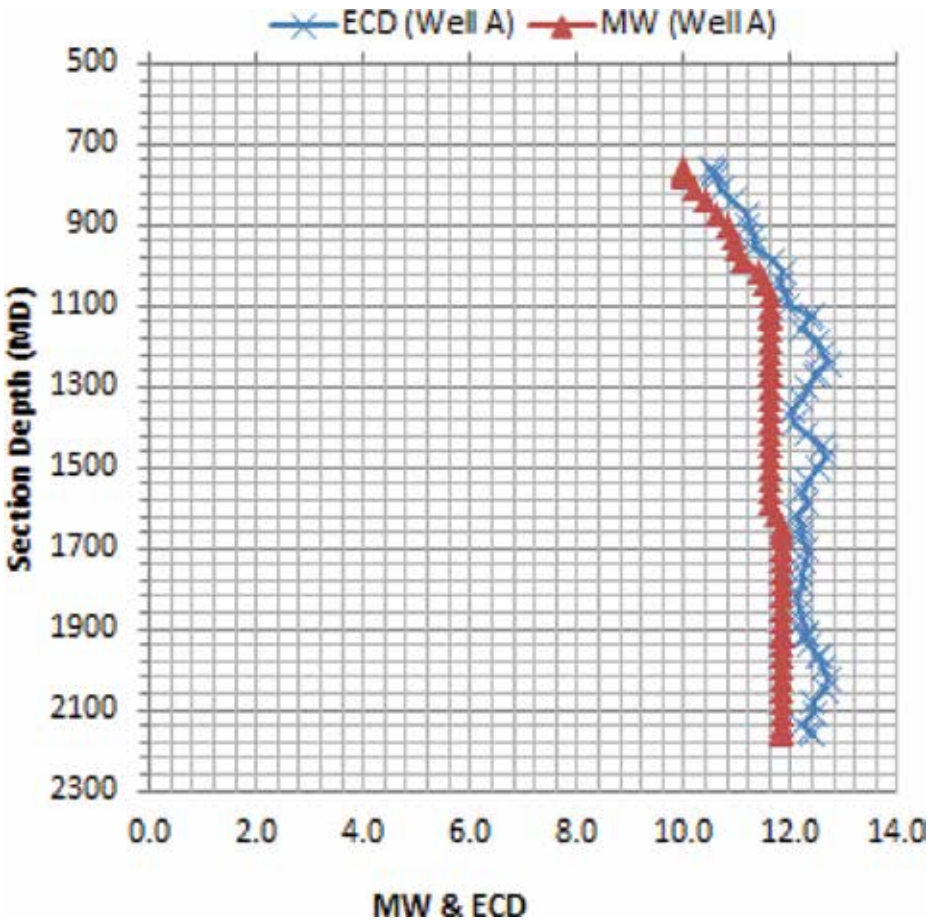


**Figure 9.** Section depth vs. MW & ECD (new design).

pressure in the column. Early tabulated data on the top section demonstrated a good ECD trend with no significant pressure spike. As drilling reached to 1124 m MDRT depth, ECD spike was increased up to 12.4 ppg. Failures to transport the cutting effectively to surface exposed the formation to pressure spike. It occurred because drilled cutting that remains in the well created tight tolerances between hole and drill string geometries. Poor hole cleaning triggered high ECD that can break the formation and losses of mud. ECD trend progressively built up, and pressure spike was observed at 1244 and 1474 m MDRT. Well circulation was commenced until the hole clean, but the entire operation progress became slows. The flow rate was ramped up in controlled manner to minimize the risk of pressure spike and high ECD. The ROP was also controlled to reduce the impact of high ECD. The average ECD additive factor was 0.6 ppg that is equivalent to 4.9% increment from original MW during mud than in dynamic condition (**Figures 9** and **10**).

Well B was drilled using new design of solid control system. The section was drilled from 750 to 2200 m MDRT. The MW used to drill this section was 10.0 to 11.9 ppg and gradually increased to maintain the hydrostatic pressure in the column. The tabulated data show that the ECD was consistent at safe drilling margin until section TD at 2150 m MDRT. No significant ECD spike was observed throughout the operation. A slight increase was observed at 1935 m MDRT with 12.32 to 12.5 ppg, but the impact is still below the fracture gradient. Increase in ECD occurred because more cutting bed accumulated on the low side of drill string. Due to

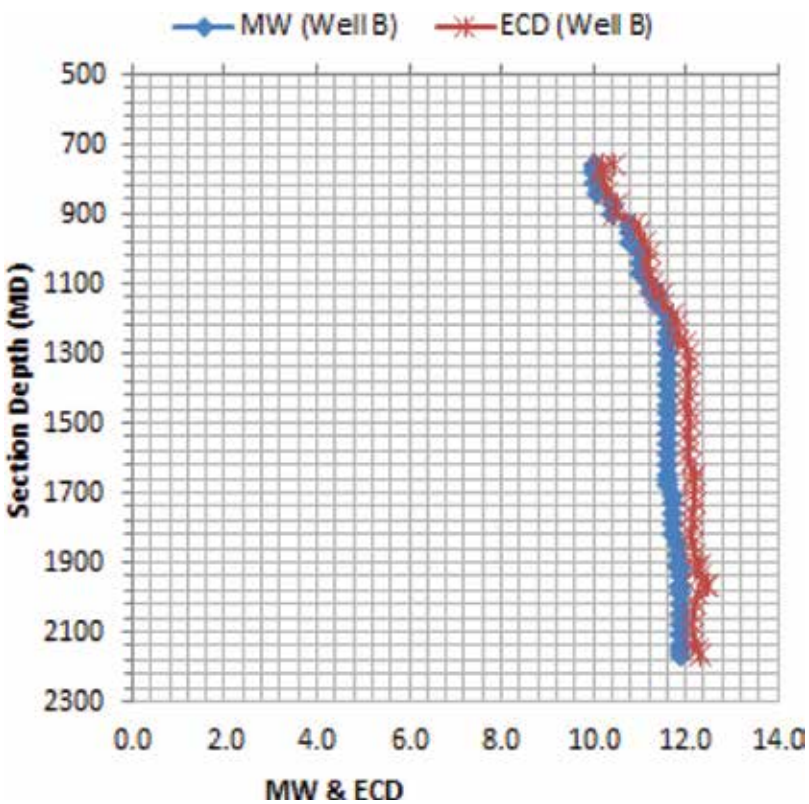


**Figure 10.** Section depth vs. MW & ECD (old design).

gravity effect at deviated hole, heavier cuttings and mud along the lower side of the hole moved at lower rate than the clean mud on the upper side. Peak performance of solid separation equipment is essentially important to ensure the LGS, YP and PV are maintained within the acceptable envelope. These parameters provide good cutting transport and no excessive pumping pressure required to break the gel. The average ECD additive factor was 0.3 ppg that is equivalent to 2.9% increment from original MW during mud flow in dynamic condition.

### 5.5. Performance of solid control system on rate penetration

The ROP trend of old design was seen concentrated at range between 40 and 60 m/h. ROP was controlled in such manner due to ECD surge. Mud properties specification was not within the recommended limit, and it significantly influenced the ROP consistency. Continuous of solid built up in the mud system altered the mud properties which eventually causing in poor drilling performance. Drilled solids circulated up the annulus increased the pressure differential and lead to slower drilling. Instantaneous maximum ROP achieved using old design SCE was 62 m/h with 48.78 m/h on average. Drilling the same section for Well B using new design solid control system showed improvement on ROP trend. Maximum instantaneous ROP was registered at 77 m/h with 61 m/h in average. Efficient solid removal using new design improved the ROP performance by 25% (**Figure 11**).

### 5.6. Performance of old design of solid control system on hooks load

Drag force is known as difference between free rotating weight and the force required to move the string up and down in the hole. Pick-up (P/U) drag force usually higher than the free rotating weight while slack-off (S/O) force is lower than the free rotating weight. String weight or

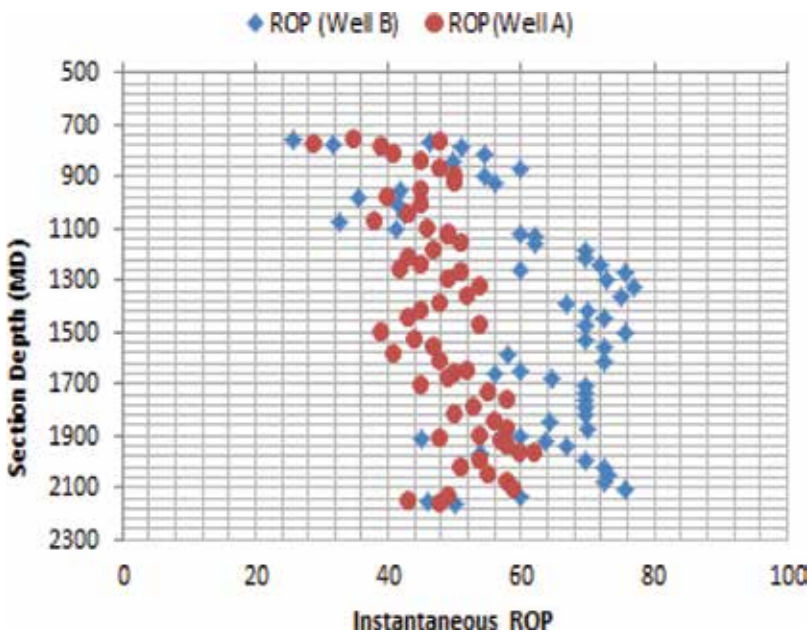


**Figure 11.** Section depth vs. ROP.

free rotating weight on this analysis represented by the green curve. Data were taken while the string was off bottom to compare0 the modeling string weight and actual weight. As designed expectation, the plots should tabulate across and along the modeling string weight at any well depth. Drilling the Well A using old design system, more solids were not properly separated from the mud. This increased the mud viscosity and altered the mud properties. In this chart, the hook load readings when P/U the drill string was tabulated between 0.2 and 0.3 FF as shown in **Figure 12**. Occasionally, the plot exceeded that friction factor line as observed at depth around 1550 and 1900 m MDRT. Pile up of drilled cuttings bed and accumulation increased the drill string contact with the wellbore. Mud circulation for hole cleaning was performed to remove the cuttings from the well. S/O weight of the drill string in this chart was observed between 0.2 and 0.3 FF. The plots were occasionally tabulated exceeding the 0.3 FF. This condition indicated that more drilled cutting was still sticking and restricting

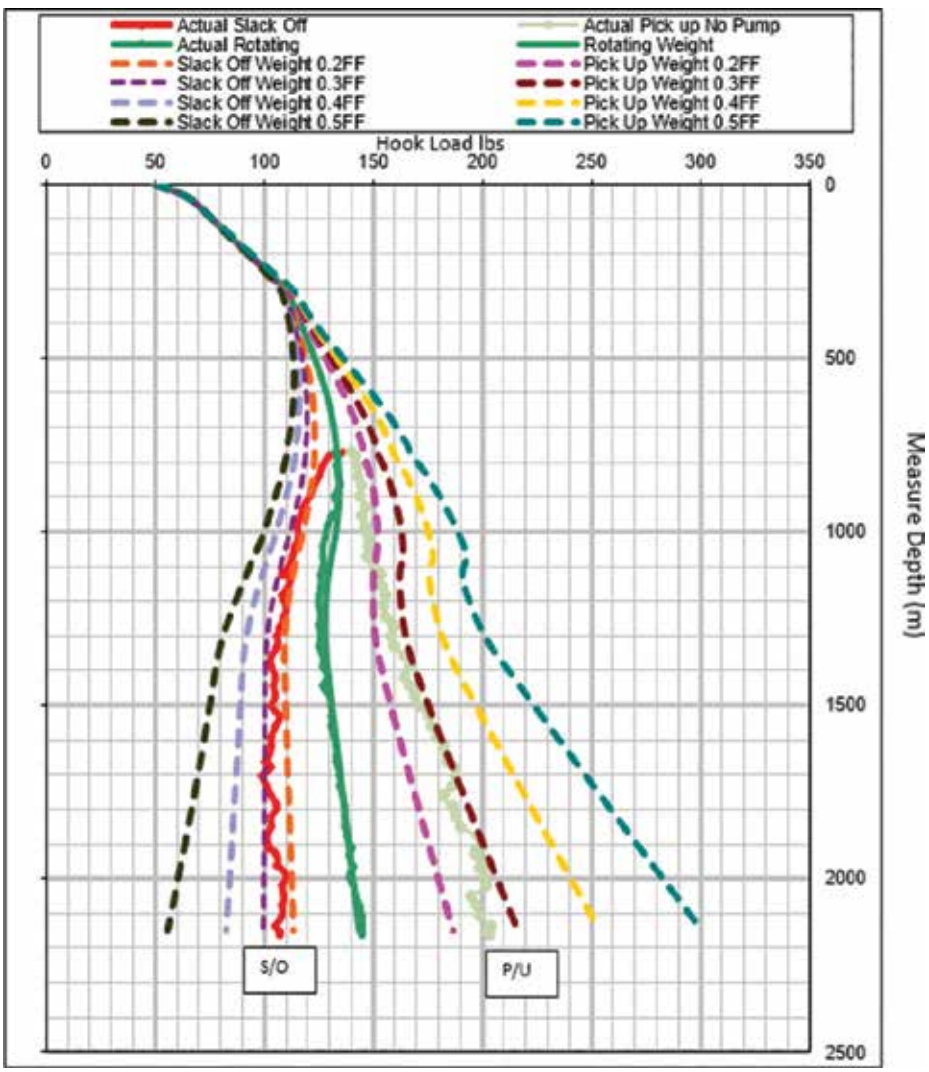


**Figure 12.** Hook load effect vs. depth (old design).

the drill string to move down. It required extra cumulative axial force to free the drill string. Lower S/O FF represents high hook load and vice versa. Failure to effectively transport the cuttings to surface result in a number of drilling problems including: excessive overpull on trips, high rotary torque, stuck pipe, hole-pack off, excessive ECDs and cutting accumulation.

### 5.7. Performance of new design of solid control system on hook load

The new design system effectively separated the drilled cuttings from the mud and allowed each of the equipment to work at peak performance. Mud properties were within the design specification with no severe solid contamination result improvement on PV, YP and LGS reading.

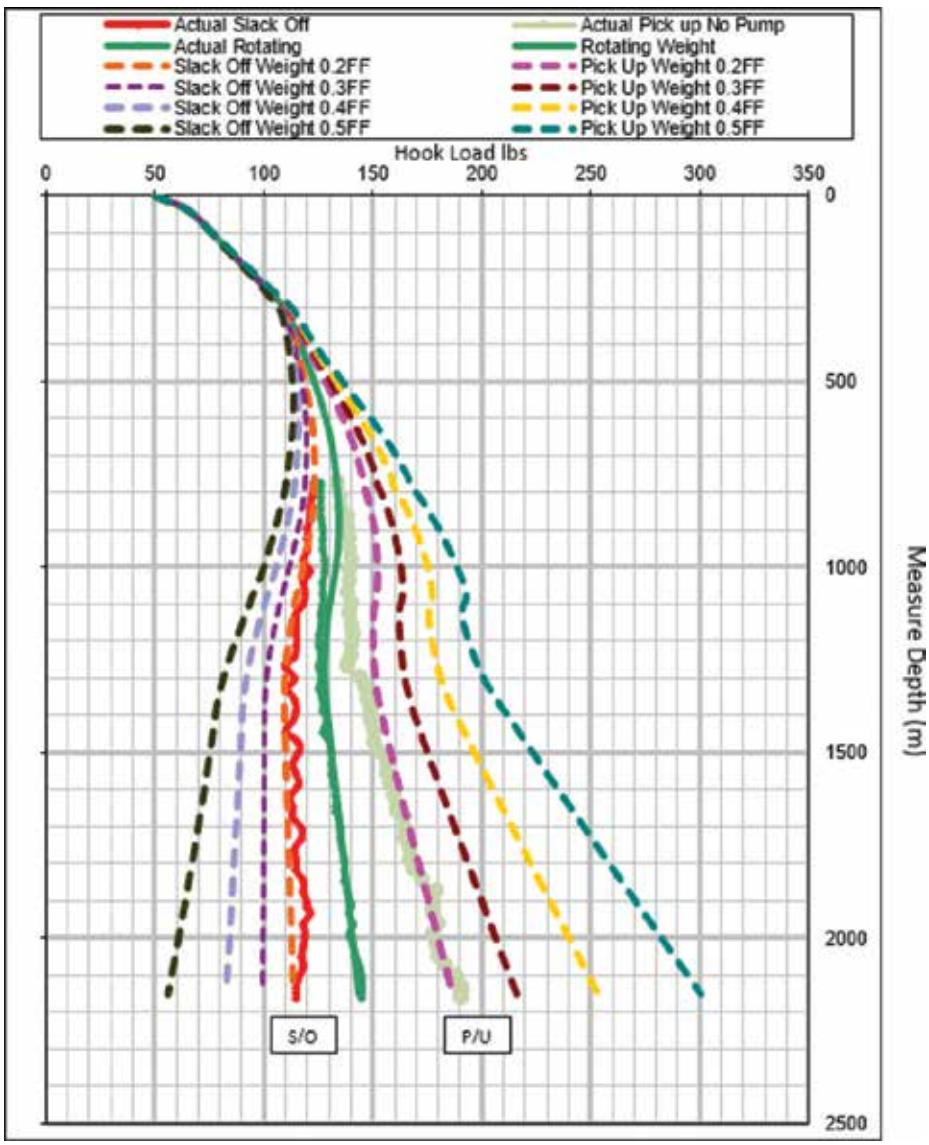


**Figure 13.** Hook load effect vs. depth (new design).

The hook load chart indicated that P/U weight was concentrated at 0.2 FF but occasionally exceeded 0.2 FF. Good control of mud return and consistent distribution flow to solid control system allowed effective solid particles separation. S/O weight of the drill string was observed tabulated below the 0.2 FF but occasionally exceeded 0.2 FF. This indication represented that the hole was not piled up with drilled cuttings. Less axial force was required to move the drill string as there was no severe contact of drilled cuttings with the string (**Figure 13**).

## 6. Conclusion

A new solid control system was developed with detailed studies on the effect of drilled solids to mud properties and drilling performance. The following conclusion can be drawn from this investigation and as an improvement of the rig solid control system.

1. The installation of mud distributor tank enhance the flow stability and regulate the circulation of mud from the well.
2. Comparing the old design while drilling 12.25-inch hole section, the new design improved the mud properties of PV by 14%, YP by 17% and LGS by 25%.
3. New design improved the ROP by 20% while drilling the 12.25-inch hole section.
4. New design improved average ECD margin by reducing additional pressure exerted using original mud from 4.9 to 2.9% at 12.25 inch. High ECD margin is not recommended because it can break the weak formation.
5. Drill string drag effect to the hook load for P/U and S/O at Old design were tabulated between 0.2 and 0.3 FF while drilling the section with New design were mostly tabulated at 0.2 FF and less.

## Acknowledgements

The authors wish to thank UTP for providing the resources and opportunity to conduct this research.

## Nomenclature

| | |
|---|---|
| PV | plastic viscosity |
| YP | yield point |
| ROP | rate of penetration |

| | |
|---|---|
| SCE | solid control equipment |
| LGS | low gravity solid |
| ECD | equivalent circulating density |
| NPT | non-productive time |
| CCC | cutting carrying capacity |
| P/U | pick up |
| S/O | slack off |
| FF | friction factor |

## Author details

Sonny Irawan* and Imros B. Kinif

*Address all correspondence to: drsonny_irawan@utp.edu.my

Universiti Teknologi PETRONAS, Seri Iskandar, Perak, Malaysia

## References

[1] Dahl B, Omland TH, Saasen A. Optimised solids control in artic environments. In: SPE Russian Oil & Gas Exploration & Production Technical Conference and Exhibition. Moscow, Russia: Society of Petroleum Engineering (SPE); October 2012

[2] Akpabio JU, Inyang PN, Iheaka CI. The Effect of Drilling Mud Density on Penetration Rate. International Research Journal of Engineering and Technology (IRJET), Dec-2015;**2**(9). e-ISSN: 2395 -0056, p-ISSN: 2395-0072

[3] Robinson L. Drilling Fluid Processing Handbook. United State of America (USA): ASME – Elsevier; 2005

[4] Dahl B, Saasen A, Omland TH. Successful drilling oil and gas by optimal drilling—fluid solid control—a practical and theoretical evaluation. SPE Drilling & Completion. 2008;**23**:409-414

[5] Moses AOA, Egbon F. Semi-analytical models of the effect of drilling fluid properties on rate of penetration (ROP). In: SPE Nigeria Annual International Conference and Exhibition. Abuja, Nigeria: Society of Petroleum Engineering (SPE); August 2011

[6] Darley HCH, Gray GR. Composition and Properties of Drilling and Completion Fluids. 5th ed. Houston: Gulf Publishing Company, Book Division; 1988

[7] Chilingarian GV, Alp E, Al-Salem M, Uslu S, Gonzales S, Dorovi R. Drilling fluid evaluation using yield point-plastic viscosity correlation. Journal of Energy Sources. Taylor & Francis; 1986;**8**(2-3):233-244. https://doi.org/10.1080/00908318608946052

[8] Robinson L. Economic Consequences of Poor Solids Control. American Association of Drilling Engineer (AADE). Houston, Texas, USA: Conference at the Wyndam Greenspoint Hotel. April 11-12, 2006

[9] Monicard RP. Drilling mud and cement slurry rheology manual. Springer; 1982:118 pages. ISBN: 9789401092463 (electronic bk.). DOI: 10.1007/978-94-010-9246-3

[10] Baumert ME, Allouche EN, Moore ID. Drilling fluid consideration in design of engineered horizontal directional drilling installation. International Journal of Geomechanics. December 2005;**5**(4):339-349

[11] Machado JC, Castilho PF. Solid control and low solids: Important binary to drill deep wells. In: Second Latin American Petroleum Engineering Conference; Caracas, Venezuela: Society of Petroleum Engineering (SPE); March 1992

[12] Paiaman AM, Ghassem MK, Salamani B, Al-Anazi BD, Masihi M. Effect of fluid properties on rate of penetration. North American Free Trade Agreement. 2009;**60**(3):129-134

[13] Saasen A, Lokingholm G. The effect of drilling fluid rheological properties on hole cleaning. In: IADC/SPE Drilling Conference; Dallas, USA: Society of Petroleum Engineering (SPE); February 2002

[14] API Recommended Practice 13D—Rheology and Hydraulics of Oil-Well Drilling Fluids 7th ed. USA: American Petroleum Institute (API); September 1, 2017

Chapter 6

# Rate of Penetration Prediction Utilizing Hydromechanical Specific Energy

Omogbolahan Ahmed, Ahmed Adeniran and Ariffin Samsuri

Additional information is available at the end of the chapter

http://dx.doi.org/10.5772/intechopen.76903

**Abstract**

The prediction and the optimization of the rate of penetration (ROP), an important measure of drilling performance, have increasingly generated great interest. Several empirical techniques have been explored in the literature for the prediction and the optimization of ROP. In this study, four commonly used artificial intelligence (AI) algorithms are explored for the prediction of ROP based on the hydromechanical specific energy (HMSE) ROP model parameters. The AIs explored are the artificial neural network (ANN), extreme learning machine (ELM), support vector regression (SVR), and least-square support vector regression (LS-SVR). All the algorithms provided results with accuracy within acceptable range. The utilization of HMSE in selecting drilling variables for the prediction models provided an improved and consistent methodology of predicting ROP with drilling efficiency optimization objectives. This is valuable from an operational point of view, because it provides a reference point for measuring drilling efficiency and performance of the drilling process in terms of energy input and corresponding output in terms of ROP. The real-time drilling data utilized are must-haves, easily acquired, accessible, and controllable during drilling operations.

**Keywords:** artificial intelligence, ROP prediction, neural network, data analytics, least square support vector regression, specific energy, drilling efficiency, extreme learning machine

## 1. Introduction

The speed at which a drill bit breaks the rock under it to deepen the hole is called rate of penetration (ROP). The ROP prediction is necessary for effective drilling and cost optimization;

therefore, it has been of great concern to drilling engineers during the last decades [1, 2]. Maximization of ROP is often directly related to the minimization of drilling costs and, therefore, it is a significant measure of drilling performance. Hydrocarbon accumulations are becoming more increasingly difficult to find and reach in terms of depth and remoteness of location, and therefore more complex wells are being drilled. Effective prediction of ROP becomes imperative in order to improve efficiency of the drilling process, enables drilling engineers, and operations team to properly estimates the time for the drilling phase of operations, the associated costs, and properly phase the operation in order to save cost. ROP prediction also helps to explain the reason behind a sudden slowness in the drilling process, and therefore helps in making informed decisions on the optimization strategy to adopt.

There are several techniques present to predict ROP, each with its own merits and demerits, and there is no acceptable universal model for all conditions, as the nature of the relationships among the parameters that affects ROP is quite complex and unique for each case. Traditional ROP model usually predicts ROP with lots of assumptions and wide range of uncertainties due to the complexity in the interactions of several parameters which affects ROP. ROP follows a complex relationship with several drilling parameters such as string rotation (RPM), weight on bit (WOB), mud weight (MW), flow rate, bit hydraulics, formation properties such as compressive strength, pore pressure gradient; mud properties, mud hydraulics, borehole deviation, size, and type of bit used. In some cases, increasing WOB and RPM could results in decreasing ROP, as there is an interaction of these inputs with other factors that affects ROP. The understating of the underlying complex relationships among these parameters is important in the accurate prediction and optimization of ROP [3].

Predictive data-driven (PDA) modeling involves searching through complex data to identify patterns and adjust the program actions accordingly. During drilling operations, lots of real-time data are being gathered with quite a number related to ROP but are riddled with lots of uncertainties and complex relationships which are better handled by data-driven analytical techniques. The ability of AI techniques, to work through complex data sets and establish a relationship or trend without prior assumptions has made it endearing to the hearts of engineers who seek to solve complex drilling engineering problems, especially when the geology and rock mechanic parameters differs from well to well, and therefore may have different recommended drilling parameters within a wide range [4].

Several researches have been carried out in predicting and optimizing ROP using AI techniques. Jahanbakhshi developed an artificial neural network (ANN) modeling for predicting ROP as a real-time analytical approach with encouraging results [5]. Bodaghi et al. showed that optimized SVR has better accuracy and robustness in the prediction of ROP compared to back propagation neural network (BPNN), and is a practicable method to implement for drilling optimization [6]. Also, Shi et al. in their study showed a promising prospect for extreme learning machine (ELM) and upper-layer-solution-aware, in predicting ROP, as they outperform the ANN model [7]. The study of Moraveji and Naderi concluded that response surface methodology, RSM statistical model provides an efficient tool for prediction of ROP as a function of controllable and uncontrollable variables with a reasonable accuracy [8]. Mantha and Samuel, using ANN, SVR, and classification regression trees (CART) in their study, shows ROP follows a complex relationship

which cannot be comprehensively explained by traditional models alone. Application of data-driven analytics using several machine learning algorithms coupled with regression analysis can help in better understanding and predicting ROP [3].

This study seeks to improve ROP prediction by proposing the utilization of HMSE parameters as inputs in the prediction of ROP by four AI techniques. The capability of the four AI techniques namely artificial neural network (ANN), extreme learning machine (ELM), support vector regression (SVR), and least-square support vector regression (LS-SVR) are compared. To demonstrate this, a case study is presented using real data from two development wells from onshore Niger Delta hydrocarbon province. The results shows all the AI techniques predicted ROP within acceptable accuracy range and provided an improved and consistent methodology of predicting ROP with drilling efficiency optimization objectives.

## 2. ROP models

ROP is an important drilling parameter as a measure of performance in terms of both drilling cost savings and drilling efficiency. It is defined as the slope of the depth evaluated over a short time. It gives a perspective of how fast or slow a particular formation is being drilled or how operational conditions affect the functioning of the drilling system. The mathematical expression of ROP is given as [9]:

$$ROP(t) = \frac{dh}{dt} \tag{1}$$

Factors affecting ROP can be divided into the following [5, 10];

- **Personnel/Rig efficiency:** this refers to the man-power and efficiency of the hardware involved in drilling operation. The experience of the personnel matters and is often a determinant in the selection of certain drilling parameters which affects ROP. The age, ratings, and technology of the drilling rig and associated hardware system also affects the efficiency of the selected drilling parameters to deliver optimum ROP output.
- **Characteristics of the formation** such as strength, hardness/abrasiveness, formations stress, elasticity, plasticity, pore pressure, balling tendency, porosity and permeability, etc. These parameters that controls ROP with varying degrees of uncertainties in the subsurface. The elasticity and ultimate strength of the formation are the most important parameters that affect ROP. In elastic environments, the normal compaction trend (NCT) indicates the increase in formation strength with increasing depth of burial. This relationship does not hold in carbonate environments. The chemical composition of the formation also affects ROP, with formation containing abrasive minerals rapidly dulling the bit while formation with gummy clay minerals clings to the bit to ball up. All these are uncontrollable factors that affect ROP [9].
- **Mechanical factors** such as RPM, bit type, and WOB can be often referred to as the bit operating conditions.

**Bit type** selection is dependent on the type of formation to be drilled with a significant effect on ROP. Some bits such as roller cone bits with large cone offset angle and long teeth are only practical for soft formations due to fast tooth wear and hence a quick loss of ROP in harder formation. The fixed cutter bit is one where there are no moving parts, but drilling occurs due to shearing, scraping, or abrasion of the rock. Fixed cutter bits can be either polycrystalline diamond compact (PDC) or grit hot-pressed inserts (GHI) or natural diamond. They can also be matrix-body or steel-body, the selection of which depends on the application and the environment of use. Matrix is desirable as a bit material, because its hardness is resistant to abrasion and erosion. It is capable of withstanding relatively high compressive loads, but, compared with steel, has low resistance to impact loading. PDC bits are generally used for drilling soft but firm, and medium-hard, nonabrasive formations that are not sticky. The choice of bit therefore has a significant impact on ROP [9].

**RPM:** this is the revolutions per minute which represents the rotational speed of the drill string. The top drive system (TDS) is a revolutionary introduction into the rig system in the early 1980s, it provides clockwise torque to the drill string to drill a borehole. **Figure 1** shows an experimental result which proves that ROP usually increased linearly with increasing values of RPM up to a certain point for a particular formation illustrated as segment a-b, provided all other drilling parameters are kept constant, after which ROP starts to diminish as seen in segment b-c. Point b, is called "the bit floundering point."

**Weight on bit (WOB):** the WOB represents the amount of axial force applied onto the bit which is then transferred to the formation causing it to break. The significance of WOB as a factor affecting ROP can be seen as illustrated in **Figure 2**. The figure shows zero ROP until the inertial breaking WOB is applied to the formation at point a. The ROP increases rapidly with increasing WOB as observed in segment a-b; then, a linear increase in ROP is observed in

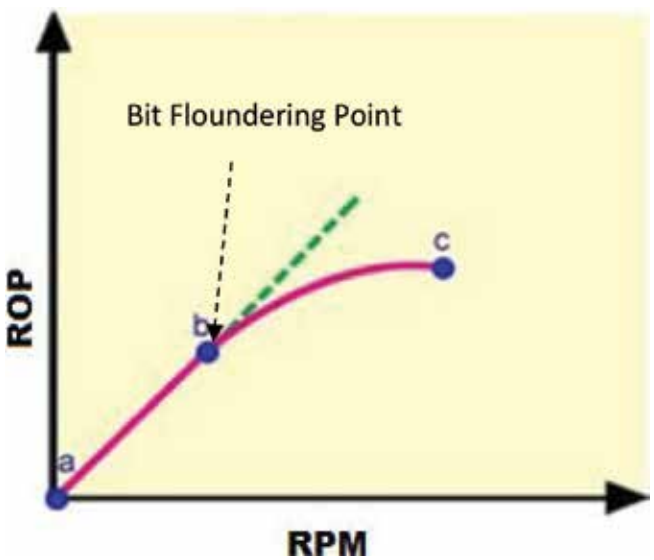


**Figure 1.** Typical response of ROP to RPM.

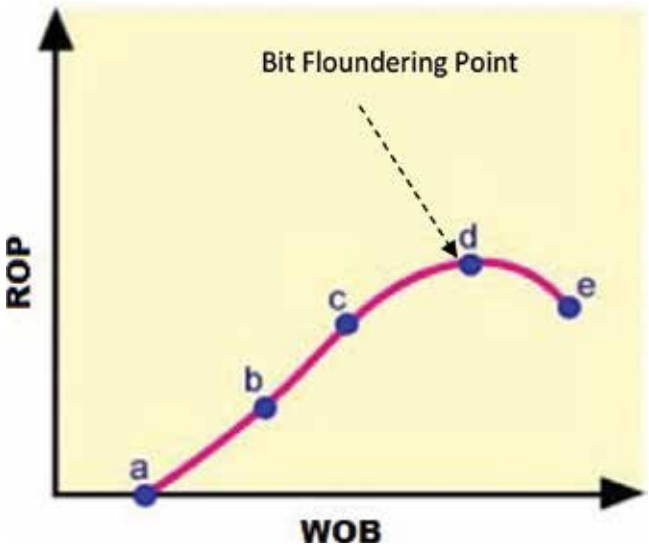


**Figure 2.** Typical response of ROP to WOB.

segment b-c followed by only a slight increase in ROP at a high value WOB in segment c-d. In extreme cases, a further increase in WOB will lead to a decrease in ROP as seen in segment d-e. The point at which this occurs is called floundering point.

- **Hydraulic factors:** this refers to the bit hydraulics, and the two main hydraulic factors with significant effects on ROP are (i) jet velocity, and (ii) bottom hole cleaning. Significant improvement in ROP could be achieved if proper nozzles were selected for a proper jetting action at the bit as drilling fluids flows at a determined flowrate through the drill string and the bit nozzles into the annulus. This promotes better cleaning action at the bit face as well as bottom hole.

  Bottom hole cleaning is an important mechanism of removing drilled cuttings from the face of the bit. The jetting action of the mud passing through the bit nozzles has to provide enough velocity and cross flow across the surface of the bit to remove the newly drilled cuttings effectively as the bit penetrates the formation. This will prevent bit balling and regrinding of drilled cuttings by moving them up the annulus to maximize drilling efficiency of the bit.

- **Drilling fluid properties**: the two main mud properties with significant impact on hole cleaning are the mud density and viscosity.

  **Mud density**: aside serving as the primary control of the well, that is, prevention of formation-fluid intrusion into the wellbore, the mud density functions as mechanical stabilization of the wellbore. Increasing the mud density beyond required to serve the aforementioned functions, is detrimental to ROP, and may cause induced losses by fracturing the formation under the *in-situ* stress condition. An increase in the mud density causes a decrease in ROP. This is because it causes an increase in bottom hole pressure

beneath the bit causing a chip hold-down effect. Hence, regrinding of drilled cuttings with adverse effect on penetration rate.

**Viscosity** tends to decrease ROP as it increases in drilling fluids. Plastic viscosity is the resistance of the drilling fluid to flow caused by mechanical friction within the fluid. With high viscosity, cuttings tend to remain stuck on the bottom of the hole causing their re-drilling and this leads to reduction in the performance of the bit. It affects the hydraulic energy available at the bit nozzles for cleaning due to parasitic frictional losses in the drill string [9].

## 2.1. ROP empirical models

There has been many proposed empirical ROP models in the last 3 decades; however, three of them are quite popular for estimating ROP, they are (i) Maurer's ROP model, (ii) Galle and Woods ROP model, and (iii) Bourgoyne-Young ROP model.

### *2.1.1. Maurer's model*

Maurer [11] developed a ROP model based on a theoretical penetration equation as a function of WOB, RPM, bit size, and rock strength derived for a roller-cone type bit. A mathematical relation between rate of drilling, WOB, and RPM based on perfect hole cleaning condition was achieved as a function of depth. The ROP equation was thus given as:

$$\frac{dF_D}{dt} = \frac{4}{\pi d_b^2}\frac{dV}{dt} \tag{2}$$

Here, $F_D$ = footage drilled by bit (ft), $t$ = time (h), $V$ = Volume of rock removed, $d_b$ = diameter of bit.

### *2.1.2. Galle and woods' model*

Galle and Woods, in their work, investigated the effects of bit cutting structure dullness, WOB, and RPM on ROP, rate of tooth wear and bearing life for roller cone bits. The result of their work is a presentation of graphs and procedures for field applications to determine the best combination of constant WOB and RPM [12]. They presented a drilling rate equation as follows:

$$\frac{dF_D}{dt} = C_{fd}\frac{\overline{W}^k}{a^p}r \tag{3}$$

Here, $C_{fd}$ = formation drillability parameter, a = $0.028125h^2 + 6.0\,h + 1$ time, hr, h = bit tooth dullness, fractional tooth height worn away, in, $p = 0.5$ (for self-sharpening or chipping type bit tooth wear), k = 1.0 (for most formations except very soft formations), 0.6 (for very soft formations), r = RPM function, $\overline{W}$= function of WOB and $d_b$, such that $\overline{W} = \frac{7.88WOB}{d_b}$.

### *2.1.3. Bourgoyne and Young ROP model*

The most popular of the ROP model is Bourgoyne and Young ROP model used to calculate the ROP. In their work, they presented a mathematical relationship using a complex drilling

model to capture the effects of changes in the various drilling parameters. They proposed an eight function empirical relationship to model the effect of most of drilling variables [1]. The equation form is

$$\widehat{ROP} = f_R(a_1, \ldots\ldots, a_8, p_2, \ldots., p_8) \tag{4}$$

$$= Exp\left(a_1 + \sum_{i=2}^{8} a_i p_i\right), \tag{5}$$

Here, $a_1$ = formation strength parameter, $a_2$ = exponent of the normal compaction trend, $a_3$ = under compaction exponent, $a_4$ = pressure differential exponent, $a_5$ = bit weight exponent, $a_6$ = rotary speed exponent, $a_7$ = tooth wear exponent, and $a_8$ = hydraulic exponent.

### *2.1.4. Hydromechanical specific energy ROP model (HMSE)*

Approaching the drilling process as a closed system in terms of energy input in the form of applied drilling parameters, and a corresponding output, in the form of ROP, brought about the concept of specific energy (SE). This concept was first introduced by Teale in [13]. Further work has been done to fully capture the mechanical and hydraulic energy input and their relationship with ROP. The HMSE concept states that "the energy required to remove a unit volume of rock comes primarily from the torque applied on the bit, the weight on bit (WOB), and the hydraulic force exerted by the drilling fluid on the formation" [14]. Specific energy is therefore a significant measure of drilling performance, especially of the cutting efficiency of bits and rock hardness [15]. The equation form is:

$$HMSE = \frac{F}{A_b} + \frac{120\pi.N.T}{A_b.ROP} + \frac{1154\eta.\Delta p_b.Q}{A_b.ROP} \tag{6}$$

Rearranging

$$ROP = \left(\frac{120\pi.N.T + 1154\eta.\Delta p_b.Q}{A_b.HMSE - F}\right) \tag{7}$$

Here, HMSE = hydromechanical specific energy in psi, F = WOB in lbs, N = RPM, T = TORQ in lb-ft, $A_b$ = bit cross sectional area in $in^2$, ROP = rate of penetration in ft/hr, Q = mud flow-in rate in gallons per minute, $\eta$ = dimensionless energy reduction factor depending on bit diameter, and $\Delta p_b$ = pressure loss at bit in psi.

The use of HMSE-derived ROP model drilling parameters have been proposed in this study because it fully captures the relevant controllable parameters that affects ROP. Also, from an operational point of view, it is valuable because it provides a reference point for measuring drilling efficiency and performance of the drilling process in terms of measuring energy input and corresponding output in terms of ROP. The SE concept became a key element for the fast drill process (FDP) [16]; the process of drilling with the highest possible ROP in terms of technical and economical limits. In early 2004, Exxon Mobil Corporation used the process to

optimized their drilling operation with a result of an astonishing increase in ROP by 133% proven the concept a useful one [16, 17].

## 3. Artificial intelligence (AI) techniques

Artificial intelligence (AI) can be described as the imitation of human intelligence processes by machines, especially computer systems. These processes include the acquisition of information from sets of data, use logic of their interdependency to reach approximate or definite conclusions while self-correcting [18]. AI was coined by John McCarthy, an American computer scientist, in 1956 at The Dartmouth Conference where the discipline was born [19]. According to artificial intelligence applications institute (AIAI), AI areas of application are; **case-based reasoning**: a technique for utilizing historical datasets to guide diagnosis and fault finding; **evolutionary algorithms**: an adaptive search technique with very broad applicability in scheduling, optimization, and model adaptation; **planning and workflow**: modeling, task setting, planning, execution, coordination, and presentation of activity-related information; **intelligent systems**: an approach of building knowledge-based systems; and **knowledge management**: the identification of knowledge assets in an organization, and support for knowledge-based work [20].

Some of the advantages of AI techniques include, but not limited to ability to model complex, nonlinear processes without priori relationship assumption between input and output variables; potential to generate accurate analysis and results from large historical databases; ability to analyze large datasets to recognize patterns and characteristics in situations where rules are unknown or relationship and dependency of variables are complex; cost-effectiveness: many AI algorithms have the advantage of execution speed, once they have been trained. The ability to train the system with data sets, instead of writing programs, makes it more cost-effective and changes can be easily implemented when need arises. Multiple algorithms can be combined taking competitive advantages of each algorithm to develop an ensemble AI tools. AI techniques can be deployed to solve routine boring tasks which would be completed faster with minimal errors and defects than human [21].

AI techniques limitations includes some of them being tagged as "black boxes," which merely attempt to chart a relationship between input and output variables based on a training data set. This raises some concerns regarding the ability of the tool to generalize to situations that were not well represented in the data set. However, application of the right domain knowledge helps to address this limitation. Other limitations are the lack of human touch, enormous processing time for large datasets and requirement for high computational resources and skills.

Despite some of the disadvantages of AI techniques, their overwhelming advantages have made them endearing in different fields, including the exploration and exploitation of oil and gas. Recent advancement in the collection and transmission of real-time drilling data coupled with insufficiency of empirical ROP models to unveil the real-time downhole conditions has made researchers to shift into AI techniques for prediction purpose. Furthermore, the effects of

| Model | Input number | Input variables | Output |
|---|---|---|---|
| ANN | 9 | UCS, bit size, bit type, drillability coefficient, gross hours drilled, WOB, RPM, drilling mud density, and AV (Apparent Viscosity) [22] | ROP |
| ANN | 20 | Differential pressure, hydraulics, hole depth, pump pressure, density of the overlying rock, equivalent circulating density, hole size, formation drillability, permeability and porosity, drilling fluid type, plastic viscosity of mud, yield point of mud, initial gel strength of mud, 10 min gel strength of mud, bit type and its properties, weight on the bit and rotary speed, bit wear, and bit hydraulic power [5] | ROP |
| ANN | 7 | Depth, bit weight, rotary speed, tooth wear, Reynolds number function, ECD, and pore pressure gradient [23] | ROP |
| ANN | 9 | Formation drillability, formation abrasiveness, bearing wear, tooth wear, pump rate, rotating time, rotary torque, WOB, and rotary speed [24] | ROP |
| SVR | 12 | Viscosity, MW, pump rate, well deviation, RPM, WOB, depth, formation, bit size, and bit tooth wear [6] | ROP |
| ANN | 6 | Rock strength, rock type, abrasion, WOB, RPM, and mud weight [25] | ROP and wear |
| ANN | 13 | Bit Type, IADC Codes, Bit diameter, Bit Status, Measure Depth, True Vertical Depth, Weight on Bit, Rotary Speed, Torque, Pump Flow Rate, Stand Pipe Pressure, mud weight, and Formation Mineralogy [26] | ROP |

**Table 1.** Summary of some recent applications of AI in ROP prediction.

all factors affecting ROP and downhole conditions are inherent in the collected surface drilling data. Applying data-driven predictive analysis has proven useful in decoding the hidden information in these drilling data.

**Table 1** shows some recent work done using artificial intelligence to predict ROP. ANN has been the most often used. What is also clear in the literature review is that the selection of input is not consistent and some may be difficult to obtain in some instances. Also, for optimization purpose while drilling, some of the variables included in the models are not controllable factors that can be adjusted in real time.

### 3.1. Some artificial intelligence techniques

Below are of some of the AI techniques considered in this study. A summary of their characteristics is presented in **Table 2**.

#### *3.1.1. Artificial neural network (ANN)*

Artificial neural networks, ANN, are designed based on the examination of biological central nervous systems and neurons, axons, dendrites, and synapses. Similarly, an ANN is composed of elements that are called "neurons," "units," or "processing elements" (PEs). Each PE has a specification of input/output (I/O) and they are connected together to form a network of nodes for mimicking the biological neural networks, hence they are called "artificial neural network," ANN.

| Artificial intelligence techniques | Characteristics | Advantages | Limitations |
|---|---|---|---|
| ANN | Nonlinearity<br>Input-output mapping, supervised learning while working through training samples<br>Evidential response<br>Neurobiological analogy<br>Very large scale integration applicability | Ability to run parallel processes and apply learning<br>Complex linear and nonlinear relationships can be derived using ANN<br>Flexible input/output Less sensitive to noise | Black box models: it is not possible to explain how the results were calculated in any meaningful way<br>Many optimizing parameters to be set in defining model to avoid overtraining<br>Requirements of elaborate training examples |
| ELM | Input weights and biases, are assigned randomly without any dependency<br>Fast learning process by using a fixed nonlinear transformation in the training phase<br>An innovative training algorithm for Single-hidden Layer Feed-forward Neural networks SLFN | Online real-time application<br>Avoids unnecessary human intervention<br>Reduces computational burden<br>Needs less training time<br>Prediction accuracy slightly better than ANN<br>Easy implementation | Suffers from uncertainty<br>Suffers generalization degradation problem<br>Black box models |
| SVR | Supervised learning<br>Maximal hyperplane is constructed to separate a high dimensional space of input vectors mapped with the feature space<br>Its core feature in control of its attractiveness is the notion of an $\varepsilon$-insensitive loss function | Invaluable for the estimation of both real valued and indicator functions<br>Handles very high dimensional data<br>Can learn very high elaborate concepts<br>More stable<br>Robust to 'outliers' (i.e., data samples outside $\varepsilon$-insensitive zone) | Consumes lots of computer resources<br>Time consuming for training, testing and validation of models<br>Uses a complex quadratic programming approach making it difficult for very large datasets<br>Black box model |
| LS-SVR | LS-SVRs are closely related to regularization networks and Gaussian processes but additionally emphasize and exploit primal-dual interpretations<br>Simplified algorithm | Requires less effort in model training in comparison to the original SVR, owing to its simplified algorithm | Highly sensitive to outliers<br>Ineffective at handling non-Gaussian noise<br>Consumes lots of computer resources |

**Table 2.** Summary of AI techniques used in the case study.

The use of ANN as a reliable universal estimator in constructing nonlinear models from data is very common. It is capable of approximating both linear and nonlinear functions defined over a range of data to the desired degree of accuracy using an appropriate number of hidden neurons, this has been proven mathematically [27]. Being data-driven models, they learn from training data presented to them and do not require any a priori assumptions about the problem, not even information about statistical distributions. In petroleum engineering, the training data may be assembled from experimental data, past field data, numerical reservoir simulation, real-time data, or a combination of these [5]. Though assumptions are not required, knowledge of the statistical distribution of the input data and domain knowledge of the problem can help to speed up training. Several issues such as the ability to run parallel processes and apply learning instead of programming have made ANN an efficient tool to be

applied in various fields of engineering [28]. In the training process, weights and biases of the network are adjusted on basis of learning rules and completing training; these fixed weights and biases act as the memory of the network.

Some of the advantages of ANN are; ability to handle linear and nonlinear models: complex linear and nonlinear relationships can be derived using neural networks. Flexible input/output: neural networks can operate using one or more descriptors and/or response variables. They can also be used with categorical and continuous data. Noise: neural networks are less sensitive to noise than statistical regression models. While some of the major limitations are; Black box models: it is not possible to explain how the results were calculated in any meaningful way. Optimizing parameters: there are many parameters to be set in a neural network and optimizing the network can be challenging, especially to avoid overtraining [23, 27, 29–32].

### *3.1.2. Extreme learning machine (ELM)*

Extreme learning machines (ELM) are derived from ANN, it is however a generally unified single layer feed-forward network framework with less requirement of human interventions and thus has been found to run faster than most conventional neuron-based techniques. This is notably due to the fact that the learning parameters of its hidden nodes, including input weights and biases, are assigned randomly without any dependency, and the simple generalized operation that is involved in the determination of the output weights. The training phase with data in the ELM algorithm is efficiently completed using a fixed nonlinear transformation which is a fast learning process. The efficiency of ELM in online or real-time applications cannot be over emphasized as it automatically determines all the network parameters analytically and therefore avoids unnecessary human intervention [33].

Also, the universal approximation ability of the standard ELM with additive or Radial Basis Function (RBF) activation function has been proved [7, 33]. Success story of the application of ELM in many real-world problems is well documented especially in classification and regression problems on very large scale datasets. ELM is very efficient and effective as an innovative training algorithm for single-hidden layer feed-forward neural networks (SLFNs) [33].

Some of the merits and limitations of ELM can be summarized as follows: ELM reduces the computation burden without sacrificing the generalization capability in the expectation sense. ELM needs much less training time compared to popular ANN and SVM/SVR. The prediction accuracy of ELM is usually slightly better than ANN and close to SVM/SVR in many applications. Compared with ANN and SVR, ELM can be implemented easily since there is no parameter to be tuned except an insensitive parameter L. It should be noted that many nonlinear activation functions can be used in ELM [33]. While the limitations are ELM suffered from both the uncertainty and generalization degradation problem and for the widely used Gaussian-type activation function, ELM degraded the generalization capability [34].

### *3.1.3. Support vector regression (SVR)*

Support vector regressions (SVRs) methodology involves a group of related supervised learning methods employed for both regression and classification problems. They fall in the

category of generalized linear classifiers (GLCs). In SVRs, a maximal hyperplane is constructed to separate a high dimensional space of input vectors mapped with the feature space. It was initially designed as a classifier only to be modified in a later study by Vapnik [35] as a support vector regressor (SVR) for regression problems. Its robustness in a single model estimation condition has been testified to [36]. Hence, it can be considered invaluable for the estimation of both real valued and indicator functions as common in pattern recognition and regression problems, respectively.

When used as a regressor, SVRs attempt to choose the "best" model from a list of possible models (i.e., approximating functions) $f(\mathbf{x}, \boldsymbol{\omega})$, where a set of generalized parameters is given by $\boldsymbol{\omega}$. Generally, "good" models are those that can generalize their good predictive performance on an out-of-sample test set. This is often determined by how well the model minimizes the cost function while training with the training data. The core feature of SVR regression in control of its attractive properties is the notion of an $\varepsilon$-insensitive loss function. SVR is suitable for estimating the dominant model under multiple model formulation, where the objective function can be viewed as a primal problem, and its dual form can be obtained by constructing Lagrange function and introducing a set of (dual) variables.

SVRs generalization characteristics are ensured by the special properties of the optimal hyperplane that maximizes the distance to training examples in a high dimensional feature space. It has been shown to exhibit excellent performance [32]. The merits and limitations of SVRs are summarized thus; merits: SVRs can deal with very high dimensional data; they can learn very elaborate concepts; usually works very well. While the limitations are: requirement of both positive and negative examples; the need to select a good kernel function; consumes lots of memory and CPU time; there are some numerical stability problems in solving the constrained [30, 37, 38]. Analysis of (linear) SVR indicates that the regression model depends mainly on support vectors on the border of $\varepsilon$-insensitive zone; SVR solution is very robust to "outliers" (i.e., data samples outside $\varepsilon$-insensitive zone). These properties make SVM very attractive for its use in an iterative procedure for multiple model estimation.

### *3.1.4. Least square support vector regressions (LS-SVR)*

LS-SVRs are reformulated versions of the original SVRs algorithm for classification and function estimation, which maintains the advantages and the attributes of the original SVRs theory. LS-SVRs are closely related to regularization networks and Gaussian processes but additionally emphasize and exploit primal-dual interpretations [39]. LS-SVR possesses excellent generalization performances and is associated with low computational costs. LS-SVR requires less effort in model training in comparison to the original SVR, owing to its simplified algorithm. It minimizes a quadratic penalty on the slack variables which allows the quadratic programming problem to be reduced to a set of matrix inversion operations in the dual space, which takes less time compared to solving the SVR quadratic problem [40]. Robustness, sparseness, and weightings can be incorporated into LS-SVRs where needed and a Bayesian framework with three levels of inference has also been developed [41]. Some of its limitations include being ineffective at handling non-Gaussian noise as well as being sensitive to outliers [42].

## 4. Case study

A case study is presented below to illustrate one of the advantages inherent in combining AI techniques with domain expert knowledge for improved prediction and optimization of drilling rate of penetration.

### 4.1. Data description

In this study, data from two development wells from onshore Niger Delta hydrocarbon province were used for the development and testing of the models, in each of the AI algorithms compared. The field is about 95 square kilometers in extent with a northwest-southeast trending dual culmination rollover anticline. The wells chosen represents the best in terms of drilling performance as measured by best ROP and bit runs for all the three hole sections considered. The formations encountered are mainly consolidated intercalation of shales and shallow marine shoreface sands with a normal compaction trend, a typical elastic depositional environment of the Niger Delta. The field is a mainly gas field with some of the reservoirs having significant oil rims.

The wells used for the study were selected for ROP prediction because they were the best in class in terms of drilling performance, a result of carefully optimized drilling parameters and practices. The repeatability of such feat is highly desirable, and hence the choice of the wells. The formations encountered are well correlated across the field with lateral continuity. These two wells fairly represents the field with Well-A located in the Eastern flank of the field while Well-B is located 8 km to the west of Well-A and just about 3 km to the field western boundary. While Well-A is highly deviated and deeper in reach with maximum inclination of 74° at total depth of 11,701 ft TVD, Well-B is slightly deviated with maximum inclination of 23° at total depth of 9000 ft TVD The wells are also similar in terms of drilling equipment, the same rig was used for their construction; bit type and bottom hole assembly (BHA) used were same, hence, they were both drilled with the same bottom hole hydraulics. Details of the bit used in the three hole sections included in this research are presented in **Table 3**.

| BHA No. | Type | Make/Model | IADC Code | Initial status | Nozzle Size | TFA | IADC Dull Grade |
|---|---|---|---|---|---|---|---|
| 16″ Hole section | | | | | | | |
| 1 | Tri-Cone bit | Baker Hughes Christensen bits/ MXL-DS3DDT | 135 | New | 22*3; 1*20 | 1.42 | 6-5-WT-A-E-1/16-FC-PR |
| 12-1/4″ Hole section | | | | | | | |
| 1 | PDC Bit | VAREL PDC(VTD713 P2DGX) | | New | 16*5; 18*2 | 1.479 | 2-2-CT-A-X-1/16-WO-TD |
| 8 1/2″ Pilot hole section | | | | | | | |
| 1 | PDC Bit | BM 563 | | New | 16*2; 13*8 | 1.17 | 1-1-WT-A-X-1-NO-TD |

**Table 3.** Bit details.

As explained in Section 2.4, the specific energy concept in the drillability of a formation is being explored in this study with particular focus on hydromechanical specific energy, HMSE. The HMSE concept states that "the energy required to remove a unit volume of rock comes primarily from the torque applied on the bit, the weight on bit (WOB), and the hydraulic force exerted by the drilling fluid on the formation" [14]. Drilling data from surface data logging (SDL) tools were used in this study. These were real-time data collected at surface and could be transmitted via satellite to a central location while drilling. Among the numerous data usually collected are; measured depth (MD), hookload (HKLD), weight on bit (WOB), pipe rotation per minute (RPM), rotary torque (TORQ), mud flow-in rate (GPM), total gas (TG), pump strokes per minute (SPM), pits volume change, mud flow-out rate percentage (FFOP%), mud weight in (MW), etc. Since ROP prediction using the hydromechanical specific energy ROP model is the focus of the research, efforts to use as many data that affects ROP were consciously made. Given the HMSE Eqs. (6) and (7) in Section 2.4, [14]. It is necessary therefore, to reorganize the collected data and focus on those with physical relationship with ROP based on the HMSE-ROP model.

It is important to mention that the surface drilling mechanics data are inexpensive to collect during drilling operations; the sensors can be calibrated without disturbing drilling operations and are a must-have for drilling operations. Hence, continuous drilling data such as MD, WOB, RPM, flow rate, mud weight, bit size, TORQ, SPP from the two wells were used in this study. Data quality checks were performed on individual wells and simple activity logic was applied to ensure only on-bottom drilling data were used. Noise, as a result of sensor issues, and spurious data points within the dataset were filtered out of the collection first using activity code to sort the data and manually removing data points that are out of range using excel spreadsheet.

### 4.2. Details of the experiment/methodology

The following approach was used in the preparation of the model using data from the selected well as follows:

1. Collect and explore the datasets: raw data from the two wells, which included several drilling equipment parameters, were explored to analyze properties of interesting attributes as it relates to the objective of the study. Eight measured drilling parameters of interest were eventually selected for this study.

2. Data integrity check: verify the data quality and identify plausibility of values from operational point of view.

3. Sorting of data: using drilling activity code to separate on-bottom parameters of the identified predictors (drilling parameters to be used for ROP prediction in the AI models) from HMSE-ROP model. Clean datasets by removing noise either as a result of sensor calibration issues or as equipment malfunctioning using operational background knowledge. The total number of drilling variables which were used as predictors of ROP is presented in **Table 4**.

| Well-Code | No of data | Utilized drilling parameters (Predictors) |
|---|---|---|
| Well-A (Dataset 1) | 3641 | WOB, RPM, TORQ, SPP, GPM, Depth, MW, Bit Size |
| Well-B (Dataset 2) | 5228 | WOB, RPM, TORQ, SPP, GPM, Depth, MW, Bit Size |

Key: weight on bit (WOB), bit rotation per minute (RPM), rotary torque (TORQ), stand pipe pressure (SPP), flow rate in gallons per minute (GPM), mud weight (MW).

**Table 4.** Streamlined datasets for each of the wells (predictors) used in the models.

Statistical properties of the data in various forms such as standard deviation, mean, median, etc., were taken before training the learning models. Statistical analysis helped to reveal certain characteristics of the datasets, one of such important characteristics is standard deviation as can be seen in **Tables 5** and **6**.

It reveals that the dataset varies widely as a result of the different lithological units penetrated, and as such data normalization was carried out as part of preprocessing. This brought the various data within same range to align their distributions and prevented biasing of the model toward large values that are present in the dataset [6].

Data splitting and model development: to ensure uniform distribution of the data point and removed effect of biased sampling, the normalized data were then randomized before used in the model development. Data from the two wells were randomly split into 70% for training, 15% for testing and 15% for validation with which the algorithms were trained, modified to come up with an acceptable model for testing in each of the artificial intelligence techniques.

| | Depth (ft) | Flowrate (gpm) | WOB (klb) | RPM (rpm) | TORQ (kf-p) | SPP (psig) | MW (ppg) | Bit Size (inch) | ROP (fph) |
|---|---|---|---|---|---|---|---|---|---|
| Min | 2681.3 | 450 | 1 | 2 | 1.33 | 1232 | 8.6 | 12.25 | 9 |
| Max | 12982.5 | 1108 | 68 | 142 | 20.32 | 4216 | 11.5 | 16 | 170 |
| SD | | 83.94 | 6.72 | 28.75 | 3.47 | 557.65 | 0.78 | — | 40.26 |
| Median | | 916 | 14 | 129 | 19.51 | 2878 | 10.4 | — | 82.6 |
| Mean | | 899.59 | 14.70 | 117.93 | 17.73 | 2878.82 | 10.29 | — | 84.43 |

**Table 5.** Statistical analysis of Well-A (Dataset A).

| | Depth (ft) | Flowrate (gpm) | WOB (klb) | RPM (rpm) | TORQ (kf-p) | SPP (psig) | MW (ppg) | Bit Size (inch) | ROP (fph) |
|---|---|---|---|---|---|---|---|---|---|
| Min | 302.4 | 375 | 2 | 10 | 1 | 317 | 8.9 | 8.5 | 2.7 |
| Max | 9264 | 2449 | 47 | 152 | 24.28 | 3522 | 10.5 | 16 | 281 |
| SD | | 135.15 | 8.43 | 51.77 | 4.47 | 629.79 | 0.51 | — | 117.10 |
| Median | | 888 | 16 | 41 | 7.06 | 2272 | 9.26 | — | 158 |
| Mean | | 887.93 | 16.05 | 79.21 | 7.94 | 2372.71 | 9.68 | — | 177.22 |

**Table 6.** Statistical analysis of Well-B (Dataset B).

Data integrity and similarity were also preserved in all methods to avoid bias in evaluating different algorithms across the four AI techniques.

Model development: the implementation of ANN was carried out using MatLab® ANN toolbox. The implementation was based on the backpropagation algorithm with momentum and adaptive learning rate, and the sigmoidal functions. In the implementation of ELM, the algorithm was based on MatLab® regularized ELM codes found in ELM algorithms [43]. The SVR and LS-SVR model was implemented using the least-square-SVM (LS-SVM) proposed by Valyon and Horvath [44] combined with other functions found in the LS-SVMlab1.8 code [45]. The code was slightly modified to include heavy tailed RBF (htrbf) kernel proposed in Chapelle et al. [46].

Train models and cross validate to select best model: in the training of ANN model, weights and biases of the networks were updated by Levenberg-Marquart (LM) algorithm while the number of hidden layers and neurons was randomly investigated from 1 to 5 and 10 to 100, respectively, in a loop. The algorithm was run for 500 times, and the best models that gave the least RMSE values in the cross-validation results were selected. Similar procedure was used in the training of the ELM models except that number of neuron range from 50 to 5000. In the training of SVR and LS-LSVR models, the algorithms hyper-parameters (e-tube (epsilon), tunning parameter (C), lambda and kernel for SVMR and tunning parameter (gam) and kernal for LS-SVMR) were optimized using cross-validation technique. For each run, a kernel function was chosen and investigated for different range of values of other parameters in a loop. The Kernel function and other corresponding hyper-parameters with the least RMSE values during cross-validation of each run were identified as the best model. **Table 7** shows the final selected model hyper-parameters.

Testing and evaluation of models: the models were tested using the testing data and the three set evaluation criteria: cc, RMSE and testing time were recorded for evaluation models.

| AI techniques | Well-A | Well-B |
|---|---|---|
| SVR | C = 9.4422e+08,<br>kernel, = 'htrbf'<br>kernel option = [0.0391, 1.04267],<br>lambda = 0.00310<br>epsilon = 0.0464 | C = 1.4035e+08,<br>kernel, = 'htrbf'<br>kernel option = [0.0733,1.01050],<br>lambda = 5.38274e-04<br>epsilon = 0.0880, |
| LS-SVR | gam = 5.750319e+02<br>kernel, = 'htrbf',<br>kernel option = [8.3120e-04, 0.4753] | gam = 990,000<br>kernel, = 'htrbf',<br>kernel option = [3.6048e-06,0.9228] |
| ANN | Activation functions = [logsig, tansig, purelin]<br>Hidden nodes = [51,19] | Activation functions = [tansig, logsig, purelin]<br>Hidden nodes = [61, 71] |
| ELM | Activation function = tribas<br>Node = 1241<br>Regularization = 15.7419 | Activation function = tribas<br>Node = 2731<br>Regularization = 81.9853 |

**Table 7.** Summary of optimized parameters used in the implementation of models.

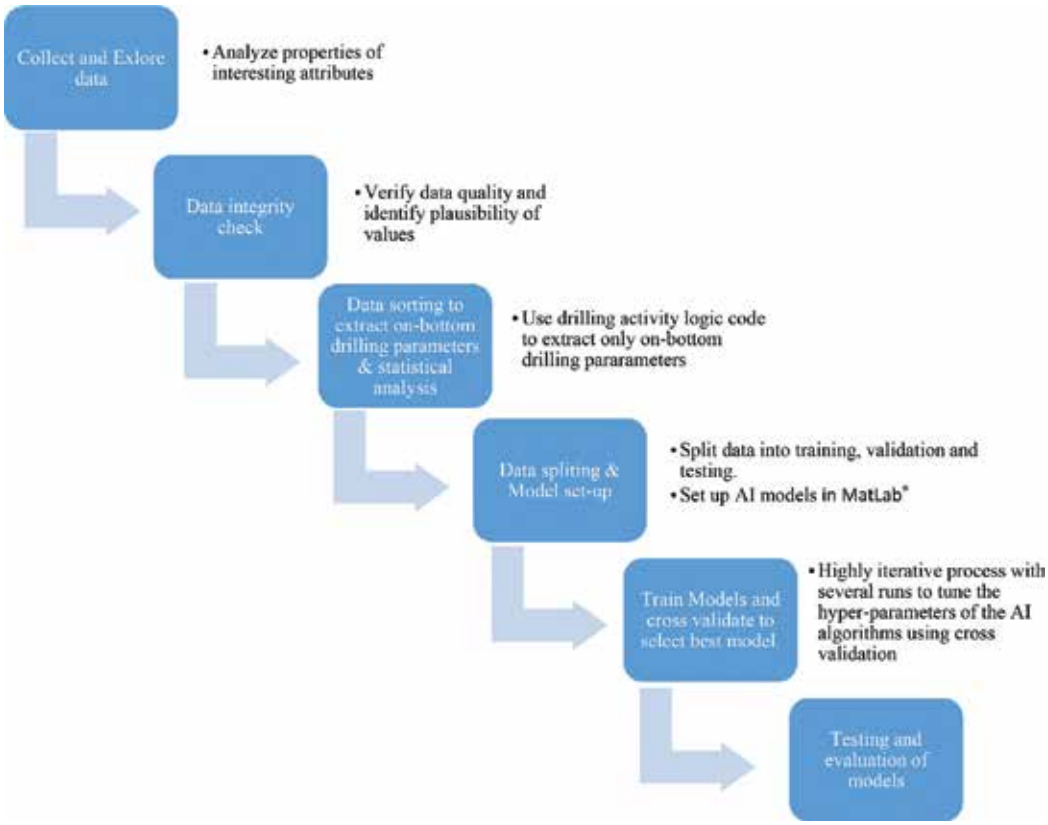


**Figure 3.** Methodology flowchart.

The flowchart presented in **Figure 3** summarizes the processes.

Data from each well were randomly split into 70% for training, 15% for testing, and 15% for validation with which the algorithms were trained, modified to come up with an acceptable model for testing in each of the artificial intelligence techniques.

To ensure uniform distribution of the data point and removed effect of biased sampling, the normalized data were then randomized before use in the model development. To avoid bias in evaluating different algorithms across the four AI being compared, data integrity and similarity were preserved in all methods. Three performance measures: root mean square error (RMSE), correlation coefficient (cc), and testing time were used to assess the performance of the algorithms.

### 4.3. Performance assessment criteria

To establish a valid evaluation of the performance of the different AI being compared, the assessment criteria used in petroleum journals were considered as the criteria for measuring performance [27, 32]. The criteria are as follows.

*4.3.1. Correlation coefficient (CC)*

This is a measure of the strength of relationship between the predicted value and the actual value being predicted. It indicates how far the model prediction deviates from the real value with high values indicating good performance and vice versa.

$$cc = \frac{\sum \left(y_a - y'_a\right)\left(y_p - y'_p\right)}{\sqrt{\sum \left(y_a - y'_a\right)^2 \left(y_p - y'_p\right)^2}} \tag{8}$$

*4.3.1. Root mean-squared error (RMSE)*

This can be interpreted as the standard deviation of the variance of the predicted value from the corresponding observed value. It is a measure of absolute fit and indicates how close the predicted values are from the actual observed values.

$$\text{rmse} = \sqrt{\frac{\left(x_1 - y_1\right)^2 + \left(x_2 - y_2\right)^2 + \ldots. + \left(x_n - y_n\right)^2}{n}} \tag{9}$$

The strategy followed is to implement the four techniques under the same data and processing conditions as described above to avoid bias in evaluating different algorithms [29, 30, 47]. Also, the design of the individual models utilized the cross-validation technique to select the optimal tuning hyper-parameters with the validation data set using the RMSE evaluation criteria to measure their performance. Runs for each of the techniques were repeated several times using a loop, in order to optimize the hyper-parameter of the models while using cross-validation to select the best model for the algorithms. The testing data is run on the model and cc, RMSE and testing time were recorded to evaluate the model for comparison.

### 4.4. Experimental results and discussion

In the implementation of each of the techniques tested for ROP prediction, the training, validation, and testing data described above were used.

- Dataset A which comprises of eight HMSE-ROP related drilling parameters from Well-A.
- Dataset B which comprises of eight HMSE-ROP-related drilling parameters from Well-B.

The datasets are presented in **Table 8**.

| Dataset | Drilling parameters (Predictors) |
|---|---|
| A | Depth, WOB, RPM, TORQ, Flowrate, SPP, MW and Bit Size for Well-A |
| B | Depth, WOB, RPM, TORQ, Flowrate, SPP, MW and Bit Size for Well-B |

**Table 8.** Drilling parameters used in each of the two datasets.

| | Training RMSE | Testing RMSE | Training CC | Testing CC | Testing Time |
|---|---|---|---|---|---|
| SVR | 14.39394 | 23.29097 | 0.937030 | 0.808604 | 2.839218 |
| ANN | 27.26942 | 27.58479 | 0.737530 | 0.715336 | 0.031200 |
| LS-SVR | 10.82009 | 21.57755 | 0.966169 | 0.837852 | 2.730018 |
| ELM | 23.17740 | 27.08876 | 0.819712 | 0.731162 | 0.078000 |

**Table 9.** Dataset A results.

| | Training RMSE | Testing RMSE | Training CC | Testing CC | Testing Time |
|---|---|---|---|---|---|
| SVR | 10.73935 | 21.71836 | 0.980072 | 0.910637 | 5.725237 |
| ANN | 26.41347 | 28.04187 | 0.866958 | 0.845982 | 0.031200 |
| LS-SVR | 3.69279 | 18.83404 | 0.997702 | 0.933733 | 5.460035 |
| ELM | 25.01964 | 27.98157 | 0.881806 | 0.846528 | 0.140401 |

**Table 10.** Dataset B results.

**Tables 9** and **10** show the results of the four AI algorithms used for ROP prediction in the study. After several runs, the best model in each were tested and evaluated to be adjudged the best. The algorithms were independently tested with eight drilling parameters presented in **Table 8**.

### 4.5. Discussion of results

Each of the four AI techniques tested exhibited its competitive performance as shown in the results. **Figures 4–6** show the performance of the four techniques in each of the dataset both during the training and testing, and therefore revealed their respective comparative strong and weak points. The comparative results of the four AIs applied to the two datasets using the same drilling parameters were plotted and are as shown in **Figure 4**.

RMSE and CC as earlier defined are measures of performance in terms of accuracy, with the algorithm exhibiting lowest RMSE and highest CC being the most accurate predicting algorithm. In **Figure 4**, a cross-plot of the testing correlation coefficient (cc) against the testing root mean square error (RMSE) shows that in Well-A the best performance in terms of accuracy in the algorithms is produced by LS-SVR followed closely by SVR while the least accurate performance is seen in ELM and ANN. The same pattern is repeated in Well-B with LS-SVR exhibiting the best performance and ANN and ELM performance are not remarkably far from each other. The overall best performance is LS-SVR performance in Well-B. This is as a result of the data density in Well-B as seen in **Table 3**. Therefore, LS-SVR provides an excellent function estimation capability.

By comparing the testing time as seen in **Tables 7** and **8**, and plotting in **Figure 5**, it is evident that among the four algorithms tested, LS-SVR and SVR in both wells require considerable amount of time for model testing, while ANN and ELM require the minimum time for the

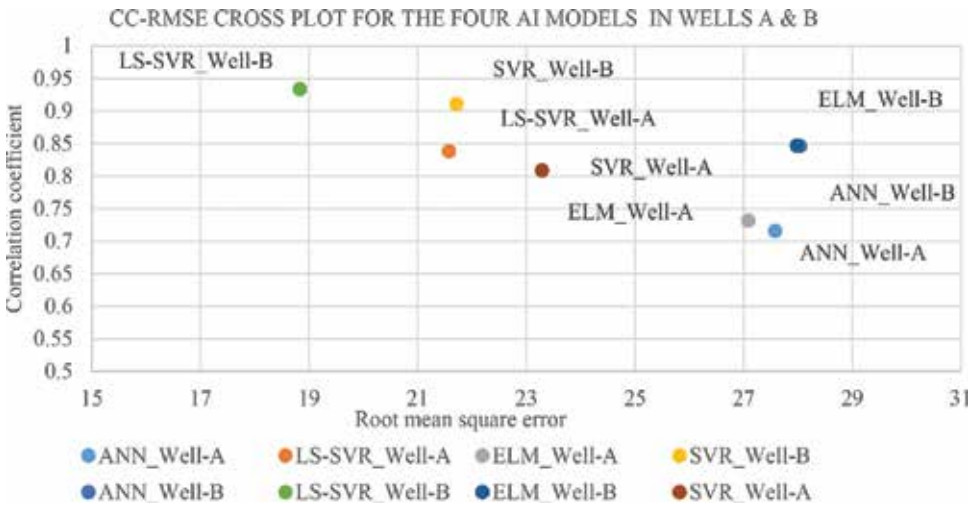


**Figure 4.** CC-RMSE plot showing testing results for dataset 1 and 2 for wells A and B, respectively.

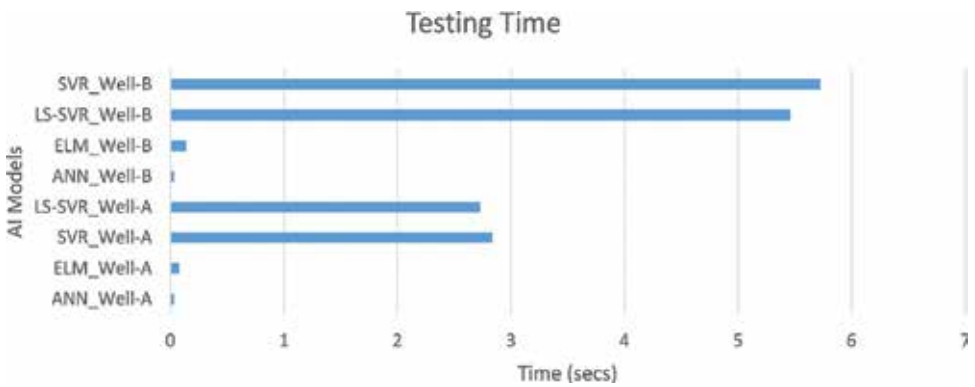


**Figure 5.** Testing time for each of the algorithms tested with the two datasets.

same process. The density and amount of data used for Well-B as can be seen in **Table 3**, is evidently responsible for the extra time it takes for testing the model.

The application of domain knowledge and in particular, the utilization of specific energy as a concept in selecting the controllable drilling parameters used in the prediction of ROP has proven valuable with all the AI models showing accuracy within acceptable range. A depth plot of actual ROP against the predicted ROP from all the AI models is presented in **Figure 6**. As can be observed, the qualitative difference is quite elusive showing that the four AI models are good predictors with reasonable accuracy.

In summary, the LS-SVR produces the best ROP model for the two dataset in term of accuracy, while it requires considerable amount of testing time of the four AI techniques compared. Therefore, it is more suitable for situations where accuracy is most desirable. Whereas, ELM and ANN requires the shortest testing execution time and are less accurate, they are more

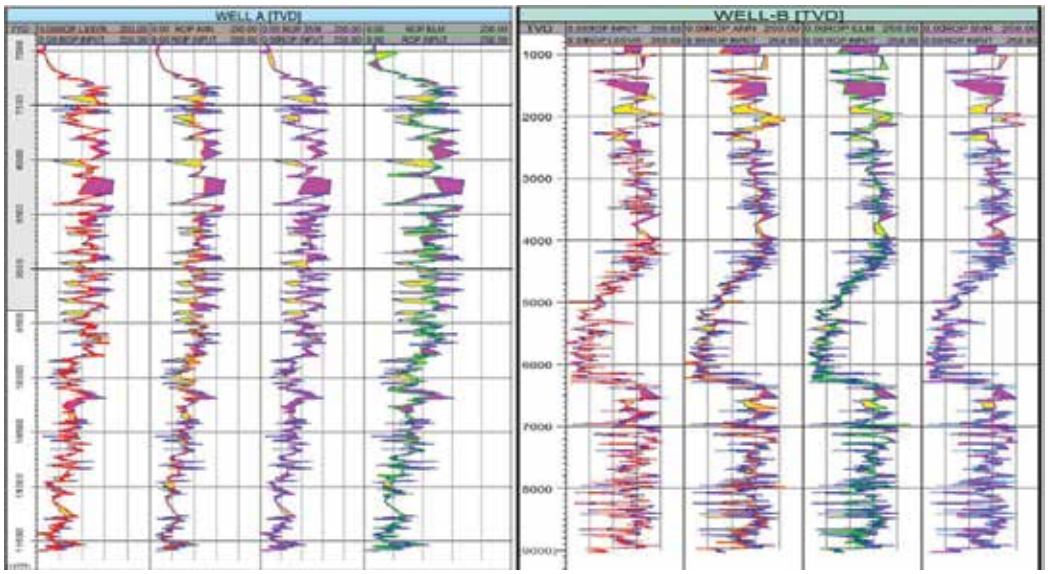


**Figure 6.** AI predicted ROPs plotted against actual ROP for Well-A and -B.

suitable for scenarios where the execution time critical. It must however be stated, that the use of drilling domain knowledge in the choice of drilling parameters has enhance the accuracy of all the AI algorithm predicted ROPs to be within acceptable range, while using variables from HMSE-ROP model as input.

## 5. Conclusion

AI techniques have increasingly proved to be of immense value in the oil and gas industry where it has been employed by different segments of the industry. Traditional methods has not been able to manage such huge impacts in such a short time as AI methods because of its ability to decipher hidden codes and complex relationships within the enormous data collected daily during drilling operations. However, application of the right domain expert knowledge has shown improved performance in the deployment of AI techniques. This technique and its application leads to time and cost saving, minimized risk, improved efficiency and solutions many optimization problems. The ability of the technique to retrain itself with life data within a shorter time has made it a major founding block for drilling automation.

This paper presents an improved methodology of predicting ROP with real-time drilling optimization in mind. Recent studies in the use of AI in the prediction of ROP shows some inconsistency in the selection of input variables. The parameters used in this study are the must haves and easily accessible parameters which can mostly be adjusted while drilling and are therefore controllable. The utilization of HMSE-ROP model has also enhanced the performance of the models as a result of selecting few variables with established relationship to ROP even though nonlinear. All the methods used provided good degree of accuracy, and therefore presented the engineers with options to use whichever algorithm is suitable for their

scenarios. It is therefore recommended that the HMSE variables should always be included in the data attributes in the prediction of ROP as they are good predictors.

## Nomenclature

| | |
|---|---|
| AI | artificial intelligence |
| AIAI | artificial intelligence applications institute |
| ANN | artificial neural network |
| BHA | bottom hole assembly |
| CART | classification regression trees |
| CIT | computational intelligence techniques |
| CPU | computer processing unit |
| $d_b$ | diameter of bit |
| DEO | drilling efficiency optimization |
| DSE | drilling specific energy |
| ELM | extreme learning machine |
| $F_D$ | footage drilled by bit, ft |
| GHI | grit hot-pressed inserts |
| GLC | generalized linear classifiers |
| GPM | gallon per minute |
| HMSE | hydraulic mechanical specific energy |
| IADC | international association of drilling contractors |
| LSSVR | least square support vector regression |
| LWD | logging while drilling |
| MATLAB | matrix laboratory |
| MD | measured depth |
| MWD | measurement while drilling |
| NPT | non-productive time |
| $\Delta p_b$ | pressure loss at bit in psi |
| PDA | predictive data-driven analysis |
| PDC | polycrystalline diamond compact |

| | |
|---|---|
| PDM | positive displacement motor |
| Q | mud flow-in rate in gallons per minute |
| RMSE | root mean square error |
| ROP | rate of penetration, ft/h |
| RPM | rotation per minute |
| SDL | surface data logging |
| SE | specific energy |
| SFLA | shuffled frog leaping algorithm |
| SLFN | single-hidden layer feedforward neural |
| SPM | strokes per minutes |
| SPP | stand pipe pressure |
| SVR | support vector regression |
| t | time, h |
| TDS | top drive system |
| TG | total gas |
| TRQ | torque |
| TVD | true vertical depth |
| WDM | warren drilling model |
| WOB | weight on bit, lbs |
| $C_{fd}$ | formation drillability parameter |
| $\overline{W}$ | function of WOB and db |
| $\eta$ | dimensionless energy reduction factor depending on bit diameter |

## Author details

Omogbolahan Ahmed[1]*, Ahmed Adeniran[2] and Ariffin Samsuri[1]

*Address all correspondence to: saomogbolahan2@live.utm.my

1 Faculty of Chemical and Energy Engineering, Universiti Teknologi Malaysia, Johor Bahru, Johor, Malaysia

2 Department of Systems Engineering, King Fahd University of Petroleum and Minerals, Dhahran, Saudi Arabia

## References


[1] Young FS Jr. A multiple regression approach to optimal drilling and abnormal pressure detection. Society of Petroleum Engineers Journal. 1974;**14**:371

[2] Ansari HR, Sarbaz Hosseini MJ, Amirpour M. Drilling rate of penetration prediction through committee support vector regression based on imperialist competitive algorithm. Carbonates and Evaporites. 2017;**32**(2):205-213

[3] Mantha B, Samuel R. ROP Optimization Using Artificial Intelligence Techniques with Statistical Regression Coupling. SPE Annu. Tech. Conf. Exhib.; 2016

[4] Sugiura J, Samuel R, Oppelt J, Ostermeyer GP, Hedengren J, Pastusek P. Drilling Modeling and Simulation: Current State and Future Goals. Spe, no. Downton 2012; 2015

[5] Jahanbakhshi RKR. Real-time prediction of rate of penetration during drilling operation in oil and gas wells. American Rock Mechanics Association. 2012;**53**(3):127

[6] Bodaghi A, Ansari HR, Gholami M. Optimized support vector regression for drilling rate of penetration estimation. Open Geosciences. 2015;**7**(1):870-879. https://doi.org/10.1515/geo-2015-0054

[7] Shi X, Liu G, Gong X, Zhang J, Wang J, Zhang H. An efficient approach for real-time prediction of rate of penetration in offshore drilling. Mathematical Problems in Engineering. 2016;**2016**

[8] Moraveji MK, Naderi M. Drilling rate of penetration prediction and optimization using response surface methodology and bat algorithm. Journal of Natural Gas Science and Engineering. 2016;**31**:829-841. DOI: 10.1016/j.jngse.2016.03.057

[9] Hossain ME, Al-Majed AA. Fundamentals of Sustainable Drilling Engineering. wiley; 2015:374-412. https://doi.org/10.1002/9781119100300

[10] Sui D, Nybo R, Azizi V. Real-time optimization of rate of penetration during drilling operation. IEEE Int. Conf. Control Autom. ICCA, no. 978; 2013. pp. 357-362

[11] Maurer WC. The 'perfect - cleaning' theory of rotary drilling. Journal of Petroleum Technology. 1962;**14**(11):1270-1274

[12] Galle E, Woods H. Best constant weight and rotary speed for rotary rock bits. Drilling and Production Practice. 1963

[13] Teale R. The concept of specific energy in rock drilling. International Journal of Rock Mechanics and Mining Science and Geomechanics Abstracts. 1965;**2**:57

[14] Mohan K, Adil F, Samuel R. Tracking drilling efficiency using hydro-mechanical specific energy. SPE/IADC Drill. Conf. Exhib., no. SPE/IADC 119421; 2009. pp. 1-12

[15] Shewalla M, Smith JR. Measure of specific energy during drilling of rocks. Electronic Journal of Geotechnical Engineering. 2015;**20**(16):6675-6686

[16] Dupriest FE, Koederitz WL. Maximizing Drill Rates with Real-Time Surveillance of Mechanical Specific Energy. SPE/IADC Drill. Conf., no. SPE/IADC 92194; 2005. pp. 1-10

[17] Koederitz WL, Johnson WE. Real-time optimization of drilling parameters by autonomous empirical methods. SPE-IADC Drilling Conference Proceeding. 2011;**1**:386-401

[18] Siddique N, Adeli H. Computational intelligence: Synergies of fuzzy logic, neural networks and evolutionary computing. United Kingdom: John Wiley and Sons, University of Ulster; 2013. DOI: 10.1002/9781118534823

[19] Smith C, Brian M, Ting H, Gary Y. The History of Artificial Intelligence. no. December. University of Washington; 2006. pp. 1-27

[20] AIAI. Artificial Intelligence Applications Institute. 2017. http://www.aiai.ed.ac.uk/. [Online]. Available: http://www.aiai.ed.ac.uk/. [Accessed: 01-Jan-2018]

[21] Bello O, Teodoriu C, Engineering G, Yaqoob T, Oppelt J, Holzmann J, Obiwanne A. SPE-184320-MS Application of Artificial Intelligence Techniques in Drilling System Design and Operations: A State of the Art Review and Future Research Pathways; 2016

[22] Meng CUI, Mengci SUN, Jinwen Z, Kai K, Yucai LUO. Maximizing drilling performance with real-time surveillance system based on parameters optimization algorithm. Advances in Petroleum Exploration and Development. 2014;**8**(1):15-24

[23] AlArfaj I, Khoukhi A, Eren T. Application of advanced computational intelligence to rate of penetration prediction. Proc. - UKSim-AMSS 6th Eur. Model. Symp. EMS 2012; 2012. pp. 33-38

[24] Bilgesu HI, Tetrick LT, Altmis U, Mohaghegh S, Ameri S. A New Approach for the Prediction of Rate of Penetration (ROP) Values. SPE Eastern Regional Meeting; 1997

[25] Moran DP, Ibrahim HF, Purwanto A, Osmond J. Sophisticated ROP Prediction Technology Based on Neural Network Delivers Accurate Results Sophisticated ROP Prediction Technology Based on Neural Network Delivers Accurate Results. IADC/SPE Asia Pacific Drill. Technol. Conf. Exhib.; 2010. pp. 1-9

[26] Amer MM, Aramco S, Abdel P, Dahab S, Abdel-alim P. SPE-187969-MS An ROP Predictive Model in Nile Delta Area Using Artificial Neural Networks Artificial Neural Network (ANN); 2017

[27] Akande KO, Olatunji SO, Owolabi TO, AbdulRaheem A. Comparative analysis of feature selection-based machine learning techniques in reservoir characterization. Society of Petroleum Engineers. 2015:1-12

[28] Haykin S. Neural Networks: A Comprehensive Foundation. 2nd ed. Upper Saddle River, NJ, USA: Prentice Hall PTR; 1998

[29] Koskim E, Gs J, Kontkanen P, Myllym P, Tirri H. Comparing Soft Computing Methods in Prediction of Manufacturing Data

[30] Erturk E, Sezer EA. A comparison of some soft computing methods for software fault prediction. Expert Systems with Applications. 2015;**42**(4):1872-1879

[31] Gola G, Nybo R, Sui D, Roverso D. Improving Management and Control of Drilling Operations with Artificial Intelligence. SPE Intell. Energy …; 2012. pp. 1-7

[32] Anifowose F, Adeniye S, Abdulraheem A. Recent advances in the application of computational intelligence techniques in oil and gas reservoir characterisation: A comparative study. Journal of Experimental and Theoretical Artificial Intelligence. 2014;**26**(4). https://doi.org/10.1080/0952813X.2014.924577

[33] Huang G-B, Zhu Q, Siew C, GHÃ, Zhu Q, Siew C, Huang G-B, Zhu Q, Siew C. Extreme learning machine: Theory and applications. Neurocomputing. 2006;**70**(1–3):489-501

[34] Lin S, Liu X, Fang J, Xu Z. Is extreme learning machine feasible? A theoretical assessment (part II). IEEE Transactions on Neural Networks and Learning Systems. 2015;**26**(1):21-34

[35] Cortes C, Vapnik V. Support-vector networks. Machine Learning. 1995;**20**(3):273-297

[36] Vapnik VN. An overview of statistical learning theory. IEEE Transactions on Neural Networks. 1999;**10**(5):988-999

[37] Ye J, Xiong T. SVM versus least squares SVM. Journal of Machine Learning Research—Proc. Track. 2007;**2**:644-651

[38] Cherkassky V, Ma Y. SVM-based learning for multiple model estimation. ReCALL. 2002: 1-29

[39] Suykens JAK, De Brabanter J, Lukas L, Vandewalle J. Weighted least squares support vector machines: Robustness and sparse approximation. Neurocomputing. Oct. 2002;**48**(1–4):85-105

[40] Sachindra DA, Huang F, Barton A, Perera BJC. Least square support vector and multi-linear regression for statistically downscaling general circulation model outputs to catchment streamflows. International Journal of Climatology. 2013;**1106**(April):1087-1106

[41] Suyken AKJ, Van Tony G, De Brabanter J, De Moor B, Vandewalle J. Least Squares Support Vector Machines. World Scientific; 2002

[42] Lu X, Liu W, Zhou C, Huang M. Robust Least-Squares Support Vector Machine With Minimization of Mean and Variance of Modeling Error; 2017. pp. 1-12

[43] ELM algorithm code. ELM algorithm code, 2017, 2017. [Online]. Available: http://www.ntu.edu.sg/home/egbhuang/elm_kernel.html. [Accessed: 05-Apr-2017]

[44] Valyon J, Horváth G. A robust LS-SVM regression. Proceeding of World Academy of Science, Engineering and Technology. 2005;**7**(August):148-153

[45] LS-SVMlab1.8 code, 2017. LS-SVMlab1.8 code, 2017. Matlab R2009b - R2013, 2013. [Online]. Available: http://www.esat.kuleuven.be/sista/lssvmlab/. [Accessed: 05-Apr-2017]

[46] Chapelle O, Haffner P, Vapnik VN. Support vector Machines for Histogram-based Image Classification. Transactions on Neural Networks. Sep. 1999;**10**(5):1055-1064

[47] Wang L, Kisi O, Zounemat-Kermani M, Gan Y. Comparison of six different soft computing methods in modeling evaporation in different climates. Hydrology and Earth System Sciences Discussions. 2016;(May):1-51

Chapter 7

# Drilling Performance Optimization Based on Mechanical Specific Energy Technologies

Xuyue Chen, Jin Yang and Deli Gao

Additional information is available at the end of the chapter

http://dx.doi.org/10.5772/intechopen.75827

**Abstract**

Mechanical specific energy (MSE) has been widely used to quantify drilling efficiency and maximize rate of penetration (ROP) in oil and gas wells drilling. In this chapter, MSE models respectively for directional or horizontal drilling and rotating drilling with positive displacement motor (PDM) are established based on the evaluation of virtues and defects of available MSE models. Meanwhile methods for drilling performance prediction and optimization based on MSE technologies are presented. Field data presented in this chapter indicates that the developed MSE models estimate MSE values with a reasonable approximation in the absence of reliable torque measurements, the method for optimizing drilling parameters can estimate optimum WOB values with different RPM to drill a specific formation interval with PDM. It also show that the optimum WOB is low for rotating drilling with PDM compared with the conventional drilling without PDM, increasing WOB does not always increase ROP but is more likely to decrease ROP. The drilling performance prediction and optimization methods based on MSE technologies could be effectively used to maximize ROP and allow operators to drill longer and avoid unnecessary trips, and is worthy to be applied and promoted with highly diagnostic accuracy, effective optimizing and simple operation.

**Keywords:** mechanical specific energy, drilling performance optimization, positive displacement motor, optimum WOB, maximize rate of penetration

## 1. Introduction

Maximizing ROP to reduce drilling cost in oil and gas development is the permanent objective of drilling researchers [1–4]. Numerous methods have been developed for optimizing drilling parameters to maximize ROP, and they are similar to drill rate and drill-off tests in that they observe trends in performance and attempt to identify the founder point, which is the point at

which the ROP is maximized [5]. Although these methods have enhanced drilling performance, they do not provide an objective assessment of the true potential ROP, only the founder point of the current system. Actually the process of optimizing drilling parameters should be not only drilling system specific but also formation specific. MSE is defined as the mechanical work done to excavate a unit volume of rock, it could provide an objective assessment of the drilling efficiency and an objective tool to identify the bit founder. The initial MSE model for rotating drilling system was proposed by Teale in 1965 [6]. In this model, as the majority of field data is in the form of surface measurements, which results in MSE's calculation containing even large sources of error. Then numerous investigators were motivated to develop more accurate models. These models include those presented by Pessier and Fear [7], Dupriest and Koeteritz [5], Armenta [8], Mohan et al. [9], Cherif [10], Mohan et al. [11] and they have been widely used in bit selection, drilling efficiency quantification, drilling performance monitoring, drilling performance optimization, ROP improvement and so on. Although the MSE obtained from these models are more and more precisely model the actual downhole drilling in vertical wells, currently there are few effective MSE models to precisely model the actual downhole drilling in directional or horizontal wells due to the majority of field data is in the form of surface measurements.

Moreover, in recent years, PDM has gained widespread use in the hard formation drilling to improve ROP. In rotating drilling with PDM, the power section of PDM converts hydraulic energy of mud flow into mechanical rotary power, the surface rotation is superimposed on downhole motor rotation. During slide drilling, bit rotation is generated only from the PDM as drilling fluid is pumped through the drill string. However, the PDM's performance is controlled by the combination of the rotor/stator lobe configuration, and the direct measurement of PDM rotary speed and torque in down hole has proven difficult. Therefore, currently there are also few effective MSE models to precisely model the actual downhole drilling for rotating drilling with PDM.

In this chapter, MSE models respectively for directional or horizontal drilling and rotating drilling with PDM are established based on the evaluation of key MSE models and the analysis on PDM performance, meanwhile methods for drilling performance prediction and optimization based on MSE technologies are presented.

## 2. Mechanical specific energy model development

### 2.1. Key models of mechanical specific energy

Mechanical specific energy (MSE) has been defined as the mechanical work done to excavate a unit volume of rock. Teale in 1965 initially proposed the MSE model for rotating drilling system [6].

$$MSE = \frac{WOB}{A_b} + \frac{120\pi \cdot RPM \cdot T}{A_b \cdot ROP} \tag{1}$$

In the above model, torque at the bit is a main variable. Although torque at the bit can be easily measured in the laboratory and with Measurement While Drilling (MWD) systems in the field, the majority of field data is in the form of surface measurement. While in the absence of reliable torque at the bit measurements, the calculation of MSE based on this model contains even large sources of error. Therefore, it is only used qualitatively as a trending tool.

In 1992, Pessier and Fear provided a simple method of the calculation of torque at bit while in the absence of reliable torque measurements and optimized Teale's model [7].

$$\begin{aligned} MSE &= WOB \cdot \left( \frac{1}{A_b} + \frac{13.33 \cdot \mu_b \cdot RPM}{D_b \cdot ROP} \right) \\ \mu_b &= 36 \frac{T}{D_b \cdot WOB} \end{aligned} \tag{2}$$

The above model's parameters are easy to be obtained on the ground, and its calculation precision has been improved, as a result, it has a common usage in the drilling industry. In this model, the torque of bit is calculated through WOB. However, WOB is always read based on the surface measurement, which is not the bottom hole real WOB. As for directional and horizontal drilling, there is a great difference between the bottom hole real WOB and the WOB of surface measurement [12]. And every bit has a certain mechanical efficiency in drilling even for the new bits, thus Pisser's model has a limited application and also exists a certain error in MSE calculation.

Given the bit had a certain mechanical efficiency in the actual drilling process, Dupriest, Cherif and Amadi defined a mechanical efficiency on the base of Teale model [5, 10, 13].

$$MSE = E_m \cdot \left( \frac{WOB}{A_b} + \frac{120 \cdot \pi \cdot RPM \cdot T}{A_b \cdot ROP} \right) \tag{3}$$

Dupriest and Koederitz thought peak bit efficiencies are always in the 30–40% range, therefore thought the mechanical efficiency were 35% [5]. However, this is a controversial issue due to the bits' mechanical efficiency depending on a variety of factors, and it may vary greatly from the assumed 35%. Cherif argued that the mechanical efficiency were 26–64% instead of 35% [10]. In directional and horizontal drilling, the MSE values may eventually become several times the formation CCS due to torsional friction. So Amadi and Iyalla thought the mechanical efficiency were 12.5% in directional and horizontal drilling [13]. Actually the mechanical efficiency is not only bit specific but also formation specific, and it may vary greatly from bit to bit and formation to formation, so it must be determined according to the real drilling conditions. Therefore, the model also has certain limitations.

Recently some researchers think that hydraulic energy also aids in actual drilling for certain formations, then they add the hydraulic term to the MSE function as [9, 11].

$$MSE = \frac{WOB}{A_b} + \frac{120\pi \cdot RPM \cdot T}{A_b \cdot ROP} + \frac{\beta \cdot \Delta P_b \cdot Q}{A_b \cdot ROP} \tag{4}$$

Hydraulic energy has a great influence on drilling efficiency, but its role is complex. In conventional rotating drilling, bit hydraulics mainly accounts for the removal of cuttings from the bottom hole by jet-erosion, and the jet from bit nozzles could hardly aid in rock-broken especially in the deep and hard formations. Therefore, the MSE model is suitable for high pressure jet drilling and soft formation drilling.

In the above MSE models, MSE's calculation containing even large sources of error due to the majority of field data is in the form of surface measurements. Especially in directional and horizontal drilling, WOB and torque of surface measurement differs greatly from bottom hole actual $WOB_b$ and torque [12]. Therefore, few of the above MSE models can precisely model the actual downhole drilling in directional or horizontal wells. Moreover, in rotating drilling with PDM, the surface rotation is superimposed on downhole motor rotation [14]. During slide drilling, bit rotation is generated only from the PDM as drilling fluid is pumped through the drill string. However, the direct measurement of PDM rotary speed and torque in down hole has proven difficult, so few of the above MSE models can also precisely model the actual downhole drilling for rotating drilling with PDM.

## 2.2. Mechanical specific energy model of directional or horizontal drilling

### *2.2.1. Model of bottom hole* $WOB_b$

Undersection trajectory of directional well or horizontal well can reduce drag greatly compared to a conventional tangent section due to well friction. Therefore, there is a great difference between surface measured WOB and bottom hole $WOB_b$ at the bit. The surface measured WOB is actually the bottom hole $WOB_b$ acting on the ground. Therefore, by analyzing the internal force of drill string produced by bottom hole $WOB_b$ in each well section, we can get the formula between the surface measured WOB and bottom hole $WOB_b$.

(1) In bends section.

In 2008, Aadnoy formulated the drag model in bends and straight sections [15]. In the process of drilling, assuming the string contacts lower side, so the drag model in bends section is as follows

$$F_2 = f(\alpha_2) + (F_1 - f(\alpha_1)) \cdot e^{-\mu(\alpha_2 - \alpha_1)} \tag{5}$$

where:

$$f(\alpha) = \frac{w \cdot R}{1 + \mu^2} \left\{ \left(1 - \mu^2\right) \sin\alpha + 2\mu \cos\alpha \right\} \tag{6}$$

If $WOB_b = 0$, assuming that the force at the upper end of the bend is $F_1'$, and the force at the lower end of the bend is $F_2'$. If $WOB_b > 0$, using that the force at the upper end of the bend is $F_1''$, and the force at the lower end of the bend is $F_2''$, then gives

$WOB_b = 0$:

$$F_2{}' = f(\alpha_2) + \left((F_1{}' - f(\alpha_1)) \cdot e^{-\mu(\alpha_2-\alpha_1)}\right. \tag{7}$$

$WOB_b > 0$:

$$F_2{}'' = f(\alpha_2) + \left(F_1{}'' - f(\alpha_1)\right) \cdot e^{-\mu(\alpha_2-\alpha_1)} \tag{8}$$

Eq. (7) minus Eq. (8), we get

$$F_2{}' - F_2{}'' = \left(F_1{}' - F_1{}''\right)e^{-\mu(\alpha_2-\alpha_1)} \tag{9}$$

Obviously, "$F_2{}'$-$F_2{}''$" is the internal force of drill string produced by bottom hole $WOB_b$ at the lower end of the bend, "$F_1{}'$-$F_1{}''$" is the internal force of drill string produced by bottom hole $WOB_b$ at the upper end of the bend. So we may express Eq. (9) as follows

$$F_{i2} = F_{i1} \cdot e^{-\mu(\alpha_2-\alpha_1)} \tag{10}$$

where:

$$\alpha_2 - \alpha_1 = \Delta\alpha = \Delta\gamma \tag{11}$$

(2) In straight sections.

In straight sections, the drag model is as follows in the process of drilling

$$F_2 = F_1 + w \cdot \Delta s \cdot \left(\mu \sin\alpha - \cos\alpha\right) \tag{12}$$

If $WOB_b = 0$, assuming that the force at the upper end is $F_1{}'$, and the force at the lower end is $F_2{}'$. If $WOB_b > 0$, using that the force at the upper end is $F_1{}''$, and the force at the lower end is $F_2{}''$, then gives.

$WOB_b = 0$:

$$F_2{}' = F_1{}' + w \cdot \Delta s \cdot \left(\mu \sin\alpha - \cos\alpha\right) \tag{13}$$

$WOB_b > 0$:

$$F_2{}'' = F_1{}'' + w \cdot \Delta s \cdot \left(\mu \sin\alpha - \cos\alpha\right) \tag{14}$$

Eq. (13) minus Eq. (14), we get

$$F_2{}' - F_2{}'' = F_1{}' - F_1{}'' \tag{15}$$

Apparently, "$F_2{}' - F_2{}''$" is the internal force of drill string produced by bottom hole $WOB_b$ at the lower end, "$F_1{}' - F_1{}''$" is the internal force of drill string produced by bottom hole $WOB_b$ at the upper end. So we may express Eq. (15) as follows

$$F_{i2} = F_{i1} \tag{16}$$

Therefore, in the straight sections, internal force produced by bottom hole $WOB_b$ in each cross-section of the drill string is the same. As for straight sections, $\alpha_2 - \alpha_1 = \Delta\alpha = 0$, so Eq. (16) is the same as Eq. (10). Therefore, Eq. (10) is also suitable for straight section.

(3) Formula between WOB and $WOB_b$.

In the horizontal well, on the surface

$$F_i = F_{i1} = WOB, \quad \alpha_1 = 180^\circ, \gamma = 0^\circ \tag{17}$$

At the bit

$$F_i = F_{i2} = WOB_b, \quad \alpha_2 = 180^\circ + \gamma_b \tag{18}$$

and

$$\Delta\alpha = \Delta\gamma = \gamma_b \tag{19}$$

Insert Eqs. (17), (18) and (19) into Eq. (10), then we get the formula between WOB and $WOB_b$ in horizontal well [12].

$$WOB_b = WOB \cdot e^{-\mu\gamma_b} \tag{20}$$

**Figure 1** shows the relationship between weight on the bit ratio and bottom hole inclination, it indicates that there is a big difference between the surface measured WOB and bottom hole $WOB_b$ for horizontal well drilling.

*2.2.2. Model of bottom hole torque at the bit*

Torque at the bit can be measured with MWD systems in the field. However, the majority of field data is in the form of surface measurements, it usually uses of surface torque to calculate MSE, which results in the value of MSE eventually is inflated by torsional friction. In horizontal drilling, the baseline trend of MSE may become several times the rock confined compressive strength (CCS). For this reason, Pessier and Fear introduced a bit-specific coefficient of sliding friction to express torque as a function of WOB, which has been widely used to compute MSE values in the absence of reliable torque measurements [7].

$$T = \int_0^{D_b/2}\int_0^{2\pi} \rho^2 \frac{4\mu_b WOB}{\pi D_b^2} d\rho d\theta = \int_0^{D_b/2} \frac{8\mu_b WOB}{D_b^2}\rho^2 d\rho = \frac{\mu_b \cdot WOB \cdot D_b}{3} \tag{21}$$

In Eq. (21), WOB is changed with $WOB_b$. Then we get the model of bottom hole torque at the bit [12].

$$T_b = \frac{\mu_b \cdot WOB_b \cdot D_b}{3} = \frac{\mu_b \cdot WOB \cdot e^{-\mu\gamma_b} \cdot D_b}{3} \tag{22}$$

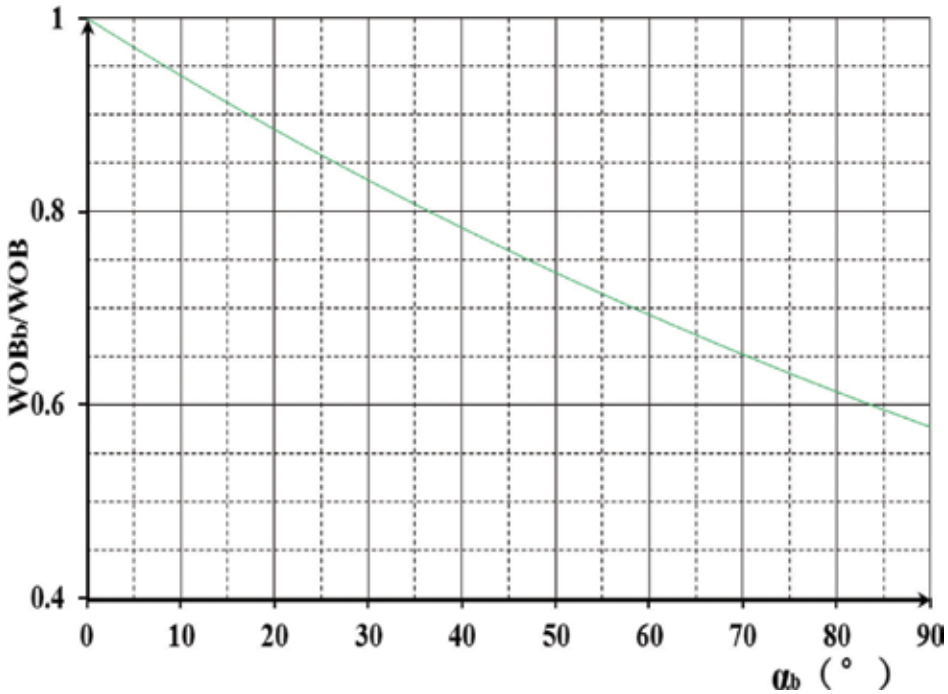


**Figure 1.** Relationship between weight on the bit ratio and bottom hole deviation angle ($\mu_b$ is set to 0.35) [12].

Usually the bit sliding coefficient of friction is assumed to be of an average value of 0.3 and 0.85 [16] for rollercone and PDC bits respectively.

### *2.2.3. Mechanical specific energy model of directional or horizontal well*

WOB and torque are key variables in MSE calculation. In directional or horizontal drilling, they are greatly inflated for well friction. Eqs. (20) and (22) are the model of bottom hole $WOB_b$ and model of bottom hole torque at the bit, which are modified by wellbore wall friction coefficient and bottom hole inclination. They can fit the bottom hole's actual working conditions. However, it has also been observed, from lab data under confined bottom hole pressure, that MSE is often substantially higher than the rock CCS, even when the bit is apparently drilling efficiently, for bit has a certain mechanical efficiency in the actual drilling process even for a new bit [5]. Finally, substitute Eqs. (20) and (22) in Teale model (Eq. (1)) and consider the mechanical efficiency ($E_m$) of the new bit, we can get a new model of MSE which can be shown as [12].

$$MSE = E_m \cdot WOB_b \cdot \left( \frac{1}{A_b} + \frac{13.33 \cdot \mu_b \cdot RPM}{D_b \cdot ROP} \right) \tag{23}$$

$$WOB_b = WOB \cdot e^{-\mu \gamma_b} \tag{24}$$

The bit sliding coefficient ($\mu_b$) of friction is assumed to be of an average value of 0.3 and 0.85 for rollercone and PDC bits respectively [16]. The drill string sliding coefficient ($\mu$) of friction is

assumed 0.25 to 0.4, usually use the value of 0.35 [17, 18]. The mechanical efficiency ($E_m$) of a new bit can be got by core samples' laboratory studies, or inversed by adjacent wells logging data.

### 2.3. Mechanical specific energy model for rotating drilling with PDM

According to the field experience, the bit's mechanical rotary energy has a much higher efficiency on rock breaking than the hydraulic energy. If the hydraulic energy of mud flow is converted into mechanical rotary power, it could improve ROP greatly. In the field, PDM has gained widespread use in the hard formation drilling to improve ROP. In rotating drilling with PDM, the power section of PDM converts hydraulic energy of mud flow into mechanical rotary power, the surface rotation is superimposed on downhole motor rotation (see **Figure 2**) [14]. Moreover, during slide drilling, bit rotation is generated only from the PDM as drilling fluid is pumped through the drill string. Due to the direct measurement of PDM rotary speed and torque in down hole has proven difficult, so currently there are few effective MSE models to precisely model the actual downhole drilling for rotating drilling with PDM.

#### *2.3.1. PDM performance*

In PDM, the power section converts hydraulic energy of mud flow into mechanical rotary power. The output parameters of its mechanical horsepower are rotor torque and rotary speed, whereas differential pressure and mud flow rate are its operational parameters. However, the direct measurement of PDM rotary speed and torque in down hole has proven difficult. The key design parameter that relates PDM output parameters to its operational parameters is PDM unit displacement. It is defined as the mud volume required to revolve a PDM rotor shaft one revolution and can be found on PDM performance data sheets. Then the ideal PDM output torque and rotary speed can be defined by [19].

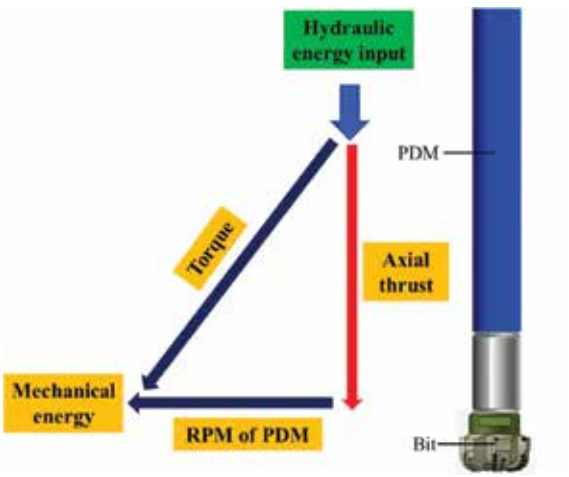


**Figure 2.** PDM converts hydraulic energy of mud flow into mechanical rotary power [14].

$$T_{ideal} = 3.066 \cdot \Delta P_m \cdot q \tag{25}$$

$$RPM_{ideal} = \frac{Q}{q} \tag{26}$$

However, in actual drilling process, leakage and torque losses play important roles in the performance of a PDM. The actual rotary speed of the PDM is decreased by the slip flow through the seal line, and the actual torque is also decreased by the resisting torque due to mechanical friction, elastomeric friction and viscous shearing of drilling fluid. The actual PDM output torque and rotary speed can be estimated by

$$T_m = T_{ideal} - \Delta T \tag{27}$$

$$RPM_m = \frac{Q - Q_{slip}}{q} \tag{28}$$

Torque losses is given by [20].

$$\Delta T = \frac{\pi^2 i^4}{2(1-i)(2-i)^3} \frac{RPM_m}{\delta} D_h^3 L_s \mu + C_f \frac{\pi(1-i^2)}{4(2-i)^2} D_h^2 p_h \Delta P_m + \frac{2F_n y}{3\pi} \tag{29}$$

Slip flow is estimate as

$$Q_{slip} = \frac{\pi \delta^3 D_h n_s \Gamma_i \tan\alpha}{12 \mu L_s L_m} \left(\frac{i}{1-i}\right) \Delta P_m \tag{30}$$

In Eqs. (29) and (30), many parameters are functions of motor geometry, property and even drilling conditions, some of them are difficult to be determined. Therefore, the prediction of $T_m$ and $RPM_m$ has proven difficult. However, in PDM the mechanical power is converted by hydraulic horsepower, and it depends on the converting efficiency of the PDM. Then the mechanical power can be predicted based on its input hydraulic power. The mechanical horsepower provided by PDM can be estimated by [21].

$$MHP = \frac{T_m}{550} \left(\frac{2\pi}{60}\right) \cdot RPM_m \tag{31}$$

The hydraulic horsepower can be given as

$$HHP = \frac{Q \cdot \Delta P_m}{1714} \tag{32}$$

Their relationship can be written as

$$MHP = \eta \cdot HHP \tag{33}$$

In Eqs. (32) and (33), the operating differential pressure drop across the motor, at a constant flow rate, can be measured by comparing off-bottom (zero torque) and on-bottom surface

standpipe pressures. Flow rate can also be easily obtained on the surface. The efficiency of a particular type of motor can be estimated based on data measured on test stands [22].

### *2.3.2. A MSE model for rotating drilling with PDM*

In rotary-drilling with PDM (see **Figure 3**), the mechanical work required to remove a unit volume of rock comes from the WOB, torque at bit provided by surface rotation and torque at bit provided by PDM rotation. The total mechanical work done by the bit in 1 h can be estimated as

$$W_{\mathrm{t}} = WOB_b \cdot ROP + 60 \cdot 2\pi \cdot RPM_s \cdot T_s + 60 \cdot 2\pi \cdot RPM_m \cdot T_m \tag{34}$$

In the above model, $RPM_s$ is bit rotary speed provided by surface rotation; $T_s$ is torque at bit provided by surface rotation; $RPM_m$ is PDM output rotary speed; $T_m$ is PDM output torque. As PDM is near above bit, bit rotary speed and torque provided by PDM can be nearly considered as PDM's output rotary speed and torque.

Please note that every bit has a mechanical efficiency for drilling when it is produced. The mechanical efficiency is mainly related to the bit's cutting structure and exists all along the drilling process [10, 11]. Given the mechanical efficiency of the new bit, the mechanical work required to break the rock drilled in 1 h can be nearly expressed as

$$W_V = W_t \cdot E_m \tag{35}$$

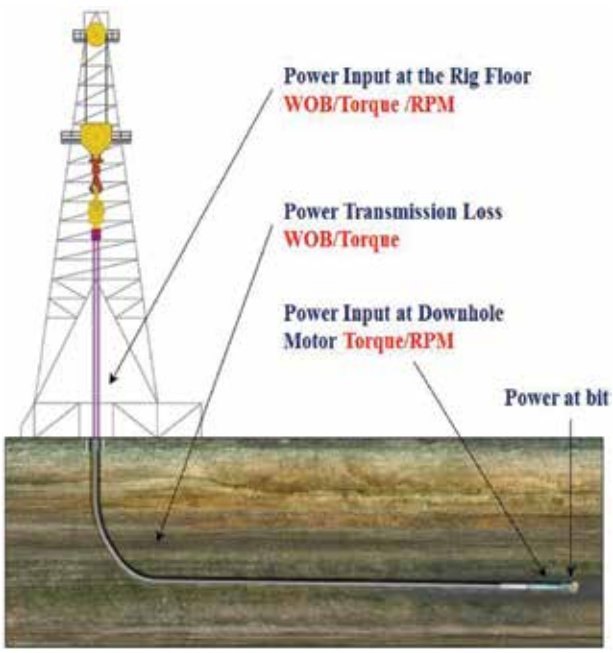


**Figure 3.** Rotating drilling system with PDM [14].

The volume of rock drilled in 1 h is

$$V = A_b \cdot ROP \tag{36}$$

MSE has been defined as the mechanical work done to excavate a unit volume of rock. By combining Eqs. (34), (35) and (36), then the MSE for rotating drilling with PDM can be expressed by

$$MSE = \frac{W_V}{V} = E_m \cdot \frac{WOB_b \cdot ROP + 60 \cdot 2\pi \cdot RPM_s \cdot T_s + 60 \cdot 2\pi \cdot RPM_m \cdot T_m}{A_b \cdot ROP} \tag{37}$$

However, the mechanical energy provided by the surface has a great transmission loss in horizontal and directional drilling. Chen et al. formulated a relationship between bottom hole WOB and the surface measured WOB and presented a method to calculate torque of bit in directional and horizontal drilling [12].

$$\begin{aligned} WOB_b &= WOB \cdot e^{-\mu_s \gamma_b} \\ \mu_b &= 36 \frac{T_s}{D_b \cdot WOB \cdot e^{-\mu_s \gamma_b}} \end{aligned} \tag{38}$$

Then the mechanical specific energy provided by the surface can be estimated as

$$\begin{aligned} &E_m \cdot \frac{WOB_b \cdot ROP + 60 \cdot 2\pi \cdot RPM_s \cdot T_s}{A_b \cdot ROP} \\ &= E_m \cdot WOB \cdot e^{-\mu_s \gamma_b} \left( \frac{1}{A_b} + \frac{13.33 \cdot \mu_b \cdot RPM_s}{D_b \cdot ROP} \right) \end{aligned} \tag{39}$$

According to Eqs. (31), (32) and (33), the mechanical specific energy provided by the down hole motor can also be estimated as

$$E_m \cdot \frac{60 \cdot 2\pi \cdot RPM_m \cdot T_m}{A_b \cdot ROP} = E_m \cdot \frac{1155.2 \cdot \eta \Delta P_m Q}{A_b \cdot ROP} \tag{40}$$

Finally, substitute Eqs. (39) and (40) into Eq.(37), we can get a new MSE model for rotating drilling with PDM [14].

$$MSE = E_m \cdot \left( WOB \cdot e^{-\mu_s \gamma_b} \left( \frac{1}{A_b} + \frac{13.33 \mu_b \cdot RPM_s}{D_b \cdot ROP} \right) + \frac{1155.2 \cdot \eta \Delta P_m Q}{A_b \cdot ROP} \right) \tag{41}$$

For slide drilling, bit rotation is generated only from the PDM as drilling fluid is pumped through the drill string. The MSE can be estimated by [14].

$$MSE = E_m \cdot \left( WOB \cdot e^{-\mu_s \gamma_b} \cdot \frac{1}{A_b} + \frac{1155.2 \cdot \eta \Delta P_m Q}{A_b \cdot ROP} \right) \tag{42}$$

Note that $\Delta P_{\mathrm{m}}$ is the pressure drop across the PDM, and $\eta$ is the efficiency of PDM but not the bit. $\mathrm{RPM_s}$ is drill pipe rotary speed.

## 3. Drilling performance prediction and optimization based on mechanical specific energy technologies

### 3.1. Confined compressive strength

Teale's laboratory experiment showed that MSE was numerically close to the unconfined compressive strength (UCS) of the formation at maximum drilling efficiency [6]. However, the tests were conducted at atmospheric conditions. In the real drilling process, MSE is numerically close to the CCS of the formation at maximum drilling efficiency. In other words, when drilling achieves a maximum drilling efficiency, the minimum MSE is reached and is roughly equal to the CCS of the rock drilled [14].

$$MSE(\min) = CCS \tag{43}$$

Therefore, MSE can be used to detect the peak drilling efficiency by surveilling MSE to see if the MSE(min) is roughly equal to the CCS of the rock drilled.

The widely practiced and accepted method for calculating CCS of rock is as follows [18].

$$CCS = UCS + D_p + 2D_p \cdot \frac{\sin\phi}{1 - \sin\phi} \tag{44}$$

In bottom-hole drilling conditions, for permeable rock, the bottom hole confining pressure can be expressed as

$$D_p = ECD_p - P_p \tag{45}$$

### 3.2. Drilling performance prediction and optimization for directional or horizontal drilling

*3.2.1. Rate of penetration model based on mechanical specific energy*

The rock strength at the rock-bit interface is best defined by CCS. Given the MSE model of directional or horizontal drilling takes the mechanical efficiency ($E_m$) of the new bit into account, so we can assume that MSE is equal to the CCS of the formation. Substituting MSE in terms of CCS, then ROP can be predicted as follows [12].

$$ROP = \frac{13.33 \cdot \mu_b \cdot RPM}{D_b\left(\frac{CCS}{E_m \cdot WOB \cdot e^{-\mu\gamma_b}} - \frac{1}{A_b}\right)} \tag{46}$$

The above ROP model is relatively simple. By using this model we can quickly predict the ROP with reasonable accuracy for all of the bit types, according to the formation properties and the drilling environment. One limitation of the ROP model is that it does not recognize the founder point of any given bit, which means it can predict a higher ROP than is achievable as WOB and RPM increase beyond the bit's optimum combination [23].

http://dx.doi.org/10.5772/intechopen.75827

*3.2.2. Drilling performance prediction and optimization method*

MSE is the amount of energy required to destroy a unit volume of rock and it provides a means of evaluating and optimizing drilling performance. By comparing MSE to the predicted CCS, as well as by comparing actual ROP to the predicted ROP, drilling performance and bit condition can be evaluated. The drilling performance can be evaluated and predicted by Eqs. (44) and (46). When MSE is equal to the predicted CCS, or actual ROP is equal to the predicted ROP, it indicates that drilling performs well and the bit is operating at its peak efficiency.

Drilling performance optimization based on MSE technologies means real-time analyzing of MSE and adjusting drilling parameters accordingly to minimize drilling problems and maximize ROP. When a bit is operating at its peak efficiency, the ratio of energy to rock volume will remain relatively constant, and MSE is nearly equal to the CCS of the formation. This relationship is used operationally by observing whether the minimum MSE is equal to the CCS of the formation while adjusting drilling parameters such as WOB or RPM to maximize ROP. If the minimum MSE remains equal to the CCS of the formation while increasing WOB, the bit is assumed to be still efficient. If MSE increases significantly and is much higher than the CCS of the formation, the bit has foundered and drilling problems may occur, such as vibrations, bit balling, bottom hole balling and dull bits. The driller then determines the most likely cause of founder and drilling problems, and adjusts parameters accordingly. Adjustments continue to be made until the MSE value is minimized equally to CCS of the formation.

Based on the relations between MSE, drilling parameters and ROP, an appropriate predicting and optimizing method can be proposed by analyzing bottom-hole conditions of drilling and determining the reasonability of drilling parameters. **Figure 4** is the flow chart of the drilling performance prediction and optimization method [12].

As shown in **Figure 4**, when MSE(min) = CCS, and ROP/WOB = constant >0, it is in the region B as **Figure 5** [12] indicate. MSE is low and nearly equal to CCS. The slope of the line is relatively constant for a given formation, bit and rotary speed. The drilling efficiency remains at its peak efficiency. In this region, the bit is not constrained by a unique inefficiency, it simply needs more energy. Just by increasing WOB or RPM, the ROP will increase greatly and eventually approach the founder point. When ROP/WOB≠constant > 0, it is close to the highest ROP that can be achieved with the current system and reached the region C. But if ROP further increases, then bit balling and bottom hole balling will occur. Therefore drilling parameters should be better set in the area near to the founder point to ensure that drilling performs efficiently and safely. Real-time MSE surveillance can be used to find the founder point. If MSE remains constant, the bit is efficient, if the MSE rises, the system is foundering.

When MSE(min) > CCS, it is in the region C, MSE is high and even several time of CCS. As ROP increases, down hole cuttings accumulate, which leads to bit balling, bottom hole balling, and constrains the energy from bit transfer to the rock, as a result ROP drops. If WOB further increases, vibrations will occur and ROP will decrease greatly. In this region, in order to extend

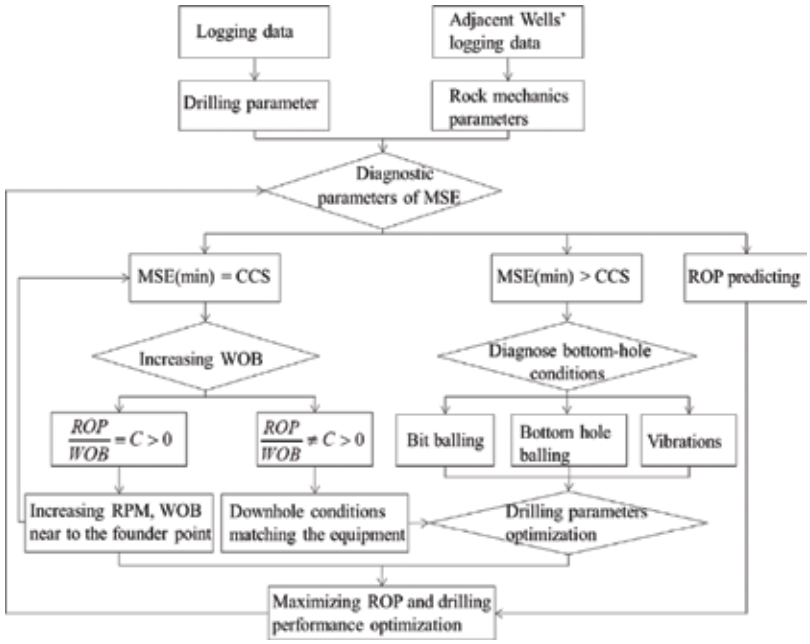


**Figure 4.** Flow chart of drilling performance prediction and optimization [12].

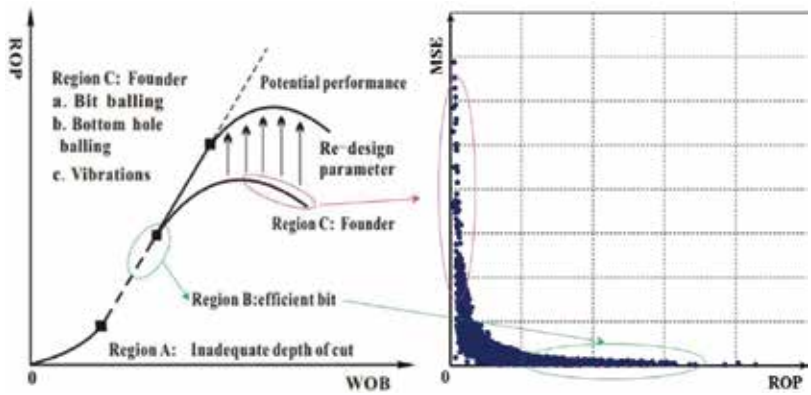


**Figure 5.** Relationship between the traditional ROP vs. WOB plot and the new MSE vs. ROP plot [12].

the range of balling period and maximize ROP, nozzles and flow rates can be modified to achieve the highest hydraulic horsepower per square inch (HSI) possible with the available rig equipment. If reaching the rated power of the equipment, WOB should reduce, and drilling parameters should be set in the intersect area between region B and region C.

### 3.3. Drilling parameters optimization for rotating drilling with PDM

Real-time optimization of drilling parameters during drilling operations aims to optimize WOB, RPM for obtaining maximum ROP [24, 25]. The process is not only formation specific

http://dx.doi.org/10.5772/intechopen.75827

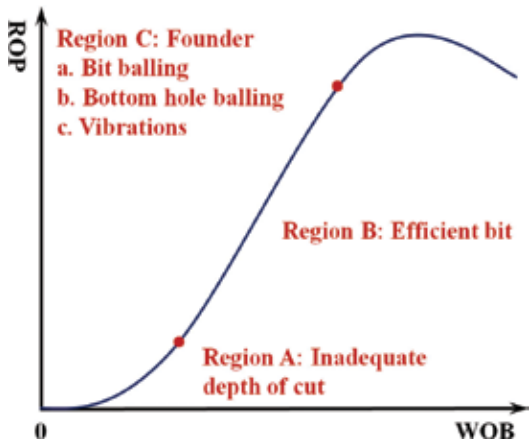


**Figure 6.** Relationship between the traditional ROP versus WOB plot [14].

but also drilling system specific. **Figure 6** shows a classic drill-off curve [5]. The point at which the ROP stops responding linearly with increasing WOB is referred to as the founder point where the ROP is maximized. The corresponding WOB at this point is taken to be the optimum WOB. **Figure 7** shows field data from three drill-off tests with an insert bit [5, 14]. It indicates that the bit is prone to founder with high RPM, and the optimum WOB decreases obviously with the increase of RPM of bit. Moreover, the founder point changes greatly with the change of RPM of bit. In rotating drilling with PDM, the surface rotation is superimposed on PDM rotation, the RPM of bit is high and could be changed greatly. It not only makes the bit be easy to reach the founder point even at low WOB, but also makes the founder point be difficult to be identified. MSE surveillance provides an objective assessment of the drilling efficiency and an

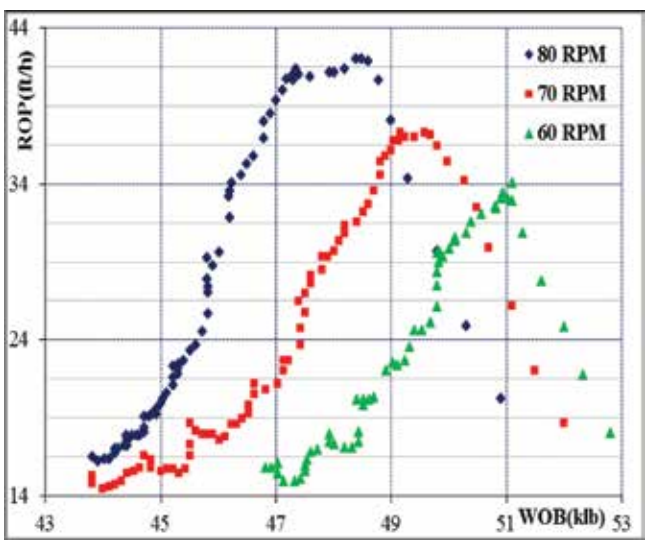


**Figure 7.** Field data from three drill-off tests [5].

objective tool to identify the founder point. Therefore, real-time optimization of drilling parameters for rotating drilling with PDM can be performed by identifying the founder point of the bit in specific formation drilling based on MSE surveillance.

As aforementioned, MSE is the amount of energy required to destroy a unit volume of rock. When a bit is operating at its peak efficiency, the ratio of energy to rock volume will remain relatively constant. The minimum MSE is reached and it correlates with the CCS of the formation. This relationship is used operationally by observing whether the MSE(min) is roughly equal to the CCS of the formation while adjusting drilling parameters such as WOB or RPM to maximize ROP. If the MSE(min) remains roughly equal to the CCS of the formation while increasing WOB, the bit is assumed to be still at its peak efficient. If the MSE(min) increases significantly and is much higher than the CCS of the formation, the bit has foundered. The causes of founder are bit balling, bottom hole balling and vibrations. If the causes of founder are not addressed when they occur, overall drilling performance will suffer and tools will be damaged.

Bit balling and bottom hole balling are terms used to describe build-up of material on the bit and bottom hole that inhibits transfer of a portion of the WOB to the cutting structure. They usually occur in soft formations, and can be relieved by increasing flow rates and reducing WOB. When drilling in hard formation with a PDM, bit balling and bottom hole balling are unlikely to occur, while vibrations are very common. Down hole vibrations include three modes: whirl (lateral), stick-slip (torsional) and bit bounce (axial). They amplify loads downhole, resulting in a host of bit and tool failures that not only increase the number of trips required, but also the costs of tool repair and replacement. Actually these vibrations in rotating drilling with PDM could be effectively eliminated by adjusting WOB or RPM on the surface.

Whirl can be effectively eliminated by reducing RPM while increasing WOB. Stick-slip can be minimized by reducing WOB and increasing RPM. As for bit bounce, if the bouncing is initiated when running high WOB and low RPM, the solution is to increase RPM and reduce WOB. Conversely, if the problem begins with higher RPM and lower WOB, the answer is to reduce RPM and increase WOB. It may also even be necessary to stop surface rotation and simply drill in slide mode (bit rotation is generated only from the PDM) through the problematic formation [26].

Assume the bottom hole is effectively cleaned, then based on the above analysis, a drilling parameters optimization method for rotating drilling with PDM can be proposed to maximize ROP and allow operators to drill longer and avoid unnecessary trips. **Figure 8** is the flow chart of the drilling parameters optimization method for rotating drilling with PDM [14], and it is based on real-time MSE surveillance to find the founder point of the bit [12]. When MSE (min) = CCS, the bit performs in the region B as shown in **Figure 6** and the drilling efficiency remains at peak efficiency. In this region, the bit is not constrained by a unique inefficiency, it simply needs more energy. Given a RPM, just by increasing WOB, the ROP will increase greatly and eventually approach the founder point.

When MSE(min) > CCS, and MSE(min) is even several time of CCS, the bit is floundering and drilling problems may occur. Adjustments of WOB and RPM need to be made until the MSE (min) value is minimized and roughly equal to the CCS of the formation. The process of

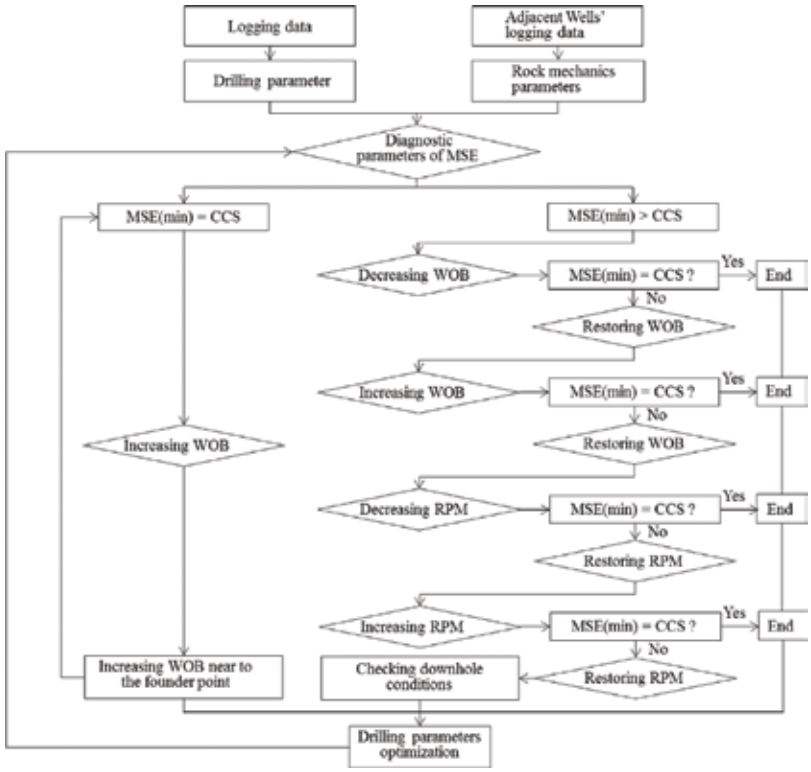


**Figure 8.** Flow chart of drilling parameters optimization for rotating drilling with PDM [14].

adjustment is shown in **Figure 8**. As drilling with PDM provides much higher RPM at the bit than the conventional rotating drilling could achieve, the bit is easy to reach the founder point even with low WOB. Further increasing WOB or RPM is more likely to decrease ROP and worsen the drilling problems. Moreover, high WOB that will generate excessive torque for the PDM may make PDM stalled, and RPM may also cause excessive vibration of the drill pipe. Therefore, the adjustment for rotating drilling with PDM is to reduce WOB first and then gradually increase WOB, and do the same manipulation for RPM until MSE(min) = CCS. The adjustment should not be in a very wide range. If MSE still much higher than the CCS of the formation after the adjustment of WOB and RPM, down hole conditions should be checked to see if the bit and PDM were damaged.

## 4. Field case

### 4.1. Field case no.1: verification of MSE model and drilling performance prediction of directional or horizontal drilling

In order to verify the accuracy of the MSE model of directional or horizontal drilling, several other key models of MSE (such as Teale model [6], Pessier model [7], Dupriest model [5]) are

carried out and compared against field data. Initially, MSE is calculated respectively by these MSE models using surface measured data and plotted vs. depth. The results are compared with the rock CCS to verify the accuracy of the MSE model of directional or horizontal drilling. Then, the actual ROP and the predicted ROP which is calculated with Eq. (46) are both plotted vs. depth to verify the accuracy of the ROP prediction model, and the drilling parameters WOB, RPM, and MSE are also plotted vs. depth to explain the observed pattern. Furthermore, actual ROP and the predicted ROP of each bit are also plotted.

This well's trajectory is designed with a kick-off point (KOP) at 2925 m with a build rate of 5°/30 m dogleg severity (DLS) until reaching 90° at 3465 m, and then steered a horizontal section to 4043 m measured depth. The log data of vertical section and horizontal section are used to calculate MSE respectively by Teale model, Pessier model, Dupriest model and the MSE model of directional or horizontal drilling. CCS is determined by Eq. (44) to verify the accuracy of these models. The comparison of MSE calculated results and CCS are showed on **Figures 9** and **10** respectively in vertical section and horizontal section. It shows that the calculation errors of Teale model, Pessier model, Dupriest mode are apparently inflated in horizontal section. The MSE estimated with the MSE model of directional or horizontal drilling has the best correlation with CCS, and the order of models from good to poor in accurately predicting correlation effect is the MSE model of directional or horizontal drilling, Pessier model, Dupriest model and Teale model. In vertical section, the correlation effect of MSE model of directional or horizontal drilling, Pessier model, Dupriest model is relatively close, but far better than Teale model. In horizontal section, MSE values calculated with Teale model is more than 10 times of CCS, and MSE values calculated with Pessier model and Dupriest model are several times of CCS. As for the MSE model of directional or horizontal drilling, its MSE values are close to CCS. The correlation effect of the MSE model of directional or horizontal drilling in horizontal section is close to that of in vertical section. So the correlation effect of the MSE model of directional or horizontal drilling is apparently better than Pessier model, Dupriest model and Teale model in both vertical section and horizontal section.

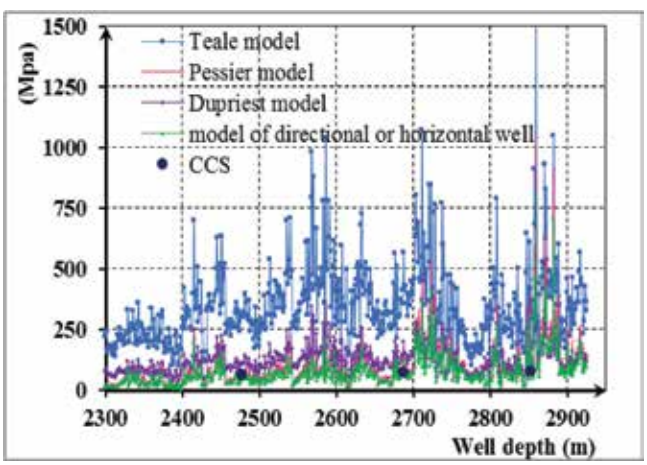


**Figure 9.** Comparison of MSE calculated results and testing CCS in vertical section.

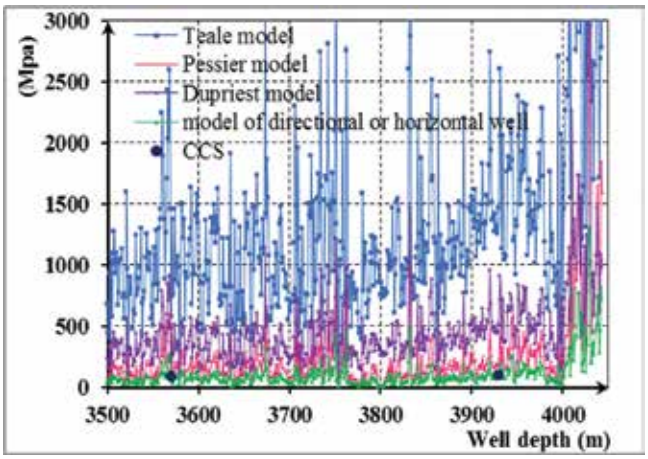


**Figure 10.** Comparison of MSE calculated results and testing CCS in horizontal section.

**Figure 11** plots the predicted ROP and the actual ROP vs. depth, and the drilling parameters WOB, RPM, and MSE are also included on **Figure 11**. The predicted ROP is calculated with Eq. (46). As indicated in **Figure 11**, the predicted ROP matches well with the actual ROP, which reveals that the ROP predict model's prediction accuracy is high, and can fully meet the needs of the field. Therefore, the MSE model of directional or horizontal drilling can be quantitatively applied. **Figure 12** plots ROP prediction accuracy of each bit. A, B, and C bit's ROP prediction accuracy respectively are 84.8% (A), 91.2% (B), 76.8% (C). In the section of 2700–2750, 2830–2890 and 3167–3215 m, the predicted ROP is higher than the actual ROP. The drilling parameters WOB, RPM, and MSE plotted vs. depth are used to explain the observed pattern in **Figure 11**.

In 2700–2750 m, MSE value increases and actual ROP reduces greatly, and the predicted ROP is higher than the actual ROP. After the WOB increases from 30 to 52 kN from 2730 to 2766 m, MSE value reduces to the baseline trend and the actual ROP increases. In this section, as the hydraulics and bit rotating speed don't change, so it can't be bit balling and bottom hole inadequate cleaning. Therefore, it is likely that whirl leads energy cannot effectively passed to the bit, as a result actual ROP decreases. And in fact, whirl is also observed in this section. In 2830–2890 m and 3167–3215 m, MSE value increases slowly and actual ROP reduces greatly, trip-out and discovery that bit was badly damaged. Change a new bit and drill with the same drill parameter, MSE value decreases and actual ROP increases.

### 4.2. Field case no.2: drilling parameters optimization for rotating drilling with PDM

To verify the new mechanical specific energy model, drilling data of a 2621-ft section of a vertical well have been used to calculate the profiles of CCS and MSE with depth. The drilling data, including WOB, surface RPM, ROP, mud flow rate and on-bottom PDM differential pressure, were recorded for every 1-ft step from 4072 to 6693 ft. The lithology is limestone and the section was drilled with 22 in bits and a 9:10 lobe ratio PDM. The efficiency of PDM is

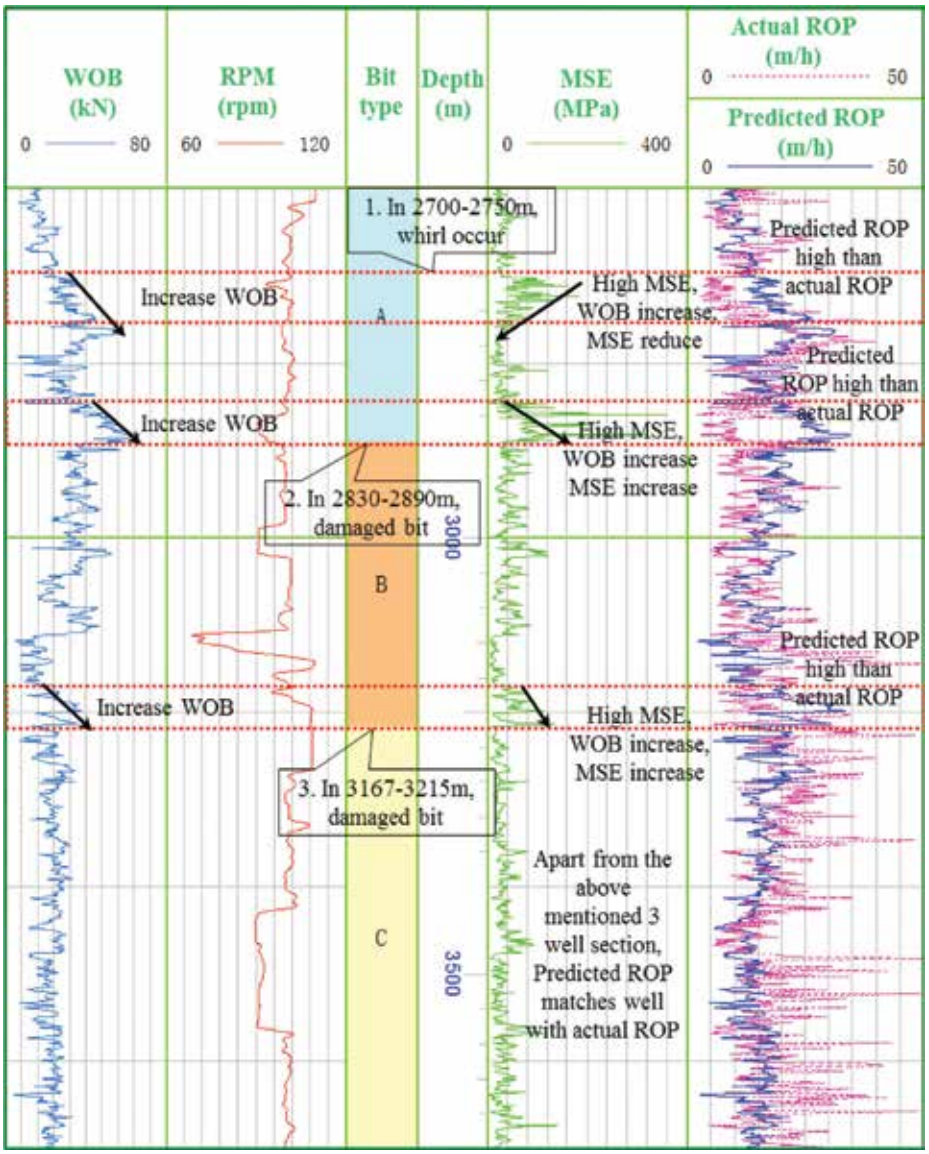


**Figure 11.** ROP predicted result and bottom-hole condition analysis.

70%. MSE is estimated by the new MSE model for rotating drilling with PDM (Eq. (41)). CCS is calculated by Eq. (44) using the field's log data. The comparison of the calculated MSE against CCS is shown in **Figures 13** and **14**. **Figure 13** shows the MSE(min) is roughly equal to the CCS of the formation almost along all the well depth apart from the well sections: 5502–5606 ft, 5948–6045 ft, 6564–6693 ft. In the sections of 5502–5606 ft and 5948–6045 ft, the applied WOB is very high and more than 46 kbl. Severe vibrations were observed in these two sections. In the section of 6564–6693 ft, relatively low WOB is applied and around 8–20 kbl. While trip-out, it is

http://dx.doi.org/10.5772/intechopen.75827

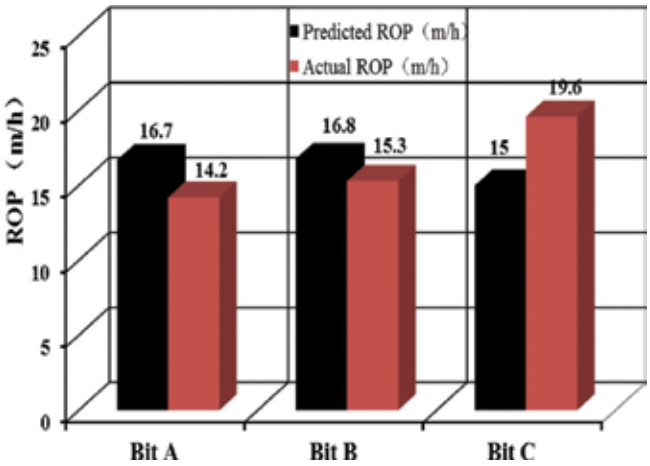


**Figure 12.** ROP predicted results of different bits type.

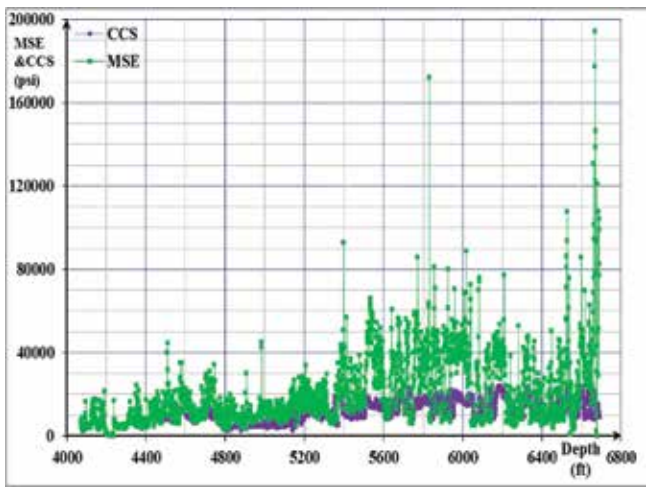


**Figure 13.** MSE and CCS vs depth.

found that the bit was badly damaged. **Figure 14** reveals that the MSE values are minimized and have good correlation with the CCS when the ROP is high, while with low ROP the MSE values are obviously higher than the CCS of the formation. Therefore, when drilling with a high efficiency and free of drilling complications, the MSE(min) estimated by the MSE Model for rotating drilling with PDM is roughly equal to the CCS of the formation along all the well depth. This indicates that the MSE Model for rotating drilling with PDM estimates MSE values with a reasonable approximation and can meet the needs of field applications.

In order to demonstrate the applicability of the proposed drilling parameters optimization method, drilling operation of a 2855-ft interval of an anhydrite and dolostone formation with a 9.5 in PDM and 16 in PDC bit is analyzed to determine the optimum WOB value in the same

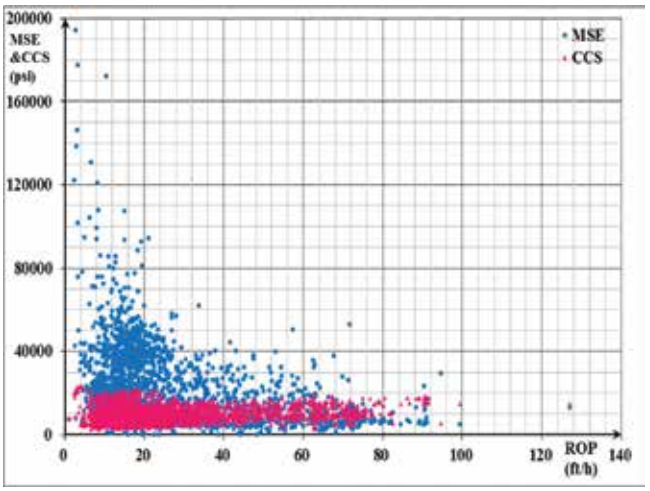


**Figure 14.** MSE and CCS vs ROP002E.

vertical well from 7651 to 10,499 ft. The PDM is a high RPM motor with a 5:6 lobe configuration which provides moderate torque values. PDM unit displacement is 6.67 gal/rev, and the PDM output rotary speed is estimated by Eq. (26).

**Figure 15** plots the drilling parameters versus depth to illustrate the sensitivity of ROP and MSE of this operation to WOB and RPM. MSE vs. ROP and the average ROP of various well

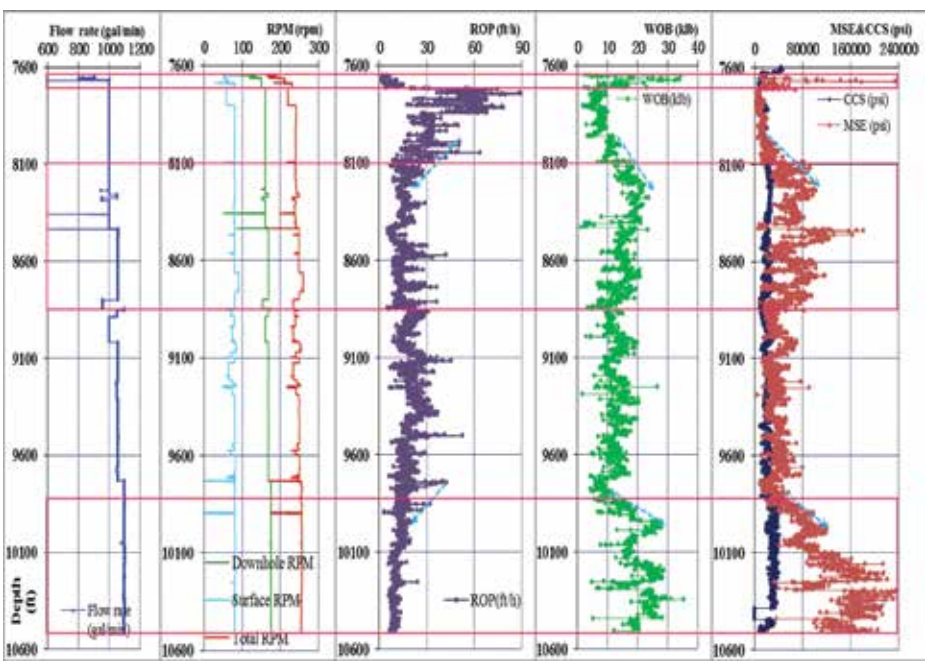


**Figure 15.** Drilling parameters optimization.

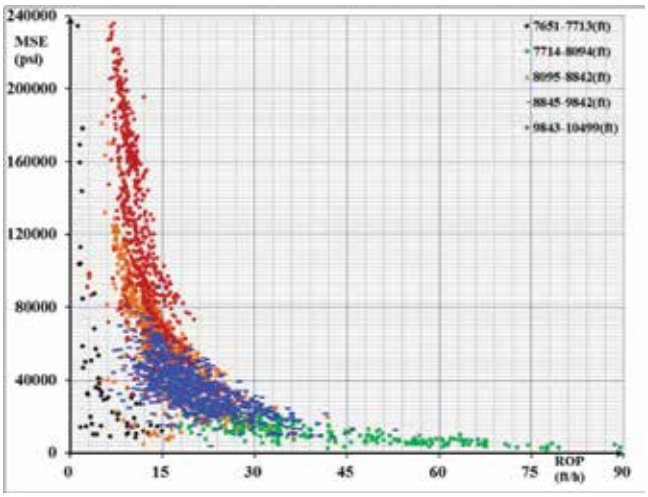


**Figure 16.** MSE vs ROP.

sections are respectively shown in **Figures 16** and **17**. From 7651 to 7713 ft, the applied WOB is as high as 34.7.4 kbl, the value of MSE is apparently greater than CCS (MSE(min) > CCS). This indicates that the bit is foundered and the average ROP is 5.9 ft/h. From 7714 to 8094 ft, WOB is adjusted to around 6.6–11 kbl and RPM almost remains at 240, then MSE(min) = CCS and the average ROP increases to 38.1 ft/h. It drills with high efficiency. At around 8084 ft, when WOB further increases from 8.8 to 11 kbl, the MSE value increases obviously and MSE(min) > CCS. From 8095 to 8842 ft, WOB increases to around 17.6 kbl. However, the MSE(min) mounts up to several times of CCS, and the average ROP decreases to 15.1 ft/h. At 8435 ft, when the flow rate increases to 1056.0 gal/min from 1001.6 gal/min and RPM increases to 249 from 240, the MSE

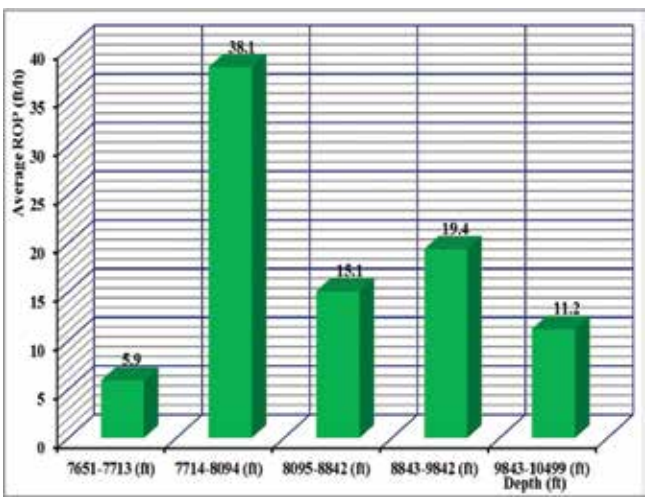


**Figure 17.** The average ROP.

value further inflates. Therefore, when RPM is around 240, the drilling system's optimum WOB is 8.8–11 kbl. At around 8843 ft, WOB is adjust to 8.8–11 kbl, the MSE value is minimized and close to the CCS of the formation. From 8843 to 9842 ft, WOB remains around 8.8–11 kbl, it drills with a relatively high efficiency and the average ROP is 19.4 ft/h. At 9731 ft, the flow rate increased to 1097.6 gal/min from 1056.0 gal/min and RPM increased to 258 from 249. The MSE value is minimized and MSE (min) = CCS while WOB reduced to 7.3–9.5 kbl. At 9888 ft, when WOB increases from 7.3 to 9.5 kbl, the MSE value rockets and MSE(min) > CCS. From 9843 to 10,499 m, WOB increases to more than 26.5 kbl, the MSE value is more than ten times of CCS and the average ROP is 11.2 ft/h. This indicates that when RPM is around 258, the drilling system's optimum WOB is 7.3–9.5 kbl.

Based on the above drilling parameters optimization analysis, it is also found that ROP is sensitive to high WOB values for rotating drilling with PDM, and increasing WOB does not always increase ROP but is more likely to decrease ROP. Moreover, the optimum WOB always changes with RPM for rotating drilling with PDM. The proposed method for optimizing drilling parameters can be used to real time estimate optimum WOB values with different RPM to drill a specific formation interval. It can be effectively and easily used, and is worthy to be applied and promoted.

## 5. Summary and conclusions

In this chapter, MSE models respectively for directional or horizontal drilling and rotating drilling with PDM are established, meanwhile methods for drilling performance prediction and optimization based on MSE technologies are presented. The following remarks provide a summary with conclusions on the basis of case studies.

1. A formula between bottom hole $WOB_b$ and the surface measured WOB is developed, and the bottom hole $WOB_b$ has been introduced to calculate torque of bit of directional or horizontal wells.
2. The MSE models respectively for directional or horizontal drilling and rotating drilling with PDM estimate MSE values with a reasonable approximation in the absence of reliable torque measurements, they can be widely used in the drilling industry.
3. ROP is sensitive to high WOB values for rotating drilling with PDM. The optimum WOB is low for rotating drilling with PDM compared with the conventional drilling without PDM, increasing WOB does not always increase ROP but is more likely to decrease ROP.
4. The method for optimizing drilling parameters can real time estimate optimum WOB values with different RPM to drill a specific formation interval with PDM. It could be effectively used to maximize ROP and allow operators to drill longer and avoid unnecessary trips in rotating drilling with PDM.
5. Drilling performance prediction and optimization methods based on MSE technologies is worthy to be applied and promoted with highly diagnostic accuracy, effective optimizing and simple operation.

http://dx.doi.org/10.5772/intechopen.75827

## Nomenclature

| | |
|---|---|
| $A_b$ | bit area ($in^2$) |
| $CCS$ | confined compressive strength (psi) |
| $C_f$ | coefficient of dry friction and is assumed to be constant for all rotational speeds |
| $D_b$ | bit diameter (in) |
| $D_h$ | diameter of the housing (in) |
| $D_p$ | $ECD_p$-$P_p$(psi) |
| $d_s$ | diameter of the shaft pitch circle (in) |
| $ECD$ | equivalent circulating density (ppg) |
| $ECD_p$ | pressure in psi exerted by an ECD in ppg |
| $E_m$ | mechanical efficiency of new bit |
| $F_i$ | internal force of drill string produced by bottom hole $WOB_b$ (lbf) |
| $F_{i1}$ | internal force of drill string at the upper end produced by bottom hole $WOB_b$ (lbf) |
| $F_{i2}$ | internal force of drill string at the lower end produced by bottom hole $WOB_b$ (lbf) |
| $F_n$ | the resultant force acting at the contact point (lbf) |
| $HHP$ | hydraulic horsepower (hp) |
| $i$ | winding ratio |
| $L_m$ | length of the PDM (in) |
| $L_s$ | total length of the seal line (in) |
| $MHP$ | mechanical horsepower provided by PDM (hp) |
| $MSE$ | mechanical specific energy (psi) |
| $n$ | number of shaft lobes of the motor (winding number) |
| $n_s$ | number of mud motor stage |
| $\Delta P_b$ | pressure drop across the bit (psi) |
| $P_h$ | pitch of the housing (in) |
| $\Delta P_m$ | differential pressure across the PDM (psi) |
| $P_p$ | pore pressure (psi) |
| $Q$ | flow rate (gal/min) |
| $q$ | PDM unit displacement (gal/ rev) |

| | |
|---|---|
| $Q_{slip}$ | Mud slip flow through the PDM (gal/min) |
| $ROP$ | rate of penetration (ft/h) |
| $RPM$ | bit rotating speed (rpm) |
| $RPM_{\text{ideal}}$ | ideal PDM rotary speed (rpm) |
| $RPM_s$ | bit rotary speed provided by surface (rpm) |
| $RPM_m$ | PDM output rotary speed (rpm) |
| $T$ | torque at bit (ft-lbf) |
| $\Delta T$ | torque loss (ft-lbf) |
| $T_{ideal}$ | ideal PDM output torque (ft-lbf) |
| $T_s$ | torque at bit provided by surface (ft-lbf) |
| $T_m$ | PDM output torque (ft-lbf) |
| $UCS$ | unconfined compressive strength (psi) |
| $V$ | volume of rock drilled in one hour (ft-in$^2$) |
| $W_t$ | total mechanical work done by the bit in one hour (ft-lbf) |
| $W_V$ | mechanical work required to break the rock drilled in one hour (ft-lbf) |
| $WOB$ | weight on bit of surface measurement (lbf) |
| $WOB_b$ | bottom hole actual weight on bit (lbf) |
| $y$ | contact semi-width (in) |
| $\alpha$ | helix angle of seal line (degree) |
| $\beta$ | coefficient of hydraulic horsepower |
| $\delta$ | clearance of the slip passage (in) |
| $\mu_b$ | bit-specific coefficient of sliding friction |
| $\mu_s$ | coefficient of friction of drill string |
| $\mu$ | viscosity of mud (cp) |
| $\gamma$ | well inclination (rad) |
| $\Delta\gamma$ | additional well inclination (rad) |
| $\gamma_b$ | inclination of the bottom hole (rad) |
| $\phi$ | rock internal angle of friction (degree) |
| $\Gamma_i$ | configuration correction factor |
| $\eta$ | efficiency of PDM |

## Acknowledgements

This work was financially supported by Science Foundation of China University of Petroleum, Beijing (No.2462017YJRC050), National Key Research and Development Project (Grant numbers: 2017ZX05009-003; 2016YFC0303303), National Natural Science Foundation of China (Grant numbers: 51434009; 51521063; 51774301).

## Author details

Xuyue Chen*, Jin Yang and Deli Gao

*Address all correspondence to: chenxuyue2011@163.com

China University of Petroleum, Beijing, China

## References

[1] Chen X, Gao D, Guo B, et al. A new method for determining the minimum gas injection rate required for hole cleaning in horizontal gas drilling. Journal of Natural Gas Science and Engineering. 2014;**21**:1084-1090, ISSN 1875-5100. DOI: 10.1016/j.jngse.2014.11.009

[2] Chen X, Gao D, Guo B. A method for optimizing jet-mill-bit hydraulics in horizontal drilling. SPE Journal. 2016;**21**(2):416-422. DOI: 10.2118/178436-PA

[3] Chen X, Gao D, Guo B. Optimal design of jet mill bit for jet comminuting cuttings in horizontal gas drilling hard formations. Journal of Natural Gas Science and Engineering. 2016;**28**:587-593, ISSN 1875-5100. DOI: 10.1016/j.jngse.2015.12.033

[4] Chen X, Gao D. The maximum-allowable well depth while performing ultra-extended-reach drilling from shallow water to deepwater target. SPE Journal. 2018;**23**(01):224-236. DOI: 10.2118/183025-PA

[5] Dupriest FE, Koederitz WL. Maximizing drill rates with real-time surveillance of mechanical specific energy. In: SPE/IADC Drilling Conference; 23–25 February, 2005, Amsterdam, Netherlands. DOI: 10.2118/92194-MS

[6] Teale R. The concept of specific energy in rock drilling. International Journal of Rock Mechanics and Mining Sciences. 1965;**2**(1):57-73

[7] Pessier RC, Fear MJ. Quantifying common drilling problems with mechanical specific energy and a bit-specific coefficient of sliding friction. In: SPE Annual Technical Conference and Exhibition; 4–7 October, 1992, Washington, D.C. DOI: 10.2118/24584-MS

[8] Armenta M. Identifying inefficient drilling conditions using drilling-specific energy. In: SPE Annual Technical Conference and Exhibition; 21–24 September, 2008, Denver, Colorado, USA. DOI: 10.2118/116667-MS

[9] Mohan K, Adil F, Samuel R. Tracking drilling efficiency using hydro-mechanical specific energy. In: SPE/IADC Drilling Conference and Exhibition; 17–19 March, 2009, Amsterdam, The Netherlands. DOI: 10.2118/119421-MS

[10] Cherif H. FEA modelled MSE/UCS values optimise PDC design for entire hole section. In: Presented at at the North Africa Technical Conference and Exhibition held in Cairo, Egypt; 20–22 February 2012. SPE 149372. DOI: 10.2118/149372-MS

[11] Mohan K, Adil F, Samuel R. Comprehensive hydromechanical specific energy calculation for drilling efficiency. Journal of Energy Resources Technology. 2015;**137**(1):12904. DOI: 10.1115/1.4028272

[12] Chen X, Fan H, Guo B, Gao D, et al. Real-time prediction and optimization of drilling performance based on a new mechanical specific energy model. Arabian Journal for Science and Engineering. 2014;**39**(11):8221-8231. ISSN 1875-5100. DOI: 10.1007/s13369-014-1376-0

[13] Kingsley A, Ibiye I. Application of mechanical specific energy techniques in reducing drilling cost in deepwater development. In: SPE Deepwater Drilling and Completions Conference; 20–21 June, 2012, Galveston, Texas, USA. DOI: 10.2118/156370-MS

[14] Chen X, Gao D, Guo B, Feng Y. Real-time optimization of drilling parameters based on mechanical specific energy for rotating drilling with positive displacement motor in the hard formation, Journal of Natural Gas Science and Engineering. 2016;**35**(Part A):686-694. ISSN 1875-5100. DOI: 10.1016/j.jngse.2016.09.019

[15] Aadnoy Bernt S. Theory and application of a new generalized model for torque and drag. In: IADC/SPE Asia Pacific Drilling Technology Conference and Exhibition; 25–27 August, 2008, Jakarta, Indonesia. DOI: 10.2118/114684-MS

[16] Rashidi B, Hareland G, Fazaelizadeh M, Svigir M. Comparative study using rock energy and drilling strength models. In: 44th U.S. Rock Mechanics Symposium and 5th U.S.-Canada Rock Mechanics Symposium; 27–30 June, 2010, Salt Lake City, Utah. ARMA-10-254

[17] Juan L et al. Research on torque and drag in extended-reach horizontal wells and its application in Chenghai-1 area. Oil Drilling & Production Technology. 2009;**31**(3):21-25

[18] Caicedo H, Calhoun W, Ewy R. Unique ROP predictor using bit-specific coefficients of slide friction and mechanical efficiency as a function of confined compressive strength impacts drilling performance. In: SPE/IADC Drilling Conference; 23–25 February, 2005, Amsterdam, Netherlands. DOI: 10.2118/92576-MS

[19] Motahhari HR, Hareland G, James JA, Aramco Saudi. Improved drilling efficiency technique using integrated PDM and PDC bit parameters. Journal of Canadian Petroleum Technology. 2010;**49**(10):45-52. DOI: 10.2118/141651-PA

[20] Robello SG. Mathematical modelling and design analysis of the power section of a positive displacement motor (PDM). PhD dissertation. Tulsa: University of Tulsa; 1997

[21] Robello SG, Stefan M. Analytical study of the performance of positive displacement motor (PDM): Modeling for incompressible fluid. In: Fifth Latin American and Caribbean Petroleum Conference and Exhibition Held in Rio de Janeiro, Brazil; Aug 30–Sep 3, 1997; DOI: 10.2118/39026-MS

[22] Macpherson JD, Jogi PN, Vos BE Measurement of mud motor rotation rates using drilling dynamics. In: SPE/IADC Drilling Conference Held in Amsterdam, The Netherlands; 27 February–1 March 2001. DOI: 10.2118/67719-MS

[23] Guerrero CA. Deployment of an SeROP predictor tool for real-time bit optimization. In: SPE/IADC Drilling Conference; 20–22 February, 2007, Amsterdam, The Netherlands. DOI: 10.2118/105201-MS

[24] Bybee K. Real-time optimization of drilling parameters. Society of Petroleum Engineers. 2011;**63**(02):48-49. DOI: 10.2118/0211-0048-JPT

[25] Eren T, Ozbayoglu ME. Real time optimization of drilling parameters during drilling operations. In: SPE Oil and Gas India Conference and Exhibition; 20–22 January, 2010, Mumbai, India. DOI: 10.2118/129126-MS

[26] Brackin V, Doster M, Mounzer F et al. Minimizing dynamic dysfunctions sets new drilling performance benchmark in Saudi gas application. In: SPE Saudi Arabia Section Technical Symposium; 9–11 May, 2009, Al-Khobar, Saudi Arabia. DOI: 10.2118/126059-MS

Chapter 8

# New Development of Air and Gas Drilling Technology

Jun Li, Yulong Yang, Boyun Guo and Gonghui Liu

Additional information is available at the end of the chapter

http://dx.doi.org/10.5772/intechopen.75785

**Abstract**

Gas drilling technology has been widely promoted and applied in recent years. Known for being capable of discovering and protecting reservoirs, improving the penetration rate and avoiding loss circulation, two key issues of gas drilling still need to be addressed. First, a more accurate way of determining the gas injection rate is needful. In this text, we present a modified mathematical model for predicting the optimum range of gas injection rate required to balance the borehole cleaning and well-integrity issues. The optimum gas injection rate should be sought between the minimum value required for hole cleaning and the maximum permissible value to avoid hole erosion. Good consistency between the model prediction and field problem-free nitrogen gas injection rate indicates the reliability of the proposed model. Second, the problem of environmental pollution and wasting of resources caused by direct discharging or combustion of the returned gas is to be solved. To address the latter issue, we introduce a new technology of gas recycling system (GRS). Our research group has carried out a comprehensive investigation, including integration design, technological process, cuttings transport analysis, separation and filter equipment selection, and control system design. The feasibility of GRS has been verified through an open-loop pilot test.

**Keywords:** air and gas drilling, optimum gas injection rate, gas recycling system, penetration rate, gas-recycling drilling

## 1. Introduction

Air and gas drilling technology is the utilization of mainly (>97% in volume) compressed air or other gases (e.g., nitrogen or natural gas) as a rotary drilling circulating fluid to carry the rock cuttings to the surface. When the gases are injected into the well with incompressible fluids such as fresh water, oil, or drilling mud, the operations are called aerated drilling or stable foam drilling if foaming agents are added to create a continuous foam circulating fluid. Due to

the strong capability of cutting transportation of the aerated drilling and foam drilling, the gas injection rate calculation is less significant compared to that in air and gas drilling. Therefore, discussion of aerated and foam drilling is beyond the scope of this chapter.

Gas injection rate is one of the basic parameters during the design process of air and gas drilling. On the one hand, overestimated value of required gas injection rate may lead to high equipment investment, high cost, and ice balling of drill bit. On the other hand, underestimated value of required gas injection rate may cause cuttings transport and pipe-sticking problems. However, how to find the optimum gas injection rate accurately remains a question.

Several criteria and methods for determining the minimum gas volume requirement have been used in the gas drilling industry. They fall into two categories: (1) the minimum velocity criterion and (2) the minimum kinetic energy criterion. The minimum velocity criterion considers the interactions between solid particles, fluids, and the boundary of flow domain (borehole wall). The concept of terminal velocity is used to determine the minimum required gas velocity at the deepest large annulus. The terminal velocity of a solid particle can be influenced by many factors, including size, shape, and density of the particle; density and viscosity of the fluid and flow regime. Among many mathematical models proposed to account for the effects of these factors, Gray's model has been widely accepted for small-size hole drilling because it considers particle-wall interaction [1, 2].

The minimum kinetic energy criterion was established in 1950s based on Angel's pioneering work [3]. The mixture of gas and solid is treated as one homogeneous phase with mixture density and velocity, i.e., interactions between particles and fluids are not considered. Several models have been presented, for example, see [3–6]. Although McCray and Cole's model permits a constant-percentage slip velocity of solid particles, it uses the same particle lift criterion as Angel's model. The criterion for the minimum volume requirement is based on the experience gained from quarry drilling with air. The minimum annular velocity to effectively remove solid particles from the borehole is usually assumed to be 15 m/s, or 50 ft./sec (ft/s), under atmospheric conditions. This velocity was believed to be high enough to remove dust-like particles in air drilling. Although big cuttings not removed from the vicinity of the bit by the circulating air are reground by the bit teeth, it would be uneconomical to lift large cuttings without first trying to control their initial size at the bit. It is reported in [7] that the gas flow rate values obtained from Angel's method were at least 25% below the actual field's needs. This motivated numerous investigators to develop more accurate models to determine the minimum required gas injection rate for gas drilling, for example, see [8–17].

Guo et al. performed a comparison of results from the model calculation and the field experience [18]. The comparison shows that, among those existing models, only the result given by Angel's is mostly consistent with actual needs. Guo et al. found that the assumption of Weymouth friction-model is the reason for the underestimation. The Weymouth friction-model is suitable for smooth pipe walls, but not for the borehole walls which are rather rough. Then Guo et al. introduced Nikuradse's friction factor into Angel's model so that the modified model become more reasonable and practical. However, due to the difficulty in determining the friction factor, the application of Guo's model is limited to some extent. The latter motivates us to develop a new mathematical model to determine the gas injection rate. Li et al. [19]

investigated the optimum range of nitrogen injection rate in shale gas well drilling. Chen et al. [20] present a method for determining the minimum gas injection rate required for hole cleaning in horizontal gas drilling.

Recent developments in gas drilling include thermal failure of rock and gas temperature prediction. Zhang et al. [21] determined the effect of fluid temperature on rock failure in borehole drilling with gas. Li et al. [22] identified the complexity of thermal effect on rock failure in gas-drilling shale gas wells. Li et al. [23] developed a closed-form mathematical model for predicting gas temperature in gas-drilling unconventional tight reservoirs. Guo et al. [24] presented an analytical thermal-model for optimization of gas-drilling in unconventional tight-sand reservoirs. Guo et al. [25] published a mathematical modeling of heat transfer in counter-current multiphase flow found in gas-drilling systems with formation fluid influx. Other recent development in gas drilling includes distribution of the sizes of rock cuttings in gas drilling [26] and gas-lift drilling [27].

Another key issue of air and gas drilling to be solved is the environmental pollution and wasting of resources caused by direct discharging or combustion of the returned gas. To address this problem, our research group developed a new gas recycling system [28–30]. Unlike the conventional gas drilling process, the returned gas is re-injected into the wellbore after treatment by separators and fine filters, rather than being discharged or burned directly. The impurity content, humidity and other parameters of the treated gas can fully meet the requirements of the gas suction standard of a compressor. Therefore, the returned gas can be recycled through compressors, and consequently, the objectives of saving resources, lowering the cost, and environmental protection are achieved.

In the current work, a modified mathematical model for predicting the minimum gas injection rate is derived, taking into account Charles' theory of particle grinding energy. The maximum required value of gas injection rate is estimated using the sonic flow criterion at a bit. The proposed model allows calculating the optimum range of gas injection rate more precisely. Also, we present our work in developing the gas recycling system, including the corresponding equipment, operating procedure, and results of a pilot test. The test results indicate a promising prospect of GRS.

The structure of the text is as follows. Section 2 presents the modified mathematical model for predicting the optimum gas injection rate and the comparison between the model prediction and the field experience. Section 3 demonstrates the newly developed gas recycling system. Section 4 concludes this chapter.

## 2. Mathematical model for gas injection rate

### 2.1. The minimum required gas injection rate

It is shown in [18] that only the result given by Angel's minimum kinetic energy criterion has a trend that is consistent with field experience, although the minimum volumetric gas requirements are underestimated. We believe that this underestimation is partially because Angel's

model does not consider the gas energy consumed on grinding cuttings from large size to small size in the borehole annular space. We propose the following equation to modify Angel's model (derivation is given in Appendix):

$$\frac{1}{2}\rho_g v_g^2 = \frac{1}{2}\rho_{g0}\left(v_{g0}\sqrt{1+n}\right)^2 \tag{1}$$

where

$$n = \frac{W_g}{\frac{1}{2}\rho_{g0}v_{g0}^2} \tag{2}$$

$$W_g = \frac{100 f_g D_h^2 W_i \rho_s h_{ROP}}{Q_{g0}}\left(\frac{1}{\sqrt{d}} - \frac{1}{\sqrt{D}}\right) \tag{3}$$

$\rho_g$ and $v_g$ in Eq. (1) are dependent on gas-flow-rate through bottom hole pressure; therefore, this equation has to be solved for $Q_{g0}$ numerically.

### 2.2. The maximum permissible gas injection rate

The excessive gas flow rate through bit can cause several problems including borehole erosion, hole deviation, and ice-balling of drill bit [2]. These problems are usually associated with the sonic flow condition at bit. The temperature of gas at bit can be much lower than expected under sonic flow conditions. This low temperature is due to the Joule-Thomson cooling effect, i.e., a sudden gas expansion below the bit orifice causes a significant temperature drop. The temperature can easily drop to below ice point, resulting in ice-balling of the bit if water exists. Even though the temperature can still be above the ice point, it could be below the dew-point of water vapor, resulting in the formation of liquid water which promotes mud ring problems in the annulus. If natural gas is used as the drilling fluid, it can form gas hydrates with water around the bit, i.e., hydrate balling. The temperature at the bit orifice downstream may be predicted by assuming an isentropic process for an ideal gas flowing through bit orifices [2]. The bit upstream temperature may be lower than the geothermal temperature at the bit depth because the down-stream gas cools the bit body, and the bit body, in turn, cools the upstream gas. The process can continue until a dynamic equilibrium with geothermal and gas temperatures is reached at the bottom of the hole. Ref. [31] presented an analytical method for predicting borehole enlargement due to low-pressure and low-temperature effects. In additional to the borehole erosion, hole deviation and ice-balling, the sonic flow condition can also cause pipe sticking problem [2].

The flow equation for subsonic flow is given by [2]:

$$Q_g = 5.6 C A_n p_{up}\sqrt{\frac{k}{S_g(k-1)\left(\frac{9}{5}t_{up}+492\right)}\left[\left(\frac{p_{dn}}{p_{up}}\right)^{\frac{2}{k}} - \left(\frac{p_{dn}}{p_{up}}\right)^{\frac{k+1}{k}}\right]} \tag{4}$$

Eq. (4) relates the upstream pressure to the down-stream pressure only in subsonic flow conditions. This relation was first presented in [32]. The boundary between the sonic flow and

subsonic flow is identified by the critical downstream to upstream pressure ratio $\frac{p_{dn}}{p_{up}} = \left(\frac{2}{k+1}\right)^{\frac{k}{k-1}}$ = 0.53 when $k$ is 1.4 for air [32]. The choke flow coefficient $C$ takes the maximum value of 1.2, according to [32]. Substituting $C$ = 1.2, $k$ = 1.4, and the critical pressure ratio of 0.53 into Eq. (4) gives an expression of the maximum gas flow rate without causing sonic flow as:

$$Q_{g\max} = \frac{3.25 A_n p_{up}}{\sqrt{S_g\left(\frac{9}{5} t_{up} + 492\right)}} \tag{5}$$

If the operating gas injection rate is higher than this value, larger orifice area $A_n$ should be utilized to expand the maximum permissible flow rate. If changing the orifice area $A_n$ is not an option, a flow diverging joint (FDJ) should be employed at the shoulder of the drill collar. Application procedure of FDJ is reported in the literature, for example, see [33].

### 2.3. Application examples

Shale sections of two wells in the Daqing Field, China, were drilled with nitrogen. Basic data are shown in **Table 1**. For the hole section in Well no. 1, Angel's model predicted the minimum required gas injection rate of 69 standard cubic meter per minute ($Nm^3$/min). For the hole section in Well no. 2, Angel's model gave the minimum required gas injection rate of 66 $Nm^3$/min.

The initial cuttings size was estimated on the basis of rate of penetration and rotary speed to be about 6 mm. The average cuttings size received at surface was observed to be about 1 mm. Assuming the major content of the shale is clay, its fragmentation energy is 6. 3 kWh/t. The $n$-value in Eq. (1) reflects the amount of fragmentation energy from the lowing gas. An empirical $n$ = 1/ 3 is assumed based on the observations that the average size of returned drill cuttings is significantly larger when the drilling string is not rotating while the gas booster is turned on.

| | |
|---|---|
| Site elevation (above mean sea level) | 200 m |
| Ambient pressure | 0.1 $MP_a$ |
| Ambient temperature | 20°C |
| Relative humidity | 10% |
| Geothermal gradient | 3C/100 m |
| Specific gravity of rock | 2.7 water = 1 |
| Hole section in Well no. 1 | 2840–3650 m |
| Hole section in Well no. 2 | 2550–3305 m |
| Bit diameter | 215.9 mm |
| Drill pipe outer diameter | 127 mm |
| Bit orifices | 14.29 mm×3 |
| Rate of penetration | 18 m/h |
| Rotary speed | 50 rpm |

**Table 1.** Basic data for the nitrogen drilling cases in the Daqing Field, China.

| Well no. | 1 | 2 |
|---|---|---|
| Hole section (m) | 2840–3650 | 2550–3305 |
| The minimum required gas injection rate ($Nm^3$/min) | — | — |
| Angel's model | 69 | 66 |
| The new model | 85 | 82 |
| The maximum permissible gas injection rate ($Nm^3$/min) | 144 | 134 |
| Field-applied gas injection rate ($Nm^3$/min) | 120 | 95 |

**Table 2.** Comparison of model-calculated data and field observations.

On the one hand, the latter phenomenon is due to the weak ability of cuttings transportation of gas, i.e., the cuttings have to be fine enough so as to be returned from the bottom. On the other hand, the excessive gas injection rate is non-commercial and may lead to the ice-balling of drill bit induced by Joule Thompson effect as we have mentioned in the previous text. Moreover, field practice and theoretical analysis have shown that the returned debris in gas drilling is extremely fine, regardless of strata types [34]. Utilizing this value in the new model expressed by Eq. (1) gives the minimum required gas injection rate of 85 and 82 $Nm^3$/min for the two hole sections in Well no. 1 and Well no. 2, respectively. The maximum permissible gas injection rates were calculated by Eq. (5) to be 144 and 134 $Nm^3$/min for the two hole sections in Well no. 1 and Well no. 2, respectively.

**Table 2** shows a comparison of model-calculated data and field-applied gas injection rates. Using the new model and a design factor of 1.15, The designed gas injection rate was $1.15\times85$, or 97.8 $Nm^3$/min. For the hole section in Well no. 1. The section was drilled with a fixed compressor capacity of 120 $Nm^3$/min, which is between the minimum required gas rate of 85 $Nm^3$/min and the maximum permissible gas rate of 144 $Nm^3$/min, with no problem of hole cleaning and hole enlargement. Using the new model and the same design factor of 1.15, the designed gas injection rate was $1.15\times82$, or 94.3 $Nm^3$/min for the hole section in Well no. 2. The section was drilled smoothly with a fixed compressor capacity of 95 $Nm^3$/min, which is between the minimum required gas rate of 82 $Nm^3$/min and the maximum permissible gas rate of 134 $Nm^3$/min. This comparison indicates a good consistency between the model-predicted optimum range of gas injection rates and the field-observed problem-free gas injection rates.

## 3. New technology of gas recycling drilling

The current gas drilling practice of handling gas returned from the borehole is to discharge it to the atmosphere directly. If the gas can be recycled in the same way as drilling mud, the energy consumption and drilling cost can be greatly reduced. The recycling system can also allow the produced gas from the reservoir to be compressed and transported to the gas gathering system in the field. The overall efficiency of gas drilling will be improved significantly.

The gas recycling system (GRS) has been investigated at the China University of Petroleum, Beijing (CUPB), for several years. A systematic research and development group at the CUPB

carried out a comprehensive study including an integration design, technological process investigation, cuttings transport analysis, separation and filter equipment selection, and control system design.

### 3.1. System description

The general idea of the GRS is to separate gas effectively from the gas-liquid-solid mixtures returned from the well and re-inject the gas back into the well. At the same time, cuttings and fluids are discharged after the separation. During the natural gas drilling process, the separated gas can be released to the gas gathering system in the field. The integrated design of the process is illustrated in **Figure 1**.

When nitrogen is used as the drilling fluid, a low-capacity nitrogen generator is employed to supply nitrogen gas and inject it into the well. If the well is deep, compressors or boosters may be used to provide the required injection pressure. When the gas pressure and volume reach the required value for recycling, the gas drilling process can be initiated. Because the nitrogen gas is recycled, only a low-capacity nitrogen generator is required for supplying a small amount of nitrogen gas to make up the losses due to leakage and to meet the requirement of additional gas volume in the wellbore as depth increases.

The major equipments in the GRS are described as follows:

**Compressors and boosters:** The compressors and boosters used in the gas recycling system are the standard equipment used in conventional gas drilling operations. After filtration, the clean nitrogen gas is introduced into the system through parallel connections.

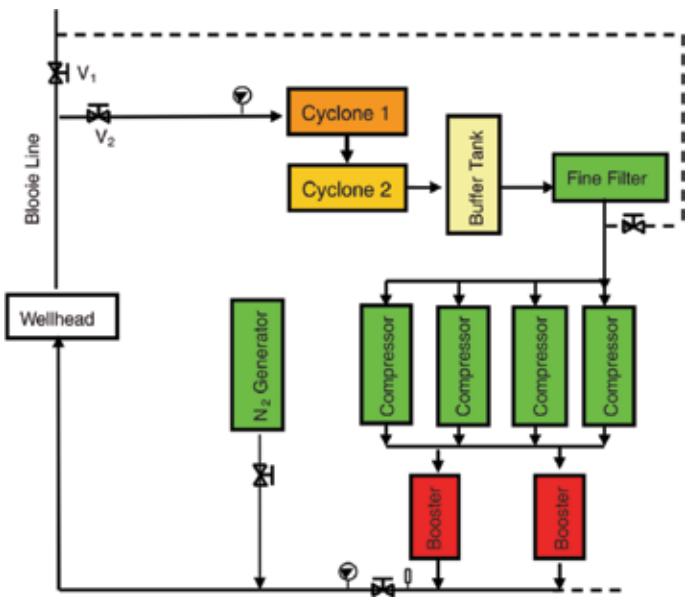


**Figure 1.** A sketch of the gas recycling system.

**Primary separator**: The primary separator separates drill cuttings of larger than 0.1 mm equivalent diameter by centrifugal force. Water is introduced into the separator to dilute the cuttings in the separator. The solid particles and liquid are discharged at the bottom of the separator. The separated gas exits the separator at the top and flows into a cyclone separator for further purification. The discharge system was designed to prevent gas loss and liquid overflow by automatically maintaining the dynamic liquid level during the solids and liquids discharge process in the pressurized separator. It is expected that any liquid hydrocarbon/condensate from the drilled formation will drain out of the system at the bottom of the separator.

**Cyclone separation unit:** Two cyclone separators are used to separate solid particles of a size larger than the 7 μm equivalent diameter. An air-lock and waste-discharge device is specially designed in the separator to guarantee the timely debris-discharging by using the recycled water and the gas tightness. Consequently, the separator can work continuously without deposition of debris. Use of the two cyclone separators in series guarantees that most, although not 100%, of the drill cuttings are removed from the gas phase. The gas phase with small particles (dust) is led to a fine filter for further purification.

**Fine filter:** The fine filter works on the principle of filtration and aggregation to remove the solid particles that are larger than the 3 μm equivalent diameter. The purity of the post-separation gas is superior to the atmospheric air in terms of particle concentration. The filtered gas is introduced to the compressors for injection into the well. Two fine filters are prepared for alternation. If the debris is overstocked in one of the fine filters, the other one is switched over duly. And the element of the overstocked filter is replaced.

### 3.2. Operating procedure

The procedure of operating the GRS is different from that of the conventional gas drilling system. The procedure is outlined as follows:

**Air displacement:** If the upper well section is drilled with mud, one can follow the conventional air drilling procedure to lift the liquid and dry the hole with compressed air in order to save the cost of nitrogen generation. When the air lift is completed, one can replace the air in the well with nitrogen gas to ensure safe drilling.

**Preparation of nitrogen gas:** The nitrogen generator is started first. The generated nitrogen gas is injected into the well by the compressors. Drilling operation is initiated when the gas pressure and gas flow rate reach the desired levels for the well condition.

**Nitrogen supplement:** The fluid mixture returned from the well is led to the separation system to remove solids and liquids. The separated gas from the gas-liquid-solid mixture is fed into the compressors and boosters and reinjected into the well. The nitrogen generator runs intermittently to make up for the gas loss in the system and the increased borehole volume as the well deepens.

**Drill pipe connection operation:** Pipe connection will cause some gas loss. The loss in the annulus can be controlled by closing the rotating head. To minimize the gas loss, one can use the check valves in the drill string to prevent backflow of nitrogen gas during pipe connections.

http://dx.doi.org/10.5772/intechopen.75785

**Treatment of drilling complications:** In case of drilling complications such as borehole collapse and excessive formation liquid influx, the nitrogen gas flow rate should be increased immediately. The nitrogen generator should be turned on as soon as possible to provide additional nitrogen gas volume. For instance, if the normal gas circulation rate is 120 $Nm^3$/min and the capacity of the membrane nitrogen is 30 $Nm^3$/min, turning on the nitrogen generator will increase the gas rate to 150 $Nm^3$/min. Because the gas is still in recycling, gas shortage will not be a problem. Moreover, as time passes, the gas volumetric flow rate in the well will continue to increase to clean the borehole.

**System control:** The process in the GRS is more complicated than that in a conventional gas drilling system. The gas supplement rate adjustment, the valve activation during pipe connection, the timely turning on/off of the nitrogen generator, etc., cannot be achieved by manual operations. An automatic control system was implemented in the developed gas recycling system to ensure operational safety.

### 3.3. Pilot test

To verify the feasibility of the GRS and the performance of the related equipment, the development group at the CUPB conducted a special test of the system on the Dayi101 well in 2010. An open loop mode was adopted to ensure the safety of the drilling operation. The assembled system is shown in **Figure 2**.

The GRS was installed in the middle of the blooie line. This arrangement was based on two considerations. First, the setup location was not close to the drilling floor to prevent its direct influence on the drilling floor operations should complications occur. Second, the location was not close to the outlet of the blooie line, thereby avoiding the impact of the igniting device on the GRS. The safe distance is essential for preventing hazardous conditions when gas leaks from the separation system.

**Figure 2.** A gas recycling system installed in Sichuan province of China.

The first objective of the pilot test was to assess the performance of the separation and filtration equipment. This was achieved by evaluating the capacity of separation and filtration equipment, including separating performance of the first and second cyclone separators, stability of the separation system, and the purity of gas at the outlet of the fine filter. The second objective of the test was to assess the adaptability of separation and filtration equipment to the drilling conditions, including normal drilling condition and complication condition such as formation fluid influx. Three working conditions were created. The first condition was the closed-gas flow test to check the liability of the separation system. The second condition was the normal gas drilling test to examine the effectiveness of the separation system. The third condition was the formation fluid influx test to inspect the adaptability of the new system.

**Gas tightness test:** After the third openhole section of Dayi 101 had been drilled with water, a gas lift was conducted to blow off water and cuttings out of the hole. It took 8 hours to dry the hole completely. The gas circulation was normal. This was a favorable condition for the tightness test of the new system. During the tightness test, the gas injection pressure was 3.8 MPa and the gas injection rate was 90 $Nm^3$/min. A small leak was found at the outlet of the second cyclone separator. After an investigation, it was confirmed that a collision had occurred to the outlet of the separator during transportation, which damaged the gaskets and caused the leak. After the gaskets were replaced, no more leaks were found during a half-hour test, which indicated that the seal was effective. It provided a sound base for conducting the subsequent tests.

**Separation test:** Water zones were encountered during drilling in the fourth openhole section. The drilling operation was immediately stopped for discharging water. During this period, a separation system test was conducted. The injection gas pressure was about 4.6 MPa and injection gas rate was 90 $Nm^3$/min. Visible dust and water were seen at the outlet of the blooie line in the beginning, as shown in **Figure 3a** and **b**. After switching to the separation system, however, the gas at the outlet was seen to be clean and no water droplets were observed, as shown in **Figure 4a** and **b**. This indicated that the formation water and cuttings had been separated effectively by the system. The white mist was caused not by the solid dust, but by the high velocity of gas. However, there was no evidence of any remaining liquid hydrocarbon/condensate in the gas stream.

Because the formation water influx was little and the amount of dust was small in the hole drying process, the system worked effectively. The next step was to test the separation system in normal drilling conditions in which a large amount of dust exists in the system.

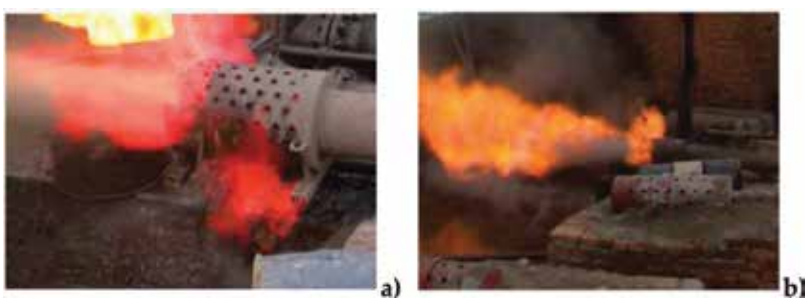


**Figure 3.** Water and dust was seen at the outlet of the blooie line before separation.

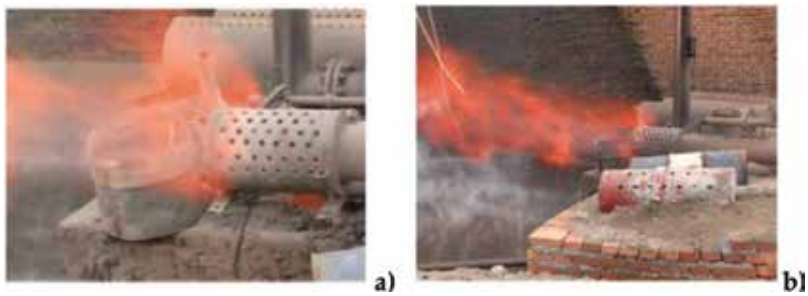


**Figure 4.** No water or dust was seen at the outlet of the blooie line after separation.

The drilling process started after the hole drying operation. To ensure operational safety, a driller was appointed to control the valve on the blooie line ($V_1$ in **Figure 1**). In case of an unforeseen situation, the $V_1$ should be immediately switched to the conventional work position.

The output at the exit of the blooie line was normal after the drilling operation began. Therefore, the inlet valve ($V_2$ in **Figure 1**) to the separation system was opened and the $V_1$ was closed. Then the full stream of the gas-liquid-solid mixture returned from the well entered the separation system. To better observe the effect, the water pump for dust removal was closed temporarily. Dust appeared at the exit of the blooie line before separation. After resuming the water injection with the pump to initiate separation, no visible dust was observed at the exit of the blooie line. The filtered gas was very clean. The test result showed that the separation was effective.

As the separated gas was prepared for recycling, its purity must meet the requirement of the compressor. Therefore, a dust concentration test was conducted for the separated gas. Before the test, the dust concentration of the air at the well site was measured to be 0.03–0.1 mg/m$^3$. The concentration monitoring instruments were installed at both the inlet and outlet of the filter. The quality parameters of the gas were recorded and analyzed automatically. The monitoring result showed that the dust concentration at the inlet of the filter was 50–80 mg/m$^3$ and that at the outlet was 0.05–0.08 mg/m$^3$. This means that the purity of the filtered gas reached the level of the

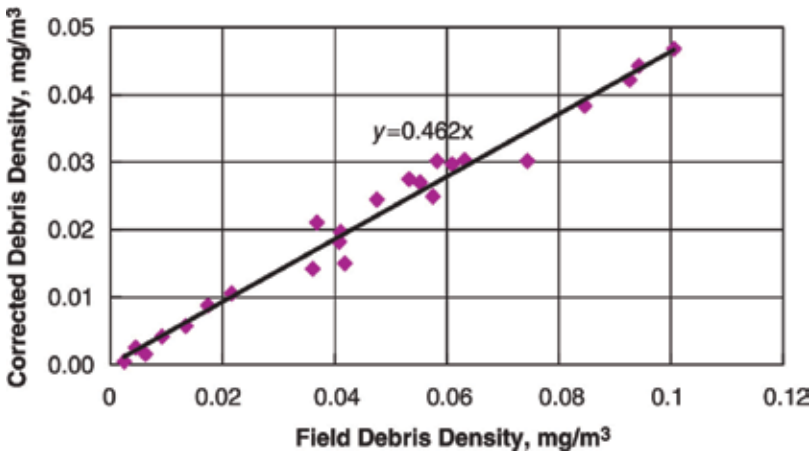


**Figure 5.** The contrast curve of TSI AM510 measurements and PALAS 3000 measurements.

atmospheric air. It is believed that the filter device completely blocked dust particles that are larger than 3 μm equivalent diameter and the purified gas met the requirement of the compressor.

In order to ensure the accuracy of the measurements, a calibration test for the on-site monitor TSI AM510 was further conducted. The calibration device PALAS 3000 is a more accurate instrument suitable for indoor test. A calibrated contrast curve is presented in **Figure 5**, which shows that the dust concentration was much lower than that of the field data. This again proves the reliability of the separation and filtration system.

It was known from the data collected by the mud logger that the stand pipe pressure increased by only 0.1 MPa because of the separation process. This is the total pressure drop in the separation system. Apparently, the separation system has negligible effect on the drilling pressure.

### 3.4. Problems and solutions

The first open-loop field test of the GRS was essentially successful. All the equipment was in working order and the separation efficiency was high. This work served as a solid base line for more closed-loop tests. The following problems were found during the test:

#### *3.4.1. Continuous discharge design*

According to the original plan, the separated cuttings should be discharged continuously by circulating water. However, the electrical motor for suction pump was not explosion-proof. It did not meet the field security requirement. Therefore, the gas discharge mode had to be adopted. All electrical equipment must be explosion-proof in the future design. In the discharge process, the working condition of the second cyclone separator was normal. However, the blooie line of the first separator was blocked for a moment. Larger size blooie line should be adopted in the future design.

#### *3.4.2. The height of the equipment and skid mounted design*

The current separation system is about 7 m high. Collision may occur easily during the transportation and installation process. This height is also inconvenient for monitoring and maintenance of the system. Therefore, the equipment's height should be reduced in the subsequent design without affecting separation efficiency. At this time, the design of a new horizontal separation system has been completed. After further improvements, a skid mounted system will be fabricated for easy transportation and equipment integration.

#### *3.4.3. System measurement and control design*

When a closed-circulation is achieved, the operating parameters such as pressure and gas flow rate should be monitored in real time for safety. Valve switching should be used with both manual and automatic modes. In addition, a real-time alarm system should be added for safe operation. Due to the constraints of time and field conditions, an onsite reading method was

used in this test. The automatic measurements and control systems should be emphasized in subsequent development.

#### *3.4.4. Compressor inlet design*

The entrance of a conventional compressor is open to air. Because the separated gas needs to be introduced to the compressor through piping, a proper parallel gas distributing manifold should be designed to fit the compressor inlet. Currently, such a manifold has been conducted and tested with conventional compressors and the result is satisfactory.

### 3.5. Operational risks

Some operational risks still exist with the new technology. These risks include: (1) quick addition of gas volume into the borehole in an emergency, (2) oxygen rust corrosion, and (3) downhole fire/explosion.

Whenever the hole cleaning raises a concern because of drill cuttings accumulation, borehole collapse, excessive formation liquid influx, and/or gas leakage, it is imperative to automatically switch on the membrane nitrogen generator for increasing gas input volume to the system. This step will minimize drilling complications and ensure smooth drilling. Since nitrogen gas is highly compressible, which does not cause an immediate pressure drop in the borehole, it may be a good practice to select between 25 and 35% of the capacity of the membrane nitrogen generator using normal nitrogen drilling practice.

Rust corrosion due to oxygen in a wet system is a concern in any nitrogen gas drilling if the oxygen filters do not perform well, whether the system is an open or a closed one. Fortunately, most membrane nitrogen generators remove oxygen to much lower than percent level and no significant risk is expected. Because $CO_2$ and $H_2S$ corrosion occurs in wet systems, they should be minimized with inhibitors whenever these gases are encountered during drilling.

Downhole fire/explosion can occur when drilling hydrocarbon-bearing zones in the presence of oxygen. For this to happen, the oxygen/hydrocarbon ratio has to be in a certain range. In systems containing natural gas and air only, the natural gas concentration needs to be between 5 and 15%, depending on pressure. Since air contains about 21% of oxygen while membrane-generated nitrogen contains less than 5% oxygen, it is uncommon to see a downhole fire/explosion in a nitrogen gas drilling operation.

## 4. Conclusions

Regarding the determination of the required gas injection rate and direct discharge of the returned gas in gas drilling, we derived a mathematical model for predicting the optimum range of gas injection rate, developed a new technology of gas recycling drilling, established a system of gas separation and filtration corresponding in the GRS, and performed a pilot test. This study allows for drawing the following conclusions:

1. Based on the modified energy criterion, the minimum required gas injection rate for hole cleaning is nearly proportional to the grinding energy contributed by the flowing gas.
2. The range of the optimum required nitrogen gas injection rate given by the newly developed mathematical model is consistent with field experience.
3. The first open-loop field test on the GRS was successful. The purity of the post-separation gas is superior to the atmospheric air in terms of particle concentration. The filtered gas met the requirement of gas compressor and circulation in the well. The success of the test has laid a good foundation for future development of the system. The GRS has been proven to be a viable and feasible innovation for reducing the cost of gas drilling. It has a huge potential to be applied to the gas drilling operations including nitrogen drilling and natural gas drilling. This technology is predicted to have a huge impact on reducing the cost of gas drilling and improving drilling performance.

## A. The minimum energy criterion for hole cleaning considering cuttings grinding

According to Angel [3], the gas stream at bottom hole should be powerful enough to have at least a kinetic energy given by the following expression:

$$\frac{1}{2}\rho_g v_g^2 = \frac{1}{2}\rho_{g0} v_{g0}^2 \tag{A.1}$$

The right-hand-side of Eq. (A.1) is equal to 142 J/m$^3$.

Angel's energy criterion underestimates the gas flow rate requirement for hole cleaning possibly because it does not consider the gas energy consumed on grinding cuttings from large size to small size in the borehole annular space. We propose the hypothesis that gas stream should have at least the kinetic energy of.

$$\frac{1}{2}\rho_g v_g^2 = \frac{1}{2}\rho_{g0} v_{g0}^2 + W_g \tag{A.2}$$

where $W_g$ is the gas energy spent on grinding cuttings, J/m$^3$.

Gas drilling produces drill cuttings of dust-like. The fine sizes of the solid particles are believed to be resulted from many times of collisions of drill cuttings to the borehole wall and drill string. If this is true, the energy spent on the collision must be from the flowing gas and the rotating drill bit and drill string. Consider the work done during the collision. Charles' equation for grinding energy has been widely used in the powder grinding industry [35]:

$$dW = -cx^{-a}dx \tag{A.3}$$

where $W$ is the energy requirement for crushing an individual particle, $x$ is particle diameter, $c$ is a proportionality coefficient, and $a$ is a diameter index. When the particle is ground from its initial diameter $D$ to its final diameter $d$, Eq. (A.3) can be integrated to obtain a relation:

$$W = k\left(\frac{1}{d^b} - \frac{1}{D^b}\right) \tag{A.4}$$

where $b = a - 1$ and $k = \frac{c}{a-1}$.

In gas drilling, the initial cuttings equivalent diameter is usually in the order of 10 mm. The final cuttings equivalent diameter is normally greater than 0.5 mm. This particle size range falls into the category of Bond Crack Propagation where $b \approx 0.5$. Eq. (A.4) then degenerates to.

$$W = W_i\left(\frac{10}{\sqrt{d}} - \frac{10}{\sqrt{D}}\right) \tag{A.5}$$

where $W$ is the energy requirement for crushing an individual particle, kWh; $W_i$ = $k$/10 represents the fragmentation energy determined in standard test [35], kWh/t.

If the energy requirement is expressed in Joule per particle, Eq. (A.5) becomes:

$$w = \frac{3.6 \times 10^6}{907} W_i\left[\rho_s\left(\frac{\pi}{6}D^3\right)\right] \times \left(\frac{1}{\sqrt{d}} - \frac{1}{\sqrt{D}}\right) \tag{A.6}$$

or

$$w = 3.97 \times 10^3 W_i \rho_s D^3\left(\frac{1}{\sqrt{d}} - \frac{1}{\sqrt{D}}\right) \tag{A.7}$$

where $w$ is the energy requirement for crushing an individual particle, J; $\rho_s$ is the density of solid particle, kg/m$^3$.

The number of drill cuttings ($m$) created by the drill bit in a unit volume of gas at standard condition can be estimated on the basis of rate of cuttings volume generation ($Q_c$), volume of individual cuttings ($V_c$), and gas injection rate ($Q_{g0}$):

$$m = \frac{\frac{Q_c}{V_c}}{Q_{g0}} \tag{A.8}$$

The rate of cuttings volume generation is expressed as:

$$Q_c = \frac{c\pi D_h^2 h_{ROP}}{4(60)} \tag{A.9}$$

where $D_h$ is the hole diameter, m; $h_{ROP}$ is the rate of penetration, m/hr.

Assuming cuttings sphericity 1.0, the volume of individual cuttings is.

$$V_c = \frac{4\pi}{3}\left(\frac{D}{2}\right)^3 \tag{A.10}$$

Substituting Eqs. (A.9) and (A.10) into Eq. (A.8) results in

$$m = \frac{D_h^2 h_{ROP}}{40 Q_{g0} D^3} \tag{A.11}$$

The energy requirement for grinding all particles in a unit volume of gas is then expressed as.

$$W = mw \tag{A.12}$$

It is understood that crushing energy should be from rotating drill bit, drill string, and the flowing gas. Assuming the fraction of the crushing energy from the flowing gas is $f_g$, we have

$$W_g = f_g mw \tag{A.13}$$

Substitution of Eqs. (A.7) and (A.11) into Eq. (A.13) yield:

$$W_g = \frac{100 f_g D_h^2 W_i \rho_s h_{ROP}}{Q_{g0}}\left(\frac{1}{\sqrt{d}} - \frac{1}{\sqrt{D}}\right) \tag{A.14}$$

Substituting Eq. (A.14) into Eq. (A.2) results in:

$$\frac{1}{2}\rho_g v_g^2 = \frac{1}{2}\rho_{g0} v_{g0}^2 + \frac{100 f_g D_h^2 W_i \rho_s h_{ROP}}{Q_{g0}}\left(\frac{1}{\sqrt{d}} - \frac{1}{\sqrt{D}}\right) \tag{A.15}$$

To make the model easy to be adopted in existing computer models, this equation can be rewritten in the same form of Angel's equation as:

$$\frac{1}{2}\rho_g v_g^2 = \frac{1}{2}\rho_{g0}\left(v_{g0}\sqrt{1+n}\right)^2 \tag{A.16}$$

where

$$n = \frac{W_g}{\frac{1}{2}\rho_{g0} v_{g0}^2} \tag{A.17}$$

## Nomenclature

| | |
|---|---|
| $A_n$ | total nozzle area, $mm^2$ |
| $C$ | choke flow coefficient (≈1.2 according to Guo and Liu [2]) |

| | |
|---|---|
| $d$ | final diameter, m |
| $D$ | initial diameter, m |
| $D_h$ | hole diameter, m |
| $F_g$ | fraction of grinding energy contributed by the flowing gas, dimensionless |
| $h_{ROP}$ | rate of penetration, m/h |
| $k$ | heat capacity ratio of gas (≈ 1.4 according to Guo and Liu [2]) |
| $p_{dn}$ | downstream pressure, MPa absolute |
| $p_{up}$ | upstream pressure, MPa absolute |
| $Q_{g0}$ | the minimum required gas volumetric flow rate at standard condition, $Nm^3/min$ |
| $S_g$ | gas specific gravity, air = 1 |
| $t_{up}$ | upstream temperature, °C |
| $W_g$ | the energy spent on grinding cuttings by the gas stream, $J/m^3$ |
| $W_i$ | fragmentation energy, 6.30 kWh/t for clay and 12.74 kWh/t for limestone |

Greek symbols

| | |
|---|---|
| $\rho_g$ | gas density at bottom hole condition, $kg/m^3$ |
| $v_g$ | gas velocity at bottom hole condition, m/s |
| $\rho_{g0}$ | gas density at standard condition (0. 1 MPa, 15°C), 1.22 $kg/m^3$ |
| $v_{g0}$ | Angel's gas velocity at standard condition for hole cleaning (0. 1 MPa, 15°C), 15 m/s |
| $\rho_s$ | density of solid particle, $kg/m^3$ |

## Author details

Jun Li[1]*, Yulong Yang[1], Boyun Guo[2] and Gonghui Liu[1]

*Address all correspondence to: lijun446@vip.163.com

1 China University of Petroleum, Beijing, China

2 University of Louisiana at Lafayette, USA

## References

[1] Gray KE. The cutting carrying capacity of air at pressures above atmospheric. Transactions of AIME. 1958;**213**:180-185

[2] Guo B, Liu G. Applied Drilling Circulation Systems. Oxford: Elsevier; 2011

[3] Angel RR. Volume requirements for air or gas drilling. Transactions of AIME. 1957;**210**: 325-330

[4] Martin DJ. Use of air or gas as a circulating fluid in rotary drilling—Volumetric requirements. Hughes Engineering Bulletin. 1952;**23**:35-42

[5] Scott JO. How to figure how much air to put down the hole in air drilling. Oil & Gas Journal. 1957;**55**:104-107

[6] McCray AW, Cole FW. Oil Well Drilling Technology. Edmund: University of Oklahoma Press; 1959

[7] Schoeppel RJ, Spare AR. Volume requirements in air drilling. In: Drilling and Rock Mechanics Conference; 25-26 January 1967; Austin, Texas. DOI: 10.2118/1700-MS

[8] Capes CE, Nakamura K. Vertical pneumatic conveying: An experimental study with particles in the intermediate and turbulent flow regimes. Canadian Journal of Chemical Engineering. 1973;**51**(1):33-38

[9] Sharma MP, Crowe CT. A novel physico-computational model for quasi: One dimensional gas-particle flows. Transactions of ASME. 1977;**22**:79-83. DOI: 10.1115/1.3448678

[10] Ikoku CU, Azar JJ, Williams CR. Practical approach to volume requirements for air and gas drilling. In: SPE Annual Technical Conference and Exhibition; 21-24 September 1980; Dallas, Texas. DOI: 10.2118/9445-MS

[11] Machado CJ, Ikoku CU. Experimental determination of solid fraction and minimum volume requirements in air and gas drilling. Journal of Petroleum Technology. 1982; **34**(11):35-42

[12] Mitchell RF. Simulation of air and mist drilling for geothermal wells. Journal of Petroleum Technology. 1983;**35**(11):27-34. DOI: 10.2118/10234-PA

[13] Puon PS, Ameri S. Simplified approach to air drilling operations. In: SPE Eastern Regional Meeting; 31 October-2 November 1984; Charleston, West Virginia. DOI: 10.2118/13380-MS

[14] Sharma MP, Chowdry DV. A computational model for drilled cutting transport in air (or gas) drilling operations. Journal of Energy Resources Technology. 1986;**108**(1):8-14. DOI: 10.1115/1.3231247

[15] Wolcott PS, Sharma MP. Analysis of air drilling circulating systems with application to air volume requirement estimation. In: SPE Eastern Regional Meeting; 12–14 November 1986; Columbus, Ohio. DOI: 10.2118/15950-MS

[16] Adewumi MA, Tian S. Hydrodynamic modeling of wellbore hydraulics in air drilling. In: SPE Eastern Regional Meeting; 24–27 October 1989; Charleston, West Virginia. DOI: 10.2118/19333-MS

[17] Tian S, Adewumi MA. Development of hydrodynamic model-based air drilling design procedures. SPE Drilling Engineering. 1992;**7**(04):241-246. DOI: 10.2118/23426-PA

[18] Guo B, Miska S, Lee RL. Volume requirements for directional air drilling. In: SPE/IADC Drilling Conference; 15-18 February 1994; Dallas, Texas. DOI: 10.2118/27510-MS

[19] Li J, Guo B, Liu G, Liu W. The optimum range of nitrogen injection rate in shale gas well drilling. SPE Drilling & Completion. 2013;**28**(1):60-64. DOI: 10.2118/163103-PA

[20] Chen X, Gao D, Guo B, Luo L, Liu X, Zhang X. A new method for determining the minimum gas injection rate required for hole cleaning in horizontal gas drilling. Journal of Natural Gas Science and Engineering. 2014;**21**:1084-1090. DOI: 10.1016/j.jngse.2014.11.009

[21] Zhang H, Gao D, Salehi S, Guo B. Effect of fluid temperature on rock failure in borehole drilling. ASCE Journal of Engineering Mechanics. 2014;**140**(1):82-90. DOI: 10.1061/(ASCE) EM.1943-7889.0000648

[22] Li J, Guo B, Yang S, Liu G. The complexity of thermal effect on rock failure in gas-drilling shale gas wells. Journal of Natural Gas Science and Engineering. 2014;**21**:255-259. DOI: 10.1016/j.jngse.2014.08.011

[23] Li J, Guo B, Li B. A closed form mathematical model for predicting gas temperature in gas-drilling unconventional tight reservoirs. Journal of Natural Gas Science and Engineering. 2015;**2**:284-289. DOI: 10.1016/j.jngse.2015.08.064

[24] Guo B, Li G, Song J. An analytical thermal-model for optimization of gas-drilling inunconventional tight-sand reservoirs. Journal of Sustainable Energy Engineering. 2016; **2016**(2):108-126

[25] Guo B, Li J, Song J, Li G. Mathematical modeling of heat transfer in counter-current multiphase flow found in gas-drilling systems with formation fluid influx. Journal of Petroleum Science. 2017;**14**:711-719. DOI: 10.1007/s12182-017-0164-3

[26] Li J, Yang S, Guo B, Feng Y, Liu G. Distribution of the sizes of rock cuttings in gas drilling. Computer Modeling in Engineering & Sciences. 2012;**2340**(1):1-18

[27] Guo B, Li G, Song J, Li J. A feasibility study of gas-lift drilling in unconventional tight oil and gas reservoirs. Journal of Natural Gas Science and Engineering. 2017;**37**:551-559. DOI: 10.1016/j.jngse.2016.11.057

[28] Liu G, Tao Q, Li J. Gas volume control techniques for circular gas drilling. Oil Drilling & Production Technology. 2009;**31**(4):32-35. DOI: 10.13639/j.odpt.2009.04.008 (in Chinese)

[29] Li J, Liu G, Han L. Study on the gas circulation system. Drilling & Production Technology. 2010;**3**(3):48-50. (in Chinese)

[30] Li J, Liu G, Guo B. Pilot test shows promising technology for gas drilling. Journal of Petroleum Technology. 2012;**64**(07):32-37. DOI: 10.2118/0712-0032-JPT

[31] Zhang H, Zhang H, Guo B, Gang M. Analytical and numerical modeling reveals the mechanism of rock failure in gas UBD. Journal of Natural Gas Science and Engineering. 2012;**4**:29-34. DOI: 10.1016/j.jngse.2011.09.002

[32] Szilas AP. Production and Transport of Oil and Gas. Amsterdam: Elsevier; 1975

[33] Guo B, Zhang Z, Gao D. Optimal use of flow-diverting joint in underbalanced gas drilling. In: SPE Asia Pacific Oil and Gas Conference and Exhibition; 20–22 September 2011; Jakarta, Indonesia. DOI: 10.2118/143309-MS

[34] Li J, Yang S, Liu G. Cutting breakage and transportation mechanism of airdrilling. International Journal of Oil, Gas and Coal Technology. 2013;**6**(3):259-270. DOI: 10.1504/IJOGCT.2013.052237

[35] Zheng S. Superfine Grinding. Beijing: China Building Materials Industry Press; 1999

*Edited by Ariffin Samsuri*

With regard to depleted oil and gas resources, increasing world energy demands and volatile economic and political world scenarios, oil and gas industry players are working very hard to find ways to cut exploration and production costs to sustain and develop the industry to provide the world with cheap energy without harming the environment. Therefore, this book intends to provide readers with a comprehensive overview of the current state of the art in drilling, such as advanced drilling operations and techniques used by the industry, particularly in floating, underbalanced drilling, smart drilling fluid, intelligent drilling, drilling optimization, and future drilling technology and development.

Published in London, UK


IntechOpen

ISBN 978-1-83881-531-8